
**Improving PTR-ToF-MS: Implementation of a
radio frequency ion funnel and an
investigation into buffer-gas doping.**

**Thesis submitted for the degree of Doctor of
Philosophy at the University of Leicester**

by

Shane Brian Barber BSc (Hons) AMRSC

Department of Chemistry

University of Leicester

September 2015

Statement of originality

The work described in this thesis was conducted by the author in the Department of Chemistry at the University of Leicester mainly during the period between October 2010 and September 2014. All the work in this thesis is original unless otherwise acknowledged in the text or by references.

.....
Shane Brian Barber

26th September 2015

Abstract

Improving PTR-ToF-MS: implementation of a radio frequency ion funnel and an investigation into buffer-gas doping.

Shane Brian Barber

September 2015

Volatile organic compounds (VOCs) are ubiquitous in the Earth's atmosphere. VOCs are produced from biogenic sources such as forests, or anthropogenic sources such as fossil fuel combustion. Many areas of research involve measuring VOCs, from atmospheric science, to medical science and homeland security with implications for health, the environment, and safety. It is crucial that VOCs are detected quickly and with a high sensitivity: proton transfer reaction - mass spectrometry (PTR-MS) offers a solution and potential enhancements of the PTR-MS technique are discussed here. A drift tube capable of simultaneously functioning as an ion funnel is demonstrated in PTR-MS for the first time enabling a much higher proportion of ions to exit the drift tube and enter the mass spectrometer than would otherwise be the case. An increase in the detection sensitivity for VOCs of up to two orders of magnitude and an increase in Limit of Detection of one order of magnitude is delivered, allowing lower concentrations of VOCs to be detected.

An alternate way to change how the drift tube behaves is to alter the buffer gas. The collision energy within the drift tube is investigated in order to ascertain what advantages changing the buffer gas from nitrogen to argon yields with respect to sensitivity and fragmentation of analytes. For several compounds, the sensitivity is increased and fragmentation reduced. If sensitivity can be increased and/or fragmentation reduced within a complex mixture of analyte ions, then analysis of these mixtures will be simplified. Finally, a standard PTR-MS instrument is compared with the ion funnel equipped PTR-MS instrument in an urban, megacity (ClearfLo campaign, London, UK) in order to test the instrument and enhanced sensitivity for field measurements.

Acknowledgments

I would like to thank the Royal Society of Chemistry's (RSC), Analytical Chemistry Trust Fund (ACTF) and the Natural Environment Research Council (NERC) for funding my PhD. I would like to thank my supervisors, Professor Andrew M Ellis and Professor Paul S Monks, for allowing me the opportunity to work with them to learn the *art* of PTR-MS.

I would like to thank everybody who has helped me with my research. The guys in the workshops, Keith, Praf, and Carl, who without their skills this research would simply not be possible. Everyone from the atmospheric department over the last four years, including (but not limited to), Rebecca, Tom, Double Dr Blake, Iain G, Rik and Zoë. Chris and Sara for making things run smoothly and allowing me to claim my expenses back!

I want to give a special mention to Dr Iain White, 'YT', for working with me during my time here and showing me the ropes, as well as the many hours on Skype giving tips and advice to help me complete this thesis.

Ellie 'Nora' Banks for sharing her grammatical knowledge and for taking the time to proof read my thesis late into the night.

And of course my amazing wife, Nicola, for putting up with many mornings, afternoons, and nights of despair, meltdowns and complaining. Without her constant support this would never have been possible.

Table of contents

	Page number
Statement of originality	ii
Abstract	iii
Acknowledgements	iv
Table of contents	v
List of tables	ix
List of figures	xii
List of abbreviations	xx
Chapter one: Introduction	1
1.1 Volatile organic compounds in the atmosphere	1
1.2 Volatile organic compounds in other areas	6
1.3 Volatile organic compound detection	7
1.3.1 Gas chromatography	7
1.3.2 Ion mobility spectrometry	9
1.3.3 Flowing afterglow technique	11
1.3.4 Selected ion flow tube - mass spectrometry	12
1.3.5 Selected ion flow drift tube - mass spectrometry	13
1.3.6 Proton transfer reaction - mass spectrometry	13
1.4 Applications of proton transfer reaction - mass spectrometry	17
1.4.1 Atmospheric chemistry	17
1.4.2 Breath analysis	19
1.4.3 Food science	21
1.4.4 Forensic science	23
1.4.5 Homeland security	24
1.5 Thesis structure	25
1.6 References	27
Chapter two: Instrumental	32
2.1 Introduction to mass, charge and mass spectrometry	32
2.1.1 Mass and charge nomenclature	32
2.1.2 Units of mass to charge ratio	32

2.2	Ionising and ionisation sources	34
2.2.1	Hard verses soft ionisation	34
2.2.2	Electron ionisation	34
2.2.3	Chemical ionisation	35
2.2.4	Chemical ionisation sources	36
2.3	Thermodynamics and kinetics of proton transfer	39
2.3.1	Thermodynamics	39
2.3.2	Kinetics	42
2.3.3	<i>E/N</i> ratio	43
2.3.4	Buffer gases	45
2.4	Time of flight mass analyser	46
2.4.1	Liner time of flight mass analyser	46
2.4.2	Reflectron time of flight mass analyser	47
2.5	Instrumentation in use at the University of Leicester	49
2.5.1	Kore ToF	49
2.5.2	Leicester ToF	52
2.5.3	Comparison of instrumentation	53
2.5.4	Instruments used in each study	54
2.6	Validation and quantification	55
2.6.1	Data normalisation	55
2.6.2	Calibration	55
2.6.3	Sensitivity and limit of detection	58
2.7	References	62

Chapter three: Characterisation of a PTR-ToF-MS fitted with a radio frequency ion funnel

3.1	Introduction	64
3.2	Experimental	67
3.2.1	The standard PTR-MS apparatus	67
3.2.2	Modified ion funnel/drift tube	67
3.2.3	Detector blanking	71
3.2.4	Operating conditions	71
3.3	Results and discussion	73
3.3.1	Preliminary observations	73

3.3.2	Effective E/N	74
3.3.3	Volatile organic compound fragmentation	78
3.3.4	Noise	79
3.3.5	Detection sensitivity and limit of detection	83
3.4	Conclusion	88
3.5	References	89
 Chapter four: The use of rare gases to control collision energy		 90
4.1	Introduction	90
4.2	Kinetics/thermodynamics of gases in the drift tube	92
4.2.1	Centre of mass collision energy calculations	92
4.2.2	Drift time	94
4.3	Previous findings	97
4.3.1	Penning Ionisation	99
4.4	Experimental	100
4.5	Results and discussion	103
4.5.1	Initial results	103
4.5.2	Hydronium clusters	104
4.5.3	Argon/nitrogen mixture	106
4.5.4	Fragmentation comparison	109
4.6	Exhaust gas analysis	118
4.6.1	Experimental	119
4.6.2	Results and discussion	120
4.7	Conclusion	123
4.8	References	126
 Chapter five: Case study - Measuring urban air samples in London, UK, with enhanced sensitivity		 128
5.1	Introduction	128
5.2	Overview of the ClearfLo campaign 2012, London, UK.	132
5.2.1	Winter IOP	133
5.2.2	Summer IOP	145
5.2.3	Winter verses summer comparison	148
5.2.4	Chamber study	152

5.2.5	Experimental	153
5.2.6	Results	153
5.3	Conclusion	163
5.4	References	165
Chapter six: Conclusion		168
6.1	Enhanced sensitivity	168
6.2	Controlling collision energy	169
6.3	Urban air measurements	171
6.4	Ongoing challenges	172
6.5	Future work	172
6.6	Final remarks	173
6.7	References	174

List of tables

Chapter one: Introduction

Table 1-1. Main chemical constituents of dry air. **1**

Table 1-2. Typical VOCs and oVOCs found in the atmosphere. Typical concentrations are shown for particular campaigns/ data source locations. **2**

Table 1-3. VOCs identified by PTR-MS (adapted from (Blake et al., 2009)). **18**

Chapter two: Instrumental

Table 2-1. Comparison of energy measurement units (adapted from (Ellis and Mayhew, 2014)). **40**

Table 2-2. List of various atoms and molecules and their corresponding proton affinities with data collected from (Goebbert and Wentold, 2004, Lindinger et al., 1998, Fernandez et al., 1998). Shown in red are possible proton donors. **42**

Table 2-3. A comparison of the mass spectrometers used throughout this thesis. **53**

Table 2-4. Details of the instruments used in each study/ field campaign. **54**

Chapter three: Characterisation of a PTR-ToF-MS fitted with a radio frequency ion funnel

Table 3-1. Electrode dimensions and spacings used in the modified radio frequency ion funnel. **70**

Table 3-2. Effective E/N for different RF voltage settings. The DC component was kept at ~ 100 V. The peak to peak voltages were made by physically measuring the pins attached to plates 26, 27, 28 and 29 (P26, P27, P28 and P29 respectively) using an oscilloscope. **78**

Table 3-3. Comparison of sensitivities and LoD for several VOCs. **85**

Table 3-4. VOCs with RF/DC sensitivity ratios (incorporating data from Table 3 3). **87**

Chapter four: The use of rare gases to control collision energy

Table 4-1. Typical signal intensities for a 1 min integration time of primary ions and sensitivities for acetone (adapted from (Inomata et al., 2008)). **98**

Table 4-2. A list of excitation energies for water and four rare gases when in an excited state (adapted from (Inomata et al., 2008)). **99**

Table 4-3. The values of E/N and the percentage of argon and nitrogen present as the buffer gas in the series of experiments. **101**

Table 4-4. The percentage ions detected at m/z 137 (protonate parent molecule) and at m/z 81 (a fragment ion) for limonene for two different E/N conditions. **104**

Table 4-5. Summary of the conditions used (E/N and % Ar, expressed as high, medium, or low) for the five chosen VOCs. **109**

Table 4-6. The three sets of 'comparable' conditions that yield equivalent E/N, equivalent collision energy, and equivalent hydronium ratio for pure argon and nitrogen buffer gases. **110**

Table 4-7. Presented here are the mass channels displayed as a % of the total ion count for hexane in three different comparable experiments carried out using both nitrogen and argon as a buffer gas. $\Delta\text{Ar-N}_2$ is the difference between the intensity of the mass channel in nitrogen subtracted from the argon measurement. **114**

Table 4-8. Summary of ion fragment distribution for limonene. **116**

Table 4-9. The two sets of 'comparable' conditions that yield equivalent E/N, equivalent collision energy, and equivalent hydronium ratio for pure argon and nitrogen buffer gases. **119**

Table 4-10. Number of peaks in a given height range (signal intensity) from the spectra of exhaust emissions for two different buffer gases at two pairs of comparative settings. **122**

Chapter five: Case study - Measuring urban air samples in London, UK, with enhanced sensitivity

Table 5-1. Ions detected using PTR-ToF-MS in the winter (blue), ions detected using RF-PTR-ToF-MS in the summer (red) or ions detected on both instruments (black). Reagent and associated ions are in italics. **149**

Table 5-2. Comparison of m/z 19 and total ion count on the PTR-ToF-MS and RF-PTR-ToF-MS. **151**

Table 5-3. Conditions within the chamber during the α -pinene oxidation experiment. **153**

Table 5-4. Mass channels observed on the PTR-ToF-MS during winter, and the RF-PTR-ToF-MS during summer. Shown also are the potential ions observed during a monoterpene oxidation experiment carried out as part of the ACIDPRUF campaign, 2012. ‘•’ means that the ion was observed. Adapted from (McCracken, 2013). **160**

List of figures

Chapter one: Introduction

Figure 1-1. Schematic of the oxidation of NO to NO₂ in the presence of ozone (Atkinson, 2000). **4**

Figure 1-2. Schematic of the oxidation of NO to NO₂ in the presence of VOCs (Atkinson, 2000). **5**

Figure 1-3. GC schematic. The sample is injected into the carrier gas at the injector point, before entering into the column, which provides separation before reaching the detector, a flame ionisation detector (FID) in this case (Ellis and Mayhew, 2014). **8**

Figure 1-4. IMS, with the ions flowing from left to right. (Ellis and Mayhew, 2014). **10**

Figure 1-5. IMS coupled to a ToF mass analyser, in this case a double reflectron (W ToF) (Kanu et al., 2008). **11**

Figure 1-6. Schematic of a FA instrument. The ions are generated upstream in the source and are then extracted into the flow tube, where neutral reagents can be added through any of the ports, before the ions are filtered by a quadrupole mass analyser and detected (Ellis and Mayhew, 2014). **12**

Figure 1-7. Schematic of SIFT-MS consisting of an ion source, quadrupole mass filter for ion selection, a carrier gas flow reactor tube and a detection quadrupole mass spectrometer (Smith and Španěl, 2005, Španěl and Smith, 2011). **12**

Figure 1-8. An early schematic showing four poles of a quadrupole mass analyser used in the separation of the ions (Helmut and Wolfgang, 1960). **15**

Figure 1-9. PTR-MS data (1 min time resolution) obtained by the University of Leicester during the ClearfLo Campaign, London, UK (2012). **19**

Figure 1-10. Change in various organosulfides with decay time of meat. (Blake et al., 2009). **22**

Figure 1-11. Correlation between the age calculated for cheese ripening using PTR-MS analysis and the actual age of the meat. (Blake et al., 2009, Aprea et al., 2007). **23**

Chapter two: Instrumental

Figure 2-1. A simple example of a hollow cathode discharge. The variable resistance provided by the ballast resistor limits the amount of current drawn and improves the stability of the discharge (Ellis and Mayhew, 2014). **37**

Figure 2-2. Americium ion source with an expanded view of the ionising reaction between an alpha particle (yellow) and a water molecule (red - oxygen, white - hydrogen). **38**

Figure 2-3. A schematic of a flight tube where the ions enter on the left, and are then reflected by the reflectron, and go on to strike the detector. (Blake, 2005). **48**

Figure 2-4. Schematic of the ion source and drift tube (reactor) on the Kore-ToF (Kore-Technology-Ltd, 2010). **50**

Figure 2-5. Schematic of the Leicester-ToF showing the drift tube, transfer chamber, mass analyser and detector. **52**

Figure 2-6. Humidity dependence of various compounds carried out on the Kore-ToF. **57**

Figure 2-7. Time series of signal intensity as measured at m/z 159 (bromobenzene) illustrating instrumental drift over a period of 3 h). **60**

Figure 2-8. Data demonstrating instrument stability for m/z 159 (bromobenzene). **60**

Chapter three: Characterisation of a PTR-ToF-MS fitted with a radio frequency ion funnel

Figure 3-1. Image of ion funnel electrodes with a large diameter tapering down to a smaller internal diameter. The 5 ceramic support rods can also be seen. **68**

Figure 3-2. Simulated ion trajectory (black lines) along a drift tube with cylindrical electrodes. The ions travel from left to right, interacting with the RF field near the electrode face (Lynn et al., 2000). **69**

Figure 3-3. Radio frequency ion funnel illustrating the electrode positioning. Taken from a Simion© simulation carried out by E. James, a student at the University of Leicester. **70**

Figure 3-4. Comparison between the LoD of isoprene under different temperature conditions in the drift tube. The blue line represents the cooler

room temperature (~24 °C) and the red line the hotter temperature (~100 °C).
74

Figure 3-5. Water cluster distribution obtained under DC-only mode as a function of E/N. 75

Figure 3-6. Water cluster ion distribution obtained in RF mode as a function of the RF peak voltage with a constant 100 V DC voltage applied to the drift tube.
76

Figure 3-7. Graph used to convert RF values to E/N values. The DC-only mode results are represented by clear diamonds and the RF mode results by solid diamonds) are fitted to the curves. The numbers refer the m/z of the water cluster ions. 77

Figure 3-8. Protonated acetaldehyde parent ion (m/z 45) and fragment (m/z 27) plotted as a function of effective E/N in RF mode operation. 79

Figure 3-9. Different views of the same background mass spectrum obtained in RF mode using a 20 s scan time on three different vertical axis scales. (a) Full scale survey scan; (b) vertically expanded view; (c) An even further vertically expanded view. 81

Figure 3-10. Selected mass channels with noise peaks as a function of RF amplitude for a 20 second scan time. 82

Figure 3-11. Selected normalised noise peaks for the same 20 seconds scan as shown in Figure 3-10 as a function of RF amplitude. 83

Figure 3-12. Multi-point calibration showing the normalised sensitivities for a seven-component VOC gas standard. The data was collected in the RF mode. The sensitivity is linear over dynamic range of at least three orders of magnitude. 84

Figure 3-13. Improvement of raw sensitivity of various compounds comparing RF mode analysis to DC-only mode analysis. The data here contains the information from Table 3 4. 87

Chapter four: The use of rare gases to control collision energy

Figure 4-1. Calculated kinetic energy with respect to the centre of mass vs E/N for three different buffer gases (Green = $\text{H}_3\text{O}^+/\text{He}$, Blue = $\text{H}_3\text{O}^+/\text{Ar}$, Red = $\text{H}_3\text{O}^+/\text{N}_2$.) The analyte has a nominal mass of 86 (hexane) and the reagent ion mass used was 19 (hydronium). Data obtained from (McFarland et al., 1973c, McFarland et al., 1973a, McFarland et al., 1973b). **94**

Figure 4-2. Drift time for differing drift tube length (blue = 10 cm, green = 7 cm, red = 5 cm) for hydronium molecules in an argon buffer gas. Data obtained from (McFarland et al., 1973c, McFarland et al., 1973a, McFarland et al., 1973b). **96**

Figure 4-3. Images of a discharge ion source used by Inomata and co-workers. (a) “ H_2O -only” discharge mode at E/N 100 Td, and (b)-(e) “ H_2O in the presence of a rare gas at E/N 40 Td. (b) He, (c) Ne, (d) Ar, and (e) Kr (taken from (Inomata et al., 2008)). **97**

Figure 4-4. Data plotted from Table 4-1. Blue = m/z 19, red = m/z 37, orange = m/z 59. The protonated acetone (m/z 59) count has been multiplied by 1000 and therefore the data is now in units of counts/ppmV. **98**

Figure 4-5. The structure of limonene. **103**

Figure 4-6. A calibration graph of limonene parent ion (m/z 137) signal with varying concentration of limonene. **104**

Figure 4-7. Hydronium and its hydrated clusters as a function of E/N when nitrogen is the buffer gas. $19 = \text{H}_3\text{O}^+$, $37 = \text{H}_3\text{O}^+.\text{H}_2\text{O}$, $55 = \text{H}_3\text{O}^+.\text{(H}_2\text{O)}_2$, $73 = \text{H}_3\text{O}^+.\text{(H}_2\text{O)}_3$, $91 = \text{H}_3\text{O}^+.\text{(H}_2\text{O)}_4$. **105**

Figure 4-8. Hydronium and its hydrated clusters as a function of E/N when argon is the buffer gas. $19 = \text{H}_3\text{O}^+$, $37 = \text{H}_3\text{O}^+.\text{H}_2\text{O}$, $55 = \text{H}_3\text{O}^+.\text{(H}_2\text{O)}_2$, $73 = \text{H}_3\text{O}^+.\text{(H}_2\text{O)}_3$, $91 = \text{H}_3\text{O}^+.\text{(H}_2\text{O)}_4$. **106**

Figure 4-9. 3D plots of the protonated parent ion for 5 different VOCs. The x-axis is E/N in Td and the y axis is the % of argon as the buffer gas in a nitrogen balance. The protonated ions masses are given for isoprene (m/z 69), benzene (m/z 79), toluene (m/z 93), ethylbenzene (m/z 107) and 2-chloroethyl sulfide (m/z 125 and 127). The contour units are counts min⁻¹. **108**

Figure 4-10. Hexane signal intensity verses E/N for argon (green) and nitrogen (blue) as the buffer gas. **111**

Figure 4-11. Simplified mass spectrum presented as relative abundance for the most prominent peak in the spectrum for hexane at equivalent E/N (68 Td). The top spectrum (blue) is for the nitrogen buffer gas, and the bottom spectrum (green) is for argon as a buffer gas. **112**

Figure 4-12. Simplified mass spectrum presented as relative abundance for the most prominent peak in the spectrum for hexane at equivalent kinetic energies (0.1 eV - nitrogen at 79 Td and argon at 52 Td. The top spectrum (blue) is for nitrogen and the bottom spectrum (green) is for argon as a buffer gas. **113**

Figure 4-13. Simplified mass spectrum presented as relative abundance for the most prominent peak in the spectrum for hexane at equivalent hydronium ratios (nitrogen at 100 Td and argon at 63 Td. The top spectrum (blue) is for the nitrogen buffer gas, and the bottom spectrum (green) is for argon as a buffer gas. **113**

Figure 4-14. Number of counts per second as a function of E/N for m/z 81 and m/z 137 for the buffer gas nitrogen (blue) and argon (green). **115**

Figure 4-15. Percentage of limonene parent ion as a total of the parent ion and fragment. **116**

Figure 4-16. The number of peaks in the mass spectrum that are a certain height (number of counts / min-1) for the same calculated kinetic energy (0.1 eV). Blue = nitrogen buffer gas, green = argon buffer gas. **120**

Figure 4-17. The number of peaks in the mass spectrum that are a certain height (number of counts min-1) for the same H₃O:H₃O⁺.H₂O) ratio (65 % H₃O⁺). Blue = nitrogen buffer gas, green = argon buffer. **121**

Chapter five: Case study - Measuring urban air samples in London, UK, with enhanced sensitivity

Figure 5-1. Map identifying the position of the North Kensington site (black rectangle), London, UK (Bannan et al., 2014). **132**

Figure 5-2. Mobile laboratory position during summer IOP set up within the playground of Sion Manning School, North Kensington, UK, with the blue shipping container belonging to the University of Leicester. **133**

Figure 5-3. 1 min time resolution series for acetaldehyde (m/z 45) over a 6 day period from 02/02/12 – 07/02/12 collected from North Kensington, London, UK. The zero point at ~06/02 12:00 is a set of background scans to verify the zero point. **135**

Figure 5-4. 1 min time resolution series for acetone (m/z 59) over a 6 day period from 02/02/12 – 07/02/12 collected from North Kensington, London, UK. The zero point at ~06/02 12:00 is a set of background scans to verify the zero point. **136**

Figure 5-5. 1 min time resolution series for butene (m/z 57) over a 6 day period from 02/02/12 – 07/02/12 collected from North Kensington, London, UK. The zero point at ~06/02 12:00 is a set of background scans to verify the zero point. **136**

Figure 5-6. 1 min time resolution series for xylene (m/z 107) over a 6 day period from 02/02/12 – 07/02/12 collected from North Kensington, London, UK. The zero point at ~06/02 12:00 is a set of background scans to verify the zero point. **137**

Figure 5-7. 1 min time resolution series for toluene (m/z 93) over a 6 day period from 02/02/12 – 07/02/12 collected from North Kensington, London, UK. The zero point at ~06/02 12:00 is a set of background scans to verify the zero point. **138**

Figure 5 8. 1 min time resolution series for benzene (m/z 79) over a 6 day period from 02/02/12 – 07/02/12 collected from North Kensington, London, UK. The zero point at ~06/02 12:00 is a set of background scans to verify the zero point. **138**

Figure 5-9. 1 h 2D-GC-MS acetone data (red) plotted on the same axis as 1 min PTR-ToF-MS acetone data (grey). The zero point at ~06/02 12:00 is a set of background scans to verify the zero point. **140**

Figure 5-10. Comparison of acetone concentration obtained during the winter IOP between data acquired by 2D-GC-MS and data obtained by PTR-ToF-MS data. **140**

Figure 5-11. 1 h 2D-GC-MS butene data (red) plotted on the same axis as 1 min PTR-ToF-MS butene data (grey). The zero point at ~06/02 12:00 is a set of background scans to verify the zero point. **141**

Figure 5-12. Comparison of butene concentration obtained during the winter IOP between data acquired by 2D-GC-MS and data obtained by PTR-ToF-MS data. **141**

Figure 5-13. 1 h 2D-GC-MS benzene data (red) plotted on the same axis as 1 min PTR-ToF-MS benzene data (grey). The zero point at ~06/02 12:00 is a set of background scans to verify the zero point. **142**

Figure 5-14. Comparison of benzene concentration obtained during the winter IOP between data acquired by 2D-GC-MS and data obtained by PTR-ToF-MS data. **142**

Figure 5-15. 1 h 2D-GC-MS toluene data (red) plotted on the same axis as 1 min PTR-ToF-MS toluene data (grey). The zero point at ~06/02 12:00 is a set of background scans to verify the zero point. **142**

Figure 5-16. Comparison of toluene concentration obtained during the winter IOP between data acquired by 2D-GC-MS and data obtained by PTR-ToF-MS data. **143**

Figure 5-17. 1 h 2D-GC-MS xylene data (red) plotted on the same axis as 1 min PTR-ToF-MS xylene data (grey). The zero point at ~06/02 12:00 is a set of background scans to verify the zero point. **143**

Figure 5-18. Comparison of xylene concentration obtained during the winter IOP between data acquired by 2D-GC-MS and data obtained by PTR-ToF-MS data. **143**

Figure 5-19. Ion funnel equipped PTR-ToF-MS taking measurements from within the mobile laboratory. **145**

Figure 5-20. An example of a 1 min mass spectrum taken on 07/08 illustrating a number of peaks including several high mass ions ($> m/z$ 150). **146**

Figure 5-21. Data obtained during the summer ClearfLo campaign. The blue points represent the ambient temperature within the container-lab (taken with a temperature probe) and the red points represent the signal intensity of m/z 21

($\text{H}_3^{18}\text{O}^+$) and were obtained on the RF funnel equipped PTR-MS instrument.

147

Figure 5-22. A comparison of a typical urban air spectra taken on the PTR-ToF-MS during winter (blue) and on the RF-PTR-ToF-MS during summer (red) illustrating the increased number of peaks present in the RF-PTR-ToF-MS obtained spectrum. **148**

Figure 5-23. Example time series comparing signal intensity from RF-PTR-ToF-MS (red) and from PTR-MS (blue) for a) m/z 57 (butene), b) m/z 59 (acetone), c) m/z 93 (toluene) and d) m/z 107 (xylene). The data to the left (0 - 40 min) are background subtracted, whilst the data from 40 – 180 min is urban air. **150**

Figure 5-24. Gas phase measurements of VOCs during the α -pinene photo-oxidation experiment (White et al., 2012). a) 3-dimensional graph of VOC evolution where the colours represent the counts s^{-1} , b) spectrum taken at 50 min, c) spectrum taken at 190 min. **154**

Figure 5-25. Time series for various measurements and ions monitored during α -pinene photo-oxidation experiment. For panels a) - h) x-axis = time after lights on/ min. For panels c) y-axis = normalised signal intensity (counts). Panel a) Temperature (red), relative humidity (blue). Panel b) Ozone (green) NO_x (red), NO_2 (purple), NO (orange). Panel c) Precursor parent ion m/z 137 (blue), fragment ion m/z 81 (red). Panel d) Pinonaldehyde (m/z 169) and its fragment ions, m/z 151, m/z 123, m/z 107, m/z 108, m/z 109. Panel e) Ion m/z 153 α -pinene oxide. Panel f) Ion m/z 155 norpinonaldehyde. Panel g) Ion m/z 157 norpinic acid. Panel h) Ion m/z 185 pinonic acid. **156**

Figure 5-26. Main paths of the α -pinene oxidation by OH, taken from (Capouet et al., 2004). **158**

Figure 5-27. Main paths of the α -pinene oxidation by O_3 (in presence of NO) taken from (Capouet et al., 2008). **159**

List of abbreviations

2D-GC-MS	2-dimensional - gas chromatography - mass spectrometry
bVOC	biogenic volatile organic compound
CI-MS	Chemical ionisation - mass spectrometry
EI	Electron ionisation
FA	Flowing afterglow
FID	Flame ionisation detector
GC	Gas chromatography
GC-MS	Gas chromatography - mass spectrometry
GD	Glow discharge
IM-MS	Ion mobility - mass spectrometry
IMS	Ion mobility spectrometry
KE	Kinetic energy
LE-ToF	'Leicester ToF'
LoD	Limit of detection
MFC	Mass flow controller
MCP	Multichannel plate
NCAS	National centre for atmospheric science, UK
NERC	National environment research council, UK
NEIS	National institute for environmental studies, Japan
oVOC	oxygenated volatile organic compound
ppbV	parts per billion by volume
ppmV	parts per million by volume
pptV	parts per trillion by volume
PERCA	Peroxy radical amplification instrument
PSS	Photostationary state
PEEK	Polyether ether ketone
PAH	Polynuclear aromatic hydrocarbons
PA	Proton affinity
PTR-MS	Proton transfer reaction - mass spectrometry
PTR-ToF-MS	Proton transfer reaction - time of flight - mass spectrometry
RF	Radio frequency
RSD	Relative standard deviation

SOA	Secondary organic aerosol
SIFDT-MS	Selected ion flow drift tube - mass spectrometry
SIFT-MS	Selected ion flow tube - mass spectrometry
SIM	Selected ion monitoring
S/N	Signal to noise ratio
SD	Source drift
ToF-MS	Time of flight - mass spectrometry
ToF	Time of flight
TDC	Time to digital converter
VOC	Volatile organic compound
VMR	Volume mixing ratio
W ToF	Double reflectron ToF mass analyser

1 Chapter one: Introduction

1.1 Volatile organic compounds in the atmosphere

The atmosphere is comprised primarily of nitrogen, oxygen, argon, and carbon dioxide (as well as a varying amount of water vapour) along with other species listed in Table 1-1 (adapted from (Warneke and Williams, 2012)). Many other components, such as volatile organic compounds (VOCs) are also present in the atmosphere and, while only constituting a small fraction of the total air mass, they play a critical role in the chemistry of the Earth's atmosphere. The most common VOC is methane, but even this only makes up 1.8 parts per million by volume (ppmV) (Bamberger et al., 2014) of the gas in the troposphere. Some other VOCs may be present in parts per billion by volume (ppbV) concentrations but many more are present at even lower levels, in the parts per trillion by volume (pptV) range and less. Attempting to detect such low concentrations of VOCs, using little sample preparation or separation, poses a significant challenge, as there is potential interference from the main components of the atmosphere, which are present at levels many orders of magnitude higher than these trace VOCs.

Table 1-1. Main chemical constituents of dry air.^a

Constituent	Molar mass / g mol ⁻¹	Volume fraction / %	
		a)	b)
Nitrogen, N ₂	28.0134	78.084±0.004	78.093
Oxygen, O ₂	31.9988	20.946±0.002	20.933
Argon, Ar	39.948	0.934±0.001	0.934
Neon, Ne	20.1797	(1.818±0.004)×10 ⁻³	1.818×10 ⁻³
Helium, He	4.002602	(5.24±0.05)×10 ⁻⁴	5.24×10 ⁻⁴
Krypton, Kr	83.798	(1.14±0.01)×10 ⁻⁴	1.14×10 ⁻⁴
Xenon, Xe	131.293	(8.7±0.1)10 ⁻⁶	8.7×10 ⁻⁶
Carbon dioxide, CO ₂	44.0095	0.0332 ^b	0.0400 ^{bc}

^a Data source: a) (Glueckauf, 1951); the CO₂ content was extrapolated from the data reviewed by (Callendar, 1940) and did not correspond to the true value at that time. b) recalculated for a CO₂ content of 400 ppmV and oxygen consumption due to the combustion of fossil fuels, assuming 48 % of CO₂ to have remained in the atmosphere.

^b In addition to a global rise, CO₂ undergoes diurnal variations locally and annual variations globally due to assimilation and respiration by plants and the release from decaying biomass.

^c 2013 Atmospheric CO₂ levels (Showstack, 2013).

Chapter one: Introduction

VOCs can be classified into two broad categories: biogenic VOCs (bVOCs) and anthropogenic VOCs. Biogenic sources are derived from natural sources, such as monoterpene emissions from trees. Anthropogenic emissions are man-made and come from sources such as the combustion engine.

A selection of VOCs and oxygenated VOCs (oVOCs), their sources and example atmospheric concentrations are presented in Table 1-2. It should be cautioned however that atmospheric concentration of these species can, and does, vary greatly depending up on where the measurement is taken, i.e. if the measurement is taken near a source of the emission or in a remote location.

Table 1-2. Typical VOCs and oVOCs found in the atmosphere. Typical concentrations are shown for particular campaigns/ data source locations.

Compound	Sources	Typical atmospheric concentration	Campaign / data source location	Reference
Methane	Farming, wetlands, energy	1.8 ppbV	Measured in Switzerland, 2013.	(Bamberger et al., 2014)
Methanol	Vegetation	~ 800 pptV (remote location)	SONEX 1997 – North Atlantic	(Singh et al., 2000)
Acetaldehyde	Common photo-oxidation product of many organic compounds in the atmosphere	~ 1 ppbV	Denver, CO, US, 1991-96	(Anderson et al., 1996)
Acetone	Biomass burning and vegetation	Up to 10 ppbV	Various measurements	(Schade and Goldstein, 2006)
Methacrolein	Product of reaction between isoprene and OH	0.2 – 5.7 ppbV	Measure in Austin, Texas, US, 1998	(Wiedinmyer et al., 2001)
Formaldehyde	Combustion of fuels	0.4 – 3.4 ppbV	Measure in Austin, Texas, US, 1998	(Wiedinmyer et al., 2001)
Monoterpene	Biogenic	50 – 200 pptV	Nova Scotia, Canada, 2004	(de Gouw and Warneke, 2007)
Isoprene	Biogenic – forest trees and other vegetation	0.3 – 6.0 ppbV	Measure in Austin, Texas, US, 1998	(Wiedinmyer et al., 2001)
Toluene	Automobile combustion and industrial processes	~1 ppbV (urban) ~120 pptV (rural)	UK National Air Quality archive data	(von Schneidmesser et al., 2010)
Benzene	Automobile combustion and industrial processes	~320 pptV (urban) ~88 pptV (rural)	UK National Air Quality archive data	(von Schneidmesser et al., 2010)

Methane is the most abundant VOC in the Earth's atmosphere. Of the non-methane hydrocarbons, the most abundant are isoprene and monoterpenes, both of which are bVOCs (Laothawornkitkul et al., 2009). These compounds are

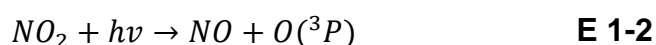
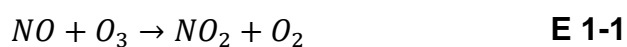
Chapter one: Introduction

emitted from trees and other plant life, and are released in copious amounts each year. The release of these bVOCs is linked to the photosynthetic cycle of plants, and also whether or not they are stressed by external conditions such as increased ozone levels, insect damage and water stress.

Although the emission of VOCs from plants is of great interest to biologists, this information also has far reaching consequences in other fields of research, such as atmospheric chemistry. bVOCs are the dominant source of all VOCs in the atmosphere and interact with the hydroxyl radical (HO_x), nitrogen oxide(s) (NO_x) and also ozone (O_3) cycles, so it is crucial that they are well understood (PORG, 1997, Kroll and Seinfeld, 2008, Hamilton et al., 2011, Healy et al., 2008).

The emission of additional (anthropogenic) VOCs can lead to an imbalance of atmospheric processes. These VOCs can come from fossil fuel combustion, biomass burning or industrial processes. An area where anthropogenic VOC emissions are prevalent is in the urban environment. One of the reasons it is important to understand VOCs in an urban context is the role that they play in the formation of ground level (tropospheric) ozone. With built-up areas comes high traffic levels, and with combustion engines being a source not only of VOCs but also NO_x , ozone can be created and have negative health impacts on the local community.

Under tropospheric conditions oxidation of NO to NO_2 in the presence of ozone can occur (E 1-1). The photolysis of NO_2 (E 1-2) then leads to the formation of ozone (E 1-3) (Mannschreck et al., 2004). The overall effect of these three equations (E 1-1, E 1-2, E 1-3) results in the setup of the NO_x photostationary state (PSS) and is shown in Figure 1-1 (Harrison, 2007). It should be noted that in the NO_x PSS there is no net production of ozone as one molecule is consumed and one molecule is produced.



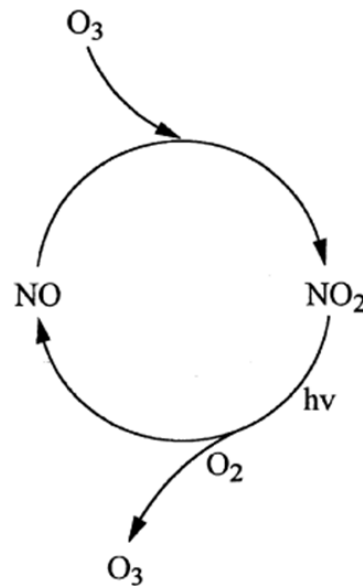
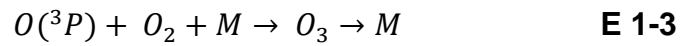
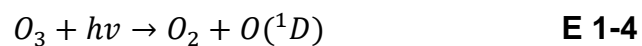
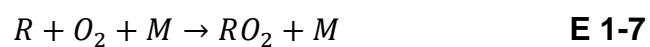


Figure 1-1. Schematic of the oxidation of NO to NO₂ in the presence of ozone (Atkinson, 2000).

There is however the possibility of oxidising NO to NO₂ that results in the production of ozone at ground level. Within the troposphere ozone can be photolysed to produce OH (E 1-4 and E 1-5).

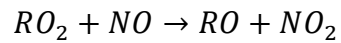


Here one ozone molecule is able to generate two OH molecules. In tropospheric environments where VOCs are present OH can react with VOCs (RH) and generate RO₂ radicals,



where M is a third body.

The radical, RO_2 , can then oxidise NO to NO_2 ,



E 1-8

NO_2 can now react to produce ozone (E1-3 and 1-4) but crucially there is now the net production of ozone, thus disrupting the PSS of NO_x and tuning it from ozone neutral (Figure 1-1) to ozone production (Figure 1-2).

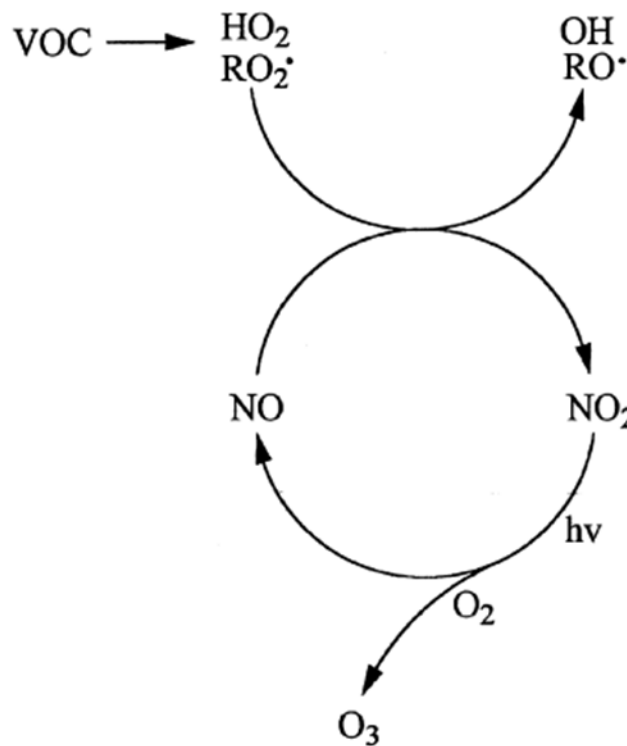


Figure 1-2. Schematic of the oxidation of NO to NO_2 in the presence of VOCs (Atkinson, 2000).

1.2 Volatile organic compounds in other areas

VOCs are also prevalent in many other areas of interest, so it is not unsurprising that the instrumentation that has proven so successful in monitoring VOCs in atmospheric studies has lent its self so well to other areas of research. While it has been discussed that plants give out VOCs, all living things including animals also emit VOCs. Humans are no exception to this, with many VOCs inside the body making their way into the blood stream, into the lungs and then expelled out of the lungs whilst breathing. These VOCs are linked to the body's metabolic processes, so it is quite possible that if someone has a particular illness, the altered processes in the body can be detected via a change in exhaled VOCs (Phillips et al., 1999).

Another application is that of the food and flavour sciences. VOCs play a crucial role in determining our perception of food and our ideas of taste (Blake et al., 2009). The food and drink industry is big business, with companies vying for consumer interest. It is little wonder then that alongside human taste-testing trials, the VOCs from the food or beverage can be analysed to help build up a picture of what exactly makes food desirable.

1.3 Volatile organic compound detection

It has previously been mentioned that VOCs are present in many systems including the atmosphere at very low levels, sometimes sub-pptV. Currently there is no single technique that is perfect for measuring VOCs in all these systems and there likely never will be. Compromises have to be made between system performance for a particular application (such as sensitivity, temporal resolution etc.) and the practicalities of the instrument (such as cost, size and transportability).

The main methods for detecting trace VOCs are gas chromatography - mass spectrometry (GC-MS), ion mobility spectrometry (IMS), selected ion flow tube - mass spectrometry (SIFT-MS) and proton transfer reaction - mass spectrometry (PTR-MS). This section will discuss these methods of VOC detection, finishing with some historical background on the development of PTR-MS. Finally it will move onto an in depth look into the various applications that PTR-MS is particularly suited for.

1.3.1 Gas chromatography

Gas Chromatography (GC) is usually regarded as the 'gold standard' of analytical techniques and is the most widely used technique for trace gas analysis. GC works by passing a gas mixture (the mobile phase) over either a solid or viscous liquid (the stationary phase), where different constituents of the mobile phase interact differently with the stationary phase, resulting in temporal partitioning of the mixture (James and Martin, 1952).

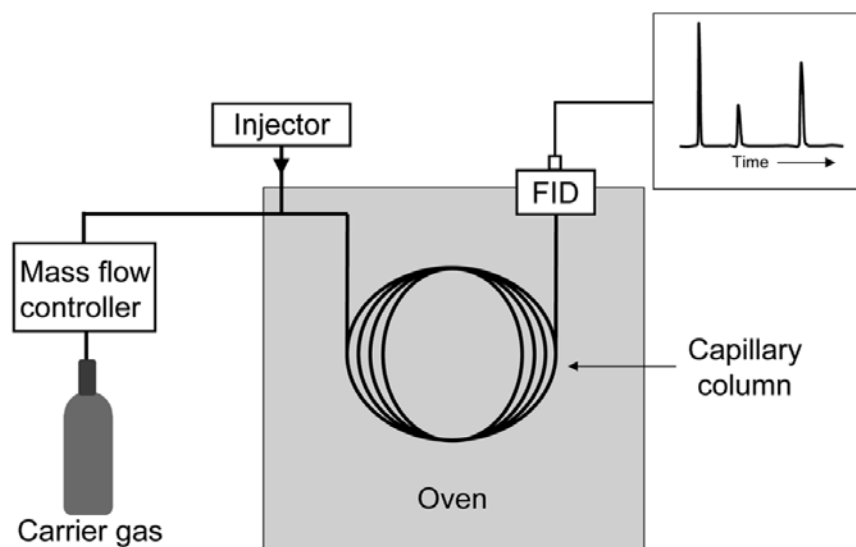


Figure 1-3. GC schematic. The sample is injected into the carrier gas at the injector point, before entering into the column, which provides separation before reaching the detector, a flame ionisation detector (FID) in this case (Ellis and Mayhew, 2014).

The separation takes place in a long coiled column in a temperature controlled oven, as shown in Figure 1-3. The partition coefficient determines how well the different types of analyte molecules in the mobile phase separate when passing through the stationary phase and this dictates the retention time obtained in the spectrum.

Modern columns are typically very long and thin, and the stationary phase is often a viscous liquid 1 μm thick that coats the inside of the columns' walls. Lengths of columns can be up to, and even exceed, 50-60 m. By varying the temperature of the oven, the gas carrying the sample flow and makeup of the column, different components can be separated with different success rates and the system can be tuned for the application at hand.

Once the components have been separated they are then fed into a detector and their retention times are recorded. There are many different types of detector that can be used based on the application at hand. For instance a flame ionisation detector (FID) is often used for detecting organic molecules. As the carbon-containing compounds enter the flame they form cations and electrons and this current is measured. The retention time can then often be used to determine the specific compounds present. However, many compounds

have overlapping retention times and this technique is not ideal for complete speciation. Consequently a mass spectrometer, such as a compact electron ionisation quadrupole, can be added to the end of the column. The analyte, after passing and separating in the column, enters the quadrupole and further analysis can be carried out. In this instance, it serves as a useful tool for compound identification as the elution time can be combined with an ion fragmentation pattern for better compound identification. By combining the retention time with molecular weight and fragmentation patterns, it is now much easier to identify and assign the correct chemical species.

Whilst sensitivities for GC-MS can be as low as 0.1 pptV for VOCs it does have several drawbacks. These include sample preparation and its temporal resolution. First of all the sample needs to be prepared in some manner, be it the extraction of a compound for analysis a sample mixture or the collection of a gaseous sample on a thermal adsorption tube. When using a thermal adsorption tube, the air sample, containing VOCs and semi-volatile organic compounds (sVOC), is passed through the tube, at which point the target analytes are adsorbed onto the tube and can then later be thermally desorbed for analysis by GC-MS. The sample has to be injected in small quantities and therefore, if the VOCs of interest are only present in the pptV range, they are unlikely to be detected. To circumvent this, a pre-concentration step will be required. Also as this is an offline technique that requires analysis time after each injection, continuous monitoring is not possible.

1.3.2 Ion mobility spectrometry

IMS has also been used for the rapid detection of a wide range of VOCs over the past couple of decades and has found use in the security and military areas due to its compact, rugged and robust instrumentation. There are currently over 5000 IMS instruments in use for the detection of explosives, drugs and chemical warfare agents (Kanu et al., 2008).

In IMS, the analyte is introduced and then ionised by any of the typical ion sources found in mass spectrometry using any number of potential reagent ions such as H_3O^+ . A schematic experimental arrangement is shown in

Chapter one: Introduction

Figure 1-4, where a radioactive source is utilised. The ions are then pulsed into a tube via a fast switching Bradbury Nielson gate (Zhu et al., 2009, Clowers et al., 2005), where electrodes then provide an electric field that drives the ions (positive ions in this case) towards the detector. In Figure 1-4 the detector is a simple Faraday plate. This tube is known as a drift tube in which there is a flow of neutral gas, often helium, which can be in either direction with respect to the direction of travel of the ions.

The ions are separated by their mobility rates, based on their size and shape (collision cross section) in the chosen neutral gas and it can be carried out at either ambient or reduced pressure. Generally speaking, the ions will be separated based on their mass, the lighter ions finding it easier to travel through the counter flowing neutral gas. However, as mentioned above, other effects such as the ion size (cross section) are also important, so IMS does not act simply as a quasi-mass spectrometer.

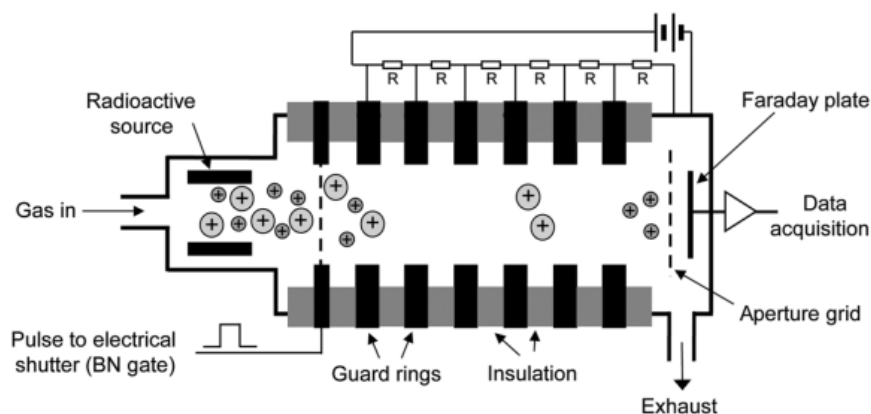


Figure 1-4. IMS, with the ions flowing from left to right. (Ellis and Mayhew, 2014).

One disadvantage of IMS, which is shared with GC, is that some compounds may not be separated from other compounds in the analyte because they have the same drift times in the drift tube. In this case, an extra means of identification can be achieved by coupling an IMS with a mass analyser (Kanu et al., 2008), such as a quadrupole or time of flight (ToF) (as shown in Figure 1-5). This combination is known as ion mobility - mass spectrometry (IM-MS).

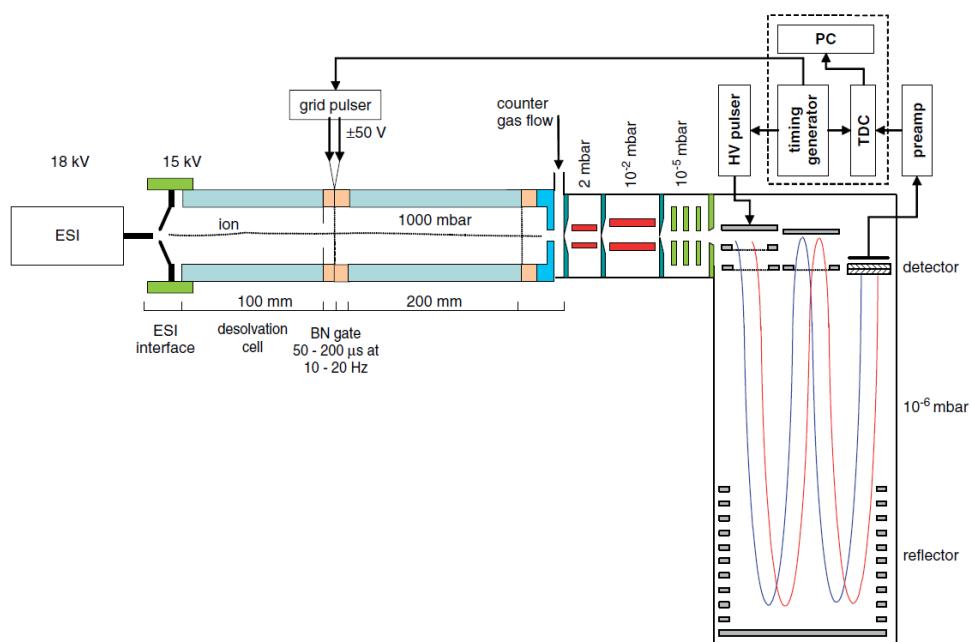


Figure 1-5. IMS coupled to a ToF mass analyser, in this case a double reflectron (W ToF) (Kanu et al., 2008).

1.3.3 Flowing afterglow technique

The Flowing Afterglow (FA) technique (Figure 1-6) was the first ion swarm technique to be employed to analyse VOCs (Newman and Mason, 2006). This technique was pivotal in pioneering the developments that would later lead to PTR-MS and for that reason it has been included here. The FA technique was first developed by Ferguson and co-workers (Fehsenfeld et al., 1966, Ferguson et al., 1969) in the 1960s and was used to study fast properties of reactions between charged molecules and neutral molecules under thermal conditions.

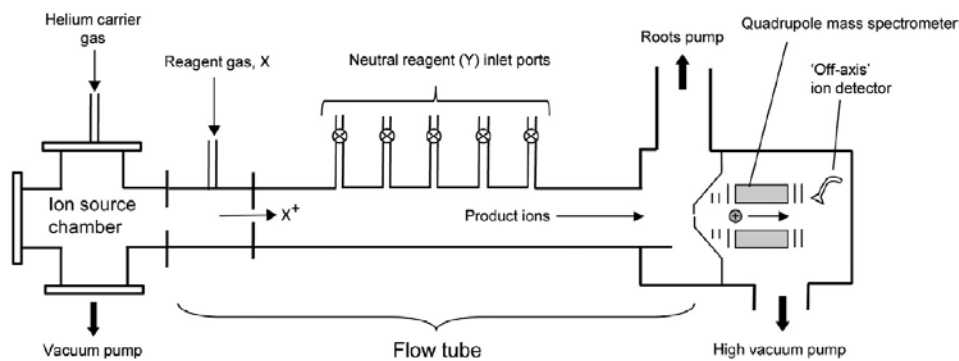


Figure 1-6. Schematic of a FA instrument. The ions are generated upstream in the source and are then extracted into the flow tube, where neutral reagents can be added through any of the ports, before the ions are filtered by a quadrupole mass analyser and detected (Ellis and Mayhew, 2014).

Whilst successful in this aim, one drawback of the FA technique is that unwanted and extensive fragmentation of the reagent gas occurred if a polyatomic molecule was used, owing to the high energies present, and it was this that facilitated the development of the techniques that will be described next.

1.3.4 Selected ion flow tube - mass spectrometry

SIFT-MS is a quantitative mass spectrometry technique for identifying VOCs and is an extension of the selected ion flow tube first developed by Adams and Smith in 1976 (Adams and Smith, 1976). All SIFT-MS instruments follow the same essential format as the one shown in Figure 1-7.

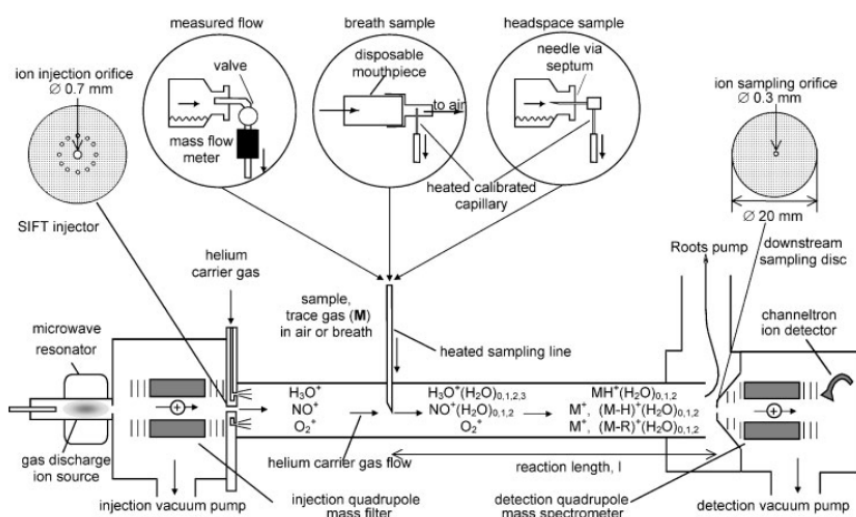


Figure 1-7. Schematic of SIFT-MS consisting of an ion source, quadrupole mass filter for ion selection, a carrier gas flow reactor tube and a detection quadrupole mass spectrometer (Smith and Španěl, 2005, Španěl and Smith, 2011).

SIFT-MS is similar to the FA technique. However, one of the crucial differences is the positioning of a quadrupole mass filter after the ion source, which is used to select only a specific reagent ion, such as H_3O^+ , into the flow tube. This does away with the problem of fragmentation arising from the reagent gas ionisation process and allows for a much cleaner spectrum. A negative impact of the mass filtering is a much lower transmission of reagent ions, which impacts on sensitivity. Despite this, very useful kinetic data is still obtained from this technique (Smith and Španěl, 2005, Španěl and Smith, 2011, Smith et al., 2014). SIFT-MS requires substantial pumping owing to the volume of gas that is being passed through the system; this makes the whole system rather large and adds costs for each additional pump required and limits transportability.

1.3.5 Selected ion flow drift tube - mass spectrometry

Selected Ion Flow Drift Tube - Mass Spectrometry (SIFDT-MS) was the final stepping stone from the FA technique, through SIFT-MS and finally onto the inception of what we know today as PTR-MS. SIFDT-MS was developed in 1994 by Lindinger and co-workers (Lagg et al., 1994). It uses a proton transfer reagent, such as H_3O^+ as its ionisation source, although other reagent ions can also be chosen. It has a very similar experimental arrangement to SIFT-MS. However, a direct current (DC) electric field along the flow tube is provided by various ring electrodes mounted along the tube, much like in IMS. As well as being used to drive the ions through the flow drift tube where the reactions take place, the extra voltage adds energy into the system by increasing the ion velocity, allowing higher energy ion-molecule reactions to be studied. Due to the ions being driven along by an electric field as well as the neutral gas flow, it acts simultaneously as both a drift tube and flow tube. This has the disadvantage of requiring a large pumping system, due to the high gas flow, as is the case with conventional SIFT-MS.

1.3.6 Proton transfer reaction - mass spectrometry

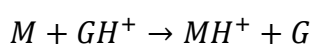
Introduced in the mid-1990s (Lagg et al., 1994, Hansel et al., 1995), PTR-MS has become an increasingly important technique for the detection and monitoring of VOCs (Blake et al., 2009, Ellis and Mayhew, 2014). The PTR-MS technique employs a drift tube with cylindrical electrodes that provide a DC electric field gradient along the drift tube. Whilst it does have a neutral gas flow,

often air, it is used for the introduction of the sample and not for the determination of ion mobility, as is the case in IMS which has been previously mentioned. The ion mobility of the analyte cannot be measured in PTR-MS as the sample is not pulsed into the drift tube; instead ion mobility does determine the reaction time of the ion-molecule reactions. Therefore the drift tube in PTR-MS can essentially be thought of as a reaction chamber, which provides an environment for the reaction between ions and molecules before the ions enter a mass analyser.

By not having a large gas flow as in the previously discussed techniques, a smaller pumping system is sufficient, thus reducing size, weight, and cost of the instrument. This now opens up a wealth of areas for *in situ* study as it can be more easily transported from the laboratory setting.

PTR-MS has very good time resolution: routinely 1 s data is measured and even sub 1 s time resolution can be achieved. However there is a trade-off between time resolution and sensitivity. PTR-MS has sufficient sensitivity to be able to measure down to the ppbV, pptV, and even sub pptV for select compounds and longer analysis times. It is also a soft ionisation technique, resulting in greatly reduced fragmentation compared to electron ionisation (EI) and this advantage will be discussed further in chapter two.

If hydronium (H_3O^+) is being used as the reagent ion, any molecule with a proton affinity (PA) higher than that of H_2O can accept a proton from H_3O^+ and become a charged species, which includes many VOCs, such as ketones, aldehydes, $> \text{C}_5$ alkanes etc., as well as sulfur and nitrogen containing compounds. Reaction E 1-9 illustrates that a proton from molecule G , (usually H_3O^+) is transferred to the analyte molecule, M resulting in a protonated species for detection.



E 1-9

If hydronium is utilised, then when measuring atmospheric samples in an air matrix, it is invisible to the main constituents of air but can measure most of the

VOCs present (this will be discussed further in chapter two) allowing for no pre-sampling techniques to be employed.

1.3.6.1 Quadrupole mass analyser

The quadrupole mass analyser was patented in 1960 and consists of four cylindrical parallel rods as illustrated in Figure 1-8 (Helmut and Wolfgang, 1960).

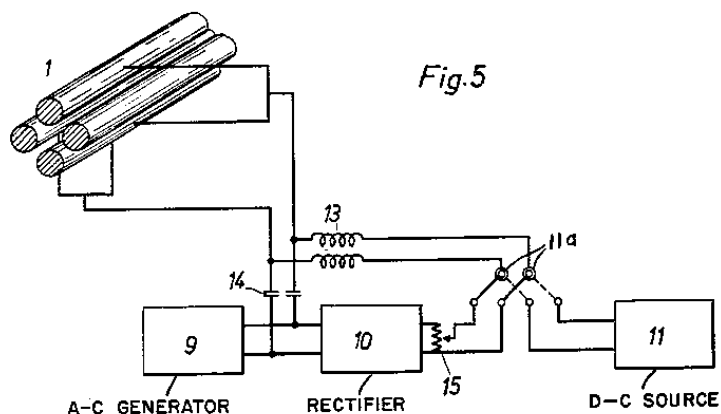


Figure 1-8. An early schematic showing four poles of a quadrupole mass analyser used in the separation of the ions (Helmut and Wolfgang, 1960).

When a sample of ions enters into one end of the quadrupole, an oscillating electric field is applied to filter out ions based on their m/z . The rods are in two pairs, each electrically connected to the opposite rod, and a radio frequency (RF) is applied and a direct voltage is superimposed onto the RF voltage. Ions then traverse the length of the rods. As the sample ions have different mass to charge ratios (m/z), all but a certain m/z will be unstable in the RF field and come into contact with the rods, annihilating its charge which renders it undetectable by the MS method. Only the ion with the m/z ratio that is stable in the field will end up reaching the detector. An advantage of this system is that if there are only a certain number of ions of interest in the sample, the quadrupole mass analyser can be set up to scan for just those particular m/z ratios. Another advantage of this type of analyser is that it is relatively compact and cost efficient in modern instruments thus making it suitable for many applications. However, the obvious downfall of this analyser is that if you wish to scan a whole range of masses, it can only convey them one at a time to the detector, thus reducing sensitivity. Quadrupole mass analysers can be used in two

modes: it can either be set to scan the whole mass range sequentially, or to focus on only pre-selected ions known as select ion monitoring (SIM) mode. If scanning the whole mass range, it measures the first mass, before sequentially scanning through all the other masses one at a time, resulting in large scan times and therefore reduced sensitivity.

Initially, PTR-MS instruments utilised quadrupole mass analysers, and whilst these are still widely used, advantages can be gained from switching to a ToF mass analyser. By switching from a quadrupole mass analyser to a ToF mass analyser, simultaneous detection over the whole mass range can be achieved. This allows for retroactive study of all the mass channels, with a higher time resolution when compared to a quadrupole mass analyser, if the whole mass spectrum needs to be analysed (as opposed to just a few select masses). The ToF principle will be discussed in much more detail in chapter two because it is the mass analyser used for this thesis.

1.4 Applications of proton transfer reaction - mass spectrometry

With the sensitivity and selectivity of PTR-MS (and PTR-ToF-MS), it is no wonder that it lends itself to a wide array of applications that involve analysis of trace gases (in fact this was why the technique was developed (Blake et al., 2009)). A few major applications along with specific examples are discussed below, although it should be noted that there are many other uses of PTR-MS that are beyond the scope of this introductory account.

1.4.1 Atmospheric chemistry

One of the most successful applications of PTR-MS has been in atmospheric and environmental chemistry. The potential to measure a wide range of VOCs in the presence of an air matrix makes this a good technique for such tasks. Whilst PTR-MS can measure many VOCs it is unable to measure VOCs and oVOCs with a proton affinity lower than that of the molecule carrying out the proton transfer, such as $< C_5$ alkanes with water. Also molecules with a low vapour pressure will not be present in the gaseous phase with enough concentration to be detected.

VOCs can be emitted by biogenic and anthropogenic sources and have a large impact on the chemistry of the atmosphere. To date, many compounds associated with atmospheric chemistry have been routinely identified by PTR-MS and these are listed in Table 1-3.

Atmospheric composition can be studied by PTR-MS to detect a wide variety of VOCs, including subsets of VOCs such as oxygenated VOCs (oVOCs) and nitrogen-containing VOCs. This, coupled with other techniques used to measure species such as NO_x , NO_y , ozone and aerosols, can help to give a detailed picture of the overall chemistry at work.

Chapter one: Introduction

Table 1-3. VOCs identified by PTR-MS (adapted from (Blake et al., 2009)).

<i>m/z</i>	Compound	Reference
28	HCN	(Karl et al., 2003)
31	HCHO	(Steinbacher et al., 2004, Inomata et al., 2007)
33	Methanol	(de Gouw et al., 2003, de Gouw et al., 2004, Holzinger et al., 2001)
42	Acetonitrile	(de Gouw et al., 2003, de Gouw et al., 2004, Sprung et al., 2001)
45	Acetaldehyde	(de Gouw et al., 2003, Kuster et al., 2004)
47	Formic acid	(Karl et al., 2004, Williams et al., 2001)
54	Acetonitrile	(Karl et al., 2003)
57	Butenes, methyl <i>tert</i> -butyl ether, butanol	(Karl et al., 2003)
59	Acetone	(de Gouw et al., 2003, Kuster et al., 2004, de Gouw et al., 2004, Sprung et al., 2001)
61	Acetic acid	(de Gouw et al., 2003)
63	Dimethylsulfide	(de Gouw and Warneke, 2007)
69	Isoprene, Furan	(de Gouw et al., 2003, Kuster et al., 2004)
71	Methyl vinyl ketone (MVK), Methacrolein	(de Gouw et al., 2003, de Gouw and Warneke, 2007)
73	Methyl ethyl ketone	(de Gouw et al., 2003)
75	Hydroxyl acetone	(Williams et al., 2001)
77	Peroxy acetyl nitrate (PAN)	(de Gouw et al., 2003)
79	Benzene	(de Gouw et al., 2003, Kuster et al., 2004)
81	Monoterpene, Hexenal	(de Gouw et al., 2003, de Gouw and Warneke, 2007)
83	Hexenol, Hexenal, hexenylacetate methylfuran, isoprene hydroxyl carbonyls	(Williams et al., 2001, Karl et al., 2001a)
85	Ehtyl vinyl ketone	(Karl et al., 2001a)
87	2-methyl-3-buten-2-ol C ₅ carbonyls, methacrylic acid	(Williams et al., 2001, Holzinger et al., 2005)
91	Peroxypropionyl nitrate (PAN)	
93	Toluene	(de Gouw et al., 2003, de Gouw et al., 2004, Kuster et al., 2004)
95	2-vinylfuran phenol	(Williams et al., 2001)
99	Hexenal	(Karl et al., 2001a)
101	Isoprene hydroperoxides	(Williams et al., 2001)
103	Peroxymethacrylic nitric anhydrides (MPAN)	
105	Styrene, peroxyisobutyric nitric anhydride (PiBN)	(Kuster et al., 2004)
107	C ₈ aromatics	(de Gouw et al., 2003, Kuster et al., 2004)
115	Heptanal	(Karl et al., 2001a)
121	C ₉ aromatics	(de Gouw et al., 2003, Kuster et al., 2004)
129	Octanal naphthalene	(Karl et al., 2001a, Karl et al., 2003)
135	C ₁₀ aromatics	(Karl et al., 2001b)
137	Monoterpenes	(de Gouw et al., 2003, de Gouw and Warneke, 2007)
139	Nopinone	(Holzinger et al., 2005)
143	Nonanal	(Karl et al., 2001a)
149	C ₁₁ aromatics methylchavicol	(Karl et al., 2003, Holzinger et al., 2005)
151	Pinonaldehydes	(Holzinger et al., 2005)
163	C ₁₂ aromatics	(Karl et al., 2003)

PTR-MS has been used in chamber studies, where the atmosphere is simulated in a controlled way using a large chamber containing known levels of ozone,

NO_x and aerosols. This allows atmospheric scientists to study atmospheric chemical processes in a controlled environment without the chemical complexity (competing/ interfering processes) present in the “real atmosphere”.

Alternatively PTR-MS has been used to study atmospheric air itself in many different places, from urban areas such as city centres to rural and even jungle locations (Blake et al., 2009, White et al., 2012). An example time series of toluene is presented in Figure 1-9 **Error! Reference source not found.** and demonstrates the high resolution data (1 min) that can be obtained when analysing atmospheric air using this technique.

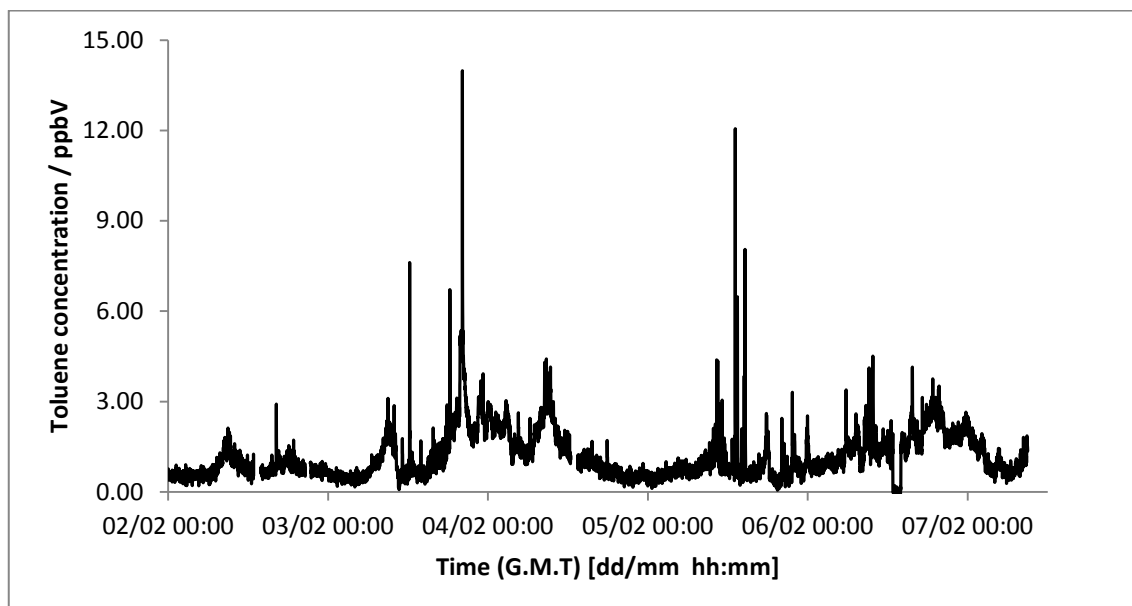


Figure 1-9. PTR-MS data (1 min time resolution) obtained by the University of Leicester during the ClearLo Campaign, London, UK (2012).

1.4.2 Breath analysis

VOCs are produced all over the body and then transported in the blood stream to the lungs, where they are exhaled in breath. As different illnesses and stresses on the body cause different combinations of VOCs to be produced, this provides a potential opportunity to develop a non-invasive medical diagnostic tool that could rapidly screen patients for certain medical conditions (Phillips, 1992).

Quantification of the various VOCs in breath analysed by PTR-MS poses a significant challenge, not least because of the high and varying humidity of the breath sample. As the humidity of the sample changes, so does the sensitivity of the VOCs detected by PTR-MS. Unwanted water clusters can form at high humidity resulting in competing ionisation pathways. This then alters the appearance of the resulting mass spectrum, however, with careful instrument set-up and calibration this problem can be minimised. Another complication is that a single compound often cannot be used for the diagnosis of one particular disease owing to the complex metabolomic processes governing the production of these metabolic VOCs. Therefore, a more holistic approach can be entertained, where the spectrum is taken as a whole, or 'fingerprint', and using statistical data analysis, certain combinations of compounds can be assigned predictors of certain diseases.

An example of this approach was provided by Phillips and co-workers, who successfully identified VOC biomarkers for the detection of lung and breast cancer (Phillips et al., 1999, Phillips et al., 2003, Phillips et al., 2006, Phillips et al., 2008, Phillips et al., 2010). These studies were carried out by collecting the breath of each patient for two minutes in an adsorption tube for pre-concentration. The adsorbed material was then thermally desorbed into a GC-MS. The data shows that it is possible to identify VOC biomarkers linked to lung and breast cancer. Unfortunately this type of analysis is an offline technique, meaning the samples are collected and then analysed in a laboratory afterwards. The next logical development would be to have real time analysis of the breath so that a decision over the likelihood of cancer (or any other disease for that matter) being present in a patient, could be determined immediately.

PTR-MS offers a solution to this problem. It has the sensitivity to detect VOCs at the levels observed in breath (down to pptV levels) without any sample pre-concentration or any subsequent and relatively slow analysis, as would be the case for GC-MS. PTR-MS can analyse gas samples at atmospheric pressure, so it is simply a case of having a patient breathe into a tube, and have some of that sample diverted off to the instrument. Whilst in practice it is not quite this trivial, it is relatively straightforward.

1.4.3 Food science

PTR-MS has been used from the beginning to analyse a whole wealth of food and drinks including:

- Coffee headspace - the headspace was monitored to discern the VOCs contained in the aroma. This provided a challenging test for PTR-MS owing to the complex mixtures present (Lindinger et al., 1998a, Yeretzian et al., 2003).
- Fruit monitoring - the headspaces of post-harvest berries were monitored for their temporal VOC profiles emitted during the ageing process in order to determine their optimum ripeness (Boschetti et al., 1999).
- Infant formula - 13 infant formulas (both powdered and liquid) of different brands were analysed by PTR-MS and GC-MS to compare the different VOCs present in order to assess early flavour perception (van Ruth et al., 2006).
- Cheese - comparisons between traditional flavour perception tests and PTR-MS have been made (Gasperi et al., 2001) as well as the study of the ageing of grana padano cheese using PTR-MS (Aprea et al., 2007).
- Red peppers - the effect of saliva on the flavour perception (emission of VOCs) of dehydrated red peppers has been carried out by PTR-MS (van Ruth and Buhr, 2003).

VOCs have the potential to play a significant role in the food industry, and in turn PTR-MS has the potential to play a crucial role in flavour perception and quality control (Blake et al., 2009). Since its inception by Lindinger, PTR-MS has been seen as a viable and useful analytical technique to study the release of VOCs when food is eaten and to better the perception of food taste and quality. Comparisons have been made between PTR-MS and the more traditional way of determining food tastes, as carried out by panel of human volunteers.

The first study into flavour release was by Taucher and co-workers in 1996 (Taucher et al., 1996), and involved a participant eating raw garlic. Breath

samples were then taken at regular intervals analysed by PTR-MS over a 30 hour period. During the analysis, several compounds from the family of organosulfur compounds, including allyl methyl sulfide, diallyl sulfide and 2-propenethiol, were detected as a result of the garlic consumption. As well as these compounds, elevated levels of acetone (already present in copious amounts on breath) were detected (~5 ppmV). This elevation in acetone was thought to be from enhanced metabolism of fatty acids.

As well as being used for flavour perception, PTR-MS has also been used as an analytical tool for the detection of food decay (Blake 2009). When meat decays, the smell changes, reflecting the breakdown products of flesh and therefore having a likely impact on VOC emission. Thus one might expect that PTR-MS could be used to determine to what extent the meat has decayed. Current techniques for detecting meat or other food decay involve bacterial testing, which can take days to carry out and can only be done on a relatively small sample set. However, PTR-MS offers a fast time resolution and a non-invasive approach that could be used to analyse anything from a warehouse to an individual piece of meat, all without damaging the product (Lindinger et al., 1998a, Lindinger et al., 1998b, Mayr et al., 2003a, Mayr et al., 2003b).

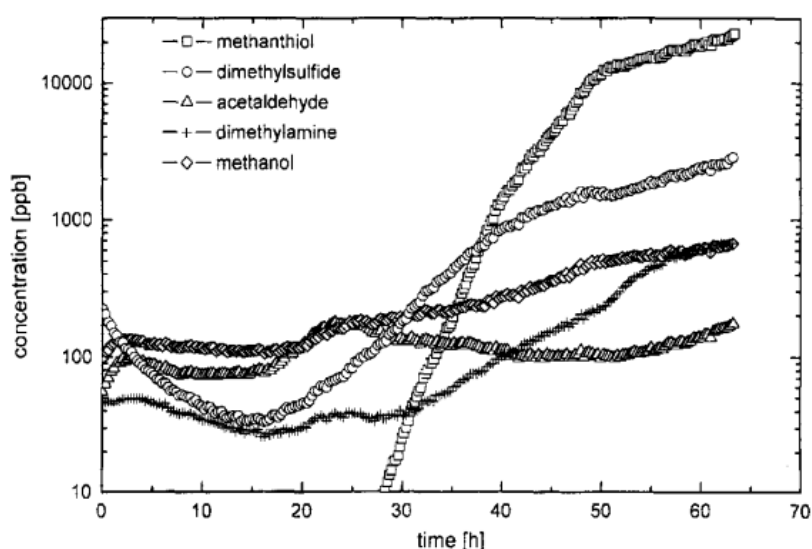


Figure 1-10. Change in various organosulfides with decay time of meat. (Blake et al., 2009).

Figure 1-10 shows how various organosulfide compounds differ in time as meat decays. At 30 hours there is a rapid change in the VOC profile and this demonstrates the beginning of the decay process.

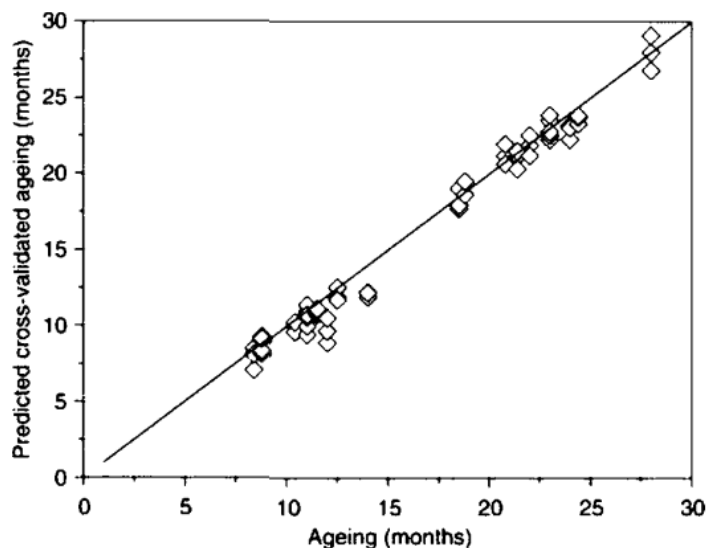


Figure 1-11. Correlation between the age calculated for cheese ripening using PTR-MS analysis and the actual age of the meat. (Blake et al., 2009, Aprea et al., 2007).

Online headspace analysis of cheese was carried out by PTR-MS in order to assess the effectiveness of this technique for the characterisation of the ageing process. Figure 1-11 illustrates that PTR-MS can successfully quantify the age of cheese using the VOC profile (16 VOCs indicative of the ripening process) when compared to the actual age (Aprea et al., 2007).

1.4.4 Forensic science

The detection of accelerants used in arson is routinely carried out by forensic scientists using GC-MS. This is an offline technique, requiring sample collection via activated carbon traps. However, PTR-MS has been shown to successfully identify different fire accelerants on different materials (Whyte et al., 2007). The head space above the burnt region was analysed, and in this way a small sample of the material could be analysed in minutes if presented to a PTR-MS instrument. Alternatively a portable variant could be taken to the scene and be used to carry out an immediate identification.

1.4.5 Homeland security

Homeland security began in the United States and still continues to follow its initial aims of protecting a nation from various terrorist threats. These threats include protecting the borders of the country from the trafficking of explosives, chemical warfare agents and illicit drugs. The most challenging aspect in detecting these types of compounds is having an instrument capable of detecting small quantities of a compound which typically has a very low vapour pressure at room temperature. PTR-MS lends itself well to this challenge due to its high sensitivity. In addition, because protonation is a soft ionisation technique, it usually leads to a protonated parent ion which instils high confidence in the molecular assignment, resulting in a reduction of false positives.

When constructing an explosive device such as a bomb, it is extremely difficult to avoid traces of the explosive getting on your person or belongings. With this in mind, it is theoretically possible to detect a bomb manufacturer even if they are not in possession of a device. Solid explosives have successfully been detected in real-time by PTR-MS in a proof of concept study (Mayhew et al., 2010). A sample of solid explosive (such as TNT or RDX), which are not visible to the unaided eye, was placed in a glass vial and heated. The PTR-MS was monitoring the headspace above the sample for the protonated peak of the explosives' constituent molecule and it was successfully detected. With further study and modification this could be a viable tool for homeland security in airports.

Chemical warfare agents, such as sarin and mustard gas, have also been detected and quantified using PTR-MS (Cordell et al., 2007). The detection of these and other chemical warfare agents could lead to a portable instrument that would quickly identify the concentrations of such compounds, both in a national security context as well as in potentially hostile areas and aid clean-up in post-conflict areas.

1.5 Thesis aims and structure

Accurately quantifying VOCs is crucial in aiding our overall understanding of the complex atmospheric processes that take place. Semi-volatile VOCs and semi-volatile oVOCs play an important role in these atmospheric processes and are potentially under reported. The reason for this under-reporting of semi-volatile VOCs and semi-volatile oVOCs is the challenge of their detection. Firstly, because of the semi-volatility, there will be fewer molecules in the gas-phase, and therefore a lower concentration of sample in atmospheric air to be measured. Secondly, careful sampling needs to be employed to minimise the chances of such molecules 'sticking' to the sample line, i.e. coming out of gas phase. Being able to measure all VOCs in order to determine the amount of ground level ozone that may be produced in an urban environment is also crucial, and has implications for public health.

The research in this thesis will first aim to improve the detection sensitivity and limit of detection for all VOCs measured by PTR-MS and will then investigate methods for reducing the complexity of mass spectra to allow for simpler interpretation.

This thesis will comprise of six chapters. Following on from this introduction chapter, which has detailed the importance of VOC detection along with methods for detection and applications of PTR-MS, is chapter two: the instrumental chapter. Here the specific instruments used for the experiments throughout this thesis are discussed, along with some of the fundamental concepts behind the instrumentation.

Chapter three explores the potential for enhanced sensitivity that arises from a modified drift tube acting as an ion funnel. This is one possible way to be able to measure lower concentration molecules, including semi volatile VOCs found in the Earth's atmosphere.

Chapter four will investigate the effect of changing buffer gas on the collision energies present in the drift tube, beginning with single compound comparisons,

Chapter one: Introduction

before analysing a complex matrix of VOCs. By altering the sensitivity, and specificity, a system could potentially be created that is suitable for monitoring specific VOCs. Simplified mass spectra would also make it easier to analyse and speciate complex data sets obtained from complex VOC mixtures, such as those obtained in an urban environment.

Urban air measurements are then carried out in chapter five, in which a standard PTR-MS is first compared to a 2D GC-MS. Then the standard PTR-MS is compared to a modified PTR-MS with ion funnel in its first field deployment. In this study the potential of the ion funnel is explored in the hope of detecting a wider range of compounds by having an increased sensitivity allowing for the detection of previously undetectable compounds.

Chapter six will form the conclusion of the thesis along with potential future work and final thoughts.

1.6 References

- ADAMS, N. G. & SMITH, D. 1976. The selected ion flow tube (SIFT); A technique for studying ion-neutral reactions. *International Journal of Mass Spectrometry and Ion Physics*, 21, 349-359.
- ANDERSON, L. G., LANNING, J. A., BARRELL, R., MIYAGISHIMA, J., JONES, R. H. & WOLFE, P. 1996. Sources and sinks of formaldehyde and acetaldehyde: An analysis of Denver's ambient concentration data. *Atmospheric Environment*, 30, 2113-2123.
- APREA, E., BIASIOLI, F., GASPERI, F., MOTT, D., MARINI, F. & MÄRK, T. D. 2007. Assessment of Trentingrana cheese ageing by proton transfer reaction-mass spectrometry and chemometrics. *International Dairy Journal*, 17, 226-234.
- ATKINSON, R. 2000. Atmospheric chemistry of VOCs and NO_x. *Atmospheric environment*, 34, 2063-2101.
- BAMBERGER, I., STIEGER, J., BUCHMANN, N. & EUGSTER, W. 2014. Spatial variability of methane: Attributing atmospheric concentrations to emissions. *Environmental Pollution*, 190, 65-74.
- BLAKE, R. S., MONKS, P. S. & ELLIS, A. M. 2009. Proton-Transfer Reaction Mass Spectrometry. *Chemical Reviews*, 109, 861-896.
- BOSCHETTI, A., BIASIOLI, F., VAN OPBERGEN, M., WARNEKE, C., JORDAN, A., HOLZINGER, R., PRAZELLER, P., KARL, T., HANSEL, A., LINDINGER, W. & IANNOTTA, S. 1999. PTR-MS real time monitoring of the emission of volatile organic compounds during postharvest aging of berryfruit. *Postharvest Biology and Technology*, 17, 143-151.
- CALLENDAR, G. S. 1940. *Quart. J. Roy. Meteor. Soc.*, 395-400.
- CLOWERS, B. H., DWIVEDI, P., STEINER, W. E., HILL JR, H. H. & BENDIAK, B. 2005. Separation of sodiated isobaric disaccharides and trisaccharides using electrospray ionization-atmospheric pressure ion mobility-time of flight mass spectrometry. *Journal of the American Society for Mass Spectrometry*, 16, 660-669.
- CORDELL, R. L., WILLIS, K. A., WYCHE, K. P., BLAKE, R. S., ELLIS, A. M. & MONKS, P. S. 2007. Detection of chemical weapon agents and simulants using chemical ionization reaction time-of-flight mass Spectrometry. *Analytical Chemistry*, 79, 8359-8366.
- DE GOUW, J., GOLDAN, P., WARNEKE, C., KUSTER, W., ROBERTS, J., MARCHEWKA, M., BERTMAN, S., PSZENNY, A. & KEENE, W. 2003. Validation of proton transfer reaction-mass spectrometry (PTR-MS) measurements of gas-phase organic compounds in the atmosphere during the New England Air Quality Study (NEAQS) in 2002. *Journal of Geophysical Research: Atmospheres (1984–2012)*, 108.
- DE GOUW, J. & WARNEKE, C. 2007. Measurements of volatile organic compounds in the earth's atmosphere using proton-transfer-reaction mass spectrometry. *Mass Spectrometry Reviews*, 26, 223-257.
- DE GOUW, J., WARNEKE, C., HOLZINGER, R., KLÜPFEL, T. & WILLIAMS, J. 2004. Inter-comparison between airborne measurements of methanol, acetonitrile and acetone using two differently configured PTR-MS instruments. *International Journal of Mass Spectrometry*, 239, 129-137.
- ELLIS, A. M. & MAYHEW, C. A. 2014. *Proton Transfer Reaction Mass Spectrometry: Principles and Applications*, Wiley.

Chapter one: Introduction

- FEHSENFELD, F. C., FERGUSON, E. E. & SCHMELTEKOPF, A. L. 1966. Thermal-Energy Ion—Neutral Reaction Rates. III. The Measured Rate Constant for the Reaction $O+(4S)+CO_2(1\Sigma)\rightarrow O_2+(2\Pi)+CO(1\Sigma)$. *The Journal of Chemical Physics*, 44, 3022-3024.
- FERGUSON, E., FEHSENFELD, F. & SCHMELTEKOPF, A. 1969. Flowing afterglow measurements of ion-neutral reactions. *Advances in Atomic and Molecular Physics*, 5, 1-56.
- GASPERI, F., GALLERANI, G., BOSCHETTI, A., BIASIOLI, F., MONETTI, A., BOSCAINI, E., JORDAN, A., LINDINGER, W. & IANNOTTA, S. 2001. The mozzarella cheese flavour profile: a comparison between judge panel analysis and proton transfer reaction mass spectrometry. *Journal of the Science of Food and Agriculture*, 81, 357-363.
- GLUECKAUF, E. 1951. *The composition of atmospheric air, in Compendium of Meteorology*, ed. by T.F. Mahone, Boston, American Meteorological Society.
- HAMILTON, J. F., RAMI ALFARRA, M., WYCHE, K. P., WARD, M. W., LEWIS, A. C., MCFIGGANS, G. B., GOOD, N., MONKS, P. S., CARR, T. & WHITE, I. R. 2011. Investigating the use of secondary organic aerosol as seed particles in simulation chamber experiments. *Atmospheric Chemistry and Physics*, 11, 5917-5929.
- HANSEL, A., JORDAN, A., HOLZINGER, R., PRAZELLER, P., VOGEL, W. & LINDINGER, W. 1995. Proton transfer reaction mass spectrometry: on-line trace gas analysis at the ppb level. *International Journal of Mass Spectrometry and Ion Processes*, 149–150, 609-619.
- HARRISON, R. M. 2007. *Principles of environmental chemistry*, Royal society of chemistry.
- HEALY, R., WENGER, J., METZGER, A., DUPLISSY, J., KALBERER, M. & DOMMEN, J. 2008. Gas/particle partitioning of carbonyls in the photooxidation of isoprene and 1, 3, 5-trimethylbenzene. *Atmospheric Chemistry and Physics*, 8, 3215-3230.
- HELMUT, S. & WOLFGANG, P. 1960. Apparatus for separating charged particles of different specific charges. Google Patents.
- HOLZINGER, R., JORDAN, A., HANSEL, A. & LINDINGER, W. 2001. Methanol measurements in the lower troposphere near Innsbruck (047° 16' N; 011° 24' E), Austria. *Atmospheric Environment*, 35, 2525-2532.
- HOLZINGER, R., LEE, A., PAW, K. & GOLDSTEIN, U. 2005. Observations of oxidation products above a forest imply biogenic emissions of very reactive compounds. *Atmospheric Chemistry and Physics*, 5, 67-75.
- INOMATA, S., TANIMOTO, H., KAMEYAMA, S., TSUNOGAI, U., IRIE, H., KANAYA, Y. & WANG, Z. 2007. Technical Note: Determination of formaldehyde mixing ratios in polluted air with PTR-MS: laboratory experiments and field measurements. *Atmospheric Chemistry and Physics Discussions*, 7, 12845-12876.
- JAMES, A. & MARTIN, A. 1952. Gas-liquid partition chromatography: the separation and micro-estimation of volatile fatty acids from formic acid to dodecanoic acid. *Biochemical Journal*, 50, 679.
- KANU, A. B., DWIVEDI, P., TAM, M., MATZ, L. & HILL, H. H. 2008. Ion mobility–mass spectrometry. *Journal of Mass Spectrometry*, 43, 1-22.
- KARL, T., CRUTZEN, P. J., MANDL, M., STAUDINGER, M., GUENTHER, A., JORDAN, A., FALL, R. & LINDINGER, W. 2001a. Variability-lifetime relationship of VOCs observed at the Sonnblick Observatory 1999—Estimation of HO-densities. *Atmospheric Environment*, 35, 5287-5300.

Chapter one: Introduction

- KARL, T., FALL, R., CRUTZEN, P., JORDAN, A. & LINDINGER, W. 2001b. High concentrations of reactive biogenic VOCs at a high altitude site in late autumn. *Geophysical Research Letters*, 28, 507-510.
- KARL, T., JOBSON, T., KUSTER, W. C., WILLIAMS, E., STUTZ, J., SHETTER, R., HALL, S. R., GOLDAN, P., FEHSENFELD, F. & LINDINGER, W. 2003. Use of proton-transfer-reaction mass spectrometry to characterize volatile organic compound sources at the La Porte super site during the Texas Air Quality Study 2000. *Journal of Geophysical Research: Atmospheres (1984–2012)*, 108.
- KARL, T., POTOSNAK, M., GUENTHER, A., CLARK, D., WALKER, J., HERRICK, J. D. & GERON, C. 2004. Exchange processes of volatile organic compounds above a tropical rain forest: Implications for modeling tropospheric chemistry above dense vegetation. *Journal of Geophysical Research: Atmospheres (1984–2012)*, 109.
- KROLL, J. H. & SEINFELD, J. H. 2008. Chemistry of secondary organic aerosol: Formation and evolution of low-volatility organics in the atmosphere. *Atmospheric Environment*, 42, 3593-3624.
- KUSTER, W., JOBSON, B., KARL, T., RIEMER, D., APEL, E., GOLDAN, P. & FEHSENFELD, F. C. 2004. Intercomparison of volatile organic carbon measurement techniques and data at La Porte during the TexAQS2000 Air Quality Study. *Environmental science & technology*, 38, 221-228.
- LAGG, A., TAUCHER, J., HANSEL, A. & LINDINGER, W. 1994. Applications of proton transfer reactions to gas analysis. *International Journal of Mass Spectrometry and Ion Processes*, 134, 55-66.
- LAOTHAWORNKITKUL, J., TAYLOR, J. E., PAUL, N. D. & HEWITT, C. N. 2009. Biogenic volatile organic compounds in the Earth system. *New Phytologist*, 183, 27-51.
- LINDINGER, W., HANSEL, A. & JORDAN, A. 1998a. On-line monitoring of volatile organic compounds at pptv levels by means of proton-transfer-reaction mass spectrometry (PTR-MS) medical applications, food control and environmental research. *International Journal of Mass Spectrometry and Ion Processes*, 173, 191-241.
- LINDINGER, W., HANSEL, A. & JORDAN, A. 1998b. Proton-transfer-reaction mass spectrometry (PTR-MS): on-line monitoring of volatile organic compounds at pptv levels. *Chem. Soc. Rev.*, 27, 347-375.
- MANNSCHRECK, K., GILGE, S., PLASS-DUELMER, C., FRICKE, W. & BERRESHEIM, H. 2004. Assessment of the applicability of NO-NO₂-O₃ photostationary state to long-term measurements at the Hohenpeissenberg GAW Station, Germany. *Atmospheric Chemistry and Physics*, 4, 1265-1277.
- MAYHEW, C., SULZER, P., PETERSSON, F., HAIDACHER, S., JORDAN, A., MÄRK, L., WATTS, P. & MÄRK, T. 2010. Applications of proton transfer reaction time-of-flight mass spectrometry for the sensitive and rapid real-time detection of solid high explosives. *International Journal of Mass Spectrometry*, 289, 58-63.
- MAYR, D., MARGESIN, R., KLINGSBICHEL, E., HARTUNGEN, E., JENEWEIN, D., SCHINNER, F. & MÄRK, T. 2003a. Rapid detection of meat spoilage by measuring volatile organic compounds by using proton transfer reaction mass spectrometry. *Applied and environmental microbiology*, 69, 4697-4705.
- MAYR, D., MARGESIN, R., SCHINNER, F. & MÄRK, T. D. 2003b. Detection of the spoiling of meat using PTR-MS. *International Journal of Mass Spectrometry*, 223–224, 229-235.

Chapter one: Introduction

- NEWMAN, K. & MASON, R. S. 2006. Organic mass spectrometry and control of fragmentation using a fast flow glow discharge ion source. *Rapid Communications in Mass Spectrometry*, 20, 2067-2073.
- PHILLIPS, M. 1992. Breath tests in medicine. *Scientific American*, 267, 74-79.
- PHILLIPS, M., ALTORKI, N., AUSTIN, J. H., CAMERON, R. B., CATANEO, R. N., KLOSS, R., MAXFIELD, R. A., MUNAWAR, M. I., PASS, H. I. & RASHID, A. 2008. Detection of lung cancer using weighted digital analysis of breath biomarkers. *Clinica Chimica Acta*, 393, 76-84.
- PHILLIPS, M., CATANEO, R. N., CUMMIN, A. R., GAGLIARDI, A. J., GLEESON, K., GREENBERG, J., MAXFIELD, R. A. & ROM, W. N. 2003. Detection of lung cancer with volatile markers in the breath. *Chest Journal*, 123, 2115-2123.
- PHILLIPS, M., CATANEO, R. N., DITKOFF, B. A., FISHER, P., GREENBERG, J., GUNAWARDENA, R., KWON, C. S., TIETJE, O. & WONG, C. 2006. Prediction of breast cancer using volatile biomarkers in the breath. *Breast cancer research and treatment*, 99, 19-21.
- PHILLIPS, M., CATANEO, R. N., SAUNDERS, C., HOPE, P., SCHMITT, P. & WAI, J. 2010. Volatile biomarkers in the breath of women with breast cancer. *Journal of breath research*, 4, 026003.
- PHILLIPS, M., GLEESON, K., HUGHES, J. M. B., GREENBERG, J., CATANEO, R. N., BAKER, L. & MCVAY, W. P. 1999. Volatile organic compounds in breath as markers of lung cancer: a cross-sectional study. *The Lancet*, 353, 1930-1933.
- PORG 1997. The Chemistry of Secondary Pollutant Formation, Report by the Photochemical Oxdants Review Group.
- SCHADE, G. W. & GOLDSTEIN, A. H. 2006. Seasonal measurements of acetone and methanol: Abundances and implications for atmospheric budgets. *Global biogeochemical cycles*, 20.
- SHOWSTACK, R. 2013. Carbon dioxide tops 400 ppm at Mauna Loa, Hawaii. *Eos, Transactions American Geophysical Union*, 94, 192-192.
- SINGH, H., CHEN, Y., TABAZADEH, A., FUKUI, Y., BEY, I., YANTOSCA, R., JACOB, D., ARNOLD, F., WOHLFROM, K. & ATLAS, E. 2000. Distribution and fate of selected oxygenated organic species in the troposphere and lower stratosphere over the Atlantic. *Journal of Geophysical Research: Atmospheres (1984–2012)*, 105, 3795-3805.
- SMITH, D. & ŠPANĚL, P. 2005. Selected ion flow tube mass spectrometry (SIFT-MS) for on-line trace gas analysis. *Mass Spectrometry Reviews*, 24, 661-700.
- SMITH, D., ŠPANĚL, P., HERBIG, J. & BEAUCHAMP, J. 2014. Mass spectrometry for real-time quantitative breath analysis. *Journal of breath research*, 8, 027101.
- ŠPANĚL, P. & SMITH, D. 2011. Progress in SIFT-MS: Breath analysis and other applications. *Mass Spectrometry Reviews*, 30, 236-267.
- SPRUNG, D., JOST, C., REINER, T., HANSEL, A. & WISTHALER, A. 2001. Acetone and acetonitrile in the tropical Indian Ocean boundary layer and free troposphere: Aircraft-based intercomparison of AP-CIMS and PTR-MS measurements. *Journal of geophysical research*, 106, 28511.
- STEINBACHER, M., DOMMEN, J., AMMANN, C., SPIRIG, C., NEFTEL, A. & PREVOT, A. 2004. Performance characteristics of a proton-transfer-reaction mass spectrometer (PTR-MS) derived from laboratory and field measurements. *International Journal of Mass Spectrometry*, 239, 117-128.

Chapter one: Introduction

- TAUCHER, J., HANSEL, A., JORDAN, A. & LINDINGER, W. 1996. Analysis of Compounds in Human Breath after Ingestion of Garlic Using Proton-Transfer-Reaction Mass Spectrometry. *Journal of Agricultural and Food Chemistry*, 44, 3778-3782.
- VAN RUTH, S. M. & BUHR, K. 2003. Influence of saliva on temporal volatile flavour release from red bell peppers determined by proton transfer reaction-mass spectrometry. *European Food Research and Technology*, 216, 220-223.
- VAN RUTH, S. M., FLORIS, V. & FAYOUX, S. 2006. Characterisation of the volatile profiles of infant formulas by proton transfer reaction-mass spectrometry and gas chromatography-mass spectrometry. *Food chemistry*, 98, 343-350.
- VON SCHNEIDEMESSER, E., MONKS, P. S. & PLASS-DUELMER, C. 2010. Global comparison of VOC and CO observations in urban areas. *Atmospheric Environment*, 44, 5053-5064.
- WARNEKE, P. & WILLIAMS, J. 2012. *The Atmospheric Chemist's Companion*, Springer.
- WHITE, I. R., GOODALL, I., BARBER, S., WYCHE, K. P. & MONKS, P. S. Gas Phase Measurements of VOCs during the ACIDPRUF Chamber Studies. ACID-PRUF Annual Science Meeting, Nov 22nd 2012. 2012 Manchester, UK.
- WHYTE, C., WYCHE, K. P., KHOLIA, M., ELLIS, A. M. & MONKS, P. S. 2007. Fast fingerprinting of arson accelerants by proton transfer reaction time-of-flight mass spectrometry. *International Journal of Mass Spectrometry*, 263, 222-232.
- WIEDINMYER, C., FRIEDFELD, S., BAUGH, W., GREENBERG, J., GUENTHER, A., FRASER, M. & ALLEN, D. 2001. Measurement and analysis of atmospheric concentrations of isoprene and its reaction products in central Texas. *Atmospheric Environment*, 35, 1001-1013.
- WILLIAMS, J., PÖSCHL, U., CRUTZEN, P., HANSEL, A., HOLZINGER, R., WARNEKE, C., LINDINGER, W. & LELIEVELD, J. 2001. An atmospheric chemistry interpretation of mass scans obtained from a proton transfer mass spectrometer flown over the tropical rainforest of Surinam. *Journal of Atmospheric Chemistry*, 38, 133-166.
- YERETZIAN, C., JORDAN, A. & LINDINGER, W. 2003. Analysing the headspace of coffee by proton-transfer-reaction mass-spectrometry. *International Journal of Mass Spectrometry*, 223, 115-139.
- ZHU, M., BENDIAK, B., CLOWERS, B. & HILL JR, H. H. 2009. Ion mobility-mass spectrometry analysis of isomeric carbohydrate precursor ions. *Analytical and bioanalytical chemistry*, 394, 1853-1867.

2 Chapter two: Instrumental

This chapter will detail the PTR-ToF-MS used in the experimental work described in this thesis. The hardware and software will be described, along with some of the fundamental aspects behind the drift tube source as well as the time of flight mass analyser. A modified drift tube incorporating an ion funnel, that was developed in this research and forms the basis of chapter three, will be discussed in that chapter as opposed to here.

2.1 Introduction to mass, charge and mass spectrometry

2.1.1 Mass and charge nomenclature

When physicists were originally studying electrically charged particles, they described them by the term 'charge to mass ratio (e/m)' as they were interested mainly in the charge of the particles. Then when chemists began to study these ions, they were interested in the compound's chemical identity; hence the mass was the most important factor, so the term was reversed to 'mass to charge ratio (m/e)'. However, as e refers to the elementary charge on the electron, m/e necessarily assumes that all molecules are singularly charged. So to avoid confusion the notation of 'mass to charge ratio' was changed to m/z , where z refers to the number of charges on the ion (Grayson, 2002). For high resolution mass spectrometry, the exact mass of the ion is used, e.g. $^1\text{H} = 1.0078$. However for lower resolution mass spectrometry which typically detects ions to the nearest mass unit, as encountered throughout this thesis, the nominal (unit) mass shall be used, i.e. $^1\text{H} = 1$.

2.1.2 Units of mass to charge ratio

When labelling the x-axis (m/z) of a mass spectrum, several different units have been used historically (Grayson, 2002). These are described below.

- Unified atomic mass unit (u) – the mass equal to $1/12^{\text{th}}$ of the unbound, rest mass of ^{12}C . This is the most commonly used unit.

Chapter two: Instrumental

- Dalton (*Da*) – the Dalton is equivalent to the *u* and is often used as an alternative notation to *u* when talking about mass spectrometry.
- Thomson (*Th*) – This is an infrequently used unit equal to u/e (*Da/e*). This unit can therefore have a negative value.
- Atomic mass unit (*amu*) – an out of date unit, it was the mass equal to $1/16^{\text{th}}$ of ^{16}O (having since been replaced by *u*). However it is still sometimes used (incorrectly), when in fact the user is referring to *u*, unless the literature is particularly old.

2.2 Ionising and ionisation sources

Ion sources come in a wide variety of configurations, ionising gaseous, liquid, and solid samples and can be operated in the regime of ambient pressure or at a reduced pressure, up to several orders of magnitude lower than atmospheric pressure. For the purpose of this thesis we will focus on the main methods of ionisation used to carry out the chemical ionisation of gaseous VOCs as well as drawing comparisons with an alternative, electron impact ionisation technique.

2.2.1 Hard verses soft ionisation

When analysing a sample, it is important to factor in how easy the resultant mass spectra can be assigned and interpreted; it is not simply enough to only be concerned with the ionisation potential, sensitivity and limit of detection of the target species. When analysing a complex sample mixture, it may be important to use an ionising technique that leaves the molecule intact, i.e. the molecular ion peak is preferentially detected. An example of soft ionisation is chemical ionisation, in which a charge is transferred from an already charged species (the reagent ion) to the target molecule. As an example in reaction E 2-1 an already protonated gaseous species (XH^+) can transfer a proton (H^+) to the neutral sample molecule (M), thus resulting in a charged species.

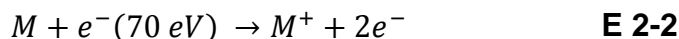


Conversely, it may be that fragmentation is acceptable, or even desired, in which case a hard ionising technique can be utilised such as electron ionisation.

2.2.2 Electron ionisation

Whilst EI sources were first invented by Dempster, they were later improved upon by Nier and Bleankey (Bleakney, 1929). In EI, the sample needs to be in the gas phase and therefore if it is a liquid or solid it must be vaporised by heating the probe tip where the analyte resides. A stream of electrons is created by thermionic emission from a wire with a current flowing through it. The gaseous analyte is then bombarded by this stream of electrons (usually at an energy near 70 eV) which can knock an electron off the analyte molecule if

collision occurs, leaving it charged as shown in reaction E 2-2 (Davis and Frearson, 1987).



EI is a hard ionisation technique due to the high kinetic energy of the ionising electron, which can cause bonds in the molecular ion to break and can therefore result in extensive fragmentation of the analyte molecule. However, this can be favourable if a single compound is being analysed and chemical identification via fragmentation pattern is required.

2.2.3 Chemical ionisation

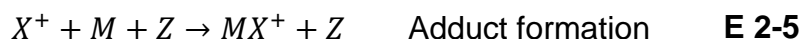
Whereas EI causes extensive fragmentation of the analyte molecule, in chemical ionisation – mass spectrometry (CI-MS) the analyte becomes charged by the transfer of charge from a previously ionised chemical species, known as the primary ion, as illustrated in reaction E 2-1. The process of charge transfer from the primary ion to the analyte molecule often results in very little excess energy in the resultant analyte ion, and thus tends to leave the ion relatively intact (a soft ionisation technique).

CI requires collisions between the primary ions and the analyte molecules (Harrison. A. G., 1983). The primary ions can be produced through various methods, including hollow cathode discharge sources (2.2.4.1) and through a radioactive alpha particle emitter (2.2.4.2), both of which will be described in detail later in this section.

Because CI requires primary ion-analyte molecule collisions for charge transfer to take place, a region of relatively poor vacuum (~1 mbar) must exist to allow a short enough mean free path length for the appropriate number of collisions to take place. Due to the poor vacuum in the source region, small orifices are used to separate differential pumping stages so that the rest of the instrument can be under high vacuum (required for detection of the ions in the mass analyser) and

to also allow for transmission of ions from one to the stage subsequent stage, without allowing too much neutral gas to move from one stage to the other.

In CI-MS, ionisation is achieved through the reaction of an ion with the analyte molecule and can take one of several potential pathways shown below (in addition to the proton transfer shown in E 2-1).



E 2-3 and E 2-4 are bimolecular reactions, whereas E 2-5 requires a third body molecule (Z) to remove energy from the system, in order for the adduct to form and not immediately dissociate.

The most commonly used reagent ion in PTR-MS is hydronium, H_3O^+ (Blake et al., 2006, Lindinger et al., 1998), and the emphasis later in this chapter and elsewhere in this thesis will be on the chemistry of this ion. However, it is worth noting that other reagent ions have been used in PTR-MS instruments including O_2^+ (Norman et al., 2007), NO^+ (Karl et al., 2012) and NH_4^+ (Blake et al., 2006).

2.2.4 Chemical ionisation sources

Outlined below are two examples of ion sources used in CI-MS. Both of these sources are used in this thesis.

2.2.4.1 Hollow cathode discharge source

A hollow cathode discharge ion source consists of a pair of electrodes with a DC potential difference applied between them. This arrangement can be seen in Figure 2-1. The negative electrode is known as the anode, and the positive the cathode. Normally the gas between the electrodes would be a poor conductor, but given a sufficient voltage, a discharge can occur in the gas between the two

electrodes. There are several different types of discharge that can occur and these are classified by the amount of current drawn:

- $\leq 1 \mu\text{A}$ - Townsend discharge
- $1 \mu\text{A} < 1 \text{ A}$ - Glow discharge
- $\geq 1 \text{ A}$ - Arc discharge

For the purposes of mass spectrometry a glow discharge (GD) (so named due to the glow of light that can be seen originating from the discharge) is utilised as an ionisation source because it provides enough electrical energy to sustain a discharge and cause ionisation without fragmenting the reagent ion.

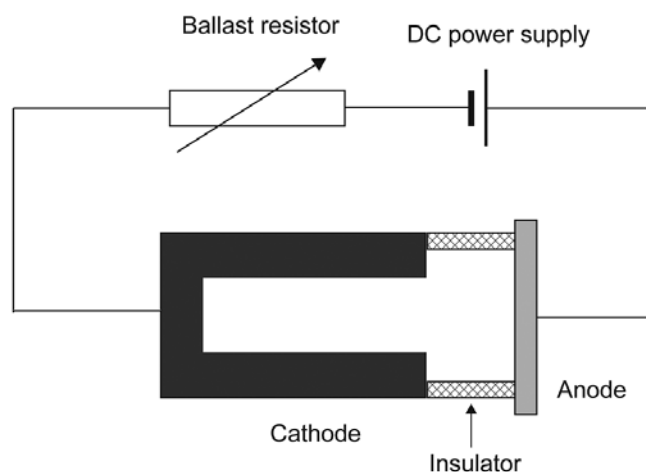


Figure 2-1. A simple example of a hollow cathode discharge. The variable resistance provided by the ballast resistor limits the amount of current drawn and improves the stability of the discharge (Ellis and Mayhew, 2014).

2.2.4.2 Radioactive ion source

A radical alternative is to use a strip of radioactive metal, such as ^{241}Am , as an alpha particle (He^{2+}) emitter in place of a hollow cathode discharge source in PTR-MS. This ion source was first developed by Hansel and co-workers (Hanson et al., 2003) and has been extensively used in the PTR-MS work by the University of Leicester team (Blake et al., 2004). The strip of radioactive metal resides in the GD region of a conventional hollow cathode set-up but in this instance no GD is required (Figure 2-2). The reagent gas, such as water vapour, is passed through this region and can collide with an alpha particle, leading to ionisation (Ellis and Mayhew, 2014).

This particular ion source gives very consistent levels of ionisation and therefore consistent hydronium production and is very reliable over a long time frame of operation. It is operated at a higher pressure than a hollow cathode ion source, which reduces back streaming, whereby the gas from the drift tube can enter the GD region, thus reducing the quantity of NO^+ and O_2^+ observed in the spectrum.

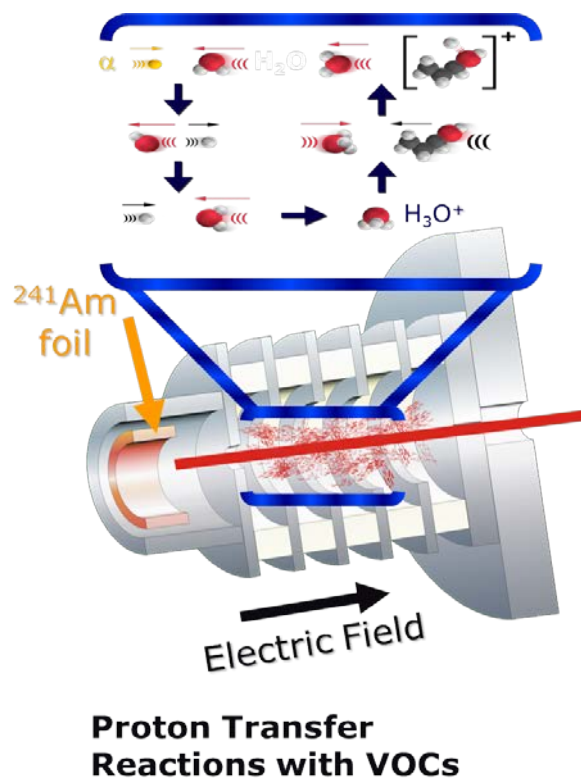


Figure 2-2. Americium ion source with an expanded view of the ionising reaction between an alpha particle (yellow) and a water molecule (red - oxygen, white - hydrogen).

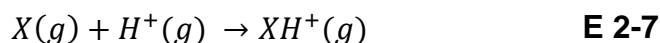
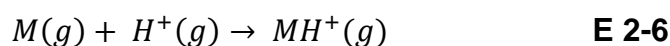
2.3 Thermodynamics and kinetics of proton transfer

Whilst CI has previously been discussed along with the different pathways for ionisation to occur (reactions E 2-1, E 2-3, E 2-4, E 2-5), the focus from here onwards will be on proton transfer (with specific reference to the hydronium ion). Therefore the thermodynamics and kinetics of this reaction are discussed in the following sections.

2.3.1 Thermodynamics

If the Gibbs energy change (ΔG) of a reaction is negative, the reaction can occur spontaneously. This does not necessarily mean that the reaction will be a fast reaction, only that thermodynamically it can occur (Ellis and Mayhew, 2014).

The thermodynamics of proton transfer can be established by considering the reactions represented in E 2-6 and E 2-7, which are the two reactions taking place within E 2-1.



Taking these two equations, it is now possible to represent proton transfer in the following terms, where (T) is the temperature and 0 represents the standard state.

$$\Delta G_T^0(\text{E 2-1}) = \Delta G_T^0(\text{E 2-6}) - \Delta G_T^0(\text{E 2-7}) \quad \text{E 2-8}$$

E 2-8 illustrates that the ΔG of proton transfer (E 2-1) can be calculated by subtracting the ΔG of the formation of XH^+ (E 2-7) from the ΔG for the formation of MH^+ (E 2-6).

Chapter two: Instrumental

A common method for determining proton transfer viability in mass spectrometry is through proton affinity (PA). PAs have been traditionally stated in units of either kJ mol^{-1} or kCal mol^{-1} . Another popular unit for energy measurement, especially when discussing electron ionisation, is the electron volt: eV. For this reason values for converting between units is given in Table 2-1.

Table 2-1. Comparison of energy measurement units (adapted from (Ellis and Mayhew, 2014)).

	eV	kJ mol^{-1}	kCal mol^{-1}
eV	1	96.48	23.06
kJ mol^{-1}	0.0104	1	0.239
kCal mol^{-1}	0.0434	4.184	1

We can see in

Table 2-2 that the inorganic constituents of air (nitrogen, oxygen etc.) have a PA far below that of H_2O and are therefore not protonated by reaction with H_3O^+ . This allows the inorganic components that make up the majority of the air to not be detected by PTR-MS and for only the detection of the organic VOCs present. Also shown is the water dimer $(\text{H}_2\text{O})_2$ with a PA of 808 kJ mol^{-1} . This presents an interesting scenario where some VOCs can be protonated only by H_3O^+ and others with high PAs by both the H_3O^+ and $\text{H}_3\text{O}^+(\text{H}_2\text{O})$ dimer. It is therefore important to bear this in mind during experiments and this will be discussed in section 2.3.3.

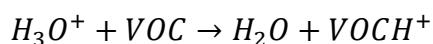
Chapter two: Instrumental

Table 2-2. List of various atoms and molecules and their corresponding proton affinities with data collected from (Goebbert and Wentold, 2004, Lindinger et al., 1998, Fernandez et al., 1998). Shown in red are possible proton donors.

Species	Formula	Mass	Proton affinity / kJ mol ⁻¹
Helium	He	4	177.8
Neon	Ne	20	203.3
Argon	Ar	40	369.0
Oxygen	O ₂	32	420.9
Hydrogen	H ₂	2	422.2
Krypton	Kr	84	424.7
Nitrogen	N ₂	28	493.7
Xenon	Xe	132	496.2
Carbon dioxide	CO ₂	44	540.6
Carbon monoxide	CO	28	592.9
Water	H₂O	18	691.2
Hydrogen Sulphide	H ₂ S	34	705.0
Formaldehyde	CH ₂ O	30	713.0
Formic acid	CH ₂ O ₂	46	741.8
Trans-2-butene	C ₄ H ₈	56	747.0
Methyl acetylene	C ₃ H ₄	40	748.0
Benzene	C ₆ H ₆	78	750.2
Propene	C ₃ H ₆	42	751.4
Bromobenzene	C ₆ H ₅ ⁷⁹ Br	156	754.1
	C ₆ H ₅ ⁸¹ Br	158	754.1
Methanol	CH ₄ O	32	754.4
Acetaldehyde	C ₂ H ₄ O	44	769.0
Ethanol	C ₂ H ₆ O	46	776.6
Acetonitrile	C ₂ H ₃ N	41	779.1
Toluene	C ₇ H ₈	92	784.1
Propanal	C ₃ H ₆ O	58	784.9
Propan-1-ol	C ₃ H ₈ O	60	787.4
Butanol	C ₄ H ₈ O	72	792.9
Xylene	C ₈ H ₁₀	106	795.0
Propan-2-ol	C ₃ H ₈ O	60	795.4
Acetic acid	C ₂ H ₄ O ₂	60	795.8
1,4-Dioxane	C ₄ H ₈ O ₂	88	797.9
Water dimer	(H₂O)₂	36	808.0
Methacrolein	C ₄ H ₆ O	70	808.7
Acetone	C ₃ H ₆ O	58	812.1
Phenol	C ₆ H ₆ O	94	815.9
Dimethyl sulphide	C ₂ H ₆ S	62	830.9
Isoprene	C ₅ H ₈	68	832.2
MVK	C ₄ H ₆ O	70	834.7
Cyclohexanone	C ₆ H ₁₀ O	98	841.1
Ammonia	NH₃	17	854.0
α-pinene	C ₁₀ H ₁₆	136	854.0
Limonene	C ₁₀ H ₁₆	136	869-873

2.3.2 Kinetics

The ionising reagent used for almost all of the experiments described in this thesis was the hydronium ion (H₃O⁺), for reasons already discussed. The proton is transferred to the VOC as shown in equation E 2-9.



E 2-9

Pseudo first order kinetics are observed when dealing with proton transfer, as hydronium ions are present in the instrument in a large excess over the concentration of analyte, i.e. $[H_3O^+] \gg [VOC]$.

Reaction E 2-10 below quantifies the rate of reaction, where k is the rate constant and t is the reaction time in the drift tube (Blake et al., 2004). The quantity of VOC that is protonated depends on the reaction time, the proton transfer rate constant for the VOC being measured, and the initial concentration of VOC. For example, acetone has a rate coefficient of $3.0 \times 10^{-9} \text{ cm}^3 \text{ s}^{-1}$ for reaction with H_3O^+ , whereas methanol has a somewhat lower rate coefficient of $2.33 \times 10^{-9} \text{ cm}^3 \text{ s}^{-1}$ (Zhao and Zhang, 2004).

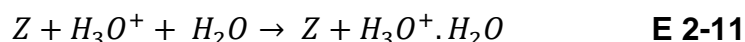
$$\frac{[VOCH^+]}{[H_3O^+]} = kt[VOC]$$

E 2-10

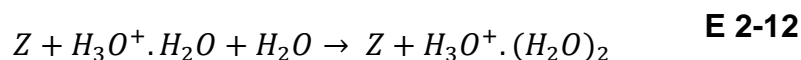
The concentration of VOC, $[VOC]$, can be calculated if the rate constant, k , and time of reaction, t , are known along with the measured protonated VOC, $[VOCH^+]$ and hydronium levels, $[H_3O^+]$.

2.3.3 E/N ratio

The ideal scenario in PTR-MS is to have a single species of reagent ion capable of ionisation. Whilst H_3O^+ is utilised, and all attempts to maximise it are carried out, water clustering can occur. This is when unreacted water molecules from the water vapour source, or from humidity in the analyte gas, react sequentially with H_3O^+ to form water clusters $H_3O^+ \cdot (H_2O)_n$, i.e.



then



where Z is a third body which removes the energy released by the association of H_3O^+ and H_2O .

To prevent water cluster ion formation, i.e. $H_3O^+.(H_2O)_n$, sufficiently energetic collisions must be present within the drift tube to break up these clusters. If water clusters are present they can create competing protonation pathways with hydronium, H_3O^+ . However unfortunately this requirement is in conflict with the desire to provide soft ionisation conditions, so a compromise has to be made.

The collision energy within the drift tube is related to the parameter E/N , where E is the electric field along the drift tube and N is the gas number density (Blake et al., 2004). The electric field is determined by the voltage, V , applied across the entire length of the drift tube (d) and is given by $E = V/d$. The number density, N (m^{-3}), which is based on conditions within the drift tube is shown in equation E 2-13, where P is the pressure in the drift tube, k_B is the Boltzmann constant and T is the temperature.

$$N = \frac{P}{k_B T} \quad \text{E 2-13}$$

E/N is measured in Townsends, Td , with units of $V.m^2$ where $1 \text{ Td} = 10^{-21} \text{ V.m}^2$.

A high E/N value results in increased fragmentation through more energetic ion-molecule collisions in the drift tube and therefore mass spectra that are typically more difficult to interpret. That is why an E/N value must be used that leads to

minimal analyte ion fragmentation whilst still creating a suitably high ratio of hydronium relative to its hydrated cluster ions (as discussed later).

2.3.4 Buffer gases

When a sample is introduced into the mass spectrometer (be it a calibrant gas, or perhaps a sample that requires dilution) then the gas that accompanies this is known as the buffer gas. Traditionally either synthetic air or nitrogen is used, as this for the most part reflects the real world conditions of the analysis, i.e. breath studies and atmospheric studies will almost exclusively be carried out in an atmosphere of air. However there are some situations where it may be possible and even beneficial to change the buffer gas from synthetic air or nitrogen to a different gas (Inomata et al., 2008). The kinetics of the drift tube are affected when the buffer gas is altered and this will be detailed, with respect to changing the balance gas to argon, forming the basis of Chapter 4.

2.4 Time of flight mass analyser

2.4.1 Linear time of flight mass analyser

The idea of a new type of mass analyser surfaced in 1946 by Stephenson during a meeting of the American Physical Society at the Massachusetts Institute of Technology (Mirsaleh-Kohan et al., 2008) and was patented (Glenn, 1956) and commercialised a few years later. The idea was to separate the ions based on the time they take to travel down a flight tube. A pulse of electric energy (in the acceleration region) forces a packet of ions into a flight tube and a field-free region. The kinetic energy of the ion E is related to its velocity v by,

$$E = \frac{1}{2}mv^2 \quad \text{E 2-14}$$

where m is the mass of the ion. The time taken for the ions to travel a set distance can be calculated by,

$$t = d \sqrt{\frac{m}{2E}} \quad \text{E 2-15}$$

where t is the time taken, d is the distance travelled by the ion, m is the mass of the ion and E is the kinetic energy of the ion.

Because all of the ions entering the flight tube are given the same initial kinetic energy and because they travel the same distance down the flight tube, then the time taken for travel is proportional to the square root of mass,

$$t \propto \sqrt{m} \quad \text{E 2-16}$$

This results in the lower mass ions travelling faster and arriving at the detector before the heavier mass ions. The detector then records the time it takes for each ion to reach it, and then in theory, using a known calibrant, the mass corresponding to each detection can be assigned.

As the quantities E and d are known in E 2-15, then by knowing the time (t) then the mass (m) of the ion can be calculated. The mass of the ion is proportional to the time (as shown in E 2-16), therefore several ions of known mass, are first used to calibrate the system. The times of the se known masses are recorded, and from this a conversion factor, relating t and m , can be calculated, allowing all future unknown masses to be calculated.

A problem, however, is that all of the ions of the same mass in reality do not start with this identical kinetic energy, as before they are given the pulse of electrical energy, they already possess a small (but not insignificant) amount of kinetic energy due to their original velocities. This resulted in a mass resolution that was so poor that it essentially made the technique useless. A solution was devised by placing a charged grid after the acceleration region which acts as a focusing element for ions of equal mass. This slows the fastest ions, increases the velocity of the slower ions, and results in closer kinetic energies across the ions of equal mass. This still had complications in that the detector would need to be mounted quite close to the acceleration region and charged grid, resulting in short flight path and less temporal separation of ions (Boesl et al., 1992).

In 1955, Wiley and McLaren (Wiley and McLaren, 1955) discovered that if a second electrical grid was added this would allow the detector to be placed much further away from the acceleration region and sufficient mass separation could be achieved.

2.4.2 Reflectron time of flight mass analyser

A modified flight tube known as a reflectron (Figure 2-3) was conceived by Alikhanov and Mamyrin (Tang et al., 1988, Mamyrin et al., 1973). The ions travel along the flight tube, enter a series of electric grids with increasing potential that slows, stops, and finally reverses their trajectory back towards the other end where the detector is now mounted. This helps to further improve the resolution of the peaks produced.

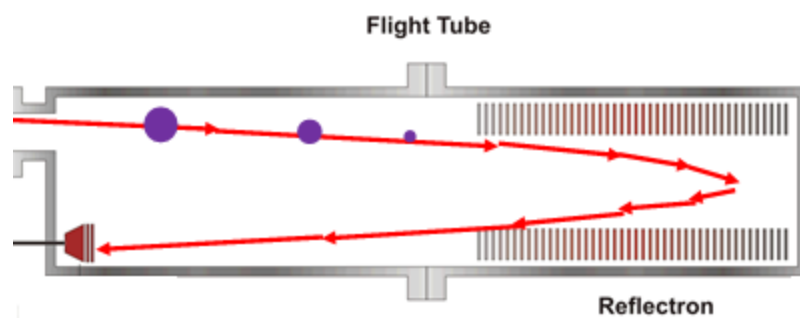


Figure 2-3. A schematic of a flight tube where the ions enter on the left, and are then reflected by the reflectron, and go on to strike the detector. (Blake, 2005).

A combination of the first two electrical grids (Wiley and McLaren, 1955), coupled with the reflectron results in extremely high mass resolution being achievable.

2.5 Instrumentation available at the University of Leicester

The experiments carried out in this thesis were conducted primarily on two instruments: one designated as the 'Kore ToF' (Kore-ToF) and the other designated as the 'Leicester ToF' (LE-ToF). The Kore-ToF has two modes of operation: one utilising a standard drift tube configuration (DC-mode) and the second with an enhanced electric field (radio frequency ion funnel) (RF-mode). These two modes will be compared in the following section and a comparison of the two setups shall be the focus of Chapter 3. The Kore-ToF is a commercial instrument provided by Kore Technology Ltd, Ely, UK, whilst the Le-ToF is a hybrid with the source having been designed in-house whilst the transfer optics, ToF mass analyser and counting system were provided by Kore Technology Ltd.

2.5.1 Kore ToF

The Kore' ToF (Kore-Technology-Ltd, 2010) consists of a hollow cathode glow discharge source and drift tube, followed by a transfer lens set-up that is coupled to a reflectron ToF mass analyser. The detector is a discrete dynode electron multiplier and ion counting is carried out by a time to digital converter (TDC) (Barber et al., 2012).

A schematic of the ion source and drift tube can be seen in Figure 2-4. Inside the GD region is a plasma at ~1-3 mbar, generated across a potential difference of 400-500 V (under standard operation). Water vapour is generated by a small chamber containing liquid H₂O that is under vacuum; this creates a stream of water vapour that enters the GD region and interacts with the plasma. Under normal operation there is a higher pressure in the GD region when compared to the source drift (SD) region and therefore there is a flow of neutral molecules from the GD region into the SD region. The voltage differential between the GD region and the lower voltages experienced in the SD region aids in extraction of ions from the GD, through the SD region and into the PTR.

The SD region is at ~1 mbar, which corresponds to a mean free path of ~0.06 mm. This results in many collisions, and thus interactions between the ions and

Chapter two: Instrumental

neutral molecules, with the effect of producing an essentially homogenous set of ions, in this case hydronium (H_3O^+) (Kore-Technology-Ltd, 2010).

As gas is provided to both the GD region (water vapour) and analyte region (analyte gas), there is a neutral gas flow gradient towards the exit of the drift tube. This means that in the GD region, the gas is almost exclusively water vapour, whilst in the drift tube there is a mixture of water and analyte gases. However, even though the analyte enters after the SD region, some back flow can occur into the GD region. This allows oxygen and nitrogen (if present in the sample) to become ionised forming O_2^+ and NO^+ ions that can be detected in the downstream mass spectrometer.

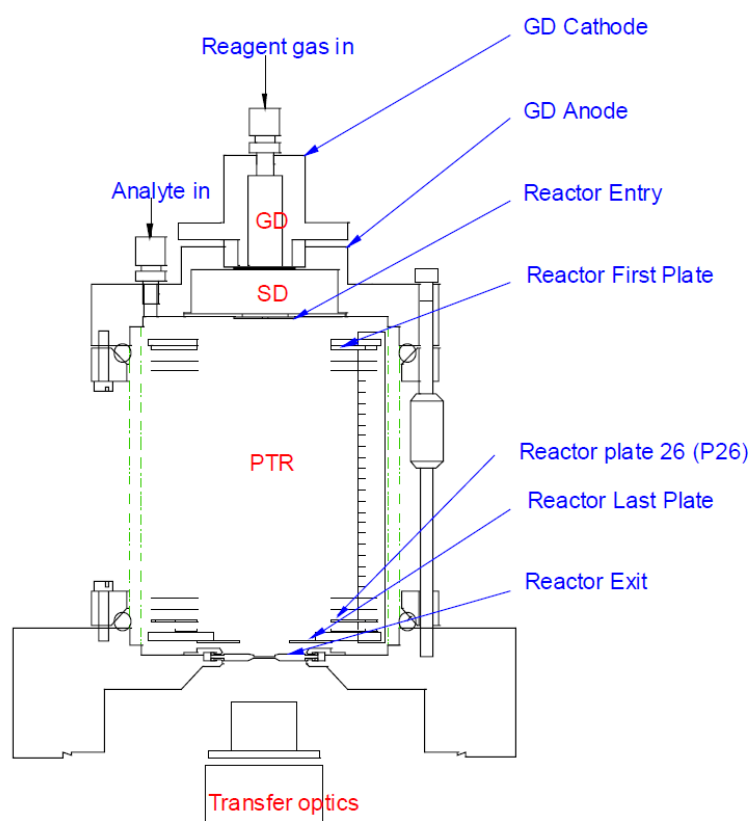


Figure 2-4. Schematic of the ion source and drift tube (reactor) on the Kore-ToF (Kore-Technology-Ltd, 2010).

The reactor exit aperture is 0.2 - 0.5 mm in diameter and the following transfer chamber is pumped by a 250 l s^{-1} turbomolecular pump. The transfer optics

consist of an einzel lens that helps to focus the stream of ions in this area in order to have a focused beam pass into the ToF source. As the ions leave the final element in the transfer assembly they are effectively free from the interaction with electric fields and continue moving through the ToF source. At regular intervals ($\sim 50 \mu\text{s}$), a pulse of -380 V is provided by a pulse extractor unit which fires a packet of ions into the flight tube (Kore-Technology-Ltd, 2010).

The ions are rapidly accelerated to $\sim 2 \text{ keV}$ and pass between two steering plates (that can be used to deflect the beam in the x and y axes) before entering a field-free region where they separate out temporally according to their m/z ratios. The ion beam then interacts with a reflectron assembly (ion mirror), as seen in Figure 2-3, which slows the ions before accelerating them back down the flight tube towards the detector (which is offset compared to the entry location).

The instrument is fitted with a flange mounted, large entrance ($8 \text{ mm} \times 32 \text{ mm}$), discrete dynode detector that detects the ions arriving at the end of the flight zone. A TDC records the arrival time of each ion and software can then be used to convert this time into a mass.

The vacuum system consists of a rotary pump that not only provides the vacuum for the drift tube region, but also doubles as a backing pump for the two turbomolecular pumps present on the instruments. One turbomolecular pump is present in the intermediary region, where the transfer optics are located, whilst the second turbomolecular pump is connected to the flight tube.

This set-up successfully takes atmospheric pressure gases, and through a system of mass flow controllers, critical orifices and pumps, allows for appropriate pressures at all stages. Thus the pressures is $\sim 1 \text{ mbar}$ in the drift tube, $\sim 10^{-4} \text{ mbar}$ in the transfer optics and finally $\sim 10^{-7} \text{ mbar}$ in the flight tube.

2.5.2 Leicester ToF

The LE-ToF is similar to the Kore-ToF in several respects and therefore this section, whilst including relevant detail, will be shorter than the account of the Kore-ToF.

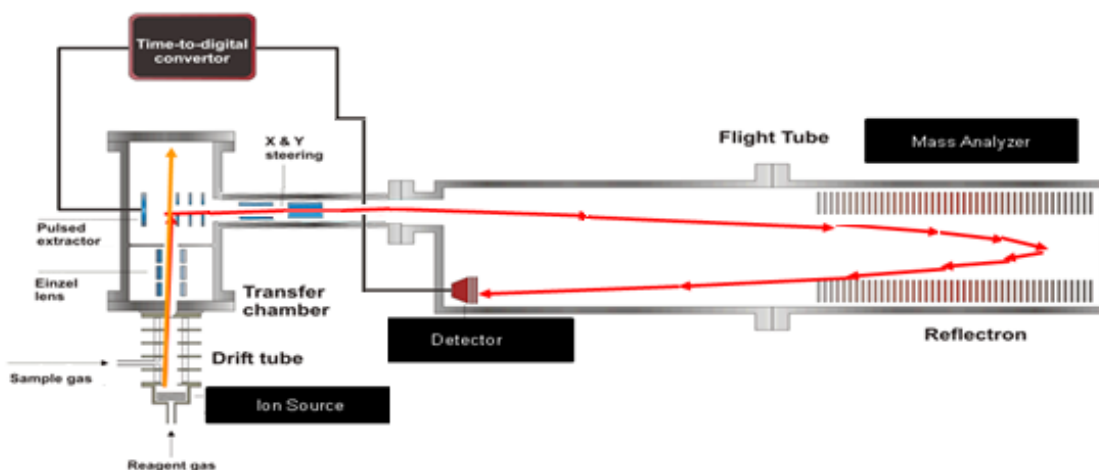


Figure 2-5. Schematic of the Leicester-ToF showing the drift tube, transfer chamber, mass analyser and detector.

The LE-ToF (Figure 2-5) utilises a radioactive (^{241}Am , 1.2 mCi, standard film, NRD Inc., Grand Island, NY) ion source as opposed to the hollow cathode discharge source in the Kore-ToF. This ion source is based around a radioactive americium band, which ionises water to hydronium through the emission of alpha particles. Water vapour generation comes from a bubbler set-up, in which a stream of pure nitrogen is passed through liquid water and is fed in to the top of the drift tube for ionisation. The drift tube is normally operated at ~6 mbar and at a voltage of ~2000-2500 V over the length of the drift tube, dependent upon experimental set-up. The ions then pass through two orifices (200 μm and 3 mm) before entering the ion transfer assembly, which consists of a three element einzel lens. Much like the Kore-ToF the ions are then pulsed into the flight tube, also a reflectron, before striking the detector.

For the LE-ToF a microchannel plate (MCP) detector is employed whilst counting of ions is provided by a TDC.

The system is pumped by three turbomolecular pumps (the transfer lens assembly and flight tube), as well as a rotary roughing pump for the drift tube. This pumping system is described in detail elsewhere (Blake, 2005).

2.5.3 Comparison of instrumentation

A general comparison of the instrumentation used in this thesis has been collated in Table 2-3 to aid the reader in understanding the differences and comparisons.

Table 2-3. A comparison of the mass spectrometers used throughout this thesis.

	LE ToF	Kore ToF, RF mode	Kore ToF, DC mode
Hydronium source	Bubbler	Vacuum water chamber	Vacuum water chamber
Ionisation source	Radioactive	Hollow Cathode	Hollow Cathode
Length of drift tube / cm	15	10	10
Length of flight tube / cm	109	45	45
Detector	MCP	Discrete dynode (m/z 19 blanked)	Discrete dynode
Binning parameters / amu^{-1}	100	20	20
Drift cell pressure / mbar	~ 6	$\sim 1-2$	~ 1.2
Flight tube pressure / mbar	9×10^{-7}	1×10^{-7}	1×10^{-7}
Drift Voltage / V	~ 2190	~ 80	~ 400
RF Voltage / V	N/A	200	N/A

2.5.4 Instruments used in each study

Throughout this thesis the three instruments previously mentioned in this chapter were used in a range of studies/ field campaigns. The instruments used in each study/ field campaign is listed below in Table 2-4.

Table 2-4. Details of the instruments used in each study/ field campaign.

Study/ field campaign details	Thesis section	Instrument name
Ion funnel PTR comparison	Chapter 3	Kore ToF, RF mode Kore ToF, DC mode
Nitrogen / argon buffer gas comparison	Chapter 4	LE ToF
ClearfLo Winter IOP	Chapter 5, section 5.2.1	Kore ToF
ClearfLo summer IOP	Chapter 5 section 5.2.2	Kore ToF, RF mode
Acidpruf chamber study	Chapter 5 section 5.2.4	Kore ToF, DC mode

2.6 Validation and quantification

2.6.1 Data normalisation

The data have been normalised so that a comparison between mass spectra obtained on different instruments or with different settings can be made. The quantity of ions detected varies from one instrument to another. In addition, for a single instrument the ion count rate can change when different settings are used, and can indeed change over time for fixed settings because of electronic voltage drifts or changes in other parameters. For this reason it is generally accepted that by 'normalising' the counts of m/z 19 hydronium to some standard value, this will reduce or increase all of the other peaks in the spectra proportionally so a fair comparison can be made between different data sets.

Data normalisation was carried out as per the following protocol. The signal obtained at m/z 19 (hydronium) was normalised to 10^6 counts. However, due to high signals at m/z 19 (especially in RF-mode on the Kore-ToF), dead time loss becomes a problem. The detector operates at a maximum detection rate of 33 kHz, meaning it can detect 33,000 ions s^{-1} for a given mass channel. If any ion reaches the detector in higher quantities than this value, then not all of the ions can be measured. To overcome this limitation, one can look at an alternative mass channel for a less abundant isotope. For example $H_3^{18}O^+$ occurs at m/z 21 and ^{18}O has a natural abundance 496 times less than ^{16}O . Consequently, analyte signals are normalised using the $H_3^{18}O^+$ signal and then the overall signal is normalised with respect to 10^6 counts of $H_3^{16}O^+$.

2.6.2 Calibration

To be able to quantitatively ascertain the concentration of a compound, the instrument requires calibration. For accurate calibration of the PTR-ToF-MS, it is essential to be able to create a steady, consistent concentration of calibration gas. Possible types of calibration sources include a permeation tube containing the compound of interest, a small amount of the compound vaporised in a tedlar bag or a calibration gas standard in a cylinder. All three of these are described below. Using these three methods it is possible to calibrate with a wide variety

of gases, over several orders of magnitude in concentration and at different humidities. It is also important when calibrating to do a multipoint calibration (i.e. calibrations carried out over a range of different concentrations) to not only reduce error, but to also determine the linear operating range of the PTR-ToF-MS. Each concentration (independent of the calibration method used) was analysed for at least 30 minutes, with the first ten minutes discarded to allow for complete equilibrium of the gas mixture.

2.6.2.1 Gas standard cylinder

Gas standard calibration cylinders (BOC special gases, UK) are premade cylinders ordered with a set concentration of VOC(s) present and are made up with either nitrogen or synthetic 'air' (80 % N₂, 20 % O₂) as the balance gas. The calibration cylinder used as part of the calibration process in this thesis contained a mixture of seven VOCs with a mixing ratio of ~1 ppmV. These were methanol, acetaldehyde, trans-2-butene, acetone, methacrolein, cyclohexanone and β-caryophyllene in a balance gas of nitrogen. A dynamic dilution was carried out using two (alicat) mass flow controllers (MFC), with one (a 500 mL min⁻¹) controlling the calibrant cylinder and another (a 5L mL min⁻¹) controlling a diluent gas before entering the drift tube.

2.6.2.2 Permeation tubes

A permeation tube (Eco-scientific, UK) consists of a tube with permeable ends that allows the emission of a calibration compound at a consistent rate. The rate of emission is calculated by the loss of mass of the calibrant, in our case a VOC, over time at a particular temperature and is calibrated (by Kin-tek laboratories, UK) to an accuracy of +/-2 % and certified typically for 6-12 months. The concentration under 0 % relative humidity conditions (C_{RH0}) can be calculated using equation E 2-17 below, where E = the emission rate (ng min⁻¹), K_0 = the conversion factor from mass emission rate to volumetric emission and is compound specific (ng min⁻¹), and F_D = the gas flow (L min⁻¹).

$$C_{RH0} = \frac{(E K_0)}{1000 F_D} \quad \text{E 2-17}$$

As the temperature is increased, the permeation tube emits at a faster rate and so it is crucial to keep the tube at a constant temperature, as even a small change in temperature can seriously affect the rate of emission. The fixed-temperature housing was provided by a Kin-tek laboratories model 491 permeation oven with a temperature-controlled heating block keeping the temperature stable to ± 0.1 °C. The permeation oven allows for a gas flow of up to 10 L min^{-1} to be used, allowing for a wide range of concentrations to be selected for a particular permeation tube. The unit houses a second heating block, so that a permeation tube certified for operations at a different temperature to the first can be added, allowing for a wider range of options when creating a complex calibration mixture. There is also a humidifying module, allowing for humid gas to be created and thus a humid calibrant sample. This is useful when determining the sensitivities for VOCs undergoing proton transfer with hydronium, as the sensitivity of the analyte will be altered by a change in humidity which can be seen in Figure 2-6.

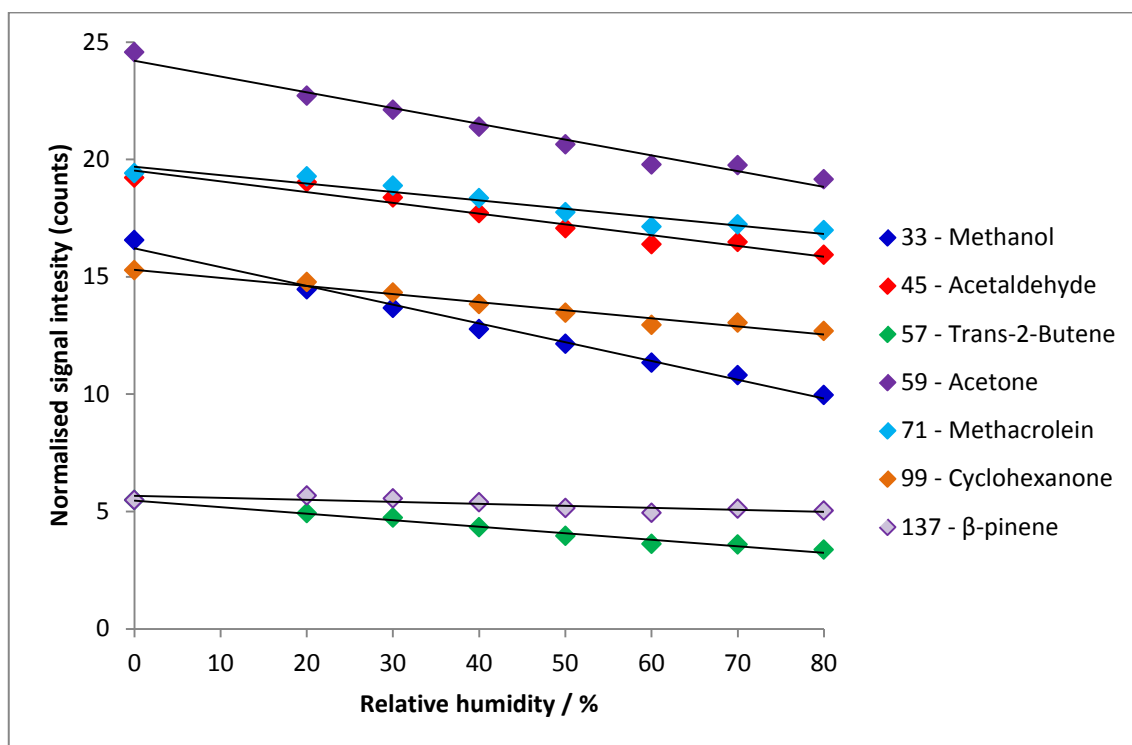


Figure 2-6. Humidity dependence of various compounds carried out on the Kore-ToF.

2.6.2.3 Tedlar bag dilution

An alternative to pre-certified calibration standards, such as a gas standard cylinder or permeation tube, is a tedlar bag dilution. First, a small quantity (1-10 μL ($\pm 0.1 \mu\text{L}$ using a 10 μL Hamilton syringe) of liquid VOC (Fischer, Sigma Aldrich) is injected into small beaker of 1-10 mL of hexane (Sigma Aldrich).

A 10 L bag is filled with 5.0 L of balance gas (either nitrogen or synthetic air) and then 1-10 μL of the VOC/hexane mixture is injected in to the bag and topped up with 5.0 L to a total of $10.0 \pm 0.1 \text{ L}$, in order to provide a thorough mixing environment and the required concentration. The resultant bag mixture is then directed into the PTR-ToF-MS and its flow is controlled by an MFC. If the VOC in question has a low vapour pressure, such as a long chain alkane, then a heat lamp was employed to raise the temperature to aid volatilisation.

Whilst this method has several steps and thus more opportunity for error propagation, it has proved useful as all that is required are readily available liquid samples of VOCs as opposed to pre-certified gas cylinder standards, which require time to order and certify. Certified calibration samples are also expensive to buy and can only be obtained for a limited selection of VOCs.

2.6.3 Sensitivity and limit of detection

2.6.3.1 Determining the concentration via the sensitivity

For a single point calibration, the average counts for a particular mass channel during a background run is recorded over a minimum of ten runs, and this is subtracted from the calibration run, also over a minimum of ten runs. The remaining number of counts is then divided by the time taken for analysis (i.e. 60 s) and the concentration used in the calibration.

Alternatively, the gradient on a multipoint calibration plot (counts verses concentration, where the concentration is background subtracted) also gives the sensitivity. Either of these methods can be employed, but it should be noted that

if using normalised counts, then there is no need to divide by the run time as the length of run time becomes irrelevant.

If for some reason the sensitivity is required for a compound that is unavailable then a theoretical estimate can be made to determine the concentration of the compound in question (Ellis and Mayhew, 2014) using equation E 2-18, where M_{VMR} is the volume mixing ratio (VMR) of the analyte in ppbV, k is the rate coefficient for reaction of the analyte with H_3O^+ , t is the reaction time, and N_d is the number density.

$$M_{VMR} = \left(\frac{MH^+}{H_3O^+} \right) \frac{1 \cdot 10^9}{kt N_d} \quad \text{E 2-18}$$

The *VMR* is used instead of standard concentration units in PTR-MS as this quantity is the same in the drift tube as it is in the atmospheric analyte.

2.6.3.2 Precision

It is essential that the precision on any given mass channel is thoroughly understood and the error reduced as much as reasonably possible in order to give the best limit of detection (LoD) as detailed in section 2.6.3.3. The signal from a calibration of bromobenzene (m/z 159) was monitored for several hours on the Kore-ToF in RF mode and is shown in Figure 2-7. The standard deviation was calculated for different data acquisition times and is shown in Figure 2-8 as a scatter plot of $\log_{10}(\text{SD}/ \text{ppbV})$ versus $\log_{10}(\text{time}/ \text{min})$. The gradient = -0.42 ± 0.04 and $r^2 = 0.95$. For randomised noise on a signal, the expected gradient would be -0.5 . A gradient of -0.42 is very reasonable, however the lower value indicates that there is instrumental drift (an increase in sensitivity in this case) and this can be seen in Figure 2-7.

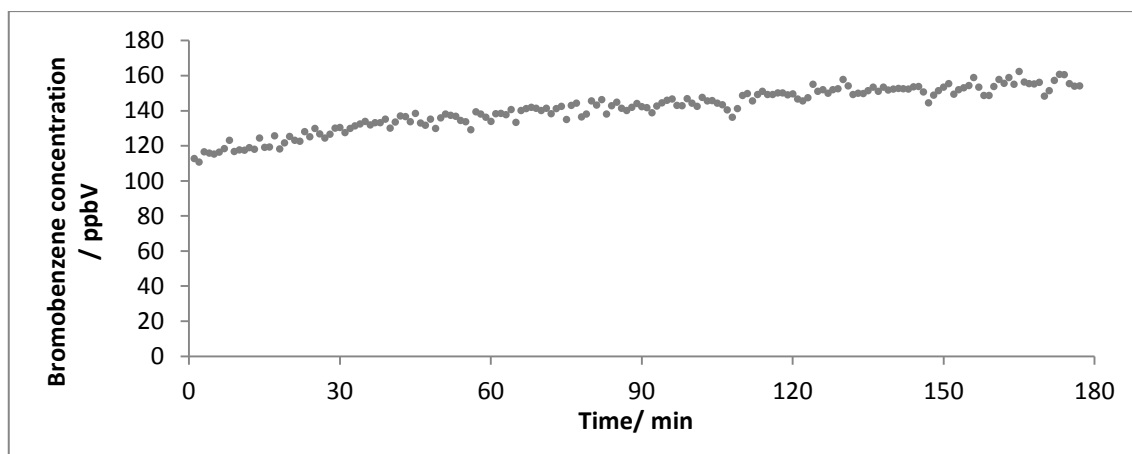


Figure 2-7. Time series of signal intensity as measured at m/z 159 (bromobenzene) illustrating instrumental drift over a period of 3 h).

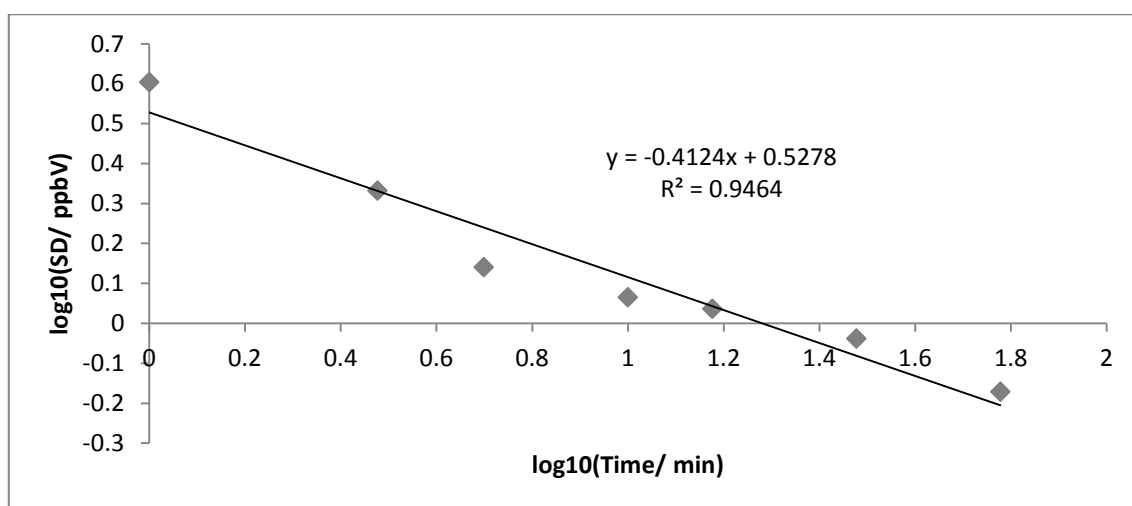


Figure 2-8. Data demonstrating instrument stability for m/z 159 (bromobenzene).

2.6.3.3 Limit of detection

Usually the LoD is calculated from normalised data. First, the signal to noise must be calculated using equation E 2-19 where S is the background-subtracted average signal from the analyte (over a minimum of ten data acquisitions) and σ_{bckgd} is the standard deviation of the background signal (over a minimum of ten data acquisitions).

$$\left(\frac{S}{N}\right) = \frac{S}{\sigma_{bckgd}} \quad \text{E 2-19}$$

The LoD_M can then be calculated using equation E 2-20 where M_{VMR} is the concentration of the analyte used in the calibration.

$$LoD_M = \frac{3 \cdot M_{VMR}}{\left(\frac{S}{N}\right)} \quad \text{E 2-20}$$

The LoD is a time-dependent quantity. As the length of the data acquisition increases, the signal-to-noise ratio improves and therefore a lower (better) LoD will be achieved. Specifically the LoD reduces with \sqrt{n} , where n is the time of the data acquisition period.

2.7 References

- BARBER, S., BLAKE, R. S., WHITE, I. R., MONKS, P. S., REICH, F., MULLOCK, S. & ELLIS, A. M. 2012. Increased sensitivity in proton transfer reaction mass spectrometry by incorporation of a radio frequency ion funnel. *Anal Chem*, 84, 5387-91.
- BLAKE, R. 2005. *Monitoring tropospheric composition using time of flight chemical ionisation mass spectrometric techniques*. PhD, University of Leicester, UK.
- BLAKE, R. S., WHYTE, C., HUGHES, C. O., ELLIS, A. M. & MONKS, P. S. 2004. Demonstration of proton-transfer reaction time-of-flight mass spectrometry for real-time analysis of trace volatile organic compounds. *Analytical Chemistry*, 76, 3841-3845.
- BLAKE, R. S., WYCHE, K. P., ELLIS, A. M. & MONKS, P. S. 2006. Chemical ionization reaction time-of-flight mass spectrometry: Multi-reagent analysis for determination of trace gas composition. *International Journal of Mass Spectrometry*, 254, 85-93.
- BLEAKNEY, W. 1929. A New Method of Positive Ray Analysis and Its Application to the Measurement of Ionization Potentials in Mercury Vapor. *Physical Review*, 34, 157-160.
- BOESL, U., WEINKAUF, R. & SCHLAG, E. 1992. Reflectron time-of-flight mass spectrometry and laser excitation for the analysis of neutrals, ionized molecules and secondary fragments. *International Journal of Mass Spectrometry and Ion Processes*, 112, 121-166.
- DAVIS, R. & FREARSON, M. 1987. *Mass Spectrometry – Analytical Chemistry by Open Learning*, London, John Wiley & Sons.
- ELLIS, A. M. & MAYHEW, C. A. 2014. *Proton Transfer Reaction Mass Spectrometry: Principles and Applications*, Wiley.
- FERNANDEZ, M. T., WILLIAMS, C., MASON, R. S. & CABRAL, B. J. C. 1998. Experimental and theoretical proton affinity of limonene. *Journal of the Chemical Society, Faraday Transactions*, 94, 1427-1430.
- GLENN, J. W. E. 1956. Time-of-flight mass spectrometer. Google Patents.
- GOEBBERT, D. J. & WENTOLD, P. G. 2004. Water dimer proton affinity from the kinetic method: dissociation energy of the water dimer. *European Journal of Mass Spectrometry*, 10, 837-846.
- GRAYSON, M. A. 2002. *Measuring Mass: From Positive Rays to Proteins.*, Philadelphia, PA, Chemical Heritage Press.
- HANSON, D., GREENBERG, J., HENRY, B. & KOSCIUCH, E. 2003. Proton transfer reaction mass spectrometry at high drift tube pressure. *International Journal of Mass Spectrometry*, 223, 507-518.
- HARRISON, A. G. 1983. *Chemical Ionisation Mass Spectrometry*, Boca Raton, FL, CRC Press.
- INOMATA, S., TANIMOTO, H. & AOKI, N. 2008. Proton transfer reaction time-of-flight mass spectrometry at low drift-tube field-strengths using an H₂O–rare gas discharge-based ion source. *J. Mass Spectrom. Soc. Jpn*, 56, 181-187.
- KARL, T., HANSEL, A., CAPPELLIN, L., KASER, L., HERDLINGER-BLATT, I. & JUD, W. 2012. Selective measurements of isoprene and 2-methyl-3-buten-2-ol based on NO⁺ ionization mass spectrometry. *Atmospheric Chemistry and Physics*, 12, 11877-11884.
- KORE-TECHNOLOGY-LTD 2010. PTR TOF-MS User Guide.

Chapter two: Instrumental

- LINDINGER, W., HANSEL, A. & JORDAN, A. 1998. On-line monitoring of volatile organic compounds at pptv levels by means of proton-transfer-reaction mass spectrometry (PTR-MS) medical applications, food control and environmental research. *International Journal of Mass Spectrometry and Ion Processes*, 173, 191-241.
- MAMYRIN, B., KARATAEV, V., SHMIKK, D. & ZAGULIN, V. 1973. The massreflect ron, a new non-magnetic time-of-flight mass spectrometer with high resolution. *Zh. Eksp. Teor. Fiz*, 64, 82-89.
- MIRSALEH-KOHAN, N., ROBERTSON, W. D. & COMPTON, R. N. 2008. Electron ionization time-of-flight mass spectrometry: Historical review and current applications. *Mass Spectrometry Reviews*, 27, 237-285.
- NORMAN, M., HANSEL, A. & WISTHALER, A. 2007. O_2^+ as reagent ion in the PTR-MS instrument: detection of gas-phase ammonia. *International Journal of Mass Spectrometry*, 265, 382-387.
- TANG, X., BEAVIS, R., ENS, W., LAFORTUNE, F., SCHUELER, B. & STANDING, K. 1988. A secondary ion time-of-flight mass spectrometer with an ion mirror. *International journal of mass spectrometry and ion processes*, 85, 43-67.
- WILEY, W. & MCLAREN, I. H. 1955. Time-of-flight mass spectrometer with improved resolution. *Review of Scientific Instruments*, 26, 1150-1157.
- ZHAO, J. & ZHANG, R. 2004. Proton transfer reaction rate constants between hydronium ion (H_3O^+) and volatile organic compounds. *Atmospheric Environment*, 38, 2177-2185.

3 Chapter three: Characterisation of a PTR-ToF-MS fitted with a radio frequency ion funnel

3.1 Introduction

The performance of the mass spectrometer is critical to the ultimate detection sensitivity available in PTR-MS and is a topic that has been discussed in detail elsewhere (Blake et al., 2009, Ellis and Mayhew, 2014). However, sensitivity is not determined solely by the ion production method, mass analyser and detector. Another factor which critically limits the detection sensitivity derives from the small exit aperture at the end of the drift tube: this size of aperture is necessary to maintain a sufficiently low pressure in the mass spectrometer while sustaining a pressure in the drift tube which is several orders of magnitude higher. Ordinarily, the vast majority of ions traversing the drift tube do not exit through this aperture, and so a large quantity of potentially useable ion signal is wasted.

This chapter will describe a method for dramatically increasing the proportion of ions that can pass from the drift tube into the mass spectrometer. The challenge is to take ions that are flowing through a region of relatively large volume and at a pressure of a few mbar (a typical pressure for a PTR-MS drift tube) and channel them through a small aperture into a much lower pressure zone. This challenge is not unique to PTR-MS: for example, it is encountered in mass spectrometers equipped with an electrospray ionisation source (Tahallah et al., 2001). The electrospray source delivers liquid at atmospheric pressure into an electrically charged capillary and the subsequent formation of ions, as the analyte leaves the capillary, occurs in a region where the optimum pressure is a few mbar. A series of differential pumping stages can then be employed to eventually deliver the ions to a mass spectrometer. The loss of ions through these pumping stages can be mitigated to some extent by the use of one or

Chapter three: Characterisation of a PTR-ToF-MS fitted with a radio frequency ion funnel

more multipole ion guides, but major losses still occur. In particular, ion guides are excellent for the collisional focusing of already relatively narrow beams of ions, but are ineffective for diffuse ion sources.

A novel solution to this problem was developed by Smith and co-workers in the late 1990s: the RF ion funnel (Shaffer et al., 1997). This RF funnel uses a series of electrodes with progressively reducing aperture sizes. A DC electrical field drives the ions axially through the funnel towards the exit aperture. In addition, an AC electric field is provided at a RF such that adjacent electrodes have opposite voltage polarities in the AC component. The RF field creates a strongly repulsive effective potential near the surface of each electrode which, coupled with the progressively diminishing aperture size, serves to focus the ions radially. This focusing effect can deliver a large increase in ion flux through the exit aperture and thus a large increase in signal at a downstream mass spectrometer. Various modifications have been made to the ion funnel design since its initial introduction (Shaffer et al., 1999, Kim et al., 2000, Julian et al., 2005, Ibrahim et al., 2006) and this has been supported by an improved understanding of the ion motion through trajectory simulations (Shaffer et al., 1999, Julian et al., 2005, Lynn et al., 2000, Tolmachev et al., 2000).

Here the RF ion funnel concept is combined with PTR-ToF-MS (RF-PTR-ToF-MS) for the first time with the majority of this material having been previously published in 2012 (Barber et al., 2012). The rationale behind this comes from the fact that the optimum pressure for operation of an RF ion funnel is close to the typical operating pressure of a drift tube in PTR-MS. This suggests that it might be possible to construct a compact drift tube which can simultaneously operate as an ion funnel and as an ion-molecule reaction vessel with a fixed reaction time. This idea has been proposed and demonstrated previously in the context of ion mobility spectrometry (Baker et al., 2007) but not for PTR-MS. This chapter describes a prototype design and explores its initial application in PTR-MS. An improvement in the detection sensitivity of between one and two orders of magnitude is observed for most of the test gases, which suggests that

Chapter three: Characterisation of a PTR-ToF-MS fitted with a radio frequency ion funnel

the RF ion funnel/drift tube may significantly enhance the performance of PTR-MS.

Chapter three: Characterisation of a PTR-ToF-MS fitted with a radio frequency ion funnel

3.2 Experimental

3.2.1 The standard PTR-MS apparatus

As described in more detail in chapter 2, the standard PTR-MS instrument consists of a hollow cathode discharge ion source, a drift tube and ion transfer lens assembly, and a reflectron TOF-MS. H_3O^+ ions are generated via a DC electrical discharge through water vapour. After passing through a source drift region, which maximizes the production of H_3O^+ , the ions then pass through a 2 mm aperture into the drift tube, where they encounter the analyte. The drift tube is pumped by a mechanical pump with an effective speed of $\sim 3 \text{ l s}^{-1}$, and a pressure of $\sim 1 \text{ mbar}$ is maintained in this region under normal operating conditions.

In the standard PTR-MS version of this instrument the drift tube consists of a series of equally spaced disk electrodes with a central aperture of 40 mm diameter. This arrangement delivers a uniform electric field along the drift tube. In the current study the electrode structure is modified to allow part of the drift tube to act as an ion funnel, as described in a separate section below. At the end of the drift tube is a 400 μm orifice, which allows ions to enter the ion transfer zone for the ToF-MS. This ion transfer assembly consists of collection/collimating optics and feeds ions into the source region of the reflectron ToF-MS. The reflectron, which is pumped by a 70 l s^{-1} turbomolecular pump, has a total effective ion flight path of $\sim 1.2 \text{ m}$. Ions are detected at the end of their trajectory by a large entrance (8 mm \times 32 mm) discrete dynode detector. The ion signal is then amplified and fed into a proprietary pulse counting system for data acquisition, which consists of a TDC interfaced to a PC. Data display and processing was carried out using the GRAMS software package provided by the manufacturer.

3.2.2 Modified ion funnel/drift tube

The ion funnel consists of 29 stainless steel plates of 0.2 mm thickness mounted on precision machined ceramic rods at an even spacing of 3.2 mm per plate. The orifice diameters of the plates through the first half of the stack is 40

Chapter three: Characterisation of a PTR-ToF-MS fitted with a radio frequency ion funnel

mm, as used in the standard drift tube reactor. In the second half of the drift tube, the orifice diameter steadily decreases to 6 mm at the final plate before the exit orifice.

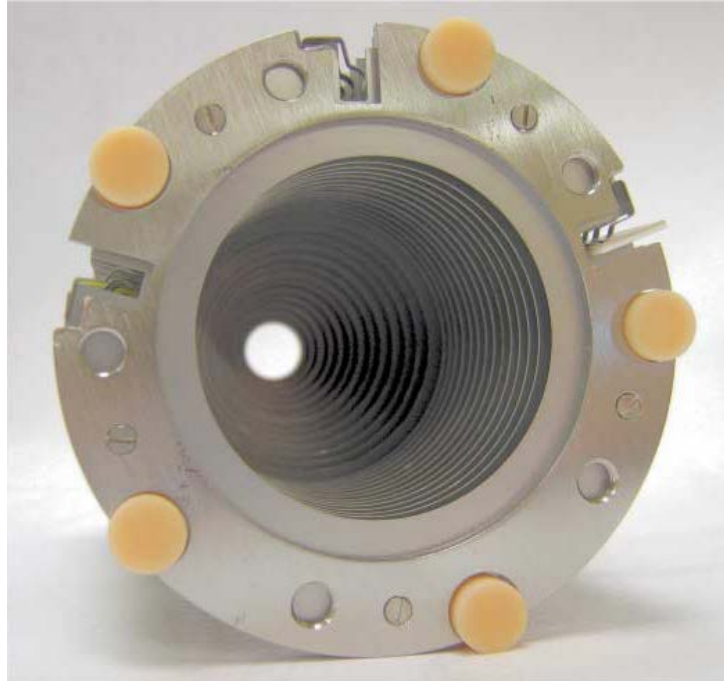


Figure 3-1. Image of ion funnel electrodes with a large diameter tapering down to a smaller internal diameter. The 5 ceramic support rods can also be seen.

To avoid the trapping of ions in axial potential wells (where the ions can still exit the final orifice), particularly those with low m/z , the following condition must be satisfied (Kelly et al., 2010),

$$2\pi \frac{\rho}{\delta} \exp\left(\frac{-2\rho}{\delta}\right) \ll 1$$

where ρ = electrode orifice diameter and $\delta = d/\pi$ where d = electrode spacing. The above condition is easily satisfied for the electrode geometries used in this work.

The path of the ions through the ion funnel are essentially linear, until they come into proximity with the electrodes at which point they are funnelled

Chapter three: Characterisation of a PTR-ToF-MS fitted with a radio frequency ion funnel

towards the exit aperture, the trajectories have been simulated in Figure 3-2 by Lynn and co-workers.

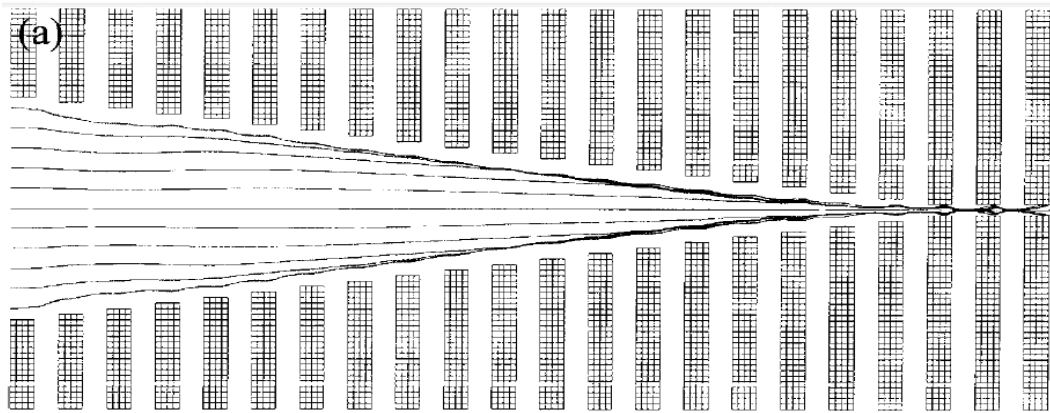


Figure 3-2. Simulated ion trajectory (black lines) along a drift tube with cylindrical electrodes. The ions travel from left to right, interacting with the RF field near the electrode face (Lynn et al., 2000).

A resistive divider, consisting of a ceramic substrate patterned with thin film resistors, is used to deliver the static voltages to individual plates, with vacuum feedthroughs providing connections to the ends of the divider. The DC voltage across the reactor may be varied between 30 and 450 V. When operating in RF mode, (i.e. with the addition of the RF field), the lower end of this scale gave the best results in terms of detection sensitivity. Capacitor chains are used to feed a balanced RF input voltage to the plates in the downstream half of the drift tube.

The RF voltage is provided by a proprietary AC generator whose output transformer is arranged to be in resonance with the load capacitance. This resonance is used to achieve a roughly sinusoidal waveform at around 800 kHz, with adjustable amplitude up to about 200 V peak to peak.

Table 3-1 provides information relating to the internal dimensions and spacing of the electrodes within the modified ion funnel drift tube and a model example of the geometry of the electrodes is shown in Figure 3-3.

Chapter three: Characterisation of a PTR-ToF-MS fitted with a radio frequency ion funnel

Table 3-1. Electrode dimensions and spacings used in the modified radio frequency ion funnel.

Electrode number	Internal diameter / mm	Length / mm
1-14	40.0	13.4
15	36.8	15.0
16	34.8	16.0
17	32.8	17.0
18	30.4	18.2
19	28.0	19.4
20	26.0	20.4
21	23.6	21.6
22	21.6	22.6
23	18.8	24.0
24	16.8	25.0
25	14.4	26.2
26	12.4	27.2
27	10.0	28.4
28	8.0	29.4
29	6.0	30.4

In Figure 3-3 the ions enter from the left and are accelerated to the right through combination of the DC electric field and the RF electric field.

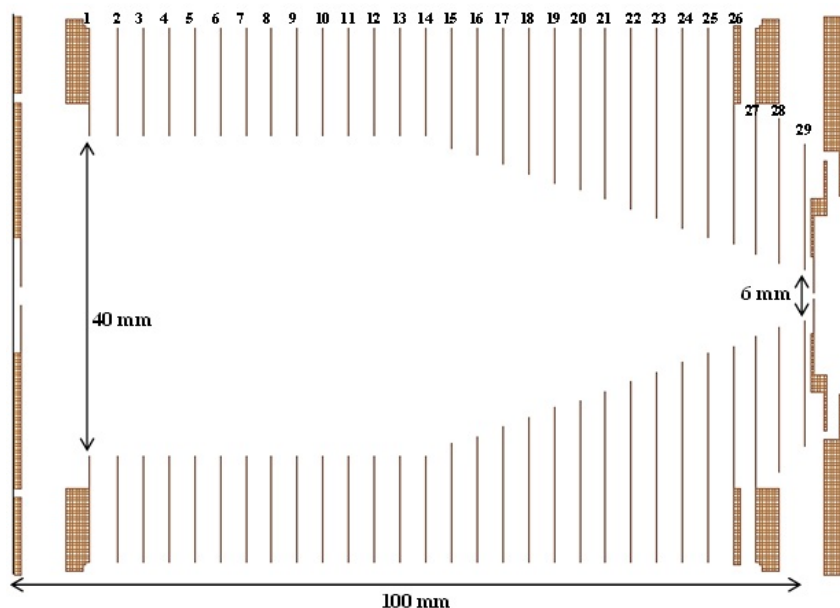


Figure 3-3. Radio frequency ion funnel illustrating the electrode positioning. Taken from a Simion© simulation carried out by E. James, a student at the University of Leicester.

The packet of ions travels down the flight tube in a field-free region, but due to the fact they have ~10 eV of kinetic energy (KE) perpendicular to the flight tube (the initial velocity), they enter the flight tube at a slight angle, hence the

Chapter three: Characterisation of a PTR-ToF-MS fitted with a radio frequency ion funnel

detector is off centre with respect to the centre of the flight tube. Due to the large increase in signal when in the RF mode (see the following section), with hydronium being by far the most prevalent ion, a decision was made to blank mass channel 19 on the detector to preserve the lifetime of the detector, as discussed below.

3.2.3 Detector blanking

Due to the increased ion count expected to reach the detector with the modified drift tube, a decision was taken to limit the wear and increase the operational lifetime of the detector. Most of the wear on a discrete dynode detector occurs on the last few plates, as this is where the highest number of electron impacts takes place so it is crucial that these are reduced to an acceptable level. The blanking procedure still allows the ions at m/z 19 to hit the first dynode but the voltage on the second dynode is momentarily raised to the same potential as the first, resulting in no cascade of electrons. This pulse is synchronised to occur just before the time when an ion corresponding to m/z 19 would strike the detector and lasts until just after that point, such that it does not affect the detection of ions above, or below that of m/z 19. The pulse leaves trace signals on the resulting spectra, one just before the m/z 19 peak and one just after. It is crucial to remember that these two signals are not ions and can be discarded.

3.2.4 Operating conditions

The ion funnel delivered a large increase in the H_3O^+ ion count rate detected at m/z 19 when compared to when the ion funnel is not in use. For the optimized ion funnel, a reading of 6×10^6 Hz was observed, whereas in the optimized DC-only mode using exactly the same electrode configuration, an H_3O^+ count rate of 5×10^5 Hz was observed. The factor of 12 higher ion count rate in the RF mode is exactly what was being sought, but it also has the disadvantage of contributing to rapid degradation of the ion detector if allowed to persist, as well as overloading the TDC. The ToF-MS detector was therefore equipped with a purpose-built gating system to prevent ions with m/z 19 from generating a cascade of electrons and hence wear in the detector as discussed in section 3.2.3. Instead, the H_3O^+ count rate was deduced by monitoring the $\text{H}_3^{18}\text{O}^+$

Chapter three: Characterisation of a PTR-ToF-MS fitted with a radio frequency ion funnel

signal at m/z 21 and using the known $^{16}\text{O}:^{18}\text{O}$ natural abundance ratio (496:1) to determine the count rate of H_3O^+ .

3.2.4.1 Gas delivery

Gas delivery was carried out using MFCs to deliver the analytes into the drift tube at a typical flow rate of 85 mL min^{-1} . To assess the analytical performance, a variety of VOCs at known concentrations were delivered in both the DC-only and RF funnel modes of operation. The source of gases was a calibrated gas mixture, from a gas cylinder, containing methanol, acetaldehyde, trans-2-butene, acetone, methacrolein, cyclohexanone, and β -pinene at known concentrations (BOC Special Gases; nominal mixing ratio 1 ppmV for each compound, with an estimated uncertainty of $\pm 10 \%$) in a balance gas of nitrogen. These compounds were chosen for several reasons; they have a wide mass range, m/z 33 - m/z 137 for the protonated parent ions, and they are a representative selection of different types of VOC including an alcohol, aldehyde, ketone, alkene and a mono-terpene. For these experiments, this mixture was subjected to a 10-fold static dilution to generate a new mixture with roughly 100 ppbV of each component, with the balance gas being nitrogen. Subsequent dilutions were then performed dynamically by feeding the cylinder gas into a gas standards generator (Kintek 491 M) and diluting in nitrogen.

Other compounds were also analysed, by using permeation tubes or Tedlar bag dilutions, to assess further sensitivity changes and fragmentation patterns. These methods of calibration have been discussed previously in Chapter 2.

3.3 Results and discussion

3.3.1 Preliminary observations

When the instrument was first operated in the RF mode, the optimised settings from the DC mode were used. This resulted in a very small count rate, and it was realised, not surprisingly, that different conditions would be needed to see an acceptable sensitivity. The voltages applied to the discharge ion source and drift tube had to be lowered markedly, from ~400 V at the start of the drift tube (PTR In) to ~80 V. The GD pressure was changed from 1.4 mbar to 1.9 mbar and the inlet flow rate reduced from 190 mL min⁻¹ to 85 mL min⁻¹. This means that in general, for E/N calculations, the nominal E has been reduced and N has been increased. However, this is an issue that will be discussed in more detail later in section 3.3.2.

3.3.1.1 Drift tube temperature

Figure 3-4 shows a comparison between the Limits of Detection (LoD) of isoprene when analysed under cold and hot conditions. This was investigated as it is often necessary to heat certain parts of the instrument or gas lines when analysing compounds that are easily deposited onto the inlet lines or the drift tube walls. All parameters other than the temperature were kept constant in this comparison.

The source and drift tube were heated by raising the overall ambient temperature by enclosing the drift tube in a heated enclosure (oven) and using a fan to circulate the warm air. There is also a heater on the flange between the end of the drift tube and the transfer region in order to stop this area acting as a significant heat sink. The flange (inlet reading) was heated to 100 °C and the ambient temperature in the oven (source reading) was heated to around 90 °C for these hot tests. The cold tests were conducted at 24 °C /room temperature. In Figure 1-3 it can be seen that at a higher temperature, the LoD worsens dramatically. This would indicate that it is beneficial to run the instrument at room temperature. The higher temperature increases the noise levels and also reduces the sensitivity of the instrument, creating a much worse signal-to-noise

Chapter three: Characterisation of a PTR-ToF-MS fitted with a radio frequency ion funnel

(*s/n*) ratio. The *S/N* ratio is essentially what controls the LoD; therefore if it is higher, a lower LoD can be achieved. In this instance, with isoprene being analysed, the cold *S/N* ratio is ~600 whereas the hot *S/N* ratio is ~7. The reason for the large increase in noise is likely to be that compounds on the surface of the instrument desorb and increase the quantity of background gas, and therefore the number of 'noise' ions detected. While this value has reduced over time as more contamination is removed through heating, the noise is still higher than if operated under cold conditions.

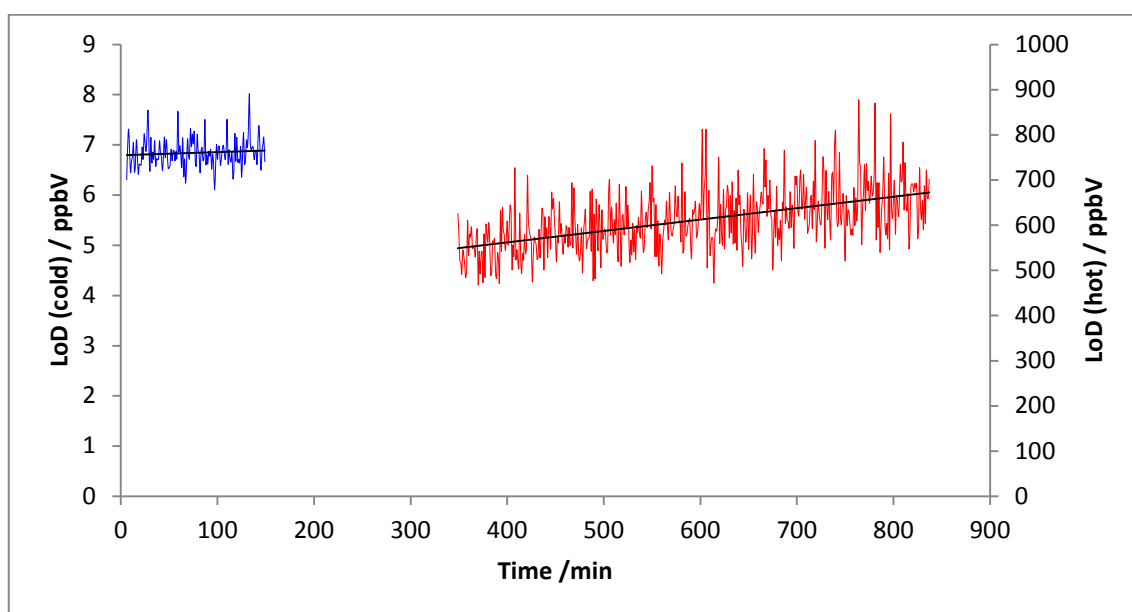


Figure 3-4. Comparison between the LoD of isoprene under different temperature conditions in the drift tube. The blue line represents the cooler room temperature (~24 °C) and the red line the hotter temperature (~100 °C).

3.3.2 Effective *E/N*

Application of an electric field along the drift tube draws ions through the reaction zone and delivers a series of energetic ion-molecule collisions, which serve to minimize the formation of cluster ions, particularly hydrated hydronium ions, $\text{H}_3\text{O}^+(\text{H}_2\text{O})_n$. Without this feature, both the mass spectrometric and the kinetic analysis would be excessively complex. The electrodes in a drift tube are normally equally spaced along the length of the tube, thus creating an axially uniform electric field. The standard means of expressing the drift tube

Chapter three: Characterisation of a PTR-ToF-MS fitted with a radio frequency ion funnel

conditions is through the quantity E/N , where E is the electric field and N is the number density of the gas.

For a standard drift tube containing gas at a known pressure and with a uniform DC electric field, E/N is a well-defined quantity. A typical operating E/N in PTR-MS is in the region of 120 Td. However, the effective E/N of a combined ion funnel/drift tube, with its contribution from both DC and AC electric fields, is no longer obvious. Here a simple empirical view is taken of the effective E/N by seeking operating conditions for the ion funnel/drift tube that match the performance of the same drift tube when operated under the optimum DC-only conditions (Figure 3-5).

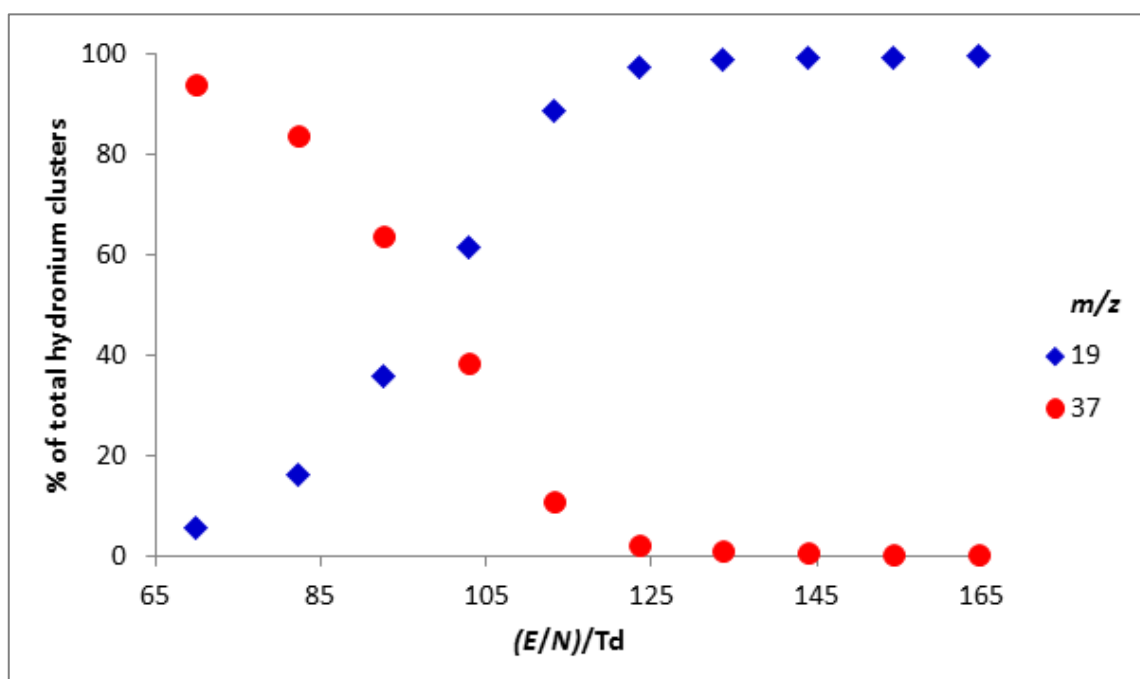


Figure 3-5. Water cluster distribution obtained under DC-only mode as a function of E/N .

The performance criterion used for this comparison is the degree of hydration of H_3O^+ . As mentioned above, under ideal conditions for PTR-MS, the H_3O^+ ion is by far the dominant source of protons. Figure 3-5 shows the signals observed in mass channels corresponding to both H_3O^+ and $H_3O^+(H_2O)$ as a function of E/N for the drift tube with the RF switched off and the DC voltage across the drift tube varied (to change the E/N). In this DC-only mode, the hydrated

Chapter three: Characterisation of a PTR-ToF-MS fitted with a radio frequency ion funnel

hydronium cluster ions dominate at low E/N but H_3O^+ becomes the most abundant ion at $E/N \approx 100$ Td. Ideal conditions for operating the drift tube in this mode of operation would be at $E/N \approx 125$ Td, since under these conditions less than 5 % of H_3O^+ is in its hydrated form. As mentioned previously, this is a fairly typical E/N value for PTR-MS and it shows that the modified electrode structure employed here, with the converging aperture sizes, does not have a major impact on the ion-molecule chemistry. Of course, one could operate at an even higher E/N , which would further reduce $\text{H}_3\text{O}^+(\text{H}_2\text{O})_n$ cluster levels relative to H_3O^+ through increasingly energetic ion-molecule collisions. However, this is generally undesirable if taken too far because it leads to excessive fragmentation of protonated analyte ions and can lead to a decrease in sensitivity as the reaction time for proton transfer decreases.

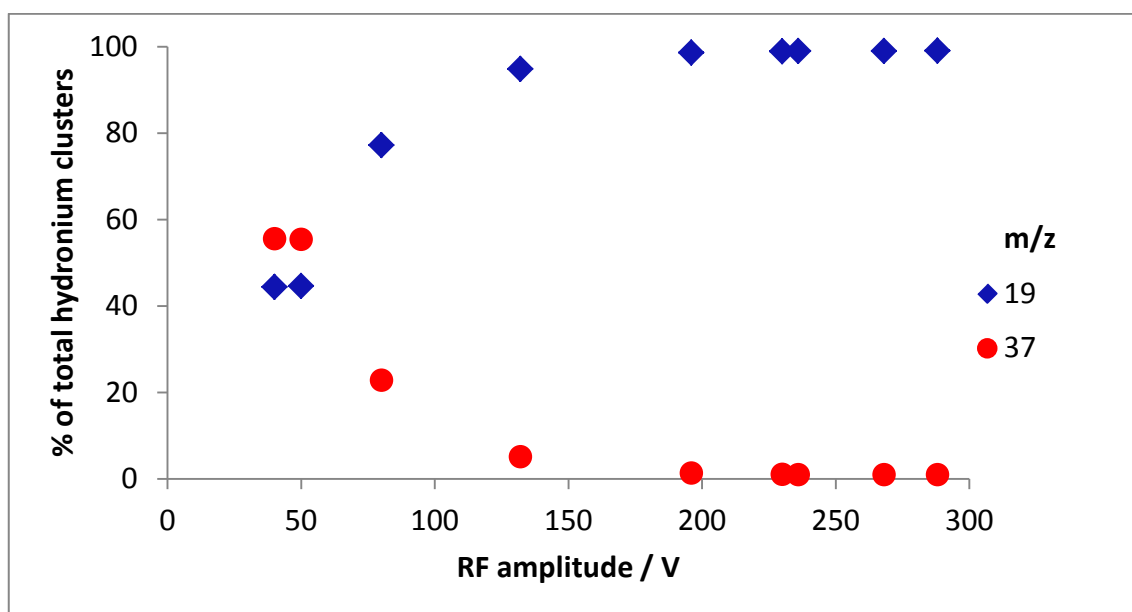


Figure 3-6. Water cluster ion distribution obtained in RF mode as a function of the RF peak voltage with a constant 100 V DC voltage applied to the drift tube.

Switching to the ion funnel mode (RF mode), operating conditions were sought when the RF field was also applied, which delivered roughly the same $[\text{H}_3\text{O}^+]/[\text{H}_3\text{O}^+(\text{H}_2\text{O})]$ ratio as seen when operating in the DC-only mode. Figure 3-6 shows how this ratio is affected by the RF conditions. The quantity being varied here was the peak-to-peak amplitude of the AC voltage, *i.e.* the DC contribution was fixed. Here the DC voltage across the drift tube was fixed at

Chapter three: Characterisation of a PTR-ToF-MS fitted with a radio frequency ion funnel

100 V, giving a DC-only contribution to the E/N of ~ 60 Td. The $[\text{H}_3\text{O}^+]/[\text{H}_3\text{O}^+(\text{H}_2\text{O})]$ ratio varies systematically with applied RF voltage in a way that is qualitatively comparable to the DC-only case, with a plateau being reached at an RF voltage of roughly 150 V peak-to-peak. This suggests that the ion funnel behaves equivalently to a DC-only drift tube under these particular conditions, but with an effective E/N that now depends on both the RF and DC electric fields. The same $[\text{H}_3\text{O}^+]/[\text{H}_3\text{O}^+(\text{H}_2\text{O})]$ ratio as obtained under optimum DC-only conditions was obtained in the RF mode when the RF voltage was 170 V. This RF voltage was used in all of the subsequent studies detailed below.

Instead of using E/N as a measure for the RF mode, the notation E/N_{eff} will be used to represent the effective E/N of the system when not in DC-only mode. An attempt to map the RF voltage to E/N_{eff} is summarised in Table 3-2 and is based on the data shown in Figure 3-7.

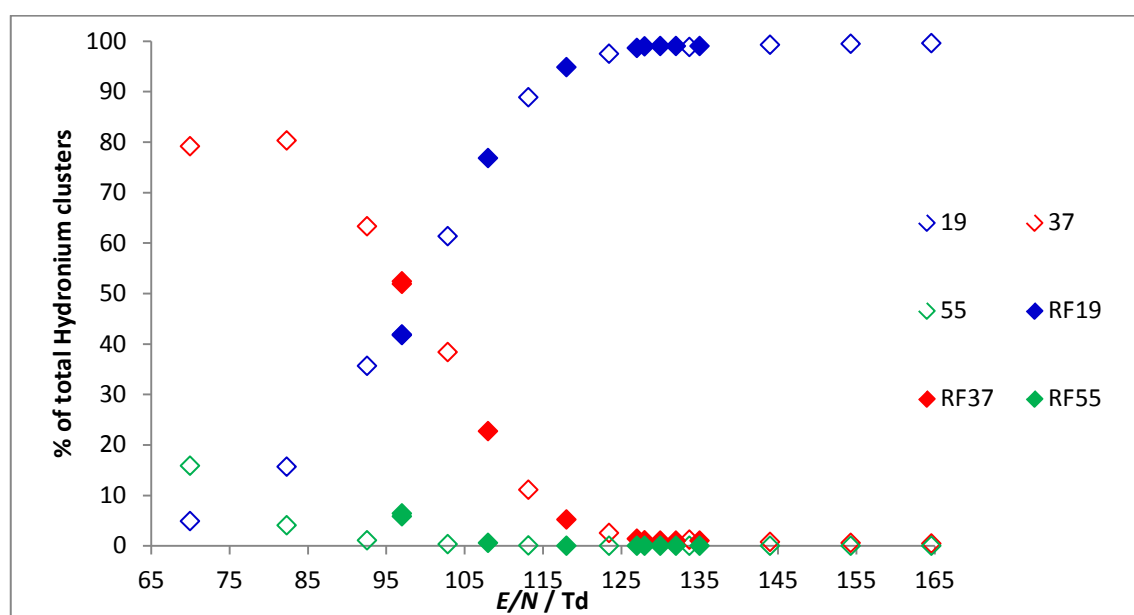


Figure 3-7. Graph used to convert RF values to E/N values. The DC-only mode results are represented by clear diamonds and the RF mode results (by solid diamonds) are fitted to the curves. The numbers refer the m/z of the water cluster ions.

Figure 3-7 is constructed by plotting the hydronium ratios obtained in RF mode on the same horizontal axis as the equivalent DC-only mode hydronium ratios

Chapter three: Characterisation of a PTR-ToF-MS fitted with a radio frequency ion funnel

(from Figure 3-5). This enables an E/N_{eff} to be calculated for any hydronium ratio obtained under RF mode conditions.

Table 3-2. Effective E/N for different RF voltage settings. The DC component was kept at ~ 100 V. The peak to peak voltages were made by physically measuring the pins attached to plates 26, 27, 28 and 29 (P26, P27, P28 and P29 respectively) using an oscilloscope.

RF setting (dial setting)	RF peak to peak voltage / V				Effective E/N ($E/N_{\text{eff}})$ / Td
	P26	P27	P28	P29	
1	73	71	66	33	96
2	74	72	68	34	96
3	80	78	74	38	108
4	132	130	126	60	118
5	196	194	184	102	127
6	230	230	217	122	128
7	236	232	218	126	130
8	268	268	248	143	132
9	269	268	260	142	133

3.3.3 Volatile organic compound fragmentation

For illustration of the effect on VOCs,

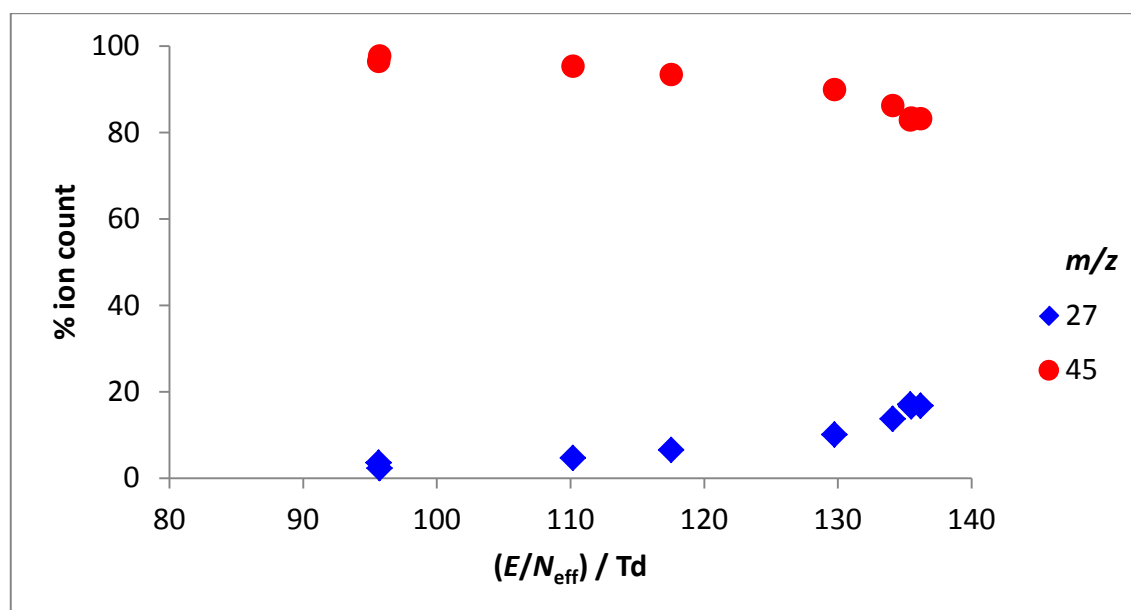


Figure 3-8 shows how the effective E/N in the RF mode of operation, inferred from the water cluster ion measurements described above, affects the signal from acetaldehyde. The principal ion product is the protonated parent molecule (m/z 45), but there is also a small quantity of a fragment at m/z 27; the latter is formed by dehydration of the protonated parent molecule. At an effective E/N of 125 Td in RF mode, the relative abundance of the dehydration fragment is

Chapter three: Characterisation of a PTR-ToF-MS fitted with a radio frequency ion funnel

slightly higher (7 %) than the corresponding measurement made in the DC-only mode (4 %), implying that the effective E/N , as calculated by the extent of reagent ion clustering, is a reasonable (but not perfect) measure of the ion-molecule collision conditions when the ion funnel is switched on.

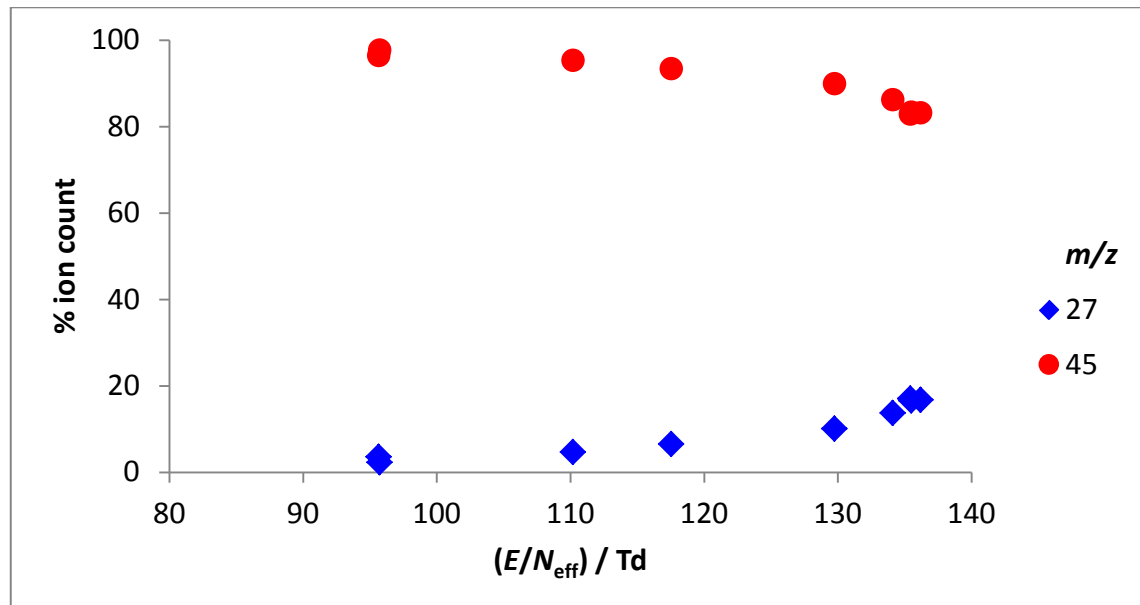


Figure 3-8: Protonated acetaldehyde parent ion (m/z 45) and fragment (m/z 27) plotted as a function of effective E/N in RF mode operation.

3.3.4 Noise

In the case of this instrument two types of noise are apparent. There appears to be well defined individual noise peaks occurring in mass channels and these are always present. i.e. at m/z 59, m/z 79, m/z 97 etc. Also, most notably, when operating in RF mode, there appears to be noise across the entire mass range, which is a combination of electrical noise and background chemical signals, as the instrument is much more sensitive when in this mode of operation. Figure 3-9 shows a single raw, pre analysis, mass spectrum for a 20 s scan period. The three images are the same spectra but with different y-axis scaling. It can be seen that when viewed at full scale, a), only the main peaks of hydronium (m/z 21, 37 and 55) can be observed, (note the large peak around m/z 19 is the result of electrical noise due to the blanking gate for this mass channel). Image b) is a vertically expanded view that gives an indication of the background peaks that are present when no compound is being analysed (blank nitrogen

Chapter three: Characterisation of a PTR-ToF-MS fitted with a radio frequency ion funnel

sample). This can result in these mass channels, such as m/z 59, having a lower LoD than otherwise possible due to the higher noise associated with the background at these locations. Finally, c), is magnified further where it can be seen that at least 2-3 counts of noise are present in nearly every mass channel, with more noise appearing at the lower end of the spectrum. The very low level peaks of 2-3 counts are simply electronic noise.

The larger peaks are also observed in another 'Kore-ToF' from the laboratory however, they are not present in the LE-ToF. One potential source for these could be from a material used in part of the construction of these two similar mass spectrometers, polyether ether ketone (PEEK), as the peaks are not present in the LE-ToF that does not contain it. It has also been suggested by the manufacturer that aluminium oxides could be the cause of some of the peaks seen, as the cathode is constructed of aluminium.

Noise in the DC-only mode has background chemical peaks in the same positions as the large peaks present in RF mode. However, in DC-only mode, there are not the individual peaks that are present at every mass channel as observed in the RF mode and therefore, the likely source of these small peaks in RF mode is electrical noise.

Chapter three: Characterisation of a PTR-ToF-MS fitted with a radio frequency ion funnel

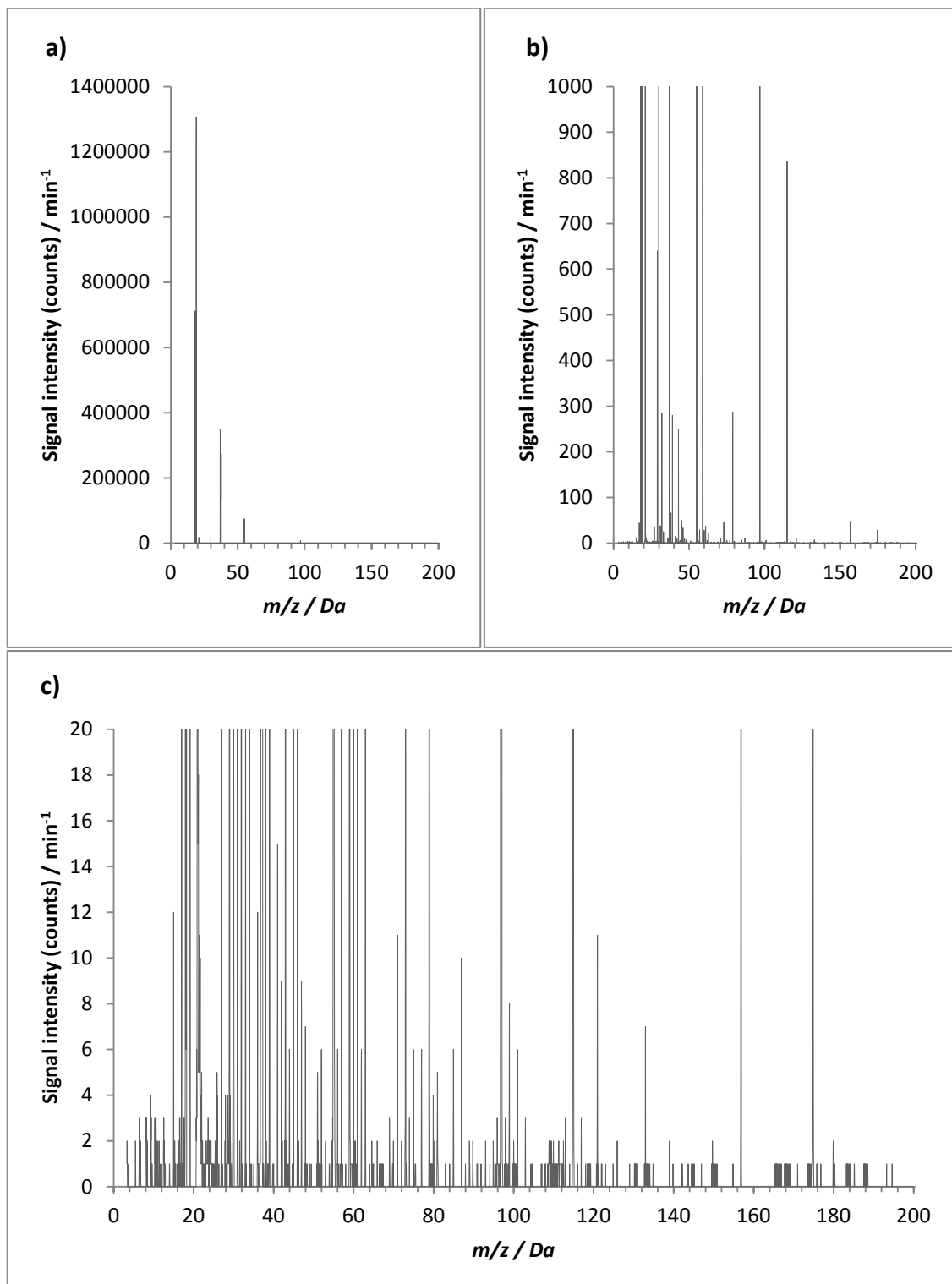


Figure 3-9. Different views of the same background mass spectrum obtained in RF mode using a 20 s scan time on three different vertical axis scales. (a) Full scale survey scan; (b) vertically expanded view; (c) An even further vertically expanded view.

Figure 3-10 and Figure 3-11 show how noise peaks vary with RF amplitude. It can be seen that in raw ion counts the noise peaks are small at RF amplitudes

Chapter three: Characterisation of a PTR-ToF-MS fitted with a radio frequency ion funnel

of below 4. This is because at these settings the overall sensitivity is very low and hence so are the noise peaks. When the counts are normalised to hydronium, however, the noise is at a minimum at RF amplitude 3. Whilst it would appear that operating the instrument in RF mode at amplitude 3 would minimise noise and maximise the LoD, the sensitivity towards compounds at this setting is also very low, which is why a compromise had to be made. RF amplitude 7 was the chosen compromise.

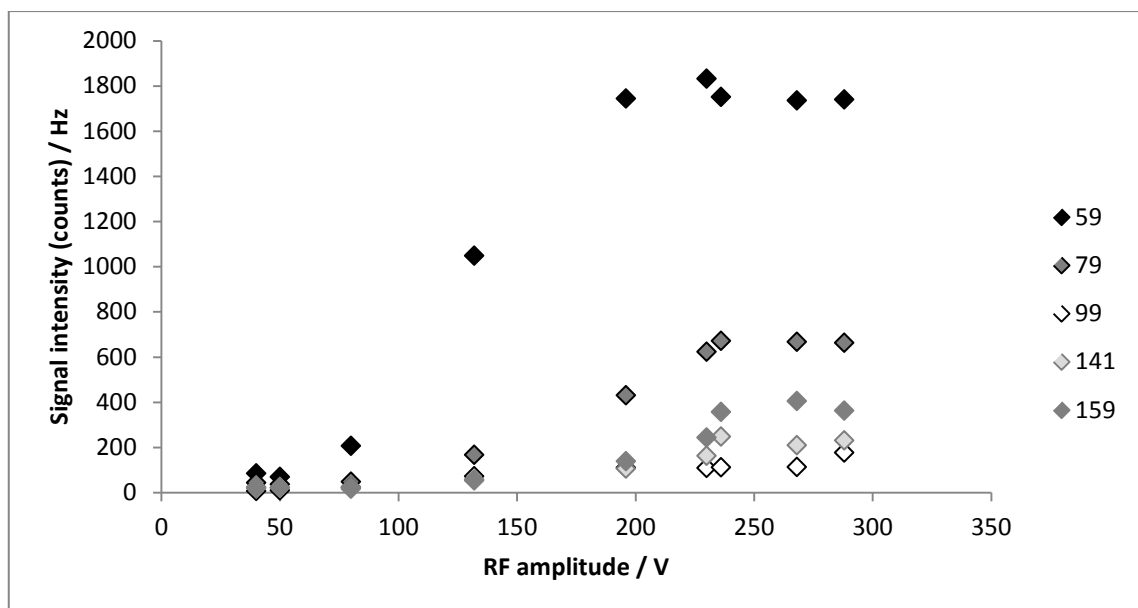


Figure 3-10. Selected mass channels with noise peaks as a function of RF amplitude for a 20 second scan time.

Chapter three: Characterisation of a PTR-ToF-MS fitted with a radio frequency ion funnel

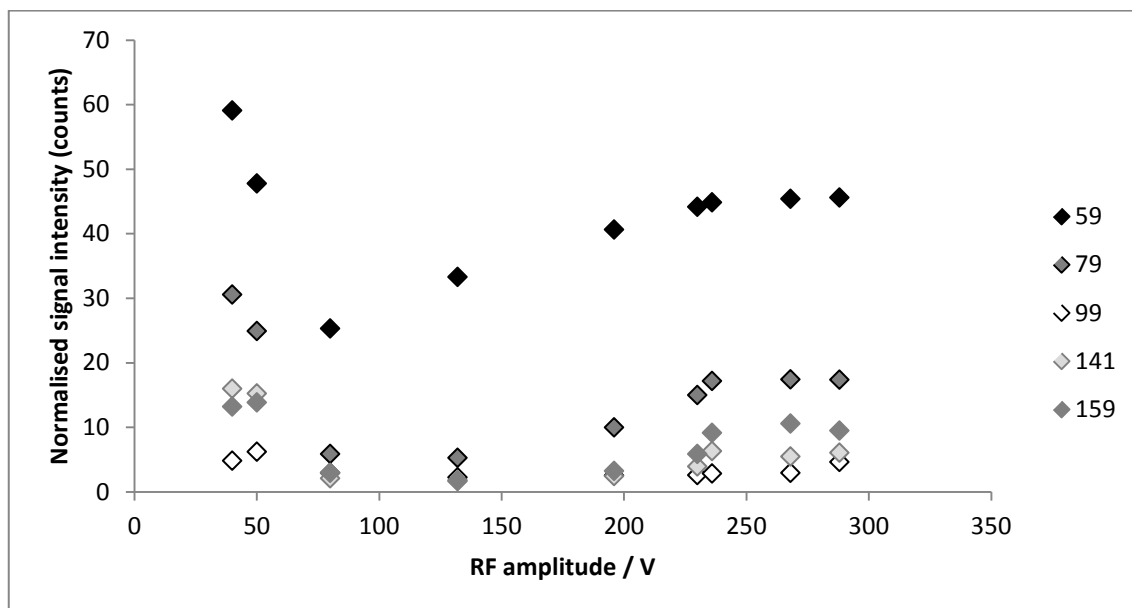


Figure 3-11. Selected normalised noise peaks for the same 20 seconds scan as shown in Figure 3-10 as a function of RF amplitude.

The precision of the instrument is discussed in section 2.6.3.2.

3.3.5 Detection sensitivity and limit of detection

The instrument was calibrated by delivering gas from a commercially prepared standard gas mixture, as detailed earlier in section 3.2.4.1. This contained seven principal components detectable by PTR-MS: methanol, acetaldehyde, trans-2-butene, acetone, methacrolein, cyclohexanone and β -pinene. The detection sensitivity was defined for these compounds as the ion count rate for a given quantity of supplied analyte. Units of Hz ppbV^{-1} were used to obtain this quantity, sometimes also known as the calibration factor, from a scatter plot of ion count rate versus the delivered quantity of each gas. The gas mixture was dynamically diluted to deliver known concentrations of each compound ranging from very low ppbV through to several hundred ppbV. For each compound, the protonated parent species was monitored to generate the data shown in Figure 3-12.

Chapter three: Characterisation of a PTR-ToF-MS fitted with a radio frequency ion funnel

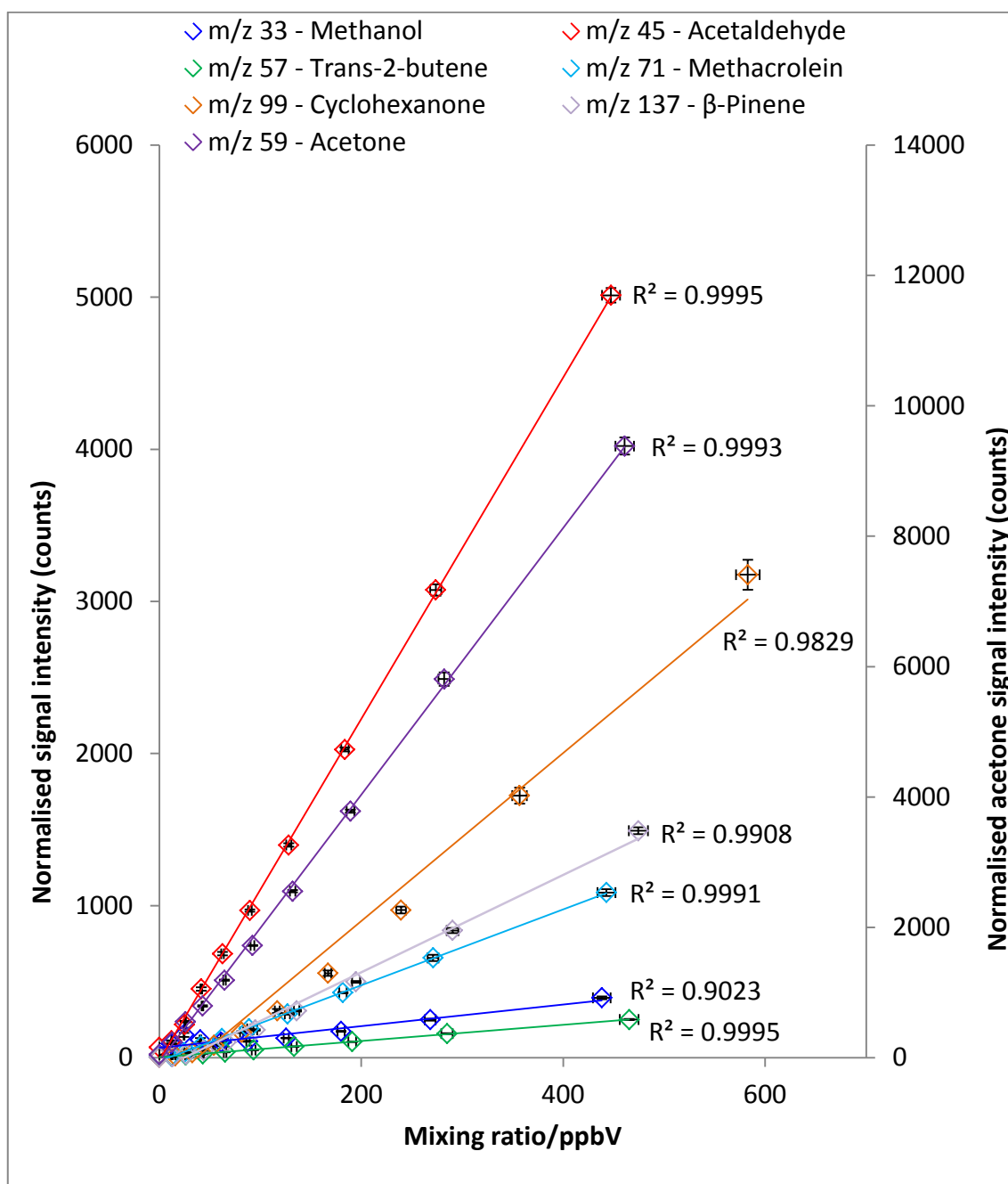


Figure 3-12. Multi-point calibration showing the normalised sensitivities for a seven-component VOC gas standard. The data was collected in the RF mode. The sensitivity is linear over dynamic range of at least three orders of magnitude.

Of the seven compounds in the gas mixture, six show excellent linear relationships between the number of ion counts and delivered concentration, with linear correlation coefficients (r^2) close to unity. The exception is methanol, but even here $r^2 \approx 0.90$. It seems likely that there is some interference with the protonated methanol signal at $m/z=33$ caused by contributions from the

Chapter three: Characterisation of a PTR-ToF-MS fitted with a radio frequency ion funnel

neighbouring O_2^+ peak at $m/z = 32$, which is observed because of some diffusion of analyte gas into the ion source region. Although small relative to H_3O^+ , the O_2^+ signal still dwarfs that from protonated methanol.

The sensitivities extracted from these plots are summarised in Table 3-3. Values are shown for both DC and RF modes of operation, along with the RF/DC sensitivity ratio. For the majority of compounds, the switch from DC to RF mode improves the sensitivity by between one and two orders of magnitude, although this is exceeded for acetone, methacrolein and cyclohexanone.

Table 3-3. Comparison of sensitivities and LoD for several VOCs ^a

Compound (m/z for MH^+)	Raw sensitivity / Hz $ppbV^{-1}$			LOD/ $pptV^b$		
	DC mode	RF mode	RF/DC	DC mode	RF mode	RF/DC
Methanol (33)	1.8	15	8	6125	1054	6
Acetaldehyde (45)	4.8	218	45	486	161	3
Trans-2-butene (57)	0.7	38	54	930	346	3
Acetone (59)	5.8	1162	200	445	30	15
Methacrolein (71)	2.4	387	161	351	26	13
Cyclohexanone (99)	3.1	686	221	271	15	18
β-Pinene (137)	1.1	164	149	425	123	3

^aThe DC data was collected at an E/N of 120 Td and the RF data was obtained at an effective E/N of 120 Td.

^bLoD determined for 20 s data collection.

The LoD (shown in equation E 3-1) in an analytical context is commonly defined as three times the background noise, *i.e.*

$$LoD = \frac{3[M]}{\left(\frac{S}{N}\right)} \quad \text{E 3-1}$$

where S is the mean background signal level at the chosen m/z , N is the corresponding noise level, and $[M]$ is the delivered concentration of compound M . Contributions to the background signal can be mass specific and will include contributions from traces of compounds present in the instrument (e.g. from components used in the instrument construction, degassing, etc.), as well as in the gas employed for background measurements. A mass-dependent background noise level was determined without any added analyte by making

Chapter three: Characterisation of a PTR-ToF-MS fitted with a radio frequency ion funnel

repeat measurements of S for a fixed integration time and then associating the standard deviation with N .

Table 3-3 also shows the LoD for the DC and RF modes of operation obtained for 20 s of data accumulation. There is a substantial improvement in LoD for all compounds in moving from DC-only operation to the RF mode. In almost all cases the LoD is reduced from several hundred pptV in the DC mode to ≤ 200 pptV in the RF mode, and in some cases is considerably better. The most marked exception is methanol, for reasons already identified above (contamination from O_2^+). Also, trans-2-butene does not fare too well, with an LoD near 350 pptV in the RF mode for 20 s data accumulation. This relatively poor LoD may partly be due to the comparatively low polarisability and the lack of a permanent dipole moment for this molecule, which will reduce the proton transfer rate when compared to the other molecules listed in Table 3-3. Furthermore, trans-2-butene has the lowest proton affinity of all of the molecules in Table 3-3 and therefore will be more susceptible to back-reaction with water vapour.

The improvement in RF/DC sensitivity ratio for various mass species is shown in Figure 3-13. The data here are from the compounds discussed in Table 3-3 as well as other VOCs analysed through the use of permeation tubes and tedlar bag dilutions. A complete list of compounds with sensitivity improvements is provided in Table 3-4.

There is a high degree of improvement across the mass range but it is most significant between m/z 45 and m/z 100. The two highest improvements come from the two ketones analysed, acetone and cyclohexanone, which also have a high proton affinity. There is of course mass dependence as shown by Figure 3-13, between m/z 45 and m/z 100, and this is a combination of the compound's structure, proton affinity and its mass. Whilst it wasn't as large, there is always a mass discrimination present with compounds in this instrument. Some compounds simply ionise and are transmitted more successfully than others,

Chapter three: Characterisation of a PTR-ToF-MS fitted with a radio frequency ion funnel

which is why this technique is ideal for detection of certain compounds but not all. The fact that the mass discrimination is larger when in RF mode shouldn't pose a significant issue for successful analysis.

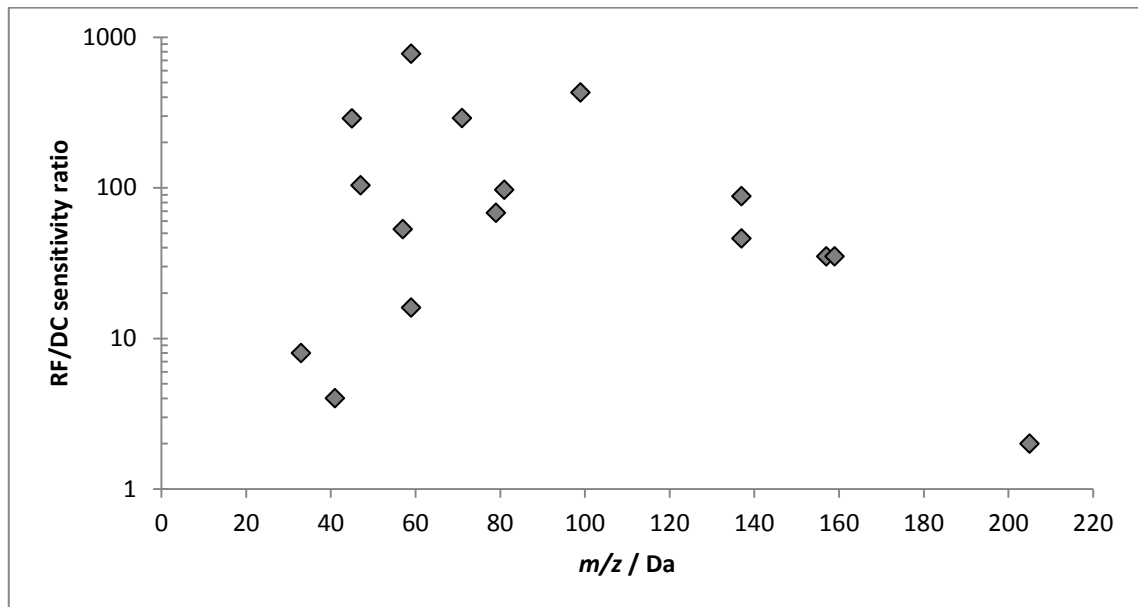


Figure 3-13. Improvement of raw sensitivity of various compounds comparing RF mode analysis to DC-only mode analysis. The data here contains the information from Table 3-4.

Table 3-4. VOCs with RF/DC sensitivity ratios (incorporating data from Table 3-3).

Compound	m/z for MH^+	RF/DC raw sensitivity ratio
Methanol	33	8
Methyl acetylene	41	4
Acetaldehyde	45	288
Formic acid	47	104
Trans-2-butene	57	53
Acetone	59	774
Pro-pionaldehyde	59	16
Methacrolein	71	290
Benzene	79	68
Limonene (fragment)	81	97
Cyclohexanone	99	428
β -Pinene	137	88
Limonene	137	46
Bromobenzene	157	35
Bromobenzene	159	35
β -Caryophyllene	205	2

3.4 Conclusion

The drift tube of a PTR-MS instrument has been modified to allow it to operate as both a conventional drift tube and as an ion funnel. This combined drift tube/ion funnel has been coupled with a mass spectrometer for the first time and the resulting PTR-MS instrument has been shown to deliver a much higher proportion of ions out of the drift tube and into the source region of the mass spectrometer. The improvement in detection sensitivity in going from the DC-only mode to the RF mode is more than two orders of magnitude for the majority of VOCs considered in this work. The dual purpose drift tube/ion funnel could easily be coupled to other types of mass spectrometer to increase the detection sensitivity and may therefore offer considerable benefits in PTR-MS work.

The LoD is currently restricted by persistent chemical background signals. The source of these signals would seem to be from materials incorporated within the instrument, rather than any extraneous sources in the laboratory. It should be possible to substantially reduce this background contamination to achieve a LoD in the single figure pptV range for 20 s of data accumulation with the current instrument, i.e. an improvement approaching two orders of magnitude relative to the DC-only mode, which would be compatible with the improvement already seen in the detection sensitivity.

Chapter three: Characterisation of a PTR-ToF-MS fitted with a radio frequency ion funnel

3.5 References

- BAKER, E. S., CLOWERS, B. H., LI, F., TANG, K., TOLMACHEV, A. V., PRIOR, D. C., BELOV, M. E. & SMITH, R. D. 2007. Ion mobility spectrometry–mass spectrometry performance using electrodynamic ion funnels and elevated drift gas pressures. *Journal of the American Society for Mass Spectrometry*, 18, 1176-1187.
- BARBER, S., BLAKE, R. S., WHITE, I. R., MONKS, P. S., REICH, F., MULLOCK, S. & ELLIS, A. M. 2012. Increased sensitivity in proton transfer reaction mass spectrometry by incorporation of a radio frequency ion funnel. *Anal Chem*, 84, 5387-91.
- BLAKE, R. S., MONKS, P. S. & ELLIS, A. M. 2009. Proton-Transfer Reaction Mass Spectrometry. *Chemical Reviews*, 109, 861-896.
- ELLIS, A. M. & MAYHEW, C. A. 2014. *Proton Transfer Reaction Mass Spectrometry: Principles and Applications*, Wiley.
- IBRAHIM, Y., TANG, K., TOLMACHEV, A. V., SHVARTSBURG, A. A. & SMITH, R. D. 2006. Improving mass spectrometer sensitivity using a high-pressure electrodynamic ion funnel interface. *Journal of the American Society for Mass Spectrometry*, 17, 1299-1305.
- JULIAN, R. R., MABBETT, S. R. & JARROLD, M. F. 2005. Ion funnels for the masses: Experiments and simulations with a simplified ion funnel. *Journal of the American Society for Mass Spectrometry*, 16, 1708-1712.
- KELLY, R. T., TOLMACHEV, A. V., PAGE, J. S., TANG, K. & SMITH, R. D. 2010. The ion funnel: theory, implementations, and applications. *Mass spectrometry reviews*, 29, 294-312.
- KIM, T., TOLMACHEV, A. V., HARKEWICZ, R., PRIOR, D. C., ANDERSON, G., UDSETH, H. R., SMITH, R. D., BAILEY, T. H., RAKOV, S. & FUTRELL, J. H. 2000. Design and implementation of a new electrodynamic ion funnel. *Analytical chemistry*, 72, 2247-2255.
- LYNN, E. C., CHUNG, M. C. & HAN, C. C. 2000. Characterizing the transmission properties of an ion funnel. *Rapid Communications in Mass Spectrometry*, 14, 2129-2134.
- SHAFFER, S. A., TANG, K., ANDERSON, G. A., PRIOR, D. C., UDSETH, H. R. & SMITH, R. D. 1997. A novel ion funnel for focusing ions at elevated pressure using electrospray ionization mass spectrometry. *Rapid Communications in Mass Spectrometry*, 11, 1813-1817.
- SHAFFER, S. A., TOLMACHEV, A., PRIOR, D. C., ANDERSON, G. A., UDSETH, H. R. & SMITH, R. D. 1999. Characterization of an improved electrodynamic ion funnel interface for electrospray ionization mass spectrometry. *Analytical chemistry*, 71, 2957-2964.
- TAHALLAH, N., PINKSE, M., MAIER, C. S. & HECK, A. J. 2001. The effect of the source pressure on the abundance of ions of noncovalent protein assemblies in an electrospray ionization orthogonal time-of-flight instrument. *Rapid Communications in Mass Spectrometry*, 15, 596-601.
- TOLMACHEV, A. V., KIM, T., UDSETH, H. R., SMITH, R. D., BAILEY, T. H. & FUTRELL, J. H. 2000. Simulation-based optimization of the electrodynamic ion funnel for high sensitivity electrospray ionization mass spectrometry. *International Journal of Mass Spectrometry*, 203, 31-47.

4 Chapter four: The use of rare gases to control collision energy

4.1 Introduction

Chapters one and two described the basic function and routine operation of PTR-MS as applied in a wide variety of studies. Over time, as the potential of PTR-MS has been realised, its exploitation has extended across different disciplines and fields of research. This has resulted in the substrates and analytes under study becoming more varied, often associated with complex sample matrices encountered within a range of environmental conditions and sampled in the gas, liquid and even solid phase. Between one novel application of PTR-MS and the next, there may be a significant change in buffer gas composition (the gas that accompanies the analyte) and, although prudent, a thorough examination into how this affects PTR sensitivity and fragmentation has often been overlooked.

In most applications, once in the drift tube, target analytes are present in a dominant matrix of the atmospheric bath gases, nitrogen and oxygen. This is because many of the systems under study (be they from the atmosphere, human breath, or head-space sampled from a chamber) are present in ambient air and so usually either synthetic air or pure nitrogen is added to the sample mixture if dilution is required due to an over-concentrated analyte mixture. Also, if a bubbler is employed to supply reagent gas in the system (as opposed to a pure water supply), then nitrogen is used as the carrier gas.

There are many applications, however, that routinely involve the buffer gas either comprising entirely of a gas that is not nitrogen or synthetic air, or a significant portion that is not nitrogen or air. When analysing exhaust fumes or gases emitted from heated shale rock, they can contain up to percent levels of gases such as CO, CO₂, CH₄ and alkanes (Jobson et al., 2005, Sommariva et al., 2014). Exhaled human breath also contains a rather large quantity of carbon

dioxide (~5 % from respiration (Smith et al., 2014, White et al., 2013)) as well as ~1 % argon already contained in the inhaled air. This constitutes ~6 % of the gas sample and therefore should not be simply ignored when analysing a complete breath sample. Another significant application is analysing the head space over cultures of anaerobic bacteria, in which the gas flowing over the sample is a hydrogen, nitrogen, carbon dioxide mixture. Here the non-nitrogen compounds constituents are up to 15 % of the total buffer gas. Furthermore, when considering these different applications, an interesting postulate arises whereby better sensitivity or less fragmentation, for a particular compound (or class of compounds), may be obtained by simply changing the composition of the buffer gas alongside careful manipulation of ionisation conditions based on the E/N ratio.

For the purpose of this thesis, the buffer gas is described as any gas entering the system that is not the analyte, or reagent ion, and these include the diluent for the analyte, and also the water vapour carrier gas used in the bubbler set-up that is used on this particular instrument, the LE-ToF. In order to both investigate how a change in buffer gas composition affects fragmentation and sensitivity, and to identify any potential benefits there may be in deliberately injecting different buffer gases into a sample mixture, a selection of VOCs were analysed using different drift tube conditions and buffer gas make-up. The aim is to determine what benefit a change in buffer gas yields, with particular emphasis on investigating which compounds not only improve in sensitivity but also fragment less, in order to apply this to a case study wherein a complex mixture requires analysis.

4.2 Kinetics/thermodynamics of gases in the drift tube

Upon changing the buffer gas within the drift tube, ion-molecule interactions are altered because the kinetic energy of the buffer gas in the drift tube is changed. If nitrogen is replaced by argon, for instance, the mean kinetic energy of the buffer gas within the drift tube will increase. In this example, the same E/N will in fact be associated with two different ionising conditions dependent on the chosen buffer gas: a phenomenon which will be explored throughout this chapter. In order to compare different buffer gas systems, kinetic energies must be calculated for each buffer gas in question. Furthermore, in altering the E/N , the drift time (or residence time) is also changed and this must be taken into account, as described below in section 4.2.2.

4.2.1 Centre of mass collision energy calculations

With regards to this study, one of the most important factors altered upon changing the gas inside the drift tube is the collision energy. The kinetic energy of the system is changed and therefore the energy between collisions is affected. The following equations (Ellis and Mayhew, 2014) can be used to calculate centre-of-mass collision energies of the reagent ion with different analytes in the presence of a buffer gas. Equation E 4-1 represents the total mean ion kinetic energy and was derived by Wannier in the 1950s (Wannier, 1951, Wannier, 1953).

$$KE_{ion} = \frac{3}{2}k_B T + \frac{1}{2}m_{ion}v_d^2 + \frac{1}{2}m_b v_d^2 \quad \text{E 4-1}$$

The first term on the right hand side of E 4-1 is the thermal contribution, where T is temperature and k_B is the Boltzmann constant. The second term is the kinetic energy of the ion as it is driven along the drift tube at velocity, v_d , where m_{ion} is the mass of the ion. The third term is one introduced by Wannier which represents the collisions between the ions and buffer gas (m_b) and can be orientated in any direction.

Wannier's equation (E 4-1) represents the kinetic energy viewed from a laboratory frame of reference. However, for the kinetic energy of an ion-

molecule reaction, it is necessary to calculate the kinetic energy relative to the centre of mass (KE_{CM}) of the colliding ion-neutral system. This is represented by E 4-2.

$$KE_{CM} = \frac{1}{2} \left(\frac{m_n m_{ion}}{m_n + m_{ion}} \right) (v_{ion}^2 + v_n^2) \quad \text{E 4-2}$$

where,

$$\frac{1}{2} m_{ion} v_{ion}^2 = KE_{ion} \quad \text{E 4-3}$$

and

$$\frac{1}{2} m_n v_n^2 = \frac{3}{2} k_B T \quad \text{E 4-4}$$

The mass and velocity of the neutral (analyte) molecule are given by m_n and v_n , respectively. If E 4-2, E 4-3 and E 4-4 are combined then we get equation E 4-5.

$$KE_{CM} = \left(\frac{m_n}{m_n + m_{ion}} \right) KE_{ion} + \left(\frac{m_{ion}}{m_n + m_{ion}} \right) \left(\frac{3}{2} k_B T \right) \quad \text{E 4-5}$$

Recognising that,

$$\left(\frac{m_{ion}}{m_n + m_{ion}} \right) = 1 - \left(\frac{m_n}{m_n + m_{ion}} \right) \quad \text{E 4-6}$$

then E 4-5 can be rearranged as,

$$KE_{CM} = \frac{m_n}{m_{ion} + m_n} \left(KE_{ion} - \frac{3}{2} k_B T \right) + \frac{3}{2} k_B T \quad \text{E 4-7}$$

E 4-7 was used to calculate the collision energies displayed in Figure 4-1 for three different buffer gases, with respect to an analyte molecule with a nominal

mass of 86 (e.g., hexane). It can be seen in Figure 4-1 that, for a given E/N , changing the buffer gas has a large impact upon the collision energies. Helium has the biggest effect on the kinetic energy of the system when compared to nitrogen whilst argon also has a significant effect. Here, the collision energy at 120 Td with a nitrogen buffer gas is equivalent to using an argon buffer gas at 59 Td and a helium buffer gas at 22 Td.

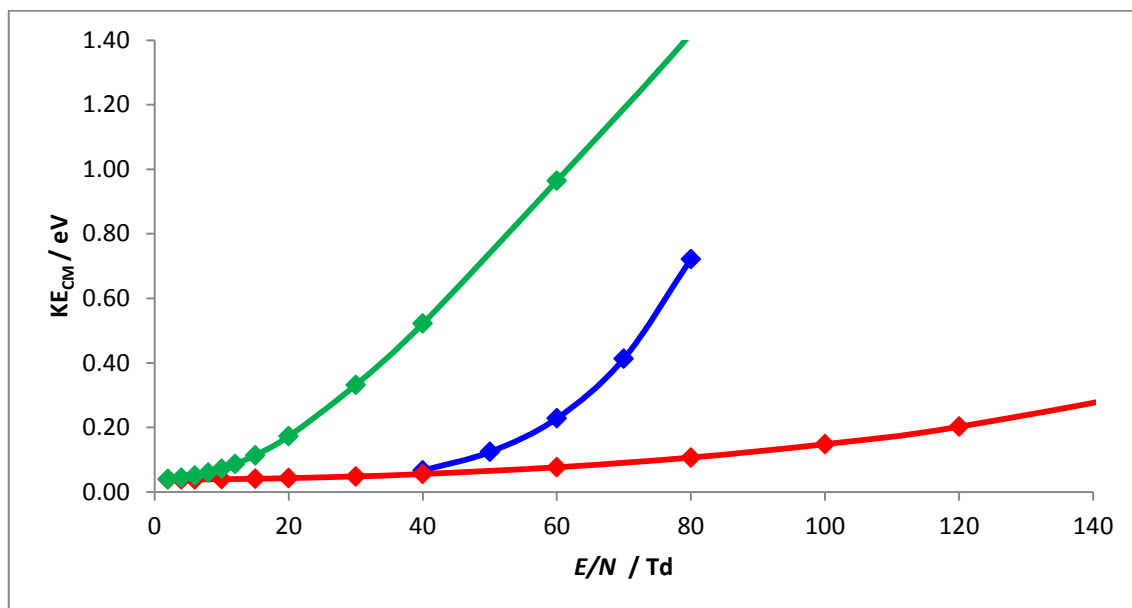


Figure 4-1. Calculated kinetic energy with respect to the centre of mass vs E/N for three different buffer gases (Green = H_3O^+/He , Blue = H_3O^+/Ar , Red = H_3O^+/N_2). The analyte has a nominal mass of 86 (hexane) and the reagent ion mass used was 19 (hydronium). Data obtained from (McFarland et al., 1973c, McFarland et al., 1973a, McFarland et al., 1973b).

4.2.2 Drift time

When a different E/N is used in the drift tube, it is important to remember that this will alter the transit time of ions through the drift tube and therefore the time available for reaction. A lower E/N reduces the velocity of the ions, providing a longer residence time due to the ions having a lower velocity.

The ion drift velocity (v_d) is represented by E 4-8 and is linearly dependent on the electric field (E) where K is the ion mobility (Ellis and Mayhew, 2014). In this case, v_d refers to the overall mean velocity of the ion cloud in the drift tube as opposed to a single selected ion.

$$v_d = K \cdot E$$

E 4-8

The ion mobility constant is a function of both pressure and temperature. It is therefore useful to introduce pressure and temperature dependence for a particular ion by introducing a reduced ion mobility (K_0) and this is related to K by E 4-9. The temperature (T) is in kelvin and the pressure (P) is in Torr.

$$K = \frac{760}{P} \frac{T}{273} K_0 \quad \text{E 4-9}$$

E 4-9 can be substituted for K into E 4-8 to give E 4-10, which now applies to a particular ion/molecule collision and can be calculated for any temperature or pressure.

$$v_d = \frac{760}{P} \frac{T}{273} K_0 E \quad \text{E 4-10}$$

We can now define N_0 as the gas number density under standard temperature and pressure (STP), i.e. 273 K and 760 Torr and rewrite E 4-10 as:

$$v_d = K_0 N_0 \frac{E}{N} \quad \text{E 4-11}$$

The drift time can be calculated by multiplying the length of the drift tube (L) by $1/v_d$ to give E 4-12.

$$t_d = \frac{L}{K_0 N_0} \frac{N}{E} \quad \text{E 4-12}$$

Based on this, the drift time can be calculated and Figure 4-2 can be constructed for different drift tube lengths at different E/N values. It can be seen that the difference in drift times for different drift tube lengths is greatest at lowest E/N , as expected.

It is thus important to be aware of this when comparing sensitivities, and also in deciding at which point the sample is introduced, as a higher residence time

allows for more reactions to take place between the analyte molecule and the reagent ion. It should be noted that the analyte enters the drift tube 10 cm before the exit aperture in the experiments described in section 4.4. Figure 4-2 shows the change of drift time when using argon as the buffer gas; however, a similarly shaped graph is produced when any buffer gas is used.

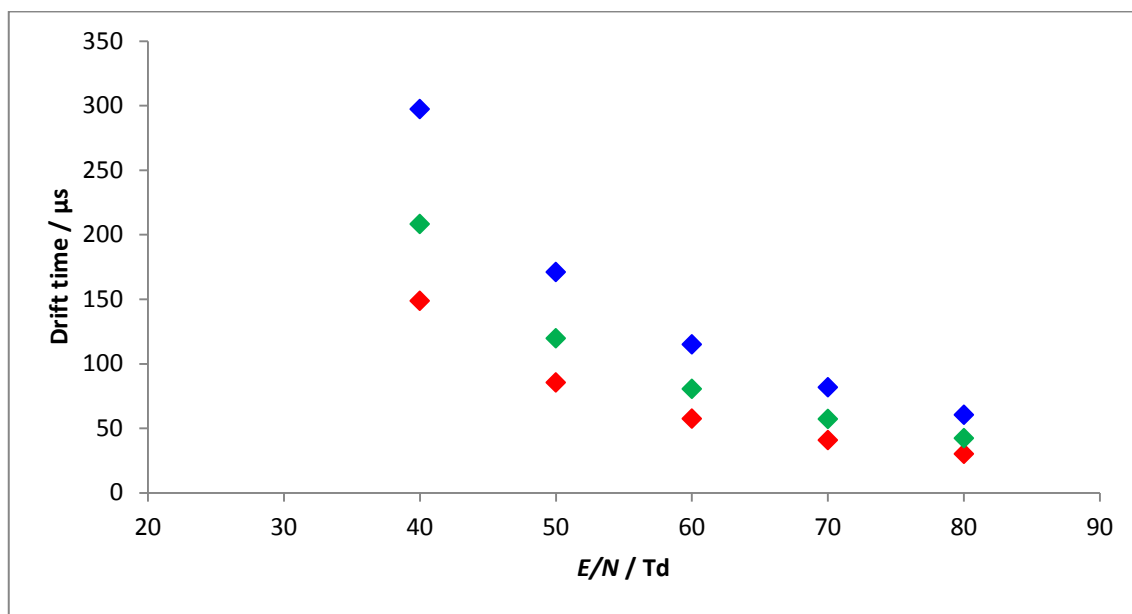


Figure 4-2. Drift time for differing drift tube length (blue = 10 cm, green = 7 cm, red = 5 cm) for hydronium molecules in an argon buffer gas. Data obtained from (McFarland et al., 1973c, McFarland et al., 1973a, McFarland et al., 1973b)

4.3 Previous findings

In 2008, Inomata and co-workers (Inomata et al., 2008) from the National Institute for Environmental Studies (NEIS), Japan, used a selection of rare gases (helium, neon, argon and krypton) as buffer gases, i.e. the gas carrying the analytes, in order to achieve a similar hydronium and VOC sensitivity whilst being able to operate the drift tube at a lower E/N compared to when nitrogen was used as the buffer gas. Their system employed a GD ion source, as can be seen in Figure 4-3, where the colour of the GD changed for each of the five different buffer gases (the four rare gases and water only (with nitrogen)). Full details of the instrument have been described in previous publications (Inomata et al., 2006, Tanimoto et al., 2007).

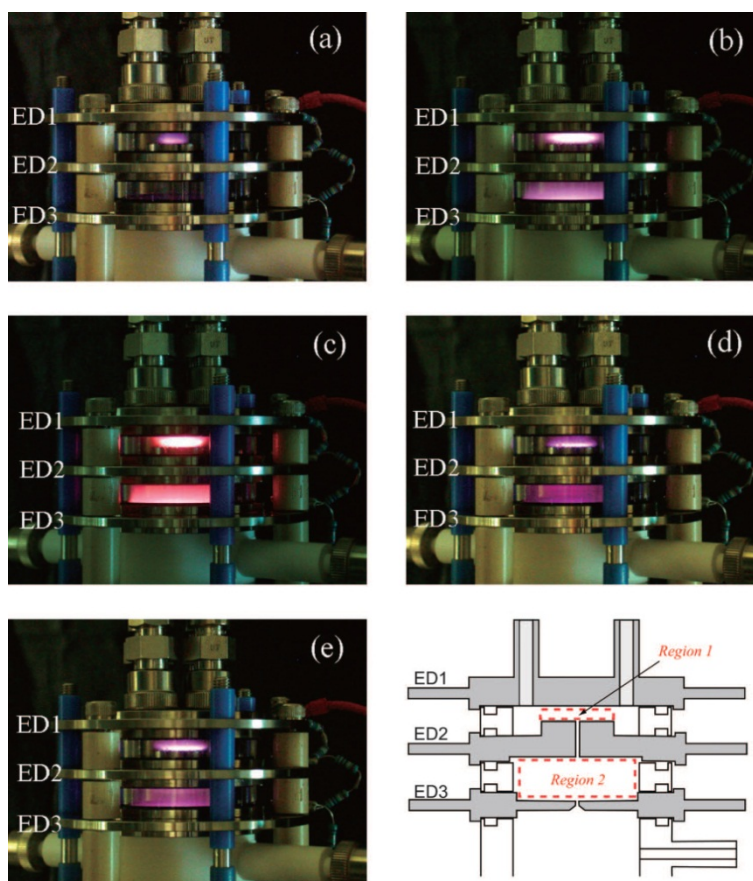


Figure 4-3. Images of a discharge ion source used by Inomata and co-workers. (a) “H₂O-only” discharge mode at E/N 100 Td, and (b)-(e) “H₂O in the presence of a rare gas at E/N 40 Td. (b) He, (c) Ne, (d) Ar, and (e) Kr (taken from (Inomata et al., 2008)).

The data in Table 4-1 indicates that for acetone, an increase in sensitivity of 5-7 times was obtained when using a rare gas at 40 Td when compared to nitrogen at 100 Td. According to the data presented by Inomata and co-workers, there is

Chapter four: The use of rare gases to control collision energy

a slight increase in the density of H_3O^+ ions for the rare gases but overall a decrease in the $\text{H}_3\text{O}^+/\text{H}_3\text{O}^+\cdot\text{H}_2\text{O}$ ratio (due to a large increase in $\text{H}_3\text{O}^+\cdot\text{H}_2\text{O}$), thus deviating from ideal PTR ionisation conditions.

Table 4-1. Typical signal intensities for a 1 min integration time of primary ions and sensitivities for acetone (adapted from (Inomata et al., 2008)).

Buffer gas	E/N / Td	H_2O^+ / counts	H_3O^+ / counts	$\text{H}_3\text{O}^+\cdot\text{H}_2\text{O}$ / counts	Acetone. H^+ / counts ppbV ⁻¹
Helium	40	14×10^2	7.6×10^5	1.9×10^6	6.0×10^2
Neon	40	7.3×10^2	8.4×10^5	1.7×10^6	7.0×10^2
Argon	40	4.9×10^2	6.0×10^5	1.2×10^6	4.9×10^2
Krypton	40	5.0×10^2	5.6×10^5	1.1×10^6	4.8×10^2
Water vapour only	100	3.6×10^2	4.0×10^5	0.3×10^6	1.2×10^2

Figure 4-4 is a graphical illustration of the data from Table 4-1. The sensitivity for acetone (m/z 59) is clearly increased when a rare gas is used as the buffer gas. However, detrimentally, there is also a large increase of around 300 - 500 % in the monohydrate water cluster ($\text{H}_3\text{O}^+\cdot\text{H}_2\text{O}$, m/z 37), especially for helium and neon; however, this could be explained by the unusually low E/N (40 Td) being used.

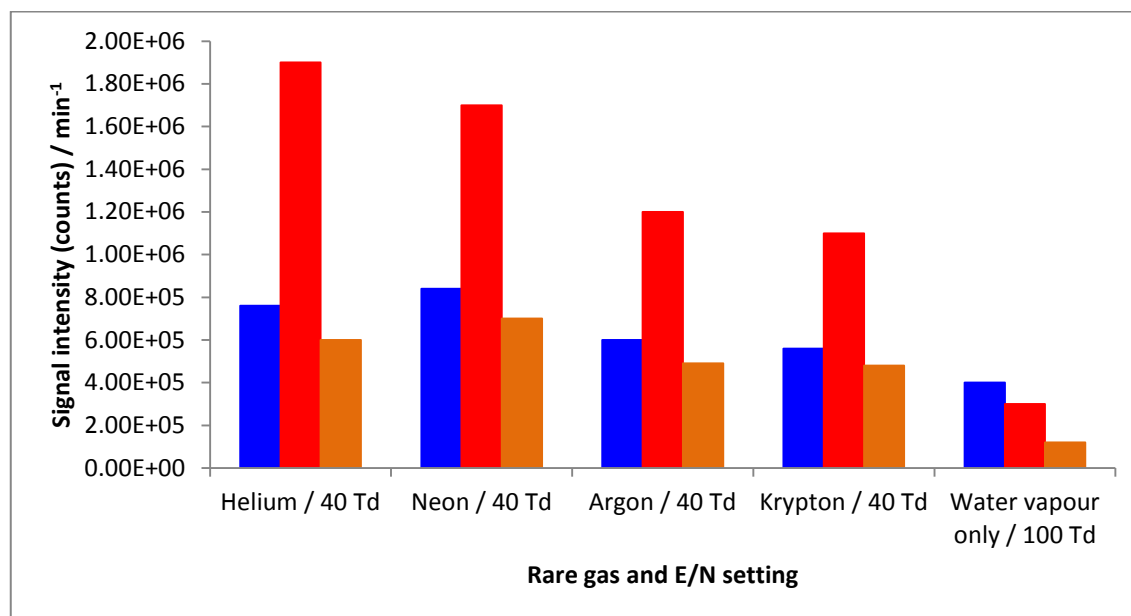
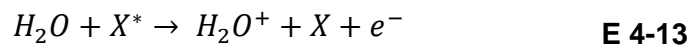


Figure 4-4. Data plotted from Table 4-1. Blue = m/z 19, red = m/z 37, orange = m/z 59. The protonated acetone (m/z 59) count has been multiplied by 1000 and therefore the data is now in units of counts/ppmV.

4.3.1 Penning Ionisation

In Table 4-1 there is also an increase in the quantity of H_2O^+ when compared to a water only system, especially when helium and neon are used as the buffer gas. This is likely due to Penning ionisation, in which the H_2O is ionised to H_2O^+ , and occurs when the electronic excitation energy of the buffer gas is higher than the ionisation energy of water. The ionisation proceeds via reaction E 4-13, (Kolts et al., 1979), where X^* is the rare gas atom in an excited state:



The excitation levels are listed in Table 4-2 and show that the quantities for krypton (10.56 eV and 9.92 eV) and argon (11.73 eV and 11.55 eV) are below that for water (12.6 eV). However, because the excitation levels in this long-lived state for neon (17.71 eV and 16.61 eV) and helium (20.61 eV and 19.81 eV) are higher than water, penning ionisation can occur when these gases are used.

Table 4-2. A list of excitation energies for water and four rare gases when in an excited state (adapted from (Inomata et al., 2008)).

Gas	Excitation energies / eV	
Krypton	10.56	9.92
Argon	11.73	11.55
H_2O	12.6	-
Neon	17.71	16.61
Helium	20.61	19.81

In the study in this thesis, argon has been chosen for further study and therefore problems arising from Penning ionisation should not become a problem.

4.4 Experimental

All of the experiments presented in this chapter were carried out on the LE-ToF previously described in chapter two, and in several publications by Blake and co-workers (Blake et al., 2004, Blake et al., 2006, Blake et al., 2009). This instrument was used instead of other PTR-MS instruments in the research group because (1) it is more suited to changes in the gas delivery system, (2) it is capable of operating at reasonably high drift pressures and (3) it uses a very stable ion source and detector which allow for easier comparison of data over time, i.e., it is possible to compare non-normalised results free from significant instrumental drift. Pure argon (99.999 % BOC gases) and pure nitrogen (99.999 % BOC gases) gas were used for the buffer gas when required. When a consistent flow of analyte was needed over a large number of runs (> 60 one min runs), then permeation tubes were used for the experiments. Tedlar bags were only used when the analysis time was around 30 min or less due to their limiting volume.

According to Inomata et al., the ratio of hydronium to hydrated hydronium, $\text{H}_3\text{O}^+:\text{H}_3\text{O}^+(\text{H}_2\text{O})$, are the same when the drift tube is operated at 100 Td with nitrogen as when operated at 40 Td with argon. Therefore, several initial experiments were carried out using these conditions in order to investigate if these operating conditions were feasible to use on this particular instrument.

The E/N was then altered to ascertain how the hydronium cluster ratios change for both argon and nitrogen (section 4.5.2). After pure gases were used as buffer gases, mixtures of argon and nitrogen were investigated, where the latter was achieved at the desired missing ratio using two mass flow controllers. These experiments were performed to investigate the feasibility of using mixtures of buffer gases and to assess the overall effect that using mixtures has on the sensitivity of VOC detection. For these sensitivity measurements, the following analytes were chosen (all delivered from permeation tubes): isoprene, benzene, toluene, 2-chloroethyl sulphide and ethylbenzene.

Chapter four: The use of rare gases to control collision energy

The conditions used are outlined in Table 4-3. All E/N settings for a single nitrogen/argon combination were analysed together, before moving on to the next nitrogen/argon combination setting, in order to give the system an opportunity to be in equilibrium, as a change in E/N (as achieved by adjusting the voltage across the drift tube) equilibrates much quicker than a change in gas composition.

Table 4-3. The values of E/N and the percentage of argon and nitrogen present as the buffer gas in the series of experiments.

E/N / Td	Nitrogen / %	Argon / %
53	100	0
53	84	16
53	65	35
53	49	51
53	33	67
63	100	0
63	84	16
63	65	35
63	49	51
63	33	67
77	100	0
77	84	16
77	65	35
77	49	51
77	33	67
101	100	0
101	84	16
101	65	35
101	49	51
101	33	67
112	100	0
112	84	16
112	65	35
112	49	51
112	33	67

Finally, a comparison of the fragmentation pattern (mass spectrum) was carried out to investigate how the drift tube behaves when under either 100 % argon buffer gas or 100 % nitrogen buffer gas at identical E/N values, then identical collision energies and finally identical equivalent hydronium clustering ratios. For this part of the study, hexane and limonene were analysed as the fragmentation pattern for these gases was well understood from previous experiments. Limonene readily fragments to a single fragment ($m/z = 81$) and

Chapter four: The use of rare gases to control collision energy

hexane undergoes fragmentation through subsequent sequential loss of $-CH_2$ from the parent ion.

4.5 Results and discussion

4.5.1 Initial results

Initially, experiments were conducted similar to those carried out by Inomata and co-workers to try and confirm their findings. Drift tube conditions of 100 Td were chosen with nitrogen as a buffer gas and 40 Td when argon was used as the buffer gas.

After the instrument was successfully operated under both of these two conditions, i.e. there was an acceptable hydronium count, then a VOC was chosen to analyse. Limonene (Figure 4-5) was the molecule of choice as it has a moderately fast rate of proton transfer of $2.54 \times 10^{-9} \text{ cm}^3 \text{ s}^{-1}$ (Zhao and Zhang, 2004) and readily fragments to only a single ion at m/z 81. Consequently, the mass channels for m/z 137 (the protonated parent molecule) and m/z 81 (the protonated fragment) could be used to ascertain changes in the fragmentation ratio, as well as the detection sensitivity.

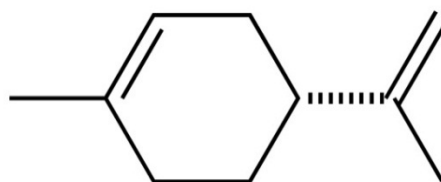


Figure 4-5. The structure of limonene.

Figure 4-6 displays a plot of the normalised ion count for protonated parent ion (m/z 137) against concentration. The horizontal axis is labelled as the reciprocal of the diluent flow, i.e. the gas flow through the permeation oven that was used to dilute the permeation tubes (containing limonene), and this is directly proportional to concentration. As this study was designed to investigate relative differences between the two buffer gases, the exact emission rate of this permeation tube was unknown, although it was in the ppmV range. Each new concentration was bracketed by a single condition throughout, that is to say, the first concentration analysed was also analysed in between the other concentrations so that any instrument drift in sensitivity could be monitored.

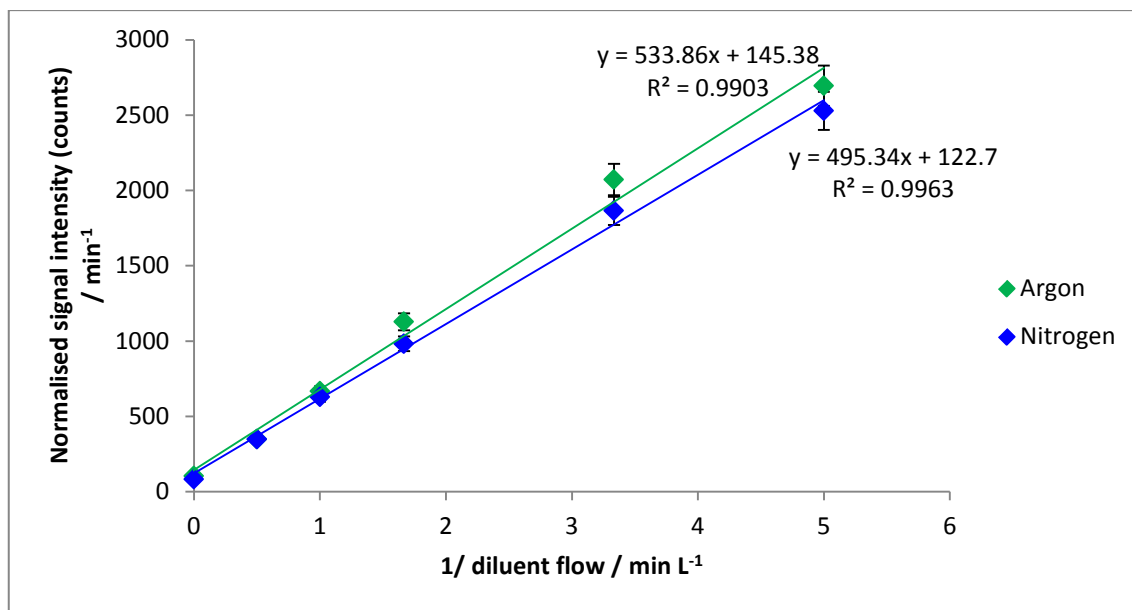


Figure 4-6. A calibration graph of limonene parent ion (m/z 137) signal with varying concentration of limonene.

Figure 4-6 shows that the number of counts of m/z 137 increased by ~ 8 % when changing the buffer gas from nitrogen (100 Td) to argon (40 Td).

Whilst this increase in sensitivity is modest, there is also a change in fragmentation ratio that should be noted. Table 4-4 shows how the percentage of parent ion is increased from 21 % to 56 % when argon is used as the buffer gas. This tells us that the total sensitivity, as determined by measurement of the protonated parent molecule only, has in fact decreased. However, the reduced fragmentation may be beneficial in that it may simplify the measurement of monoterpenes by PTR-MS within complex mixtures.

Table 4-4. The percentage ions detected at m/z 137 (protonate parent molecule) and at m/z 81 (a fragment ion) for limonene for two different E/N conditions.

	E/N / Td	m/z 81	m/z 137
Nitrogen	100	79 %	21 %
Argon	40	44 %	56 %

4.5.2 Hydronium clusters

After the preliminary work outlined in 4.5.1 demonstrated that the instrument could operate under an argon atmosphere, and that there may be some benefit in optimising the buffer gas content, a thorough investigation across different E/N conditions was carried out for argon and nitrogen. The hydronium clusters,

Chapter four: The use of rare gases to control collision energy

$\text{H}_3\text{O}^+(\text{H}_2\text{O})_n$ where, $n = (0-4)$, were successfully mapped for 35-105 Td for nitrogen and 15-75 Td for argon. It was found early on in this study that if the E/N exceeded ~ 80 Td with argon as a buffer gas then the ion source would short-out, causing the ion count to drop to ~ 0 c/s and become unusable for ~ 24 hours whilst the ion count recovered. These conditions were therefore avoided.

As the E/N of the system was increased, the water cluster ions $\text{H}_3\text{O}^+(\text{H}_2\text{O})_n$ were reduced, as shown in Figure 4-7 and Figure 4-8. For nitrogen as the buffer gas, the cross over point where H_3O^+ dominates over $\text{H}_3\text{O}^+\text{H}_2\text{O}$ is at ~ 95 Td. Under argon, however, it can be seen in Figure 4-8 that the whole graph is shifted to lower E/N values compared to nitrogen (Figure 4-7) such that the cross over point for $\text{H}_3\text{O}^+/\text{H}_3\text{O}^+\text{H}_2\text{O}$ is now ~ 65 Td.

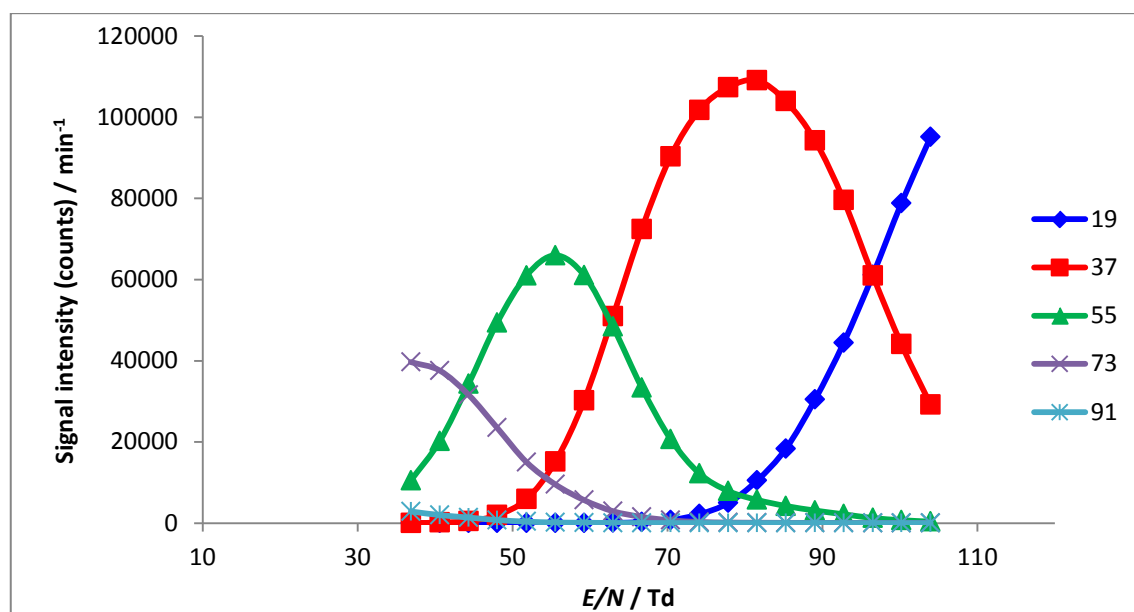


Figure 4-7: Hydronium and its hydrated clusters as a function of E/N when nitrogen is the buffer gas. 19 = H_3O^+ , 37 = $\text{H}_3\text{O}^+\text{H}_2\text{O}$, 55 = $\text{H}_3\text{O}^+(\text{H}_2\text{O})_2$, 73 = $\text{H}_3\text{O}^+(\text{H}_2\text{O})_3$, 91 = $\text{H}_3\text{O}^+(\text{H}_2\text{O})_4$.

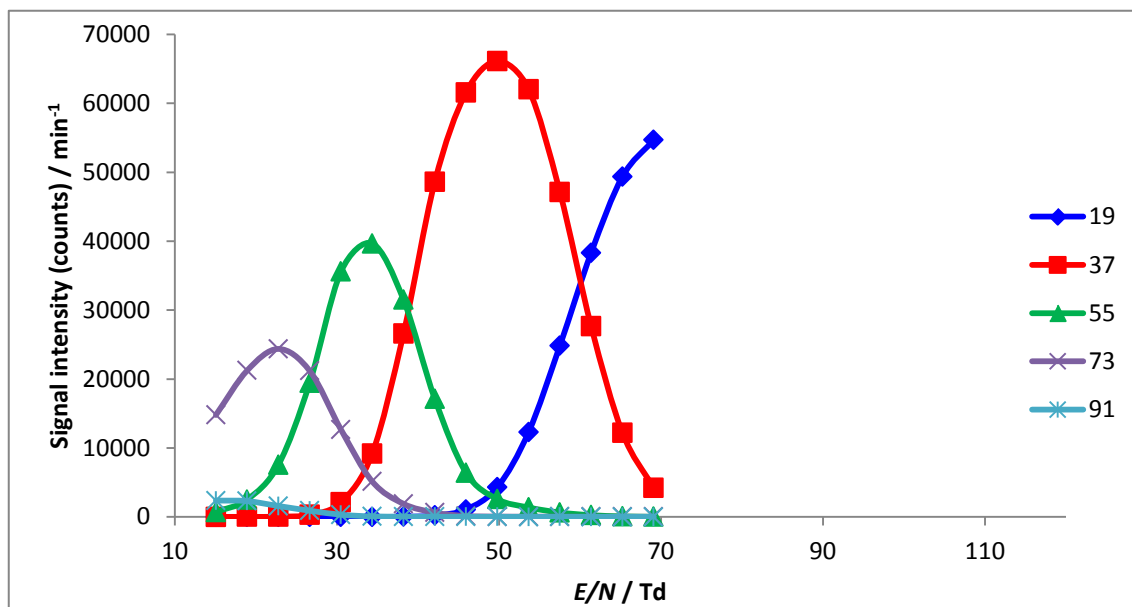


Figure 4-8: Hydronium and its hydrated clusters as a function of E/N when argon is the buffer gas. 19 = H_3O^+ , 37 = $\text{H}_3\text{O}^+\cdot\text{H}_2\text{O}$, 55 = $\text{H}_3\text{O}^+\cdot(\text{H}_2\text{O})_2$, 73 = $\text{H}_3\text{O}^+\cdot(\text{H}_2\text{O})_3$, 91 = $\text{H}_3\text{O}^+\cdot(\text{H}_2\text{O})_4$.

A shift is expected when we take into account the difference in collision energy in the drift tube from the previous centre of mass calculations (section 4.2.1.) However, those calculations indicate that equivalent hydronium cluster ratios would be observed at 65 Td for argon and 125 Td for nitrogen. Under experimental conditions as shown in Figure 4-7 and Figure 4-8 it can be seen that this isn't quite accurate, with the equivalent hydronium cluster ratio for nitrogen occurring at 95 Td.

4.5.3 Argon/nitrogen mixture

After investigating how the production of hydronium cluster ions was affected as a function of E/N , the next stage was to investigate how a mixture of nitrogen/argon as a buffer gas affects the detection sensitivity.

Buffer gas mixtures were dynamically diluted using a cylinder of pure nitrogen and a cylinder of pure argon. Mass flow controllers were used to mix these gases into a single stream at any desired mixing ratio. This stream of gas was then fed separately into the permeation tube oven and through the water bubbler, so that the whole system is kept at a homogeneous concentration of nitrogen/argon.

Chapter four: The use of rare gases to control collision energy

When selecting the chosen E/N settings for this study, a consideration was to ensure that the ion source did not 'spark': the settings chosen were listed in Table 4-3. For each E/N setting, a range of five argon/nitrogen combinations were used at 0 %, 16 %, 35 %, 51 %, and 67 % of argon in a nitrogen atmosphere. This resulted in a total of 25 different settings which were chosen to map a 3-dimensional space dictated by E/N as one dimension and the argon/nitrogen ratio as the other.

Five permeation tubes were used to provide the following VOCs for analysis: isoprene (m/z 69), benzene (m/z 79), toluene (m/z 93), ethyl-benzene (m/z 107) and 2-choloethyl-sulfide (m/z 125 and m/z 127).

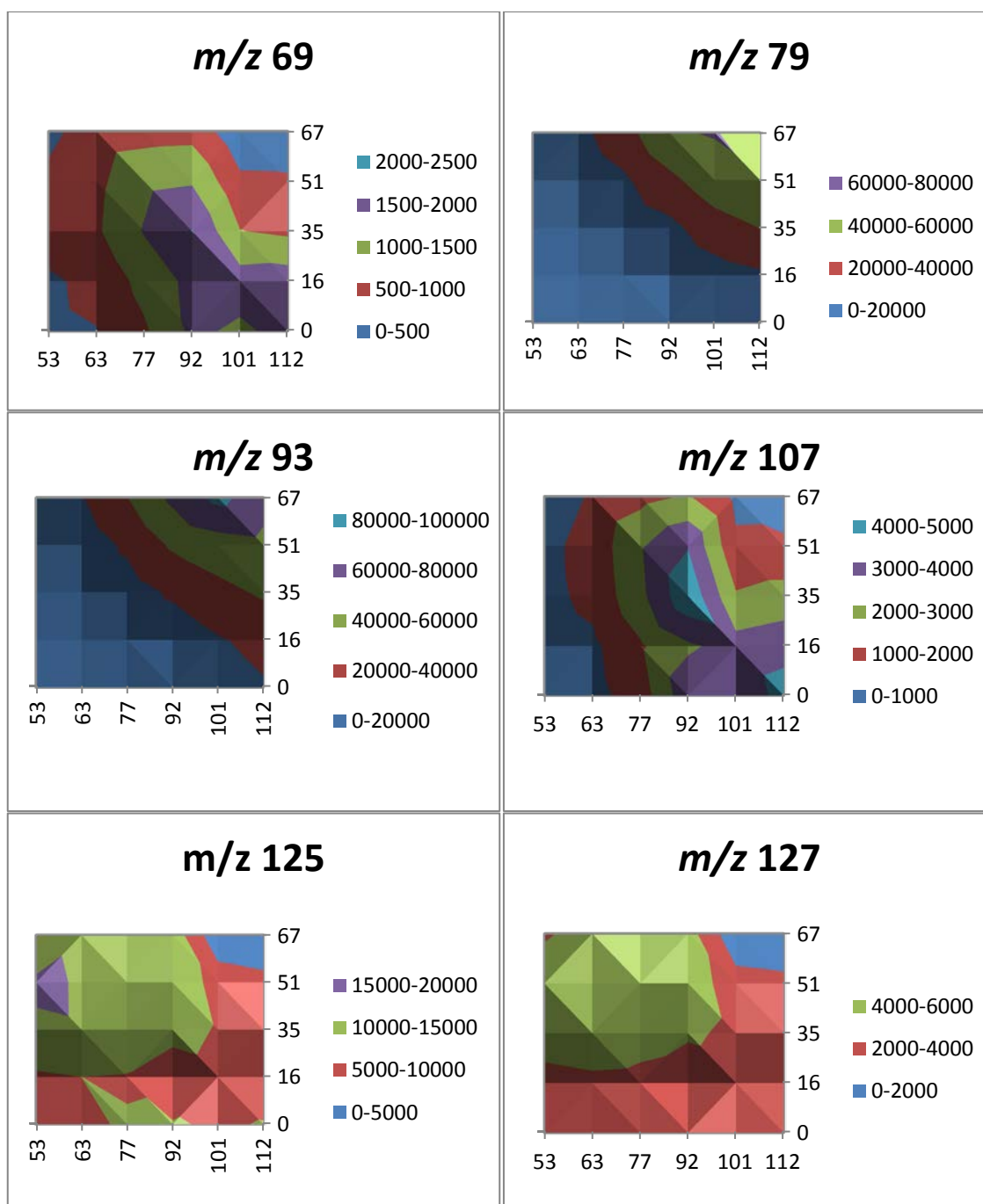


Figure 4-9. 3D plots of the protonated parent ion for 5 different VOCs. The x-axis is E/N in Td and the y axis is the % of argon as the buffer gas in a nitrogen balance. The protonated ions masses are given for isoprene (m/z 69), benzene (m/z 79), toluene (m/z 93), ethylbenzene (m/z 107) and 2-chloroethyl sulfide (m/z 125 and 127). The contour units are counts min^{-1} .

For each of the five compounds analysed, it appears that there is a different combination of E/N and argon % that gives the maximum sensitivity for the parent ion in question. This has been tabulated in Table 4-5 for ease of viewing. For all of the compounds analysed, other than 2-chloroethyl sulfide, generally the largest sensitivity was achieved when using the highest E/N (with the

correct quantity of argon and or nitrogen). Two of those (benzene and toluene), along with 2-chloroethyl sulfide, exhibit a higher sensitivity when argon is > 60 % in the system. This illustrates that the optimal conditions which produce the largest sensitivity is compound dependent. Even the three aromatic VOCs (benzene, toluene and ethyl benzene) do not all exhibit the same behaviour.

Table 4-5. Summary of the conditions used (E/N and % Ar, expressed as high, medium, or low) for the five chosen VOCs.

VOC	E/N / Td (high ¹ , medium ² , low ³)	Argon % (high ⁴ , medium ⁵ , low ⁶)
Isoprene	High	Low
Benzene	High	High
Toluene	High	High
Ethylbenzene	High/medium	Low/medium
2-chloroethyl sulfide	Low	High

¹High: $E/N > 95$ Td

²Medium: $70 \text{ Td} < E/N < 95$ Td

³Low: $E/N < 70$ Td.

⁴High: Argon > 50 %

⁵Medium: $20 \% < \text{Argon} < 50 \%$

⁶Low: Argon < 20 %

4.5.4 Fragmentation comparison

There were several variables which could be manipulated during these experiments, which makes what appears a simple inter-comparison between buffer gas experiments more difficult to interpret. The conditions chosen to examine the effect of changing the buffer gas on VOC fragmentation must therefore be carefully considered. Three sets of conditions present themselves for possible comparison: the first is to compare fragmentation patterns when matching absolute E/N values. However, this is complicated by the obvious changes that occur on the kinetics of the system i.e., in theory changing the buffer gas should yield very different results for a given E/N . The other two involve either choosing the same theoretical collision energy inside the drift tube (as calculated in section 4.2.1), or taking a more practical approach and comparing the settings under identical hydronium clustering conditions (as discussed in section 4.5.2). The three sets of conditions used in the following analysis for nitrogen and argon buffer gases are listed in Table 4-6.

Chapter four: The use of rare gases to control collision energy

Table 4-6. The three sets of ‘comparable’ conditions that yield equivalent E/N , equivalent collision energy, and equivalent hydronium ratio for pure argon and nitrogen buffer gases.

	Argon / Td	Nitrogen / Td
Same E/N	68	68
Same KE^1	52	79
Same hydronium ratio ²	63	100

¹Equivalent calculated collision energy: 0.1 eV.

²Equivalent hydronium clusters: 65 % H_3O^+ , 35 % $H_3O^+ \cdot H_2O$.

An E/N of 68 Td was chosen for the ‘same E/N ’ comparison because this was the highest E/N that an argon buffer gas could be operated at in the ‘LE-ToF’ without causing damage, (ideally though this value would be higher, such as between 100 - 120 Td if a comparison to a common setting for a nitrogen buffer gas was wanted). All three settings were analysed for two different compounds, hexane and limonene, and are presented here.

4.5.4.1 Fragmentation of hexane

The first VOC to be analysed was hexane, due to its extensive fragmentation owing to subsequent sequential $-CH_2$ loss from the parent ion. This obvious and logical fragmentation pattern allowed for simpler comparison between the various different PTR-MS settings. During each experiment, hexane was injected into a Tedlar bag (Thames Restek, UK) and mixed with the appropriate buffer gas (either argon or nitrogen). The same buffer gas was also used as the water vapour carrier gas in the bubbler set-up. Samples were analysed under a range of E/N ratios which spanned those presented in Table 4-6. In argon, this range covered 15 – 65 Td and in nitrogen, these conditions ranged from 35 Td to 110 Td. Unlike most other hydrocarbons, the alkanes undergo hydride abstraction instead of protonation when they react with hydronium, therefore producing $M-H^+$ parent ions (where M is the analyte molecule).

Figure 4-10 shows the parent ion (m/z 85) alongside the total response from all hexane ions (consisting of the parent ion along with subsequent $-CH_2$ fragments down to m/z 29). It can be seen that with increasing E/N the signal intensity gradually increases with a slight maximum before an exponential rise in signal intensity. The maximum sensitivity for the parent ion (m/z 85), as well as the sum of the parent ion and all the $-CH_2$ fragments, occurs at the largest E/N . The reason for this increase in signal intensity with increasing E/N could be due to

higher quantities of unclustered hydronium (H_3O^+) being produced at higher E/N as larger water cluster ions are dissociated by the increased collision energies in the drift tube (as seen in Figure 4-7 and Figure 4-8). An alternative explanation is that the increased E/N leads to improved ion-beam focussing, i.e. the combination of pressure and collision energy allows for a higher transmission of ions from the drift tube through the critical orifice and onto the transfer region. The signal intensity for argon at ~ 65 Td is almost double that of nitrogen at ~ 110 Td.

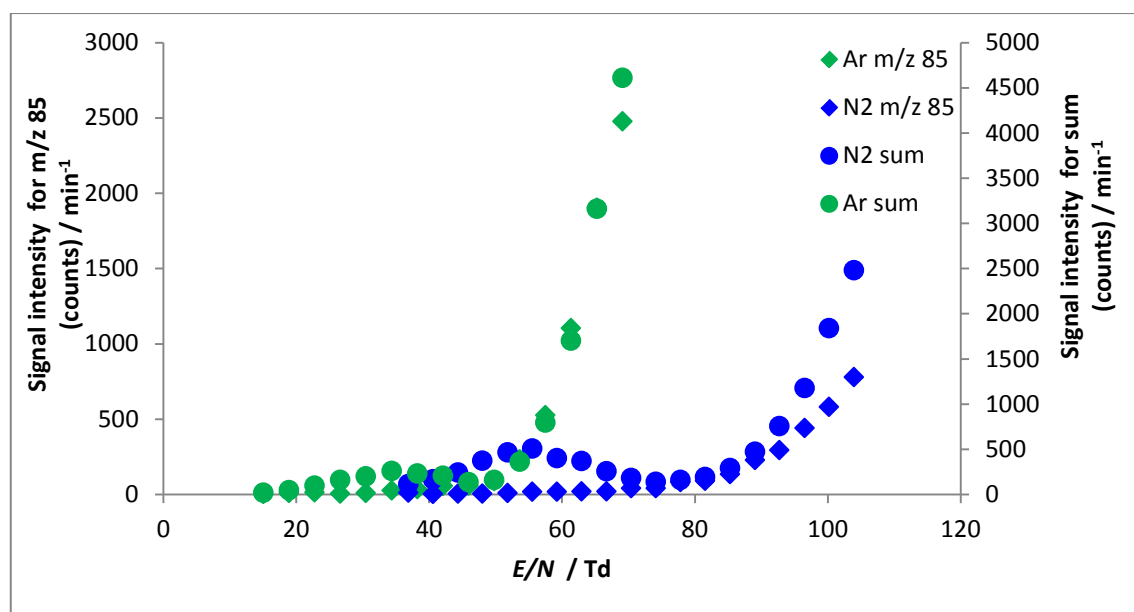


Figure 4-10. Hexane signal intensity versus E/N for argon (green) and nitrogen (blue) as the buffer gas.

Figure 4-10 shows that a higher sensitivity can be achieved for hexane at ~ 60 Td with argon (whether detecting just the parent ion at m/z 85 or for all the summed ions produced from hexane protonation) than can be achieved for ~ 110 Td in nitrogen. For every E/N setting analysed in Figure 4-10, a mass spectrum was generated. Figures 4-11 to 4-13 present mass spectra acquired under the three settings detailed in Table 4-6.

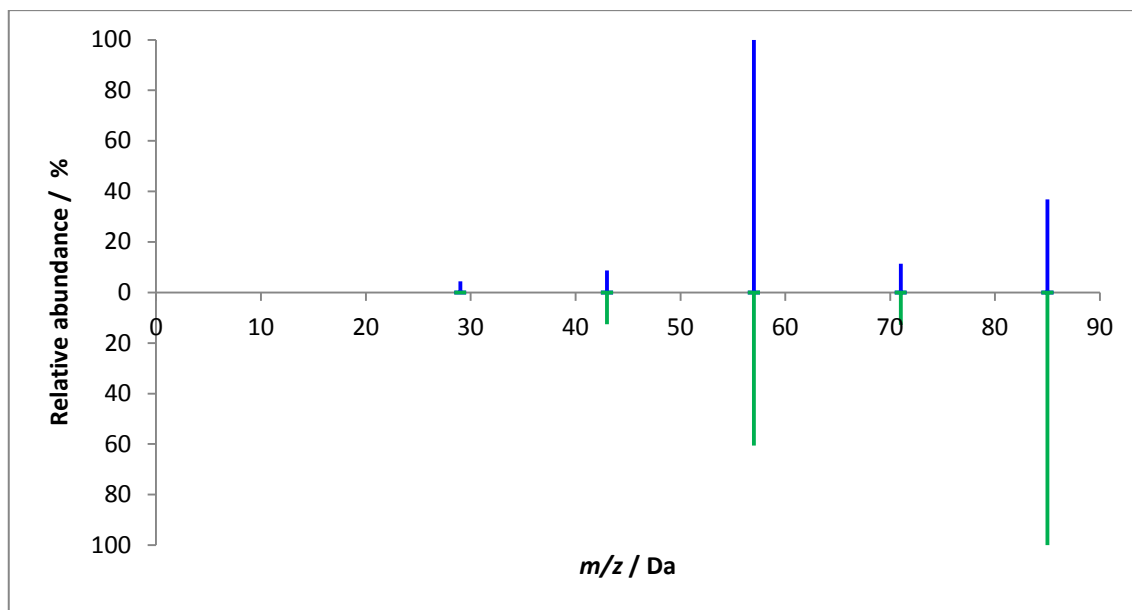


Figure 4-11. Simplified mass spectrum presented as relative abundance for the most prominent peak in the spectrum for hexane at equivalent E/N (68 Td). The top spectrum (blue) is for the nitrogen buffer gas, and the bottom spectrum (green) is for argon as a buffer gas.

Figure 4-11 compares a simplified mass spectrum (where the only ions presented are the parent ion and subsequent $-\text{CH}_2$ fragments) for both nitrogen and argon buffer gases at 68 Td. It shows that for argon under these conditions a more favourable spectrum is produced, i.e. there is less fragmentation and the parent ion dominates. For nitrogen the most prominent ion is m/z 57 with the parent ion a third of its size; however, when switching to an argon buffer gas, the m/z 57 peak is reduced and the m/z 85 (parent ion) peak is greatly increased. The amplitude of the other fragments, m/z 43 and m/z 71 stay approximately the same in both spectra whilst m/z 29 disappears completely from the argon spectrum. This demonstrates that by changing the gas from nitrogen to argon whilst keeping all other conditions identical, a shift in fragmentation readily occurs. The fragmentation differences become greater as E/N is increased.

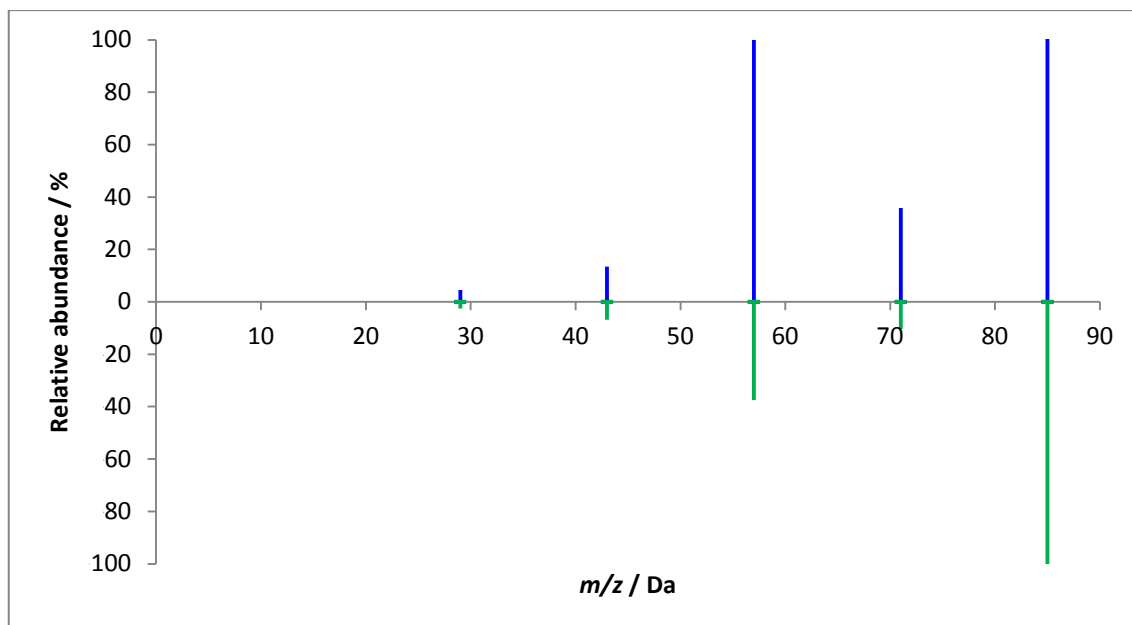


Figure 4-12. Simplified mass spectrum presented as relative abundance for the most prominent peak in the spectrum for hexane at equivalent kinetic energies (0.1 eV - nitrogen at 79 Td and argon at 52 Td. The top spectrum (blue) is for nitrogen and the bottom spectrum (green) is for argon as a buffer gas.

For the conditions employed in generating Figure 4-12, both m/z 57 and m/z 85 peaks are almost equal in magnitude for nitrogen. However for argon buffer gas, the ratio is changed substantially, with the peak at m/z 57 reduced to about a quarter of the size of the protonated parent molecule peak (m/z 85).

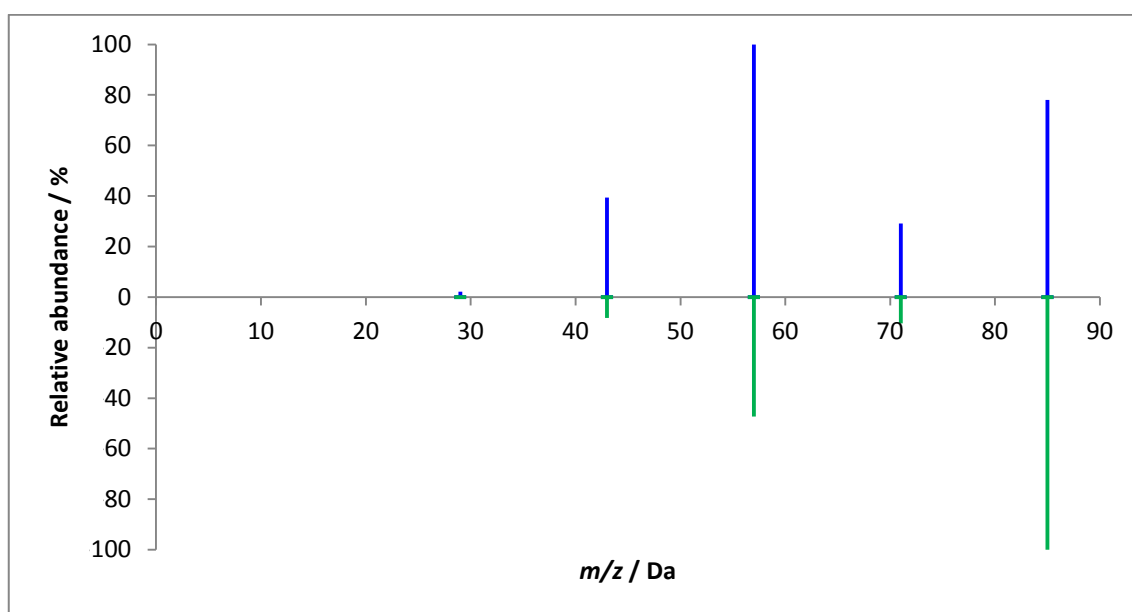


Figure 4-13. Simplified mass spectrum presented as relative abundance for the most prominent peak in the spectrum for hexane at equivalent hydronium ratios (nitrogen at 100 Td and argon at 63 Td. The top spectrum (blue) is for the nitrogen buffer gas, and the bottom spectrum (green) is for argon as a buffer gas.

Chapter four: The use of rare gases to control collision energy

Figure 4-13 compares the hexane fragmentation pattern under the same hydronium conditions (i.e., the same $\text{H}_3\text{O}^+:\text{H}_3\text{O}^+.\text{H}_2\text{O}$ ratio) for each buffer gas. Fragmentation is more extensive in nitrogen than argon. Furthermore, this is also possibly the best comparison to use from a practical point of view, since using the ratio of hydronium clusters attempts to give an exact picture of the collision dynamics going on inside the drift tube, independent of theoretical calculations. Also an E/N of 100 Td for nitrogen is only slightly below the typical values used in most PTR-MS experiments. The fragment peaks at m/z 43 and m/z 71 present in the nitrogen spectrum are greatly reduced in the argon spectrum.

Table 4-7. Presented here are the mass channels displayed as a % of the total ion count for hexane in three different comparable experiments carried out using both nitrogen and argon as a buffer gas. $\Delta_{\text{Ar-N}_2}$ is the difference between the intensity of the mass channel in nitrogen subtracted from the argon measurement.

Conditions	Buffer gas	Ions as a percentage of all ions listed					Sum of ions / %
		m/z 29	m/z 43	m/z 57	m/z 71	m/z 85	
Same E/N	Nitrogen	2.7	5.4	62.0	7.1	22.8	100
	Argon	0.1	6.7	32.6	6.9	53.7	100
	$\Delta_{\text{Ar-N}_2}$	-2.6	1.3	-29.4	-0.2	30.9	-
Same KE	Nitrogen	1.6	4.7	34.7	12.4	46.6	100
	Argon	1.6	4.4	23.8	6.6	63.8	100
	$\Delta_{\text{Ar-N}_2}$	0.0	-0.3	-10.9	-5.8	17.2	-
Same Hydronium ratio	Nitrogen	0.8	15.8	40.2	11.7	31.4	100
	Argon	0.1	4.9	28.5	6.3	60.2	100
	$\Delta_{\text{Ar-N}_2}$	-0.7	-10.9	-11.7	-5.4	28.8	-

Table 4-7 shows that for all of the conditions chosen for the argon/nitrogen comparison, when argon is used as the buffer gas, an improvement in the relative abundance in parent ion is achieved. There is also a reduction in intensity for the main fragment of hexane, m/z 57, for all three pairs of conditions analysed. The fact that none of the conditions produced identical mass spectra for the two buffer gases is also a significant finding. One might expect that, for the same theoretical ion-buffer collision energy (Figure 4-12), the fragmentation pattern should be identical for both argon and nitrogen. However, as this is not the case this indicates that this simple viewpoint is erroneous.

When equivalent hydronium levels are explored, which should indicate identical conditions within the drift tube, differences are still observed in nitrogen when compared to argon. This could be because the hydronium clusters are loosely bound as opposed to the stronger chemical bonds within the analyte, and these are each affected differently by the drift tube conditions. Also due to the kinetic energy calculations having mass dependent values (section 4.2.1), even if there is a set of conditions that provide identical fragmentation for a particular analyte molecule, it is unlikely that this will have the same effect on other analyte molecules due to this mass dependence.

4.5.4.2 Fragmentation of limonene

For the second VOC that was studied in detail, limonene, the analysis was carried out in the same manner as for hexane. Spectra were acquired under numerous E/N settings for both argon and nitrogen as buffer gases. Here, the two most abundant mass channels are m/z 81 (a fragment) and m/z 137 (the protonated parent ion). A plot of count rate versus E/N is presented in Figure 4-14.

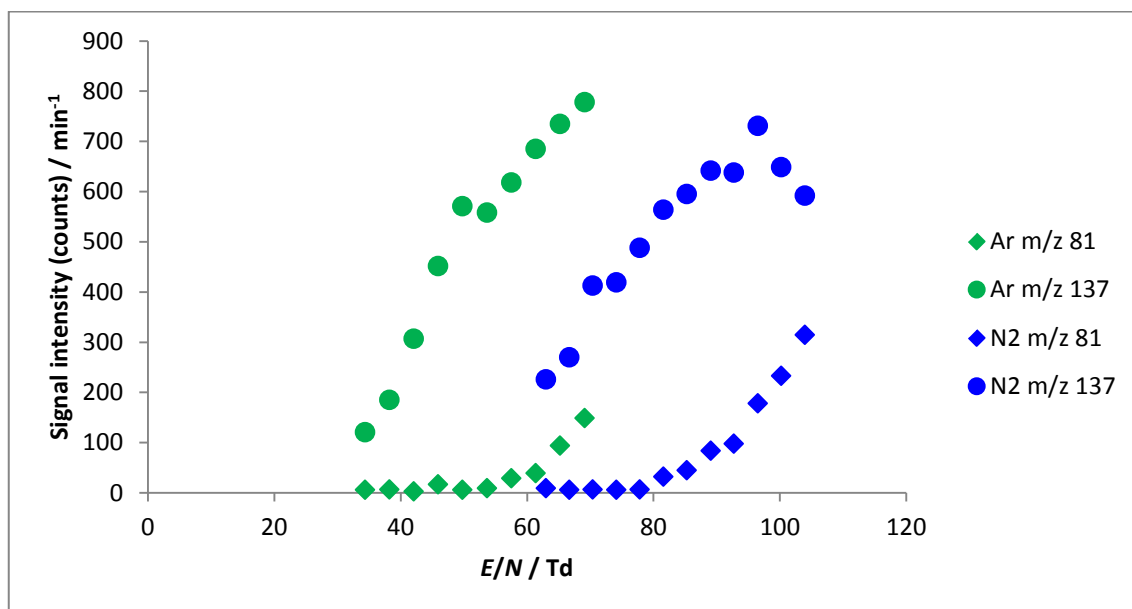


Figure 4-14. Number of counts per second as a function of E/N for m/z 81 and m/z 137 for the buffer gas nitrogen (blue) and argon (green).

In general, both the parent ion and fragment ion signals increase with increasing E/N . However, for nitrogen, the parent ion begins to decrease in abundance beyond ~ 90 Td. Presumably, this would also happen for argon if

Chapter four: The use of rare gases to control collision energy

spectra were obtained at a higher E/N , but as mentioned earlier this is not possible for practical reasons under a 100 % argon regime. Very similar sensitivities are observed for both buffer gases but there is a shift of about 40 Td lower for argon compared to nitrogen. The maximum sensitivity in argon for the parent ion occurs with around 50 % less intensity of the fragment when compared to the protonated parent molecule.

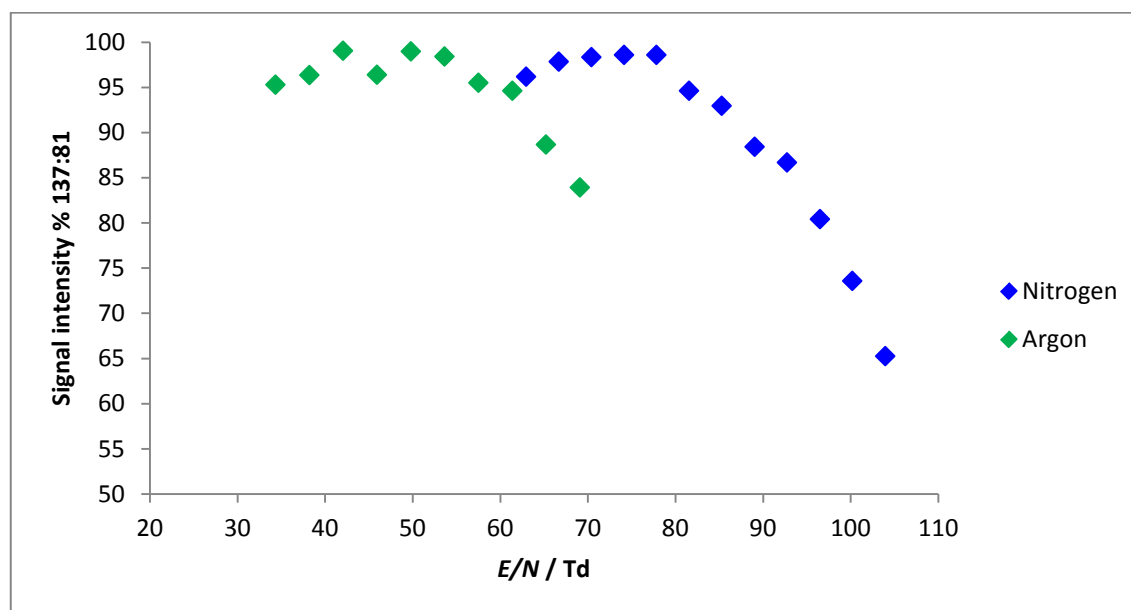


Figure 4-15. Percentage of limonene parent ion as a total of the parent ion and fragment.

Figure 4-15 shows the percentage of parent ion is > 90 % for E/N ratios < 60 Td for argon and < 80 Td for nitrogen. This then begins to reduce for both buffer gases as the E/N increases and the drift tube energy increases, causing more violent collisions and thus fragmentation of the limonene molecule.

Table 4-8. Summary of ion fragment distribution for limonene.

Conditions	Buffer gas	Peak height / Hz		% of m/z 137 ¹	Δ % change Ar-N ₂
		m/z 81	m/z 137		
Same E/N	Nitrogen	7	413	98	-14
	Argon	149	778	84	
Same KE	Nitrogen	32	564	95	3
	Argon	9	558	98	
Same hydronium ratio	Nitrogen	315	592	65	24
	Argon	94	735	89	

¹ % = $(m/z\ 137 / (m/z\ 137 + m/z\ 81)) * 100$

Table 4-8 contains a comparison of the percentage of the parent ion when compared with the fragment for the same three operating conditions detailed in

Table 4-6. When the same E/N is used, a reduction in parent ion percentage of 14 % occurs. This is due to the nitrogen setting of 68 Td being particularly soft, with little fragmentation of the limonene ion (2 %). However, a higher sensitivity is observed for the parent ion when argon is used. For the same KE almost identical sensitivity is observed, as well as very similar degrees of fragmentation. When the conditions were chosen to create the same hydronium cluster ratios, a higher intensity for the parent ion under argon was observed as well as a lower intensity for the fragment, resulting in a 24 % increase in parent ion abundance.

4.6 Exhaust gas analysis

The emission of anthropogenic VOCs into the atmosphere from any source is of great concern when the environmental and health implications are investigated. There are a wide range of sources for anthropogenic VOCs: the fossil fuel industry (mining, storage and transportation), industrial processes including organic solvents, and agriculture (Hewitt, 1998). One of the main sources of these anthropogenic VOCs is through the emission of the combustion engine. Several studies have been carried out in the urban environment such as Mexico city (Rogers et al., 2006, Molina et al., 2007), Tokyo (Kato et al., 2004, Miyakawa et al., 2005) and Barcelona (Filella and Penuelas, 2006).

As well as studying the VOCs in urban environments, studies into the composition of exhaust emissions have also taken place for both petrol and diesel engines (Jobson et al., 2005, Staehelin et al., 1998). Engine exhaust emissions contain a complex mixture of particulate compounds and gases, including many unburnt VOCs such as alkanes, alkenes and aromatic compounds and these compounds are of great interest in the urban environment where road traffic is the primary contributor of pollution. Poor air quality, especially in an urban environment, places everybody at risk, especially the young, old, and those with respiratory difficulties (Bessa et al., 2011).

Analysing exhaust emissions provides a perfect platform for studying a complex matrix of VOCs. The use of changing to a rare gas buffer gas when analysing exhaust samples and the effect of this on the fragmentation of compounds and the overall number and magnitude of the peaks present in mass spectra are assessed, with a focus on minimising fragmentation.

4.6.1 Experimental

4.6.1.1 Exhaust gas collection

The exhaust emissions from a Rover 2000i petrol engine were provided by the Engineering Department directly into a 10 L tedlar bag with appropriate fitment. All engine tests and samples were collected under the same conditions: Throttle angle 3°, Torque 20 Nm.

4.6.1.2 PTR-ToF-MS analysis

The exhaust gases were collected in chemically inert 10 L Tedlar bags (Thames Restek, UK) with polypropylene fittings for attachment to the engine exhaust system. The contents of the Tedlar bags were then analysed by the author using the LE-ToF as per the previous experiments in this chapter. A dilution method was used to prevent dead time loss from over-saturation of mass channels. 100 mL was extracted from the sample bag using a gas tight syringe, and this was injected into a second tedlar bag, which was topped up to 10 L with either inert, dry nitrogen (99.999 % BOC gases) or argon (99.999 % BOC gases) thus producing a 1:100 dilution.

To provide a comparison between an argon and nitrogen buffer gas, identical hydronium ratios ($\text{H}_3\text{O}^+:\text{H}_3\text{O}^+.\text{H}_2\text{O}$) and identical kinetic energies were compared (in a similar method to section 4.5.4) and these settings are listed in Table 4-9.

Table 4-9. The two sets of 'comparable' conditions that yield equivalent E/N , equivalent collision energy, and equivalent hydronium ratio for pure argon and nitrogen buffer gases.

	Argon / Td	Nitrogen / Td
Same KE ¹	52	79
Same hydronium ratio ²	63	100

¹ Equivalent calculated collision energy: 0.1 eV.

² Equivalent hydronium clusters: 65 % H_3O^+ , 35 % $\text{H}_3\text{O}^+.\text{H}_2\text{O}$.

4.6.2 Results and discussion

Two sets of comparative conditions were used and the resultant peak heights are compared in this section. First, a comparison of the number of peaks for a given intensity were compared for the same theoretical collision energy (0.1 eV) as calculated in section 4.2.1. Full mass spectra from m/z 15 to m/z 250 were obtained from the analysis of exhaust emissions under both nitrogen and argon buffer gases and these spectra have been background subtracted. The heights (signal intensity in counts s^{-1}) of the remaining peaks have then been divided up into four size categories: Those between 10 and 100 counts min^{-1} , those between 100 and 500 counts min^{-1} , those between 500 and 1000 counts min^{-1} , and those over 1000 counts min^{-1} . The reason to eliminate the peaks below 10 counts min^{-1} was taken in order to get a smaller number of peaks for comparison as there are many peaks below 10 counts min^{-1} and analysing them all complicated the analysis excessively.

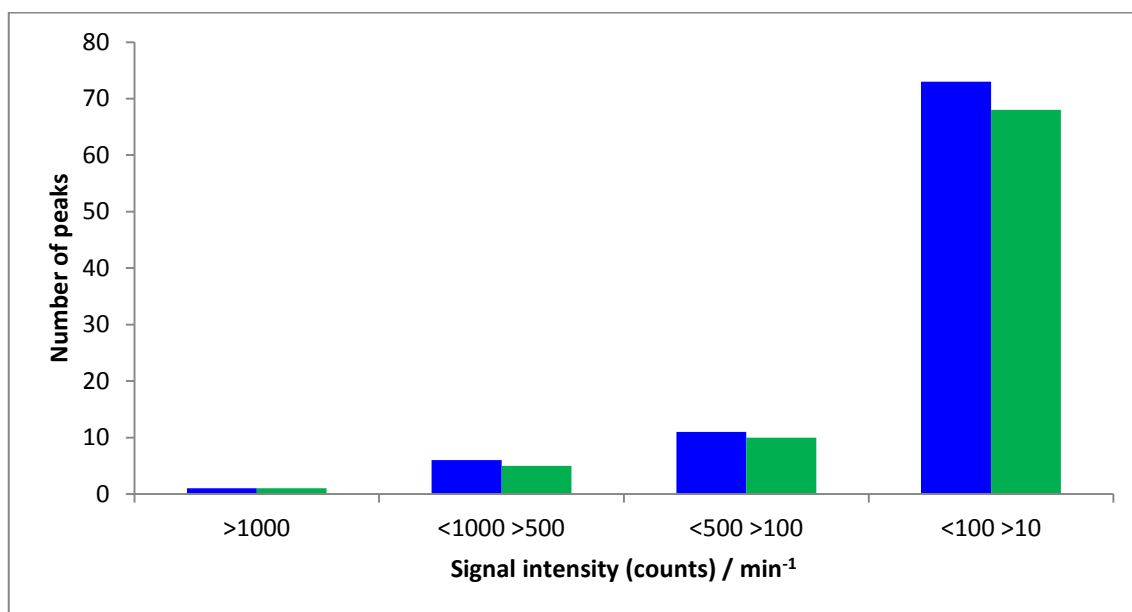


Figure 4-16. The number of peaks in the mass spectrum that are a certain height (number of counts / min⁻¹) for the same calculated kinetic energy (0.1 eV). Blue = nitrogen buffer gas, green = argon buffer gas.

Figure 4-16 shows that for the same hydronium ratio there is a small variation in the number of peaks in a given height range. For peaks > 1000 counts / min⁻¹ there is a single peak in both the nitrogen and argon spectra. However, for the other three height ranges, there is a difference in the number of peaks in the argon spectra compared to nitrogen, with the largest reduction being in the

height range $< 100 > 10 \text{ counts min}^{-1}$. With the nitrogen gas there are 73 small peaks in the range of $< 100 > 10 \text{ counts min}^{-1}$ but with argon this is reduced to 68 peaks.

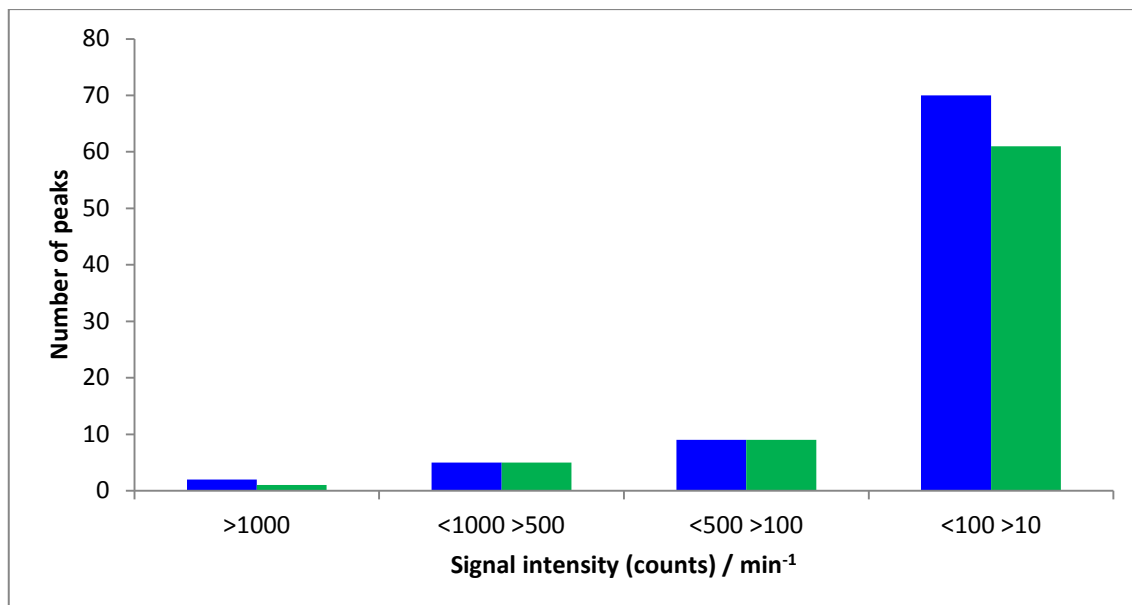


Figure 4-17. The number of peaks in the mass spectrum that are a certain height (number of counts min⁻¹) for the same H₃O:H₃O⁺:H₂O ratio (65 % H₃O⁺). Blue = nitrogen buffer gas, green = argon buffer.

When comparing the number of peaks under equivalent hydronium ratios (Figure 4-17), a similar result to Figure 4-16 is obtained. Although there is one less prominent peak above 1000 counts min⁻¹, there are the same number of peaks in the two middle height categories and a slightly larger reduction of small peaks when argon buffer gas is used. The data from Figure 4-16 and Figure 4-17 is summarised in Table 4-10. It can be seen that overall there is a reduction in total peaks for the same kinetic energy and same hydronium ratio when an argon buffer gas is used compared to nitrogen. The ion fragments observed in the argon spectrum are all observed in the nitrogen spectrum, i.e. they are a subset of the ions observed using nitrogen, not different ions.

Chapter four: The use of rare gases to control collision energy

Table 4-10. Number of peaks in a given height range (signal intensity) from the spectra of exhaust emissions for two different buffer gases at two pairs of comparative settings.

Conditions	Buffer gas	Number of peaks in a given height range				Total peaks
		>1000 c s ⁻¹	>1000 >500 c s ⁻¹	<500 >100 c s ⁻¹	<100 >10 c s ⁻¹	
Same KE ¹	Nitrogen	1	6	11	73	91
	Argon	1	5	10	68	84
	Δ_{Ar-N2}	0	-1	-1	-5	-7
Same Hydronium ratio ²	Nitrogen	2	5	9	70	86
	Argon	1	5	9	61	76
	Δ_{Ar-N2}	-1	0	0	-9	-10

¹Equivalent calculated collision energy: 0.1 eV.

²Equivalent hydronium clusters: 65 % H₃O⁺, 35 % H₃O⁺.H₂O.

4.7 Conclusion

The aim of this chapter was to first ascertain whether or not the LE-ToF could be successfully operated with a pure buffer gas other than nitrogen (or air) and then to identify both the impact and potential benefit there may be in changing the composition of the buffer gas make-up. Under the conditions suggested by Inomata and co-workers (Inomata et al., 2008), limonene was successfully analysed under argon at 40 Td and exhibited a slightly increased sensitivity (8 %) alongside, perhaps more importantly, reduced fragmentation when compared to conditions commonly used in routine analysis (100 Td and a nitrogen buffer gas).

Both buffer gases produced similar patterns with respect to the distribution of hydronium ions across the E/N range analysed. However, the pattern for argon was shifted to a lower E/N by approximately 40 Td (Figure 4-7 and Figure 4-8). Based on this finding, a pattern of hydronium ion clusters ($\text{H}_3\text{O}^+:\text{H}_3\text{O}^+.\text{H}_2\text{O}$) associated with a specific E/N ratio can be recreated when nitrogen is replaced by argon as a buffer gas. Emerging applications of PTR-MS are moving away from lab-based, single component experiments and into the field, where complex multi-component samples contain not only trace VOCs but also high concentrations of other species. This increase in other species could potentially alter buffer gas composition significantly and this has been investigated by changing the buffer gas in the PTR-MS system. Furthermore, the potential in doping the buffer with a rare gas to optimise PTR conditions for enhanced sensitivity of a specific compound or to effect the fragmentation of a specific compound is an appealing concept.

Section 4.5.3 presents a detailed study into the use of nitrogen/argon buffer gas mixes, where hexane and limonene were analysed to ascertain optimal buffer gas mixing ratios. The results showed that the optimal ratio of argon/nitrogen is highly compound dependent. For example, under harder ionisation conditions (greater than 100 Td) compounds such as benzene and toluene exhibited a greater parent ion signal when higher mixing ratios of argon were used (> 60 %). However, isoprene detection was most sensitive when the system was 100

% nitrogen. This situation is further convoluted when E/N is also manipulated to optimise sensitivity.

To further investigate the affect that rare gases have on VOC fragmentation patterns, three regimes were chosen in order to compare spectra acquired under nitrogen and argon: equivalent E/N ratios, equivalent kinetic energies and equivalent hydronium ratios. For the monoterpene, limonene, the equivalent kinetic energy and equivalent hydronium cluster ratio regimes both yielded a reduction in fragmentation, with the former achieving essentially identical fragmentation under both argon and nitrogen. Hexane, however, responded differently, with none of the regimes under study yielding comparable fragmentation conditions, and all three regimes yielding a reduction for argon of the main fragment (m/z 57) and an increase in signal intensity for the parent ion (m/z 85). The fact that limonene and hexane responded differently to a change in buffer gas may well be related to their different ionisation pathways in PTR-MS, i.e. hydride loss vs protonation. Furthermore, the fact the equivalent kinetic energy and hydronium ratio regimes produced different results for both compounds is a significant finding as it exemplifies how the change in ionisation conditions, following changing the buffer gas, affects hydronium clustering differently from VOC ion fragmentation.

When a complex mixture, such as exhaust gas, is analysed there is a slight decrease in the smallest peaks present when argon is used compared to nitrogen buffer gas. Ideally a sizable reduction would have been observed, however, if further optimisation was carried out as the process is highly compound dependant, then there is the potential for this to occur with the ultimate aim of maximising this reduction of small peaks in order to simplify interpretation/ spectral assignment.

The system described in chapter two has been carefully optimised for the detection of a wide range of compounds. Much effort has been placed into finding a compromise between ion beam focusing, lowering the E/N (to lengthen drift times and thus increase sensitivity), reducing hydronium clustering (effectively raising the E/N) and reducing the back-flow of air from the drift tube

(to minimise generation of unwanted competitive reagent ions). Thus this optimisation process represents a delicate balance between many factors and is therefore not easily manipulated. If, however, use of argon enables ionisation conditions which yield the same extent of hydronium clustering yet less VOC fragmentation (without compromising sensitivity), then this may have clear advantages for many applications. This includes, for example, the detection of alkanes (Sommariva et al., 2014): because many alkanes readily fragment into common ions, there is a clear advantage to creating softer ionisation conditions through argon-doping of the buffer.

Not only has this study provided some evidence that changing buffer gas composition may be advantageous in terms of both sensitivity and fragmentation, it has also raised several important points regarding the analysis of air mixtures where compounds exist that exceed trace concentrations. The results in section 4.5.3 suggest that if compounds exist within a sample at a concentration such that the bulk composition of the buffer gas is affected, the sensitivity towards the VOC analytes may also be affected. This effect may be negated if external calibrants are used to determine concentrations, provided they contain all components which contribute to the buffer gas mixture. However, if this is not possible (as is often the case with a breath sample or exhaust fumes) or if concentrations are calculated theoretically, results must be amended to take into account the buffer gas make-up, analogous to the corrections required to take into account changing humidity. Furthermore, these corrections are compound-dependent. It is apparent that much work is required to fully understand the buffer gas system and the results presented in this study merit further investigation.

4.8 References

- BESSA, V., DARWICHE, K., TESCHLER, H., SOMMERWERCK, U., RABIS, T., BAUMBACH, J. I. & FREITAG, L. 2011. Detection of volatile organic compounds (VOCs) in exhaled breath of patients with chronic obstructive pulmonary disease (COPD) by ion mobility spectrometry. *International Journal for Ion Mobility Spectrometry*, 14, 7-13.
- BLAKE, R. S., MONKS, P. S. & ELLIS, A. M. 2009. Proton-Transfer Reaction Mass Spectrometry. *Chemical Reviews*, 109, 861-896.
- BLAKE, R. S., WHYTE, C., HUGHES, C. O., ELLIS, A. M. & MONKS, P. S. 2004. Demonstration of Proton-Transfer Reaction Time-of-Flight Mass Spectrometry for Real-Time Analysis of Trace Volatile Organic Compounds. *Analytical Chemistry*, 76, 3841-3845.
- BLAKE, R. S., WYCHE, K. P., ELLIS, A. M. & MONKS, P. S. 2006. Chemical ionization reaction time-of-flight mass spectrometry: Multi-reagent analysis for determination of trace gas composition. *International Journal of Mass Spectrometry*, 254, 85-93.
- ELLIS, A. M. & MAYHEW, C. A. 2014. *Proton Transfer Reaction Mass Spectrometry: Principles and Applications*, Wiley.
- FILELLA, I. & PENUELAS, J. 2006. Daily, weekly, and seasonal time courses of VOC concentrations in a semi-urban area near Barcelona. *Atmospheric Environment*, 40, 7752-7769.
- HEWITT, C. N. 1998. *Reactive hydrocarbons in the atmosphere*, Academic press.
- INOMATA, S., TANIMOTO, H. & AOKI, N. 2008. Proton transfer reaction time-of-flight mass spectrometry at low drift-tube field-strengths using an H₂O-rare gas discharge-based ion source. *J. Mass Spectrom. Soc. Jpn*, 56, 181-187.
- INOMATA, S., TANIMOTO, H., AOKI, N., HIROKAWA, J. & SADANAGA, Y. 2006. A novel discharge source of hydronium ions for proton transfer reaction ionization: design, characterization, and performance. *Rapid communications in mass spectrometry*, 20, 1025-1029.
- JOBSON, B., ALEXANDER, M. L., MAUPIN, G. D. & MUNTEAN, G. G. 2005. On-line analysis of organic compounds in diesel exhaust using a proton transfer reaction mass spectrometer (PTR-MS). *International Journal of Mass Spectrometry*, 245, 78-89.
- KATO, S., MIYAKAWA, Y., KANEKO, T. & KAJII, Y. 2004. Urban air measurements using PTR-MS in Tokyo area and comparison with GC-FID measurements. *International Journal of Mass Spectrometry*, 235, 103-110.
- KOLTS, J. H., SETSER, D. W. & SETSER, D. W. 1979. *Reactive Intermediates in the Gas Phase. Generation and Monitoring Academic Press, New York.*
- MCFARLAND, M., ALBRITTON, D., FEHSENFELD, F., FERGUSON, E. & SCHMELTEKOPF, A. 1973a. Flow-drift technique for ion mobility and ion-molecule reaction rate constant measurements. II. Positive ion reactions of N⁺, O⁺, and H₂⁺ with O₂ and O⁺ with N₂ from thermal to [inverted lazy s] 2 eV. *The Journal of Chemical Physics*, 59, 6620-6628.
- MCFARLAND, M., ALBRITTON, D., FEHSENFELD, F., FERGUSON, E. & SCHMELTEKOPF, A. 1973b. Flow-drift technique for ion mobility and ion-molecule reaction rate constant measurements. III. Negative ion reactions of O⁻ with CO, NO, H₂, and D₂. *The Journal of Chemical Physics*, 59, 6629-6635.
- MCFARLAND, M., ALBRITTON, D., FEHSENFELD, F., FERGUSON, E. & SCHMELTEKOPF, A. L. 1973c. Flow-drift technique for ion mobility and ion-molecule reaction rate constant

- measurements. I. Apparatus and mobility measurements. *The Journal of Chemical Physics*, 59, 6610-6619.
- MIYAKAWA, Y., KATO, S. & KAJII, Y. 2005. Calibration of the Proton Transfer Reaction Mass Spectrometry (PTR-MS) Instrument for Oxygenated Volatile Organic Compounds (OVOCs) and the Measurement of Ambient Air in Tokyo. *Taiki Kankyo Gakkaishi*, 40, 209-219.
- MOLINA, L., KOLB, C., FOY, B. D., LAMB, B., BRUNE, W., JIMENEZ, J., RAMOS-VILLEGAS, R., SARMIENTO, J., PARAMO-FIGUEROA, V. & CARDENAS, B. 2007. Air quality in North America's most populous city—overview of the MCMA-2003 campaign. *Atmospheric Chemistry and Physics*, 7, 2447-2473.
- ROGERS, T., GRIMSRUD, E., HERNDON, S., JAYNE, J., KOLB, C. E., ALLWINE, E., WESTBERG, H., LAMB, B., ZAVALA, M. & MOLINA, L. 2006. On-road measurements of volatile organic compounds in the Mexico City metropolitan area using proton transfer reaction mass spectrometry. *International Journal of Mass Spectrometry*, 252, 26-37.
- SMITH, D., ŠPANĚL, P., HERBIG, J. & BEAUCHAMP, J. 2014. Mass spectrometry for real-time quantitative breath analysis. *Journal of breath research*, 8, 027101.
- SOMMARIVA, R., BLAKE, R. S., CUSS, R. J., CORDELL, R., HARRINGTON, J. F., WHITE, I. R. & MONKS, P. S. 2014. Observations of the Release of Non-Methane Hydrocarbons from Fractured Shale. *Environmental science & technology*.
- STAEHELIN, J., KELLER, C., STAHEL, W., SCHLÄPFER, K. & WUNDERLI, S. 1998. Emission factors from road traffic from a tunnel study (Gubrist tunnel, Switzerland). Part III: Results of organic compounds, SO₂ and speciation of organic exhaust emission. *Atmospheric Environment*, 32, 999-1009.
- TANIMOTO, H., AOKI, N., INOMATA, S., HIROKAWA, J. & SADANAGA, Y. 2007. Development of a PTR-TOFMS instrument for real-time measurements of volatile organic compounds in air. *International Journal of Mass Spectrometry*, 263, 1-11.
- WANNIER, G. H. 1951. On the motion of gaseous ions in a strong electric field. I. *Physical Review*, 83, 281.
- WANNIER, G. H. 1953. Motion of gaseous ions in strong electric fields. *Bell System Technical Journal*, 32, 170-254.
- WHITE, I. R., WILLIS, K. A., WHYTE, C., CORDELL, R., BLAKE, R. S., WARDLAW, A. J., RAO, S., GRIGG, J., ELLIS, A. M. & MONKS, P. S. 2013. Real-time multi-marker measurement of organic compounds in human breath: towards fingerprinting breath. *Journal of Breath Research*, 7.
- ZHAO, J. & ZHANG, R. 2004. Proton transfer reaction rate constants between hydronium ion (H₃O⁺) and volatile organic compounds. *Atmospheric Environment*, 38, 2177-2185.

5 Chapter five:

Case study - Measuring urban air samples in London, UK, with enhanced sensitivity

5.1 Introduction

One of the main driving forces behind the development of PTR-ToF mass spectrometry came from the atmospheric sciences (Blake et al., 2009, Ellis and Mayhew, 2014). In order to observe the complex atmospheric processes involving VOCs and their oxidative products taking place in the atmosphere, measurement techniques must not only detect concentrations of gas-phase species at trace levels but must also do so with fast temporal resolution. Not only does the PTR technique lend itself to this application, as it enables direct, near real-time sampling, but in using a ToF mass analyser many VOCs can be detected simultaneously. Goldstein and Galbally (Goldstein and Galbally, 2007) suggest that to date, 10^5 different VOCs have been detected in the atmosphere across the different ecosystems and environments found on Earth. One such environment has been gaining increasing attention from the atmospheric community in recent years as its emergence only came about towards the end of the twentieth century: that of the megacity.

A megacity is defined as a city with a population of over 10 million inhabitants, currently comprising 30 cities across the globe (Salam et al., 2003, Parrish et al., 2009, von Schneidemesser et al., 2010, von Schneidemesser and Monks, 2010, Rogers et al., 2006). The urban environment has long been studied by atmospheric scientists, as it represents a rich source of both anthropogenic and biogenic chemicals which, once emitted into the atmosphere, affect both climate and human health. Since the London smog episodes of the 1950s, pollution has been carefully monitored in cities world-wide. However poor air quality still places many people at risk (Bessa et al., 2011) and the concept of a megacity has given rise to new challenges and issues in pollution abatement strategy (Stone et al., 2007, Nakajima et al., 2007).

Chapter five: Case study - Measuring urban air samples in London, UK, with enhanced sensitivity

Chapter three of this thesis describes the development and testing of an ion funnel equipped PTR-ToF-MS (hereafter referred to as RF-PTR-ToF-MS due to it being operated exclusively in RF-mode) with enhanced sensitivity and better limit of detection allowing for the potential for more VOCs to be detected. A megacity environment, such as London, offers an ideal test-bed for the deployment of the newly developed ion funnel system: there is great importance in measuring VOCs in the field, emitted from both anthropogenic and biogenic sources. Much of the pollution in London is vehicular whilst bVOCs play a vital role in many chemical processes. Anthropogenic VOCs commonly found in the urban environment, harmful to human health, include aromatic compounds such as benzene, ethyl benzene, toluene, xylene and polynuclear aromatic hydrocarbons (PAHs) (Wilson, 2012, Harrison et al., 2009). Also noteworthy is the known carcinogen, 1,3-butadiene. Biogenic compounds comprise terpenoids including, for example, the unsaturated cyclic monoterpene limonene. Furthermore, many compounds are associated with multiple sources (e.g. isoprene is emitted from both biogenic and anthropogenic sources) (Henze and Seinfeld, 2006).

All of the above mentioned compounds have proton affinities large enough that they have the potential to be measured by PTR-MS (Zhao and Zhang, 2004). Around 2.4 PgC (10^{15} g of carbon) are released into the atmosphere each year as VOCs with almost half from vegetation (1.0 PgC) (Guenther, 2002). The oxidation of VOCs results in a wide range of oVOCs that vary by molecular weight and volatility. Some of these oVOCs may provide nucleation points for the formation of secondary organic aerosol (SOA) (Kroll and Seinfeld, 2008, Healy et al., 2008, Hamilton et al., 2011).

When considering the lifetime of oxidative species such as OH (< 1 s), it is clear that VOCs should be measured in as fast a timeframe as is currently possible, particularly when calculations are made such as the hydrocarbon clock method (Arnold et al., 2007, Barnet et al., 2012). Previous methods of non-methane hydrocarbon quantification included pre-concentration and separation steps

Chapter five: Case study - Measuring urban air samples in London, UK, with enhanced sensitivity

which significantly limit analysis time (Warneke et al., 2003, Goldstein and Galbally, 2007, Hamilton et al., 2004). Time averaging over long timeframes potentially loses information useful in terms of calculating exposure and source-apportionment. Furthermore, a determination of the quantities of VOCs present in the boundary layer is crucial if a complete understanding of the tropospheric oxidative capacity is to be fully understood (Arakaki and Faust, 1998, Ehhalt and Schmidt, 1978, Watson et al., 1992, Andreae and Crutzen, 1997).

During the winter campaign of the megacity study, MEGAPOLI, conducted in Paris, Dolgorouky et al. found discrepancies in measured and calculated OH reactivity, noting that missing OH reactants were most likely highly oxidized compounds created in photochemically processed air masses of anthropogenic origin (Dolgorouky et al., 2012). Lu et al. (Lu et al., 2012) suggested that an OH source mechanism is missing in current atmospheric models, either related to biogenic emissions or to their photochemical daughter products as so far unidentified chemical processes are needed to explain high OH levels that were observed in Southern China during their study in the Pearl River Delta.

Finally, Ren et al. found that night-time measurements in New York could be rationalised if a missing OH production rate was included based on the ozonolysis of unsaturated terpenes, capable of significant OH yields (Ren et al., 2003). The increased sensitivity provided by the RF funnel may enable the detection of highly reactive species, including biogenic species and highly oxidised VOCs, which may be less volatile and may be present at lower concentrations. Compared to other methods of VOC detection which utilise preconcentration techniques, PTR-MS is well suited to the analysis of oVOCs given that it is a direct sampling technique coupled with their fast rates of proton transfer.

During studies into SOA formation, both gas and liquid phase VOCs have been identified and analysed using a variety of techniques. In general however, a discrepancy tends to exist for semi-volatile material which could potentially be

Chapter five: Case study - Measuring urban air samples in London, UK, with enhanced sensitivity

measured in both phases. Identifying these species may hold the key to verifying the mechanism of SOA formation (Janssen et al., 2012).

The first half of this chapter focuses on the deployment of a standard PTR-ToF-MS instrument into an urban megacity environment during the winter intensive measurement period (IOP) of the ClearLo (Clean air for London) campaign, London, UK. The benefits of PTR-MS over alternative measurement techniques are highlighted alongside an evaluation of the performance of this device in an urban environment. During the second leg of the campaign, the modified ion funnel equipped RF-PTR-ToF-MS was deployed providing an opportunity to compare its performance to the standard PTR-ToF-MS and evaluate its use for urban VOC measurements. This represents the first time this instrument has been deployed in the field, with the aim that ultimately its increased sensitivity may enable the detection of semi-volatile VOCs and highly oxidised species.

Chapter five: Case study - Measuring urban air samples in London, UK, with enhanced sensitivity

5.2 Overview of the ClearfLo campaign 2012, London, UK.

The ClearfLo campaign was a collaborative project funded by the Natural Environment Research Council (NERC), conducted by the National Centre for atmospheric Science (NCAS) with the aim of setting up air quality monitoring sites across London to measure boundary layer pollution (Bohnenstengel et al., 2014). The project was made up by researchers from many institutions including: the University of Manchester, King's College London, the University of Birmingham, the University of York, the University of Leeds, the University of Hertfordshire, the University of East Anglia, the University of Leicester, and NERC CEH (Edinburgh).

Seven sites were chosen across the London area in order to deploy long term measuring equipment (as well as utilising already existing infrastructure) and also to carry out two intensive periods of measurement (a winter and summer IOP) during 2012.

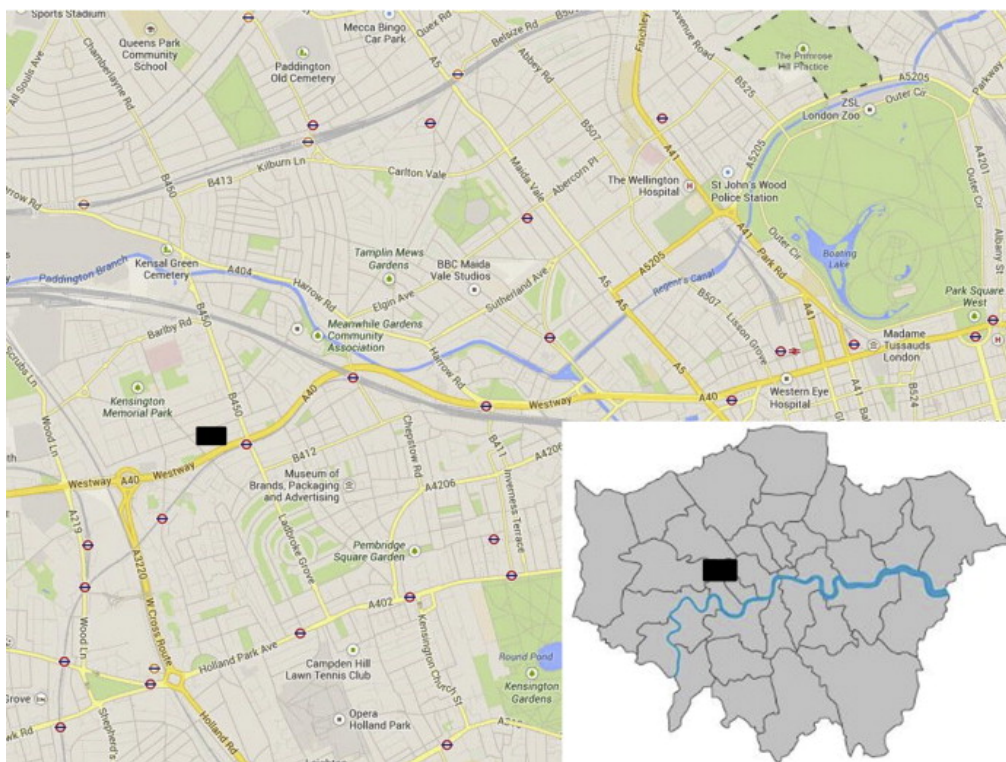


Figure 5-1. Map identifying the position of the North Kensington site (black rectangle), London, UK (Bannan et al., 2014).

Chapter five: Case study - Measuring urban air samples in London, UK, with enhanced sensitivity

The two intensive measurement periods were located in North Kensington, at Sion Manning School, UK, as shown in Figure 5-1. A converted shipping container houses the University of Leicester's mobile laboratory set-up (as seen in Figure 5-2) and this can be adapted to be able to host a whole suite of instruments appropriate to the campaign in question.



Figure 5-2. Mobile laboratory position during summer IOP set up within the playground of Sion Manning School, North Kensington, UK, with the blue shipping container belonging to the University of Leicester.

During the winter IOP, a standard PTR-ToF-MS instrument was used, this instrument is a 'Kore-ToF' as described in chapter two, with a standard, original drift tube, as opposed to a modified ion funnel equipped instrument that is described in chapter three. During the summer IOP, the RF-PTR-ToF-MS was used in order to explore how this particular instrument behaved under field deployment conditions with its enhanced sensitivity.

5.2.1 Winter IOP

The first intense campaign was carried out during the winter, in January and February of 2012. The mobile laboratory contained a suite of instruments to

Chapter five: Case study - Measuring urban air samples in London, UK, with enhanced sensitivity

collect meteorological data (meteorological station and spectral radiometer), peroxy radical concentrations through peroxy radical amplification (PERCA) (Green et al., 2006) and VOC concentrations (PTR-ToF-MS). PTR-ToF-MS data collection and analysis was performed in the same manner for both winter and summer campaigns. A 4 m, heated ¼" teflon sample tube, with inlet was mounted ~3 m above ground allowing it to be above the roofline of the mobile laboratory. A 10 L min⁻¹ rotary pump was used to draw the sample through the heated sample line at a fast rate in order to reduce sticking of the VOCs to the Teflon walls before the sample was diverted into the PTR-ToF-MS for analysis. For the winter IOP campaign the instrument setup and data acquisition was jointly carried out by the author and Dr I. Goodall (University of Leicester, Atmospheric group). The initial data analysis, i.e. removal of data from the instrument and applying calibration values to the data, was carried out by Dr I. Goodall. The 2D-GC-MS data were provided by our collaborators at the University of York and the comparison and conclusion drawn between the data sets are the work of the author.

5.2.1.1 Results

A number of VOCs (including acetaldehyde, acetone, butene, xylene, toluene, and benzene) were detected by PTR-ToF-MS during the winter IOP and are shown below in Figure 5-3, Figure 5-4, Figure 5-5, Figure 5-6, Figure 5-7 and Figure 5-8. These time series' run almost continually from the 2nd February until the 7th of February 2012. A zero point calibration was carried out at ~ midday on the 6th of February and this can be seen in all of the time series as a zero concentration value.

In all of the VOC time series, there is a consistent base line (i.e. no instrument drift) as well as a lot of fine structure, something that is only observable when using 1 min resolution data obtained by PTR-ToF-MS. Hourly GC-MS data would only allow for 24 data points per day, whereas with 1 min resolution, 1440 data points are obtained, allowing for a greater level of detail to be analysed. As the monitoring site was an 'urban background' site the general levels of VOC

Chapter five: Case study - Measuring urban air samples in London, UK, with enhanced sensitivity

detected can be thought of as those levels away from an immediate source of pollution when in an urban environment. Any spikes within the data, i.e. above the average of the background concentration, reflect pollution events. Narrow spikes in the data indicate that the emission source is close by and has not had time to mix with the surrounding air. A broad peak could imply that the VOC has been transported to the measurement site and has had time to mix with the surrounding air into a broader signal.

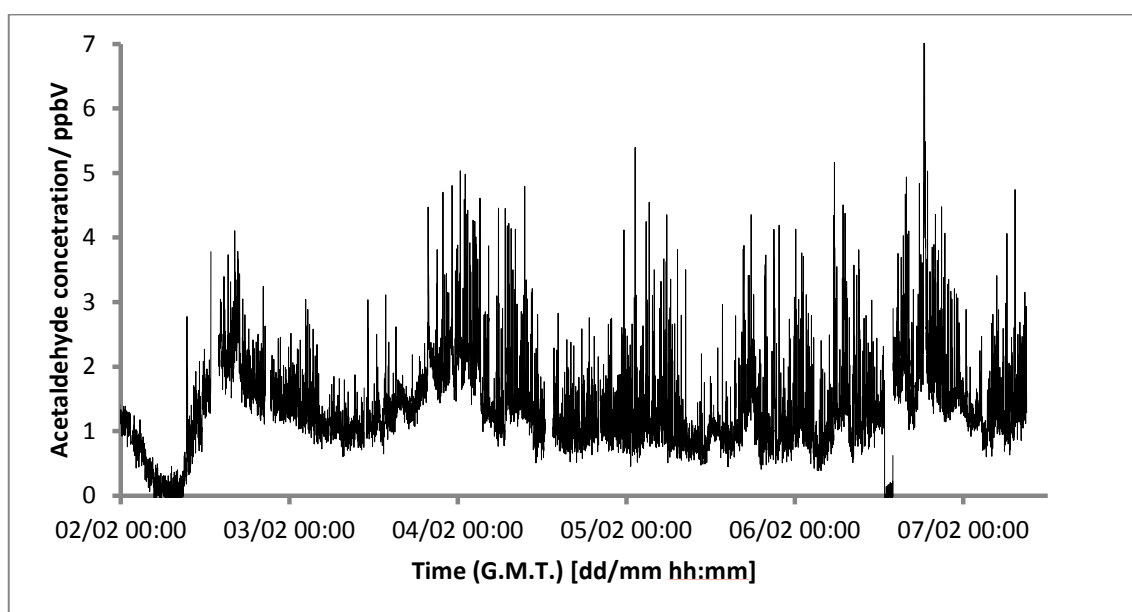


Figure 5-3. 1 min time resolution series for acetaldehyde (m/z 45) over a 6 day period from 02/02/12 – 07/02/12 collected from North Kensington, London, UK. The zero point at ~06/02 12:00 is a set of background scans to verify the zero point.

The measurements for acetaldehyde (Figure 5-3) are consistently above 1 ppbV with a maximum measurement of 7 ppbV. There appears to be two broad peaks occurring at ~12:00 2nd August and ~00:00 4th August. These could be the result of pollution released away from the measuring site that has had sufficient time to mix with nearby air. There are also many peaks above the 1 ppbV up to 5 ppbV that last for only a few minutes at a time.

Chapter five: Case study - Measuring urban air samples in London, UK, with enhanced sensitivity

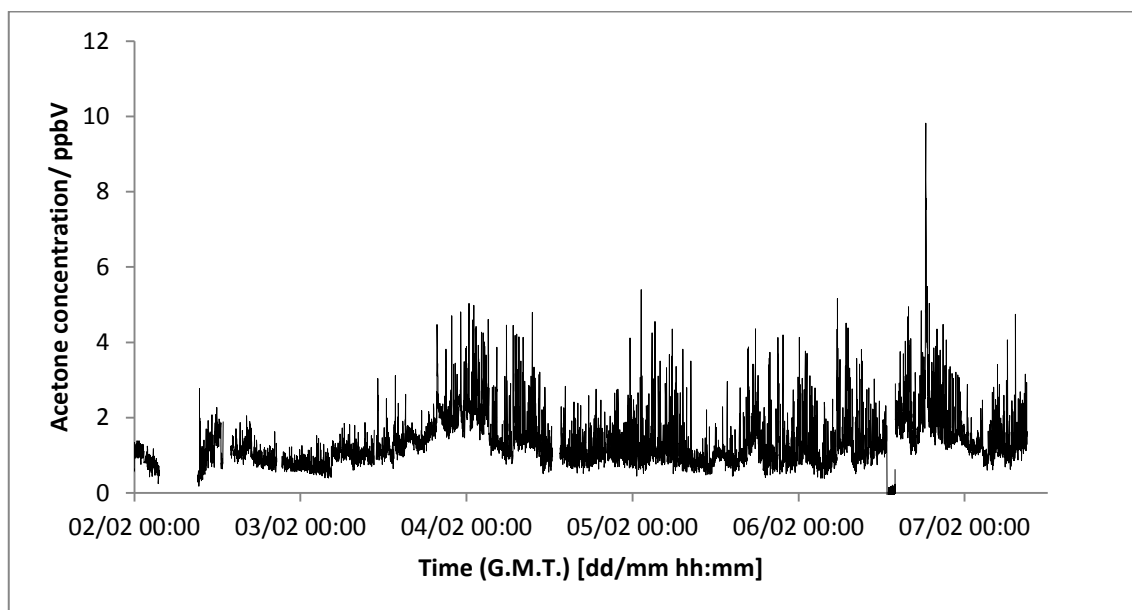


Figure 5-4. 1 min time resolution series for acetone (m/z 59) over a 6 day period from 02/02/12 – 07/02/12 collected from North Kensington, London, UK. The zero point at ~06/02 12:00 is a set of background scans to verify the zero point.

The acetone concentration (Figure 5-4) is generally between 1-2 ppbV with small pollution events in the time scale of minutes appearing from ~19:00 3rd August.

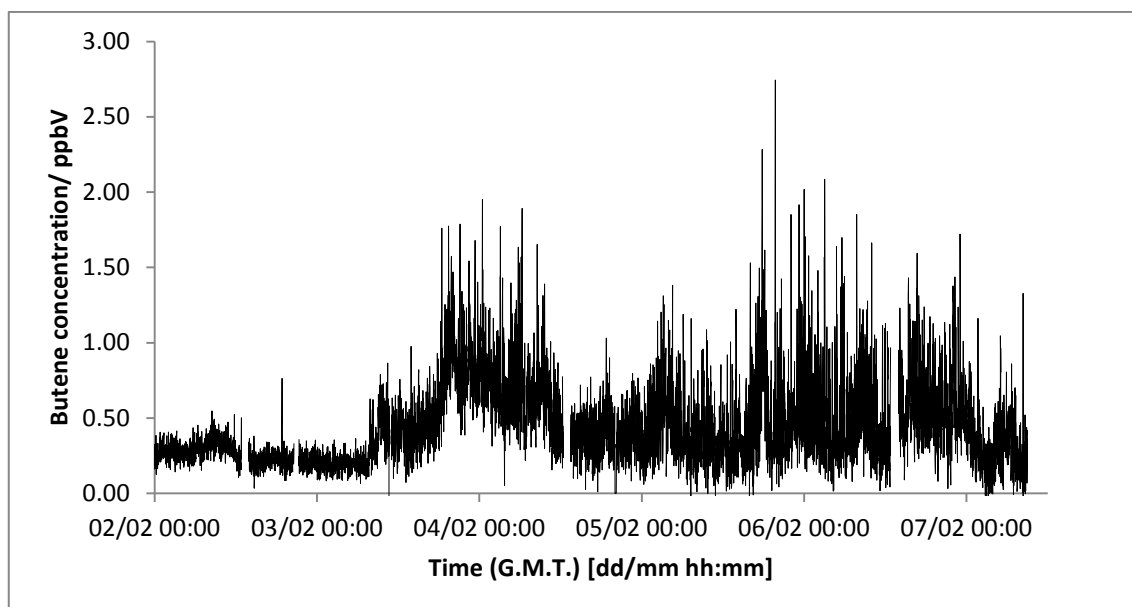


Figure 5-5. 1 min time resolution series for butene (m/z 57) over a 6 day period from 02/02/12 – 07/02/12 collected from North Kensington, London, UK. The zero point at ~06/02 12:00 is a set of background scans to verify the zero point.

Chapter five: Case study - Measuring urban air samples in London, UK, with enhanced sensitivity

Between 00:00 1st August until 12:00 3rd August the concentration of butane (Figure 5-5) is ~ 0.3 ppbV. There is then a broad peak for a period of 24 hours before the concentration drops again. This concentration however is variable; it generally ranges from 0.1 ppbV to 1.5 ppbV. Butene corresponds to m/z 57 and this channel is known to have contributions from other ions therefore some of the structure seen in the time series could be a contribution from other VOCs.

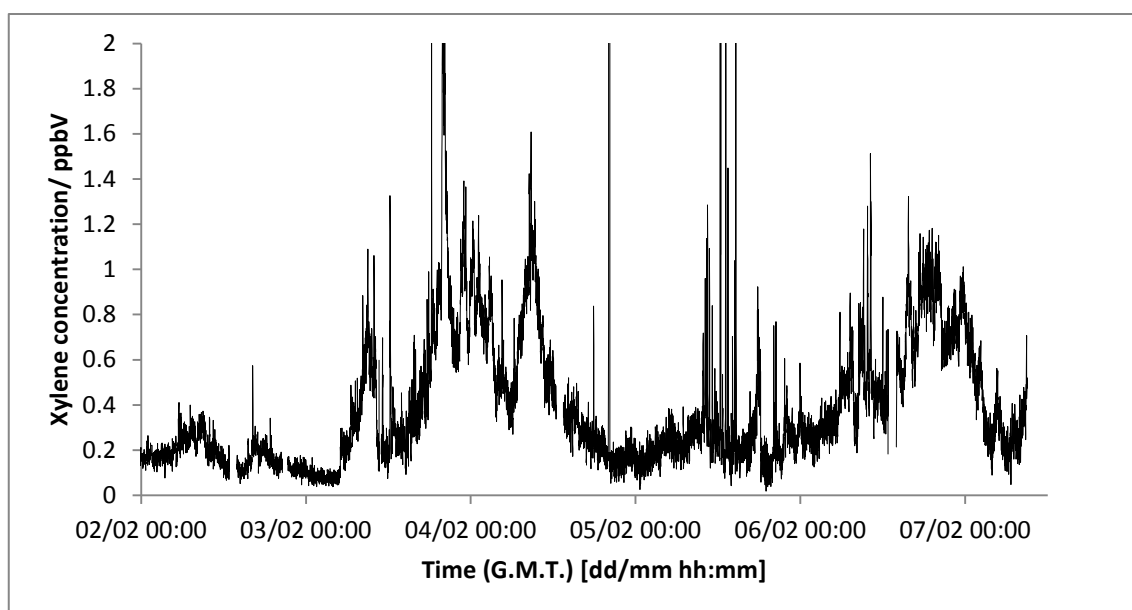


Figure 5-6. 1 min time resolution series for xylene (m/z 107) over a 6 day period from 02/02/12 – 07/02/12 collected from North Kensington, London, UK. The zero point at ~06/02 12:00 is a set of background scans to verify the zero point.

Xylene (Figure 5-6) shows two very broad peaks. The first between ~ 12:00 on the 3rd of August and ~12:00 on the 4th of August and the second between 7:00 and 00:00 on the 6th of August. This suggests that there were two pollution events at a point far enough away from the measuring site that mixing in to the nearby air mass had taken place. On top of that broad peak there are also some smaller, more localised pollution events.

Chapter five: Case study - Measuring urban air samples in London, UK, with enhanced sensitivity

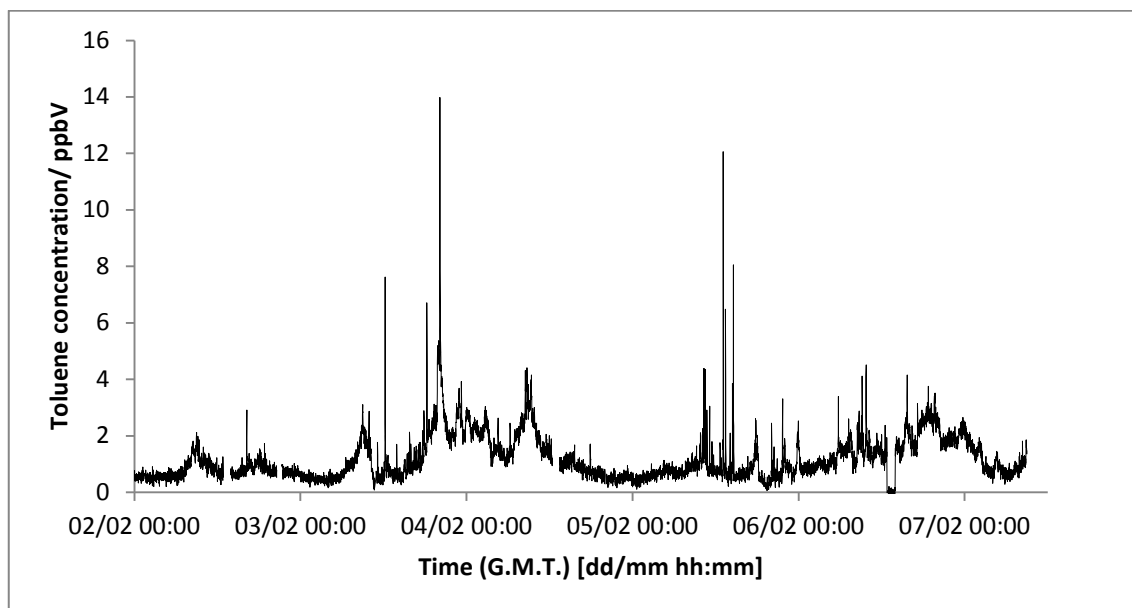


Figure 5-7. 1 min time resolution series for toluene (m/z 93) over a 6 day period from 02/02/12 – 07/02/12 collected from North Kensington, London, UK. The zero point at ~06/02 12:00 is a set of background scans to verify the zero point.

The time series for toluene (Figure 5-7) appears to broadly follow that of xylene. There are two broad pollution events although these are less pronounced than with xylene and also several large, short time frame, spikes in toluene.

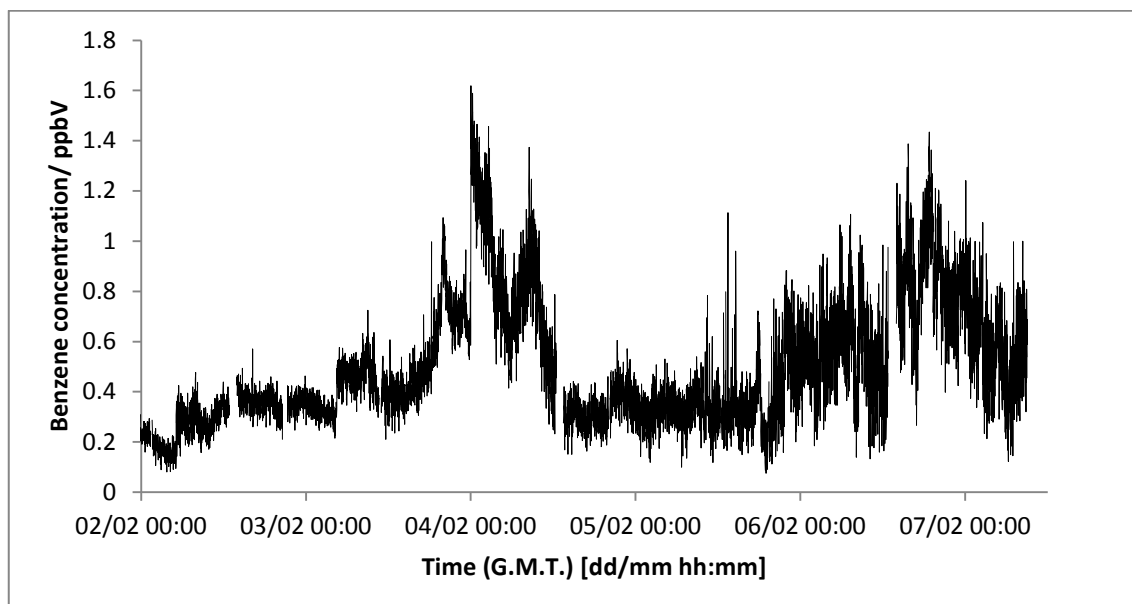


Figure 5-8. 1 min time resolution series for benzene (m/z 79) over a 6 day period from 02/02/12 – 07/02/12 collected from North Kensington, London, UK. The zero point at ~06/02 12:00 is a set of background scans to verify the zero point.

Chapter five: Case study - Measuring urban air samples in London, UK, with enhanced sensitivity

The time series for benzene (Figure 5-8) again shows these two broader peaks. There is variation within the benzene concentration in the time scale of minutes but there are a few large peaks in concentration through the time series.

5.2.1.2 GC-MS comparison

The University of York operated a two dimensional Gas Chromatography-Mass Spectrometer (2D-GC-MS) as part of their contribution to the ClearLo campaign (detailed in (Hamilton et al., 2004), (Özel et al., 2010) and (Hopkins et al., 2011)). This instrument separates the compounds using two GC columns, allowing speciation of the VOCs to be carried out and can detect a wide range of VOCs similar to the VOCs detectable by PTR-ToF-MS. The 2D-GC-MS produces one data point every 60 min with the sample for each data point being collected within the initial 10 min with each 60 min period. The data below represents the first comparison between the University of York operated 2D-GC-MS and the University of Leicester's PTR-ToF-MS during an outdoor field campaign.

Time series for various VOCs monitored by both PTR-ToF-MS and 2D-GC-MS over the period 2nd August – 7th August are shown below. In each case the first graph for each compound is a comparison between the 1 min PTR-ToF-MS data and the 1 h 2D-GC-MS data. The second graph for each compound shows the correlation between each data set. The 2D-GC-MS only collects sample for 10 minutes of every hour. The corresponding 10 min portion of PTR-ToF-MS data from each hour was averaged and that has been correlated with the appropriate 2D-GC-MS measurement.

Visually there is a good agreement in the time series between the two instruments for all compounds compared, especially for toluene (Figure 5-15), and xylene (Figure 5-17). The GC-MS data generally corresponds to the lower edge of the PTR-ToF-MS measurements. There are many peaks (pollution events) that are observed when looking at 1 min PTR-ToF-MS data that cannot be seen in the GC-MS data.

Chapter five: Case study - Measuring urban air samples in London, UK, with enhanced sensitivity

When the corresponding data is correlated between the instruments (Figure 5-10, Figure 5-12, Figure 5-14, Figure 5-16, Figure 5-18 there is varying degrees of correlation. A linear line of best fit with equation $y = mx + c$ was added to each correlation plot. Acetone ($r^2 = 0.39$, $m = 0.60 \pm 0.07$, $c = 0.62 \pm 0.09$ ppbv) and butene ($r^2 = 0.42$, $m = 0.721 \pm 0.08$, $c = 0.24 \pm 0.02$ ppbv) show the weakest correlation. Benzene has good agreement with $r^2 = 0.64$, $m = 1.02 \pm 0.07$ and $c = 0.07 \pm 0.03$ ppbv. Whist the gradient is equal to 1 (within its uncertainty), the correlation coefficient r^2 is only 0.64. Xylene ($r^2 = 0.91$, $m = 0.91 \pm 0.01$, $c = 0.10 \pm 0.01$ ppbv) and toluene ($r^2 = 0.90$, $m = 1.30 \pm 0.04$, $c = 0.26 \pm 0.03$ ppbv) have very good agreement. It can be seen with all of the VOC comparison that the gradient varies; it is neither always above 1 nor always below 1.

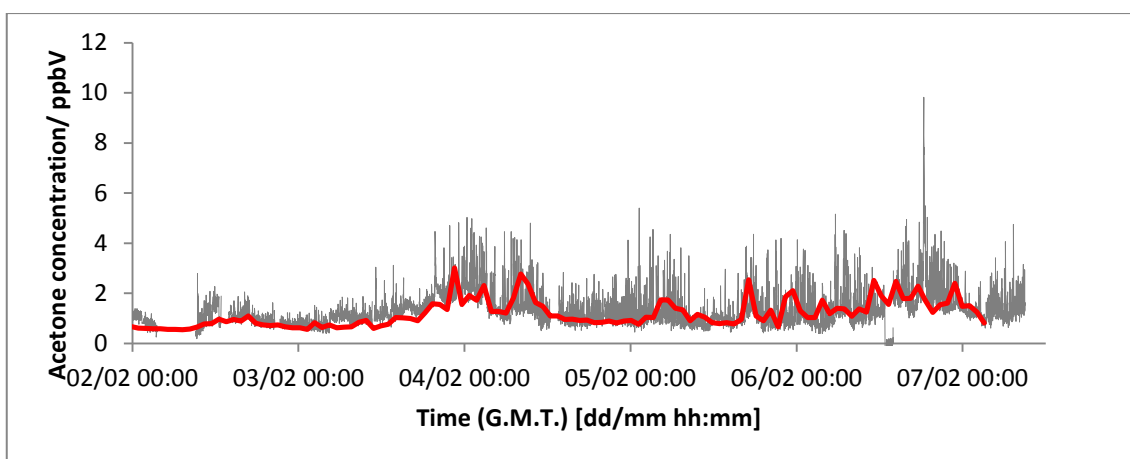


Figure 5-9. 1 h 2D-GC-MS acetone data (red) plotted on the same axis as 1 min PTR-ToF-MS acetone data (grey). The zero point at ~06/02 12:00 is a set of background scans to verify the zero point.

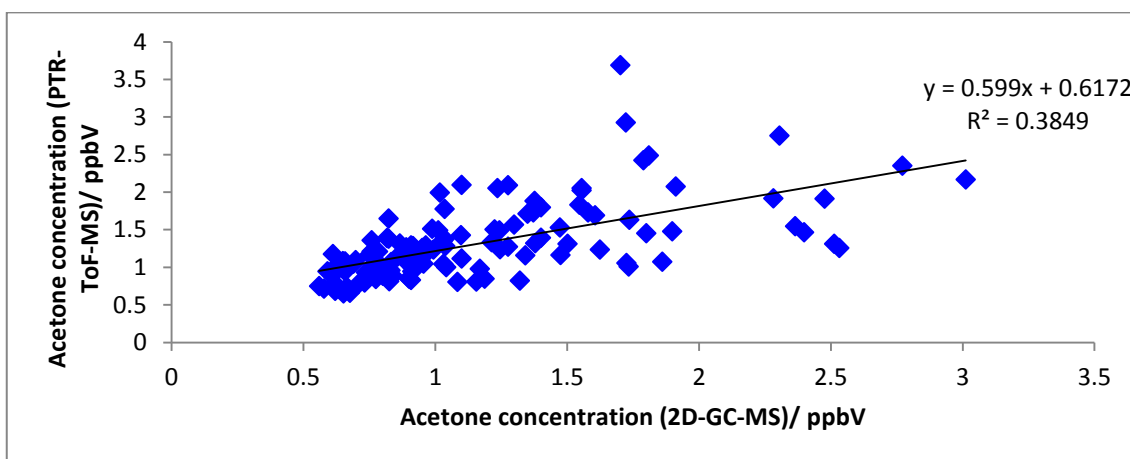


Figure 5-10. Comparison of acetone concentration obtained during the winter IOP between data acquired by 2D-GC-MS and data obtained by PTR-ToF-MS data.

Chapter five: Case study - Measuring urban air samples in London, UK, with enhanced sensitivity

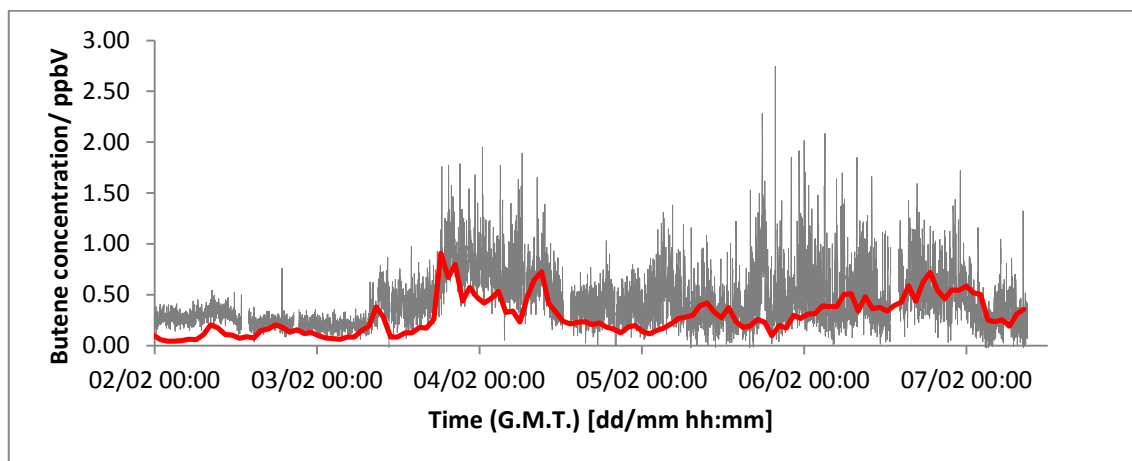


Figure 5-11. 1 h 2D-GC-MS butene data (red) plotted on the same axis as 1 min PTR-ToF-MS butene data (grey). The zero point at ~06/02 12:00 is a set of background scans to verify the zero point.

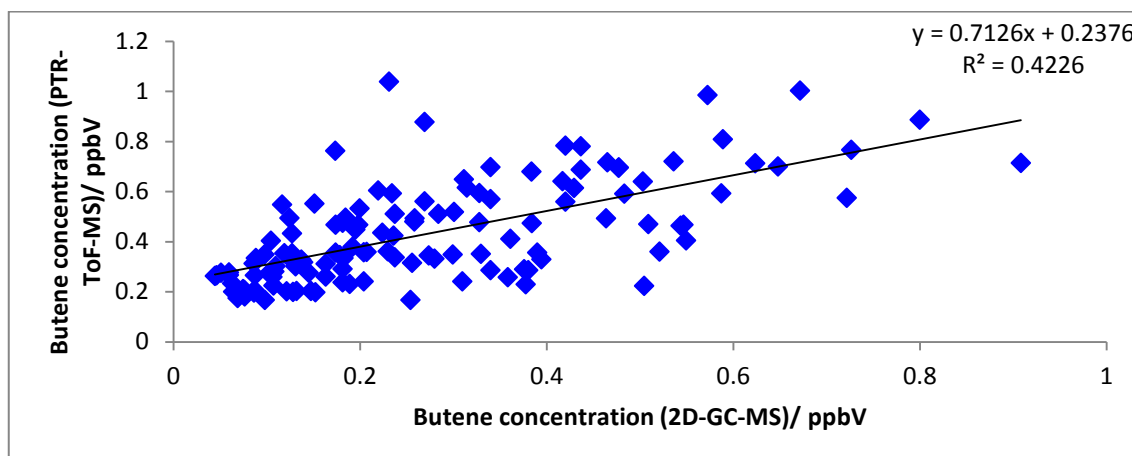


Figure 5-12. Comparison of butene concentration obtained during the winter IOP between data acquired by 2D-GC-MS and data obtained by PTR-ToF-MS data.

Chapter five: Case study - Measuring urban air samples in London, UK, with enhanced sensitivity

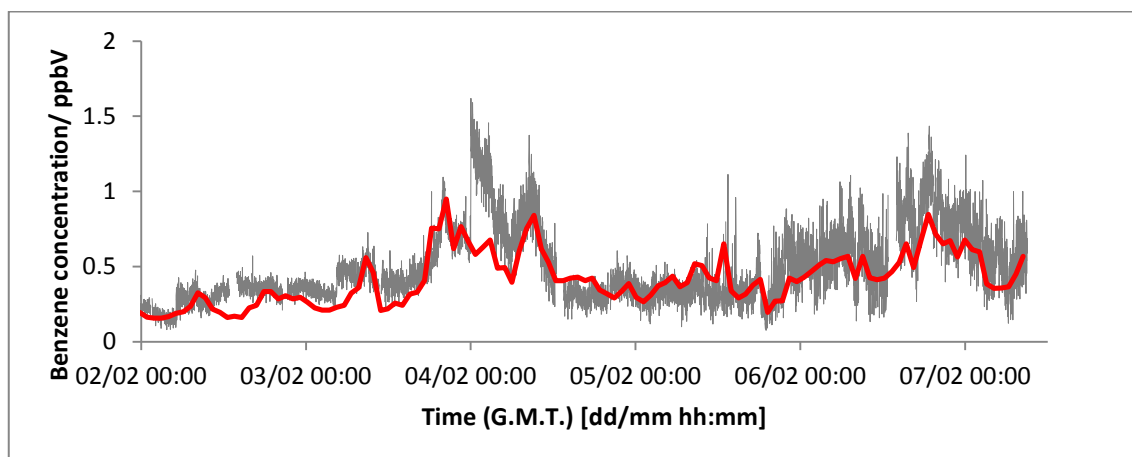


Figure 5-13. 1 h 2D-GC-MS benzene data (red) plotted on the same axis as 1 min PTR-ToF-MS benzene data (grey). The zero point at ~06/02 12:00 is a set of background scans to verify the zero point.

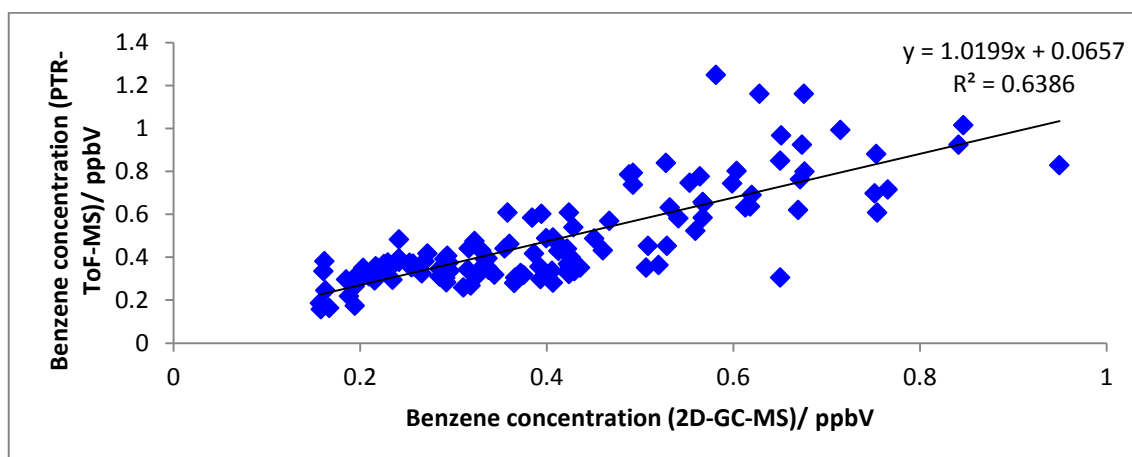


Figure 5-14. Comparison of benzene concentration obtained during the winter IOP between data acquired by 2D-GC-MS and data obtained by PTR-ToF-MS data.

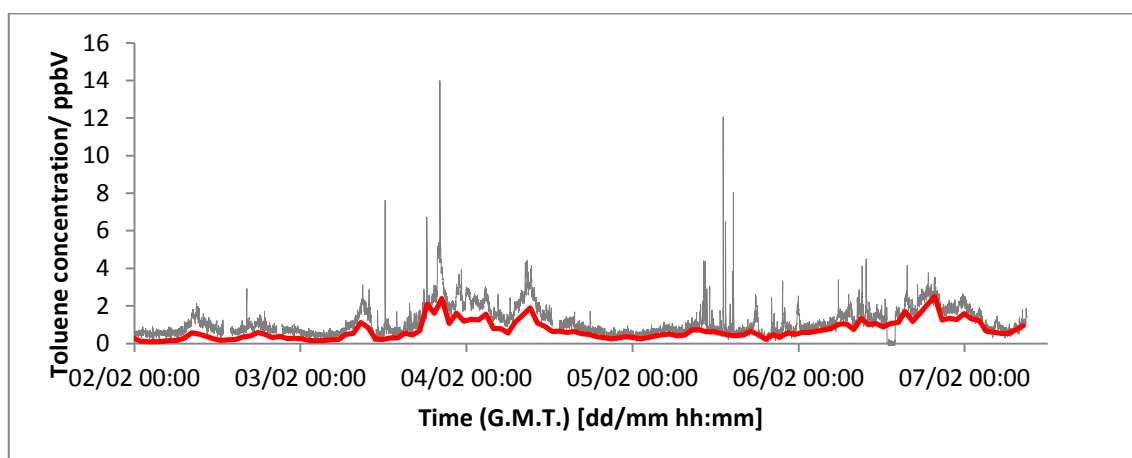


Figure 5-15. 1 h 2D-GC-MS toluene data (red) plotted on the same axis as 1 min PTR-ToF-MS toluene data (grey). The zero point at ~06/02 12:00 is a set of background scans to verify the zero point.

Chapter five: Case study - Measuring urban air samples in London, UK, with enhanced sensitivity

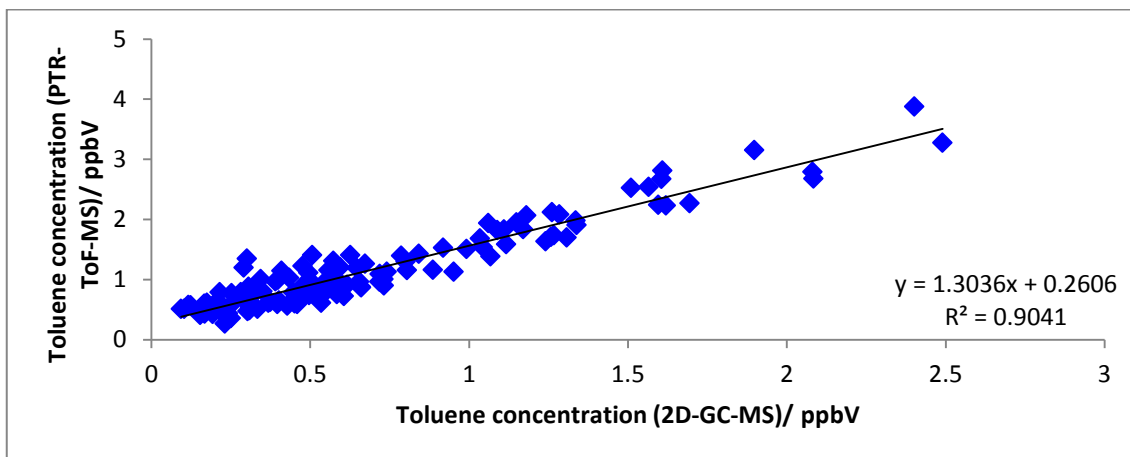


Figure 5-16. Comparison of toluene concentration obtained during the winter IOP between data acquired by 2D-GC-MS and data obtained by PTR-ToF-MS data.

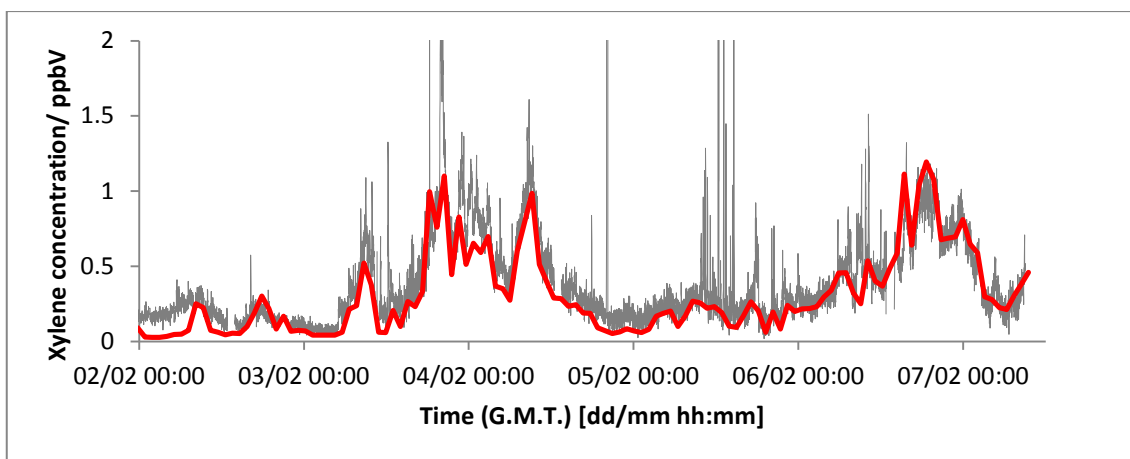


Figure 5-17. 1 h 2D-GC-MS xylene data (red) plotted on the same axis as 1 min PTR-ToF-MS xylene data (grey). The zero point at ~06/02 12:00 is a set of background scans to verify the zero point.

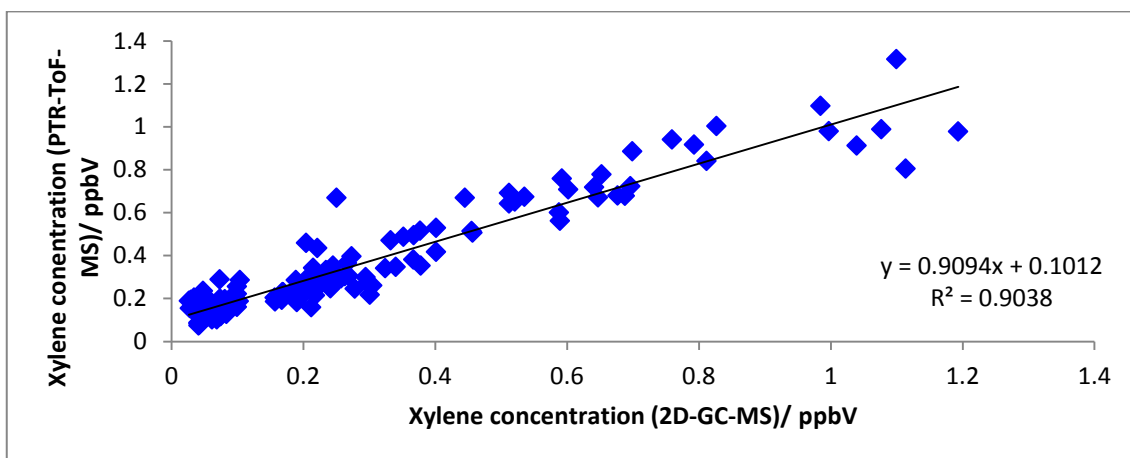


Figure 5-18. Comparison of xylene concentration PTR-ToF-MS data obtained during the winter IOP between data acquired by 2D-GC-MS and data obtained by PTR-ToF-MS data.

Chapter five: Case study - Measuring urban air samples in London, UK, with enhanced sensitivity

Overall there is relatively good agreement between the two instruments although this does vary by compound (ion). The reason for the discrepancy between the two instruments could be down to several reasons. The calibrations methods for each instrument are different and also the sampling methods are different. This could result in different compounds being analysed more effectively than others. However, the main source of error is likely to be more than one ion of the same m/z being measured by PTR-ToF-MS. In a complex VOC mixture, i.e. the urban atmosphere, there will be many VOCs present. These VOCs have the potential to fragment and contribute a signal to more than one mass channel within the PTR-ToF-MS and this can lead to interference between the competing ions. For example, both toluene (m/z 93) and xylene (m/z 107) will have a benzene ion fragment, corresponding to m/z 79, which thus interferes with the benzene (m/z 79) signal. The smaller the m/z , the more likely that a larger VOCs could fragment into that particular ion, which could be why butene and acetone do not correlate as well as the larger compounds.

As previously discussed, the data obtained via PTR-ToF-MS has a much higher time resolution (1 min) than that of the GC-MS data (1 h). This allows many pollution events (spikes in the data) to be seen in the PTR-ToF-MS that simply cannot be detected by GC-MS with its 1 h time resolution. This information is critical when determining a person's exposure to VOCs. A 2012 study carried out by Cocheo and co-workers (Cocheo et al., 2000) into personal exposure to benzene found that personal exposure could not simply be calculated as a time weighted average of outside and inside pollution levels. It is crucial to understand the specific exposure a person may have to a pollutant. An hourly, or 24 hourly average measurement will not accurately reflect exposure. It can be seen from the time series that there are many peaks in concentration, which last for as little as 1-5 minutes. People often do not spend, for example, an hour at the road side where pollution levels may be high and therefore it is important that if a person is in a polluted environment for 5 minutes that the concentration of those 5 minutes of exposure is known. A higher time resolution (such as

Chapter five: Case study - Measuring urban air samples in London, UK, with enhanced sensitivity

when PTR-ToF-MS is utilised) allows these brief pollution events to be detected and a much more accurate picture can be produced of the VOC concentration.

5.2.2 Summer IOP

The summer IOP took place during July 2012 and the University of Leicester's mobile laboratory was set up in an identical position to that of the winter IOP. The field laboratory itself contained essentially the same instrumentation as the winter IOP; a meteorological station, spectral radiometers, a PERCA to measure peroxy radical concentration and a PTR-ToF-MS for VOC measurements. For this IOP however, the ion funnel equipped RF-PTR-ToF-MS that formed the basis of chapter three was used in order to provide a level of increased sensitivity in order to measure VOCs previously below the limit of detection. The RF-PTR-ToF-MS was set up and operated by the author and all data analysis relating to the summer IOP was completed by the author.

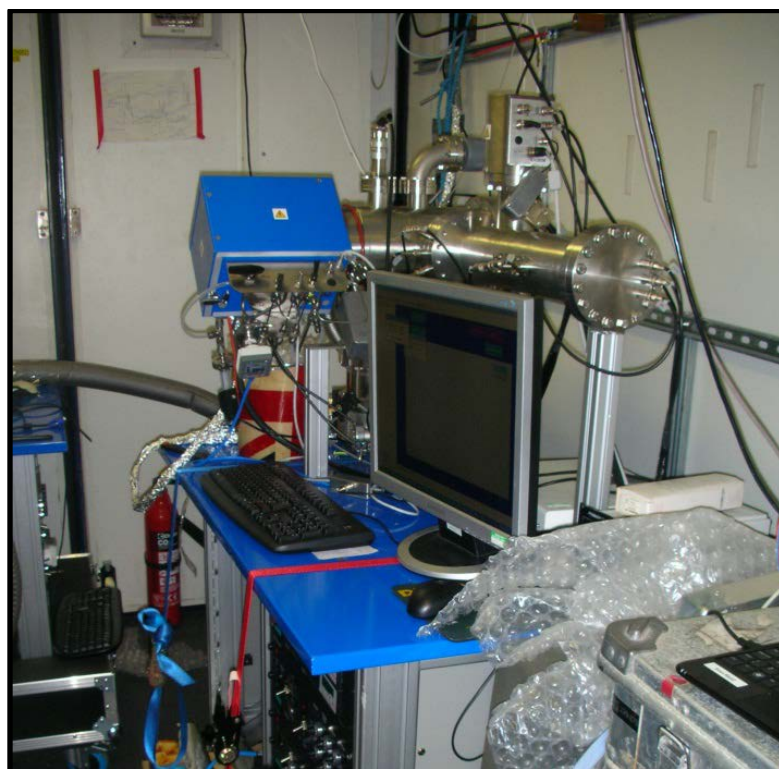


Figure 5-19. Ion funnel equipped PTR-ToF-MS taking measurements from within the mobile laboratory.

The increased sensitivity provided by the ion funnel, means that in any given spectrum, there are more peaks, and therefore potentially more compounds

Chapter five: Case study - Measuring urban air samples in London, UK, with enhanced sensitivity

being detected in urban air. Figure 5-20 is a typical mass spectrum of an urban air sample taken on the 7th August 2012, towards the start of the summer IOP reflecting typical urban air, i.e. no pollution event present.

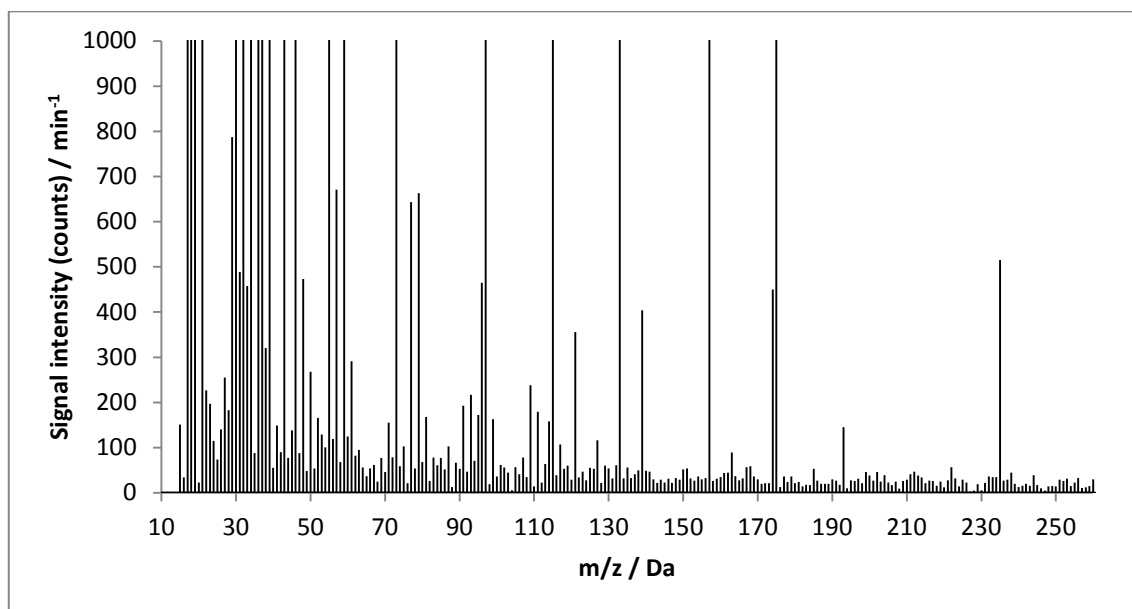


Figure 5-20. An example of a 1 min mass spectrum taken on 07/08 illustrating a number of peaks including several high mass ions ($> m/z$ 150).

Unfortunately, the data falls down when taken as a time series. The instrument is usually in a temperature controlled air conditioned laboratory; however out on campaign during the summer months, with a damaged air condition system in the container-lab, meant large temperature variation, and hence variation in sensitivity. An example of the temperature variation within the container-lab is shown in Figure 5-21 (red points). It can be seen that as the temperature fluctuates so does the hydronium count (blue points). The reasons for this change in hydronium level is down to the temperature; temperature fluctuations change the levels of water vapour entering the instrument and also alters the pressure and temperature within the PTR reactor resulting in sub-optimal instrument conditions.

This change in hydronium (reagent ion) sensitivity results in a change in VOC detection sensitivity making data acquisition and interpretation very challenging.

Chapter five: Case study - Measuring urban air samples in London, UK, with enhanced sensitivity

The fluctuating hydronium level causes the sensitivity of the instrument to fluctuate on an hourly time scale and this produces data that are very hard to speciate and calibrate for. This temperature affect can be seen on all PTR-MS instruments and is not a problem unique to the RF-funnel equipped PTR-MS instrument. Thus the poorer performance for the RF-funnel instrument presented in this section is a consequence of the more difficult operating conditions during the summer IOP, and does not reflect any fundamental issues with operating RF-funnel instruments for atmospheric field work. For this reason the PTR-MS instruments should ideally always be operated in a temperature controlled environment.

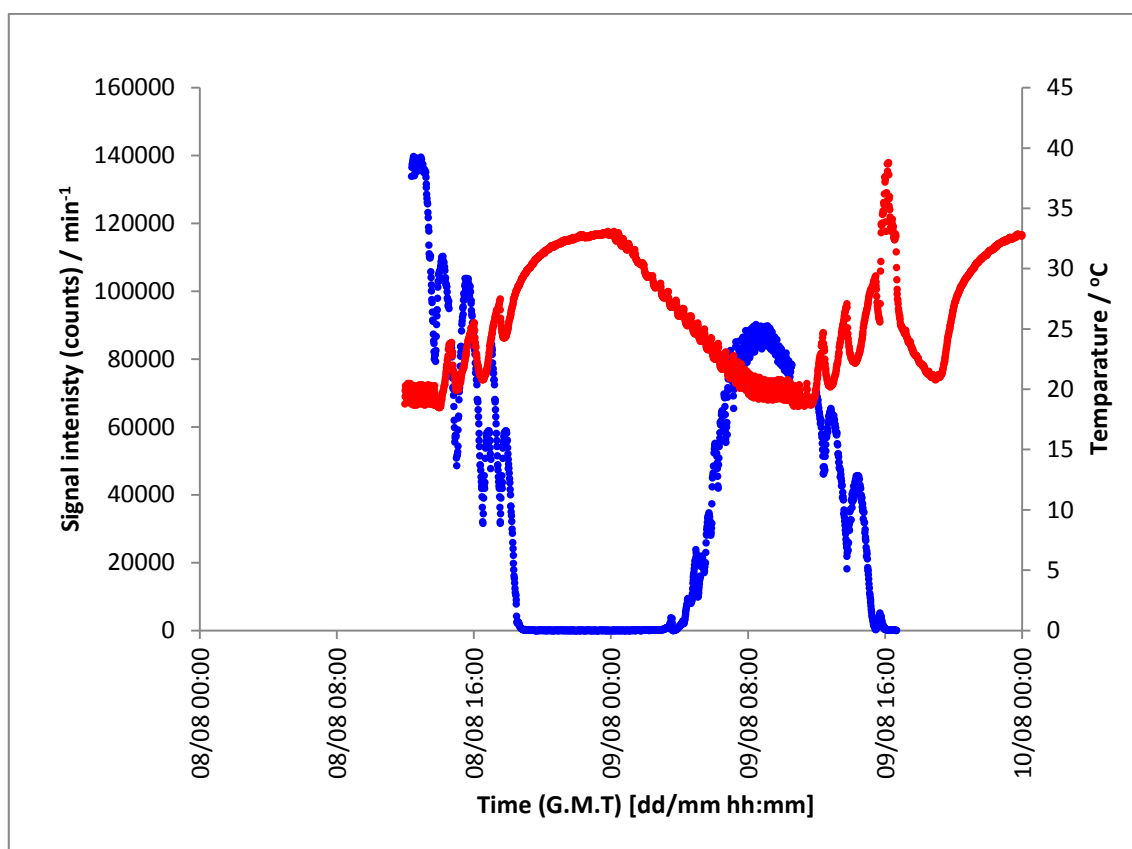


Figure 5-21. Data obtained during the summer ClearLo campaign. The blue points represent the ambient temperature within the container-lab (taken with a temperature probe) and the red points represent the signal intensity of m/z 21 ($H_3^{18}O^+$) and were obtained on the RF funnel equipped PTR-MS instrument.

However at times when the temperature was stable enough to have a strong, consistent reagent ion signal, good VOC sensitivity was obtained. This is discussed in section 5.2.3.

Chapter five: Case study - Measuring urban air samples in London, UK, with enhanced sensitivity

5.2.3 Winter verses summer comparison

A spectrum was selected from both the winter and summer IOP and is presented for comparison in Figure 5-22. These spectra were chosen for comparison as they represented a similar (within 5 %) $\text{H}_3\text{O}^+ \cdot \text{H}_2\text{O}$ ratio and also were taken during times where no pollution events were taking place and at a similar ambient humidity, i.e. they show typical background air in an urban atmosphere. It should be noted that whilst only a single spectrum is shown, the number of peaks shown are typical across the duration of the campaigns.

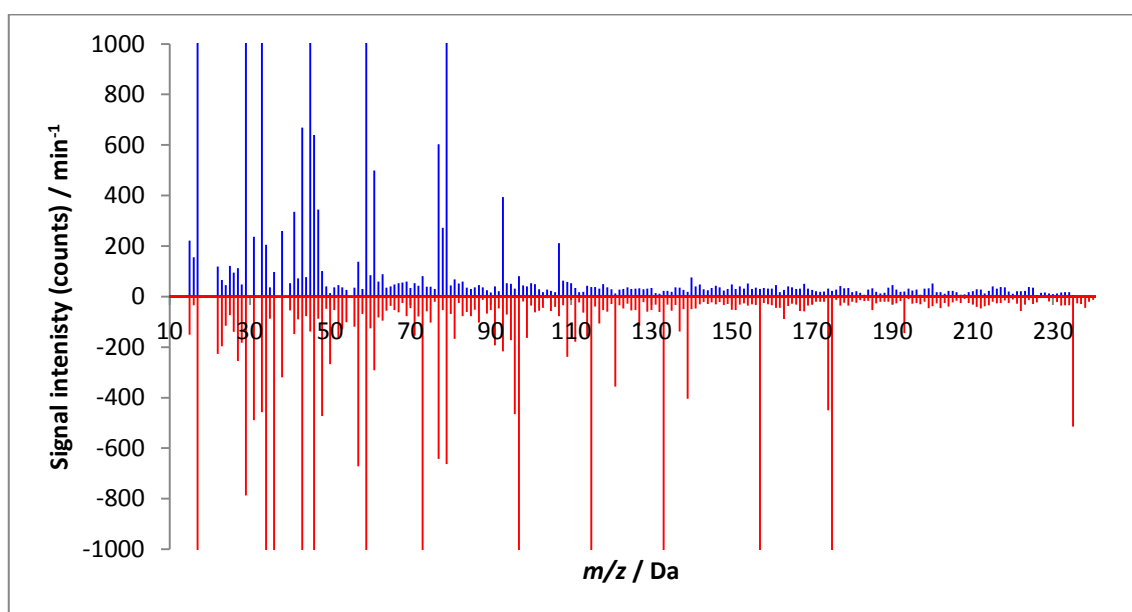


Figure 5-22. A comparison of a typical urban air spectra taken on the PTR-ToF-MS during winter (blue) and on the RF-PTR-ToF-MS during summer (red) illustrating the increased number of peaks present in the RF-PTR-ToF-MS obtained spectrum.

Many of the peaks observed in the winter spectrum are also observed in the summer spectrum. However it can be seen that there are also many other ions present in the summer that were not present in the winter. The increased number of peaks present is the result of not only enhanced sensitivity being demonstrated by the RF-PTR-ToF-MS when compared to the standard instrument used in the winter IOP (as shown in Figure 5-23), but also because of the many bVOCs and associated compounds being present during the summer months. The ions seen in those two spectra are listed in Table 5-1.

Chapter five: Case study - Measuring urban air samples in London, UK, with enhanced sensitivity

Table 5-1. Ions detected using PTR-ToF-MS in the winter (blue), ions detected using RF-PTR-ToF-MS in the summer (red) or ions detected on both instruments (black). Reagent and associated ions are in italics.

<i>m/z</i>					
15	16	17	18	19	21
22	23	25	26	27	28
29	30	31	32	33	34
35	36	37	38	39	41
42	43	44	45	46	47
48	50	51	52	53	54
55	56	57	58	59	60
61	62	63	67	69	71
72	73	75	77	78	79
80	81	83	84	85	87
89	91	93	94	95	96
97	99	101	103	107	108
109	111	113	114	115	117
121	127	132	133	137	139
140	163	174	175	193	235
268					

The ions that are displayed in Table 5-1 are those that are a minimum of 60 counts / min⁻¹ above the background in Figure 5-20. Whilst many more peaks are visible in Figure 5-22, those in Table 5-1 are the salient peaks and should be considered primarily in future analysis.

Chapter five: Case study - Measuring urban air samples in London, UK, with enhanced sensitivity

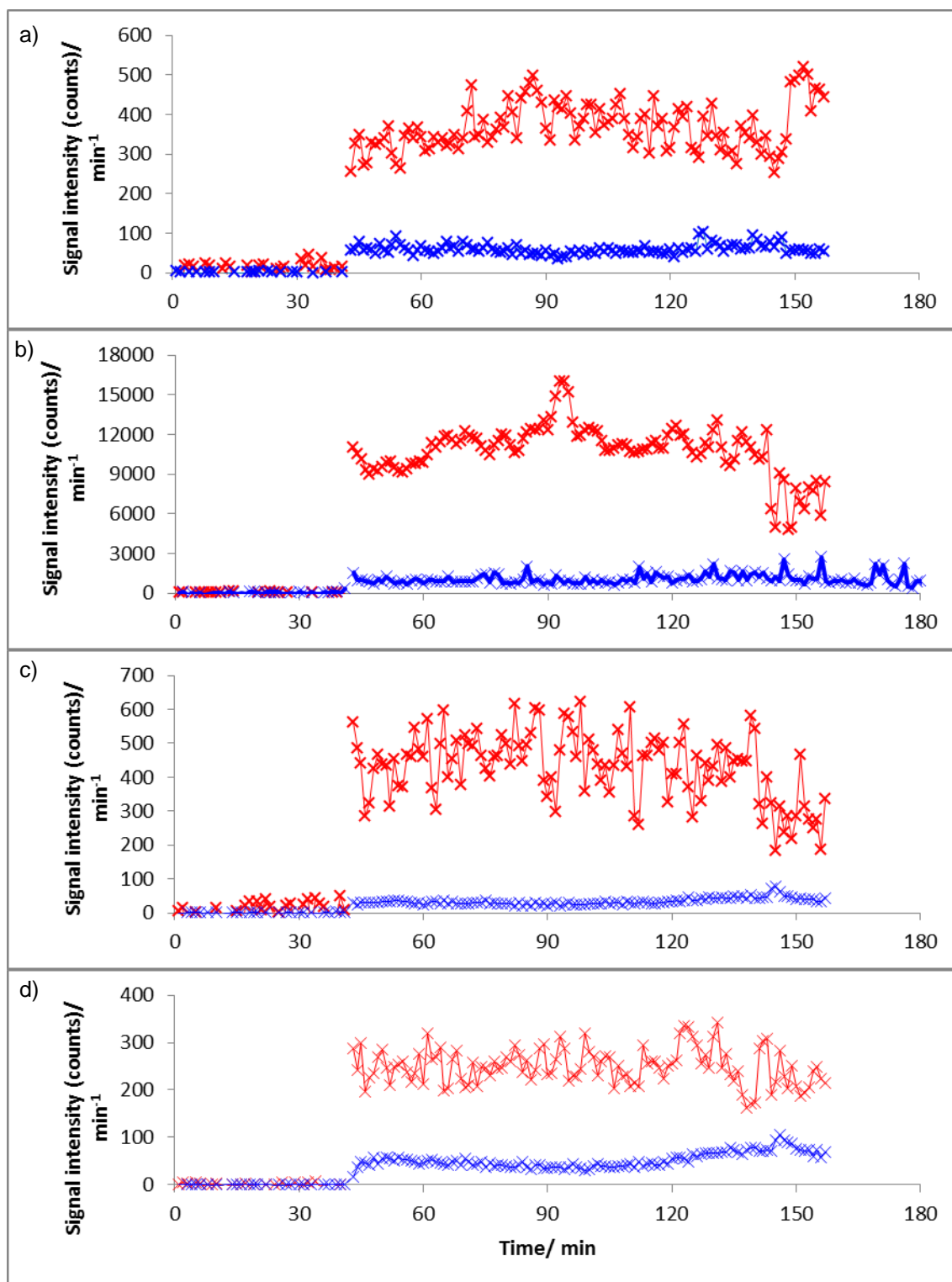


Figure 5-23. Example time series comparing signal intensity from RF-PTR-ToF-MS (red) and from PTR-MS (blue) for a) m/z 57 (butene), b) m/z 59 (acetone), c) m/z 93 (toluene) and d) m/z 107 (xylene). The data to the left (0 - 40 min) are background subtracted, whilst the data from 40 - 180 min is urban air.

The panels in Figure 5-23 demonstrate the enhanced sensitivity that can be obtained using the RF-PTR-ToF-MS. The flat line on the left hand side of each

Chapter five: Case study - Measuring urban air samples in London, UK, with enhanced sensitivity

panel (0-40 min) is a series of background scans taken when a hydrocarbon trap is connected to the inlet. This background ion signal is then subtracted from all measurements. It can be seen that for the four compounds shown, that there is a large increase in signal sensitivity between the two instruments. The highest in increase in signal is for m/z 59 (Figure 5-23 b). Both time series have the fine structure associated with an urban air mass, however the RF-PTR-ToF-MS (red) signal is ~10 times higher (at ~10000 counts / min⁻¹) when compared to the PTR-ToF-MS signal (at ~1000 counts / min⁻¹). This signal has structure that simply could not be seen on a GC-MS, where this data set would only comprise of three 1 h data points.

Overall the performance of the RF-PTR-ToF-MS over the standard PTR-ToF-MS is significant when utilised for urban air measurements within a megacity environment. This had been established by the number of salient peaks shown in Figure 5-22 and Table 5-1 as well as the increase in signal intensity demonstrated in

Figure 5-23. Furthermore, another metric for measuring performance of VOC detection is the total ion count of the mass spectrometer. That is to say, that the more ions it detects, translates to a higher sensitivity and potential for more comprehensive VOC detection. Table 5-2 compares the overall performance of the two instruments; the data for both instruments is obtained using the two spectra in Figure 5-22. The RF-PTR-ToF-MS detects over 10 times the raw ion count than that of the PTR-ToF-MS. If the data are normalised to take into account the hydronium level, then there is over a three times increase.

Table 5-2. Comparison of m/z 19 and total ion count on the PTR-ToF-MS and RF-PTR-ToF-MS.

Instrument	m/z 19 ³ / min ⁻¹	Total ion count ¹ / min ⁻¹	Normalised total ion count ^{1,2}
PTR-ToF-MS	24195	33622	2802
RF-PTR-ToF-MS	75171	368072	9872

¹ Total ion count not including reagent ions (m/z 18, m/z 19, m/z 21, m/z 30, m/z 32, m/z 37, m/z 39, m/z 55).

² Normalised to 10⁶ H₃O⁺.

³ m/z 19 is calculated by multiplying m/z 21 (H₃¹⁸O⁺) by 496 in order to obtain values for H₃¹⁶O⁺.

Chapter five: Case study - Measuring urban air samples in London, UK, with enhanced sensitivity

5.2.4 Chamber study

Chamber studies offer an alternative way to study atmospheric chemistry because they provide a well-constrained, synthetic atmosphere that can be manipulated and analysed. Often elevated concentrations of VOCs and other gases are injected in to the chamber and can be analysed in order to study the oVOC products and to generate SOA.

During the ACIDPRUF (Aerosol-Cloud Interactions - A Directed Programme to Reduce Uncertainty in Forcing) chamber study, carried out at the University of Manchester during 2012 (McCracken, 2013, White et al., 2012), the oxidation products of the VOCs, as well as particle number, were used to better understand SOA formation. Different VOCs were injected into the environment chamber to represent compounds of both anthropogenic and biogenic origins, including α -pinene, β -caryophyllene and toluene. Owing to the artificially high concentration of VOCs injected into the chamber, oVOC oxidation products can be generated at easily observable concentration, whereas in comparable urban air measurements these oVOCs are below the limit of detection of the instruments that are monitoring VOCs.

For the ACIDPRUF campaign the University of Leicester provided a 'Kore ToF' PTR-MS to monitor and measure VOCs. The set up and running of the instrument was carried out by the author along with Dr I. White and Dr I. Goodall of the University of Leicester. The initial data analysis, i.e. removal of data from the instrument and storage on the university of Leicester server, and background subtraction was carried out by Dr I. White and Dr I. Goodall. Further analysis was carried out by the author. An undergraduate student, D. McCracken, was present during the campaign and under the supervision of Dr I. White, the author and Dr I. Goodall. D. McCracken produced a report detailing a list of VOCs observed in the chamber and this is referenced in the appropriate section in this chapter. Measurements regarding the conditions used in the chamber, i.e. ozone and NO_x concentrations, were provided by the University of Manchester.

Chapter five: Case study - Measuring urban air samples in London, UK, with enhanced sensitivity

5.2.5 Experimental

The α -pinene photo-oxidation experiment (exp120601) carried out on 1st June 2012 provides a representative example of measurements obtained by PTR-MS during ACIDPRUF. The aim of this particular experiment was to investigate SOA formation during the oxidation of α -pinene, the results of which are, in the following section 5.2.6. The chamber was kept at 20-25 °C and ~60 % relative humidity. 25 ppbV of NO_x (as NO₂) was injected in to the chamber along with 45 ppbV of ozone (as an additional source of OH). A seed aerosol was used, ammonium sulphate (NH₄)₂SO₄, in order to provide a surface for the aerosol to grow on. Finally the VOC (α -pinene) was injected in to the chamber as a liquid and heated in order to create a vapour. The lights were then turned on and the reaction monitored. The conditions for the experiment are summarised in in Table 5-3.

Table 5-3. Conditions within the chamber during the α -pinene oxidation experiment.

α -pinene concentration/ ppBv	50
NO _x as NO ₂ concentration/ ppbV	20-25
Ozone concentration/ ppbV	45
Relative humidity/ %	~60
Temperature/ °C	20-25

5.2.6 Results

As mentioned previously VOCs were measured by PTR-ToF-MS and these results will be discussed in this section. A data request for aerosol water uptake was made to the University of Manchester, however unfortunately this data could not be provided. Correction methods can normally be applied to the data for wall losses however for this particular experiment it could not. Therefore a comparison between the time profiles of oVOC formation and aerosol growth could not be carried out.

Chapter five: Case study - Measuring urban air samples in London, UK, with enhanced sensitivity

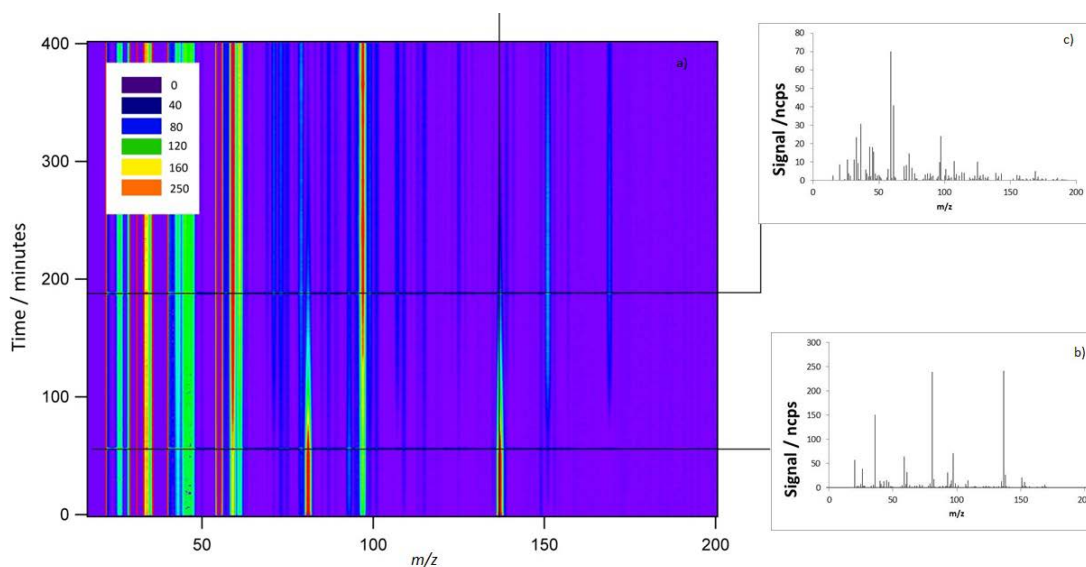


Figure 5-24. Gas phase measurements of VOCs during the α -pinene photo-oxidation experiment (White et al., 2012). a) 3-dimensional graph of VOC evolution where the colours represent the counts s^{-1} , b) spectrum taken at 50 min, c) spectrum taken at 190 min.

Figure 5-24 a) provides a 3-dimensional graph illustrating how the α -pinene precursor ion m/z 137 and its fragment ion at m/z 81 decay from 0 min onwards as the α -pinene is oxidised. Other ions are produced immediately as the monoterpene is oxidised whilst others, secondary products, can be seen to be generated from ~ 80 min onwards. The spectra, b) and c) help to illustrate how different a spectrum taken at the start, with primary products looks when compared to a spectrum taken half way through the experiment, at ~ 190 min where secondary products have formed. After ~ 360 min, the entire quantity of α -pinene precursor has been oxidised as evidenced by the m/z 137 ion signal's decay to zero.

Further conditions and specific ion are plotted in Figure 5-25. Temperature and relative humidity profiles are provided in Figure 5-25 a) and show a consistent environment of $20 - 25$ $^{\circ}C$ and $60 - 65$ % relative humidity throughout the time period of the experiment. Figure 5-25 b) illustrates how the level of ozone reduces from its initial injection of ~ 45 ppbV down to ~ 30 ppbV at the end of the experiment. Figure 5-25 c) shows the precursor molecule α -pinene (m/z 137) and its fragment ion (m/z 81) reacting from when the lights are turned on and photo-oxidation begins until approximately 360 min when there is no VOC left. Both ions have identical profiles which indicates no additional contribution

Chapter five: Case study - Measuring urban air samples in London, UK, with enhanced sensitivity

to those mass channels from other ions. oVOC time series are presented in panels d) - h). The main first generation oxidation product is pinonaldehyde which is produced through the oxidation of α -pinene with both OH and ozone (as shown in Figure 5-26 and Figure 5-27). Figure 5-25 d) shows its production and then reduction as it is oxidised further. Fragments ions are also observed at various masses and these are also shown. The fragment ions do not all have the exact same profile. This implies that there is a contribution to some of these mass channels from other species, likely fragments of other oVOCs produced during the experiment. α -pinene oxide, panel e), was produced immediately when α -pinene was injected and reacted with the ozone already present in the chamber before lights on. Figure 5-25 f), g) and h) are also oVOC products and their evolution was tracked throughout the entirety of the experiment. They were not present before the lights were turned on, but they were produced once the photo-oxidation reactions were initiated.

Chapter five: Case study - Measuring urban air samples in London, UK, with enhanced sensitivity

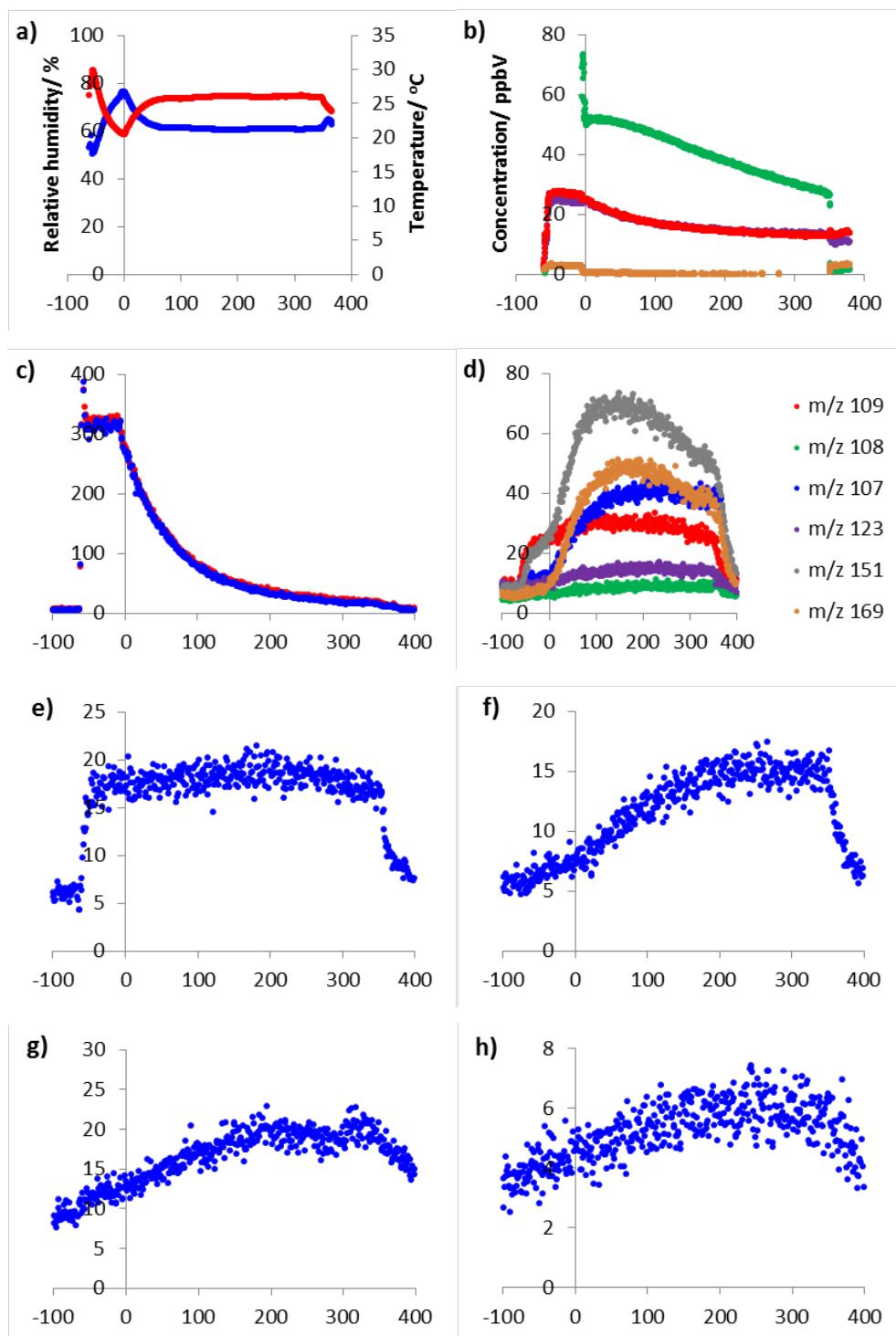


Figure 5-25. Time series for various measurements and ions monitored during α -pinene photo-oxidation experiment. For panels a) - h) x-axis = time after lights on/ min. For panels c) y-axis = normalised signal intensity (counts). **Panel a)** Temperature (red), relative humidity (blue). **Panel b)** Ozone (green) NO_x (red), NO₂ (purple), NO (orange). **Panel c)** Precursor parent ion *m/z* 137 (blue), fragment ion *m/z* 81 (red). **Panel d)** Pinonaldehyde (*m/z* 169) and its fragment ions, *m/z* 151, *m/z* 123, *m/z* 107, *m/z* 108, *m/z* 109. **Panel e)** Ion *m/z* 153 α -pinene oxide. **Panel f)** Ion *m/z* 155 norpinonaldehyde. **Panel g)** Ion *m/z* 157 norpinic acid. **Panel h)** Ion *m/z* 185 pinonic acid.

Chapter five: Case study - Measuring urban air samples in London, UK, with enhanced sensitivity

The ions observed in panels d) – h) are predicted to occur from modelling the oxidation chemistry of α -pinene. Capouet and co-workers provide a model for the oxidation of α -pinene in the presence of OH (Capouet et al., 2004) (Figure 5-26) and ozone (Capouet et al., 2008) (Figure 5-27). Oxidation of α -pinene and its products would have occurred by reaction with both OH and ozone under the conditions of ACIDPRUF exp120601, and for this reason both mechanisms are included. Pinonaldehyde can be seen in both mechanisms, and pinonic acid and norpinionaldehyde are products from the ozone reactions in Figure 5-27.

It can be seen that there are many intermediary compounds and ions produced during the oxidation of α -pinene and a difficulty in using only PTR-ToF-MS to monitor these VOCs is speciation. PTR-ToF-MS provides high temporal resolution for the monitoring of VOCs but can only analyse the mass to the nearest m/z unit and therefore not differentiate between isobaric compounds. Ideally these VOCs and the oxidation products should be analysed alongside GC-MS in order to validate speciation.

Chapter five: Case study - Measuring urban air samples in London, UK, with enhanced sensitivity

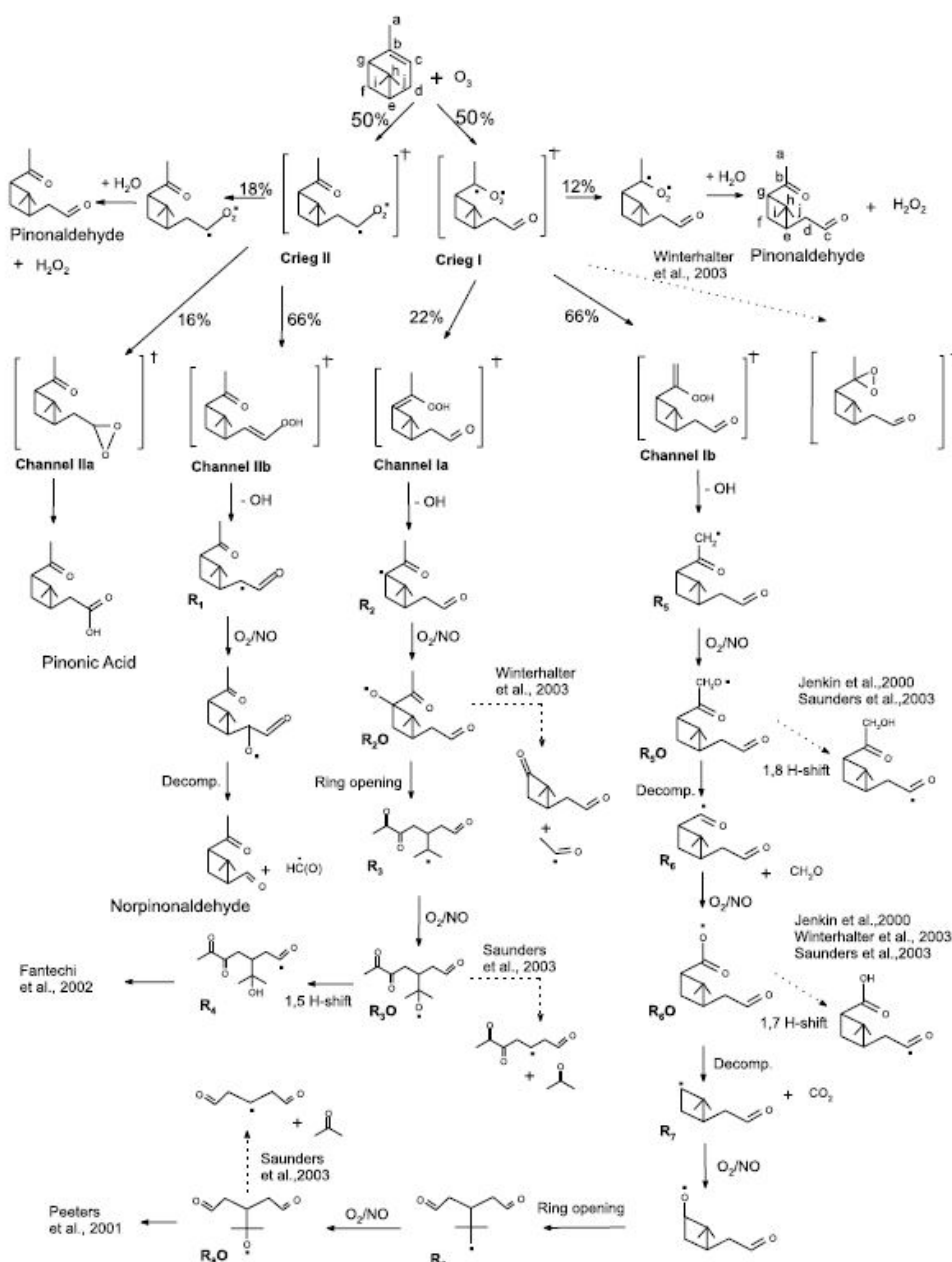


Figure 3. Main paths of the α -pinene oxidation by O_3 (in presence of NO). Alternative routes proposed in the literature are represented by the dotted arrows.

Figure 5-27. Main paths of the α -pinene oxidation by O_3 (in presence of NO) taken from (Capouet et al., 2008).

The ions from the monoterpene (α -pinene) oxidation experiment are listed in Table 5-4 with potential ion identification (McCracken, 2013). Along with the ions observed in the chamber study, those ions that were also detected during the ClearLo winter IOP by PTR-ToF-MS and the ClearLo summer IOP by RF-PTR-ToF-MS are listed.

Chapter five: Case study - Measuring urban air samples in London, UK, with enhanced sensitivity

Table 5-4. Mass channels observed on the PTR-ToF-MS during winter, and the RF-PTR-ToF-MS during summer. Shown also are the potential ions observed during a monoterpene oxidation experiment carried out as part of the ACIDPRUF campaign, 2012. ‘•’ means that the ion was observed. Adapted from (McCracken, 2013).

<i>m/z</i>	PTR-ToF-MS (Winter)	RF-PTR-ToF-MS (Summer)	Potential ion observed during monoterpene oxidation
15	•	•	Methyl group
16	•	•	
17	•	•	Hydroxyl cation
18	•	•	Water
19	•	•	Hydronium H ₃ O ⁺
21	•	•	Hydronium H ₃ ¹⁸ O ⁺
22	•	•	
25	•	•	Ethynyl radical
26	•	•	
27	•	•	
28		•	
29	•	•	Formaldehyde
30	•	•	NO ⁺
31	•	•	Formaldehyde
32	•	•	O ₂ ⁺
33	•	•	Methanol
34	•	•	Methanol isotope
35		•	
36	•	•	
37	•	•	Water cluster H ₃ O ⁺ .H ₂ O
38	•	•	
39	•	•	Water cluster H ₃ ¹⁸ O ⁺ .H ₂ O
41	•	•	
42	•	•	
43	•	•	
44	•	•	
45	•	•	Acetaldehyde
46	•	•	Acetaldehyde isotope
47	•	•	Formic acid
48	•	•	Formic acid isotope
50		•	
51		•	
52		•	
53		•	
54		•	
55	•	•	Water cluster H ₃ O ⁺ .(H ₂ O) ₂
56		•	
57	•	•	
58		•	
59	•	•	Acetone
60	•	•	Acetone isotope
61	•	•	Acetic acid
62		•	Acetic acid isotope
63	•	•	
67		•	
69		•	Isoprene, pinonic acid fragment
71		•	Pinonic acid fragment
72		•	
73	•	•	
75		•	Hydroxy acetone
77	•	•	
78	•	•	

Chapter five: Case study - Measuring urban air samples in London, UK, with enhanced sensitivity

<i>m/z</i>	PTR-ToF-MS (Winter)	RF-PTR-ToF-MS (Summer)	Potential ion observed during monoterpene oxidation
79	•	•	
80		•	
81		•	
83		•	
84		•	
85		•	
87		•	
89		•	
91		•	
93	•	•	
94		•	
95		•	Norpinonaldehyde fragment
96		•	
97	•	•	
99		•	
100			
101		•	5,6-dihydroxyhexane-2,3-dione fragment
103		•	
107	•	•	Pinonaldehyde fragment
109		•	Pinonaldehyde fragment / norpinonaldehyde fragment
111	•	•	
113	•	•	
114		•	
115		•	Pinonic acid fragment / 3,4-dioxopentanal
117		•	
121		•	
127		•	3-oxo-2,2dimethyl-cyclobutyl-1-methanal / pinic acid fragment
132		•	
133		•	
137		•	Monoterpene
139		•	Nopinone/ pinonic acid fragment / pinonaldehyde - 2x methyl
140	•		Nopinone/ pinonic acid fragment isotope
163		•	
174		•	Norpinic acid isotope / 5-hydroxy-4-methylcyclohex-3-en-1-yl nitrate
175		•	3-hydroperoxy-5,6-dioxoheptanal
193		•	
235		•	
268		•	

It can be clearly seen that many oVOCs are produced from the oxidation of one precursor molecule (α -pinene). Whilst several of these ions were observed during the winter IOP, many more of these were also observed during the summer IOP. As mentioned previously, during a chamber study many of the ions that are detected cannot be routinely detected in the field due to the much lower concentrations present in the atmosphere; however, with the added sensitivity that RF-PTR-ToF-MS affords, many of the compounds can be

Chapter five: Case study - Measuring urban air samples in London, UK, with enhanced sensitivity

monitored successfully and have been detected. It should be noted however that the ions observed during the ClearfLo campaign, at an urban background site, could be from sources other than that of monoterpene oxidation as well as fragments of other larger compounds as the urban background provides a rich diversity of both anthropogenic and biogenic VOCs in its atmosphere.

Chapter five: Case study - Measuring urban air samples in London, UK, with enhanced sensitivity

5.3 Conclusion

PTR-MS has been utilised for the measurement of atmospherically relevant species since its inception, but has only ever been able to detect the more concentrated VOCs present in the atmosphere. Now the enhanced sensitivity afforded by RF-PTR-ToF-MS, has enabled species previously only detectable in chamber studies to be detected in urban air experiments.

The ClearfLo winter IOP demonstrated that the PTR-ToF-MS equipped with a standard drift tube could successfully monitor VOCs relating to air pollution (e.g. toluene) over a weekly time frame and were compared with a 2D-GC-MS to verify the results. Owing to the 1 min resolution that can be obtained from PTR-ToF-MS measurements, many features that cannot be observed through 60 min GC-MS data can now be analysed. This is crucial if one is assessing a person's exposure to pollution and also allows for a more accurate source apportionment of VOCs.

During the summer IOP, with the enhanced sensitivity offered by the RF-PTR-ToF-MS, more peaks were detected as a result of this increased sensitivity, with many of these having not been detected during the winter campaign (as listed in Table 5-4), and therefore they could potentially be from bVOCs (or their oVOC counterparts). This creates the potential to use more atmospherically relevant VOC concentration when carrying out chamber studies owing to the enhanced sensitivity and capability of RF-PTR-ToF-MS.

Improved temperature control is required when operating the ion funnel and therefore speciation of these compounds was not possible. The system could be modified with the flight tube, and other components, being temperature controlled in order to minimise this problem. An internal standard could also be used to help track sensitivity changes in real-time throughout the entire experiment and would then require the data to be normalised to this internal calibrant. A potential internal calibrant could be bromobenzene, as it would occupy two mass channels (m/z 157 and m/z 159) that are not routinely used in

Chapter five: Case study - Measuring urban air samples in London, UK, with enhanced sensitivity

analysis, has a characteristic isotopic pattern and the levels of bromobenzene expected in urban air measurements would be very low.

Chapter five: Case study - Measuring urban air samples in London, UK, with enhanced sensitivity

5.4 References

- ANDREAE, M. O. & CRUTZEN, P. J. 1997. Atmospheric aerosols: Biogeochemical sources and role in atmospheric chemistry. *Science*, 276, 1052-1058.
- ARAKAKI, T. & FAUST, B. C. 1998. Sources, sinks, and mechanisms of hydroxyl radical (\bullet OH) photoproduction and consumption in authentic acidic continental cloud waters from Whiteface Mountain, New York: the role of the Fe (r)(r= II, III) photochemical cycle. *Journal of Geophysical Research: Atmospheres (1984–2012)*, 103, 3487-3504.
- ARNOLD, S., METHVEN, J., EVANS, M., CHIPPERFIELD, M., LEWIS, A., HOPKINS, J., MCQUAID, J., WATSON, N., PURVIS, R. & LEE, J. 2007. Statistical inference of OH concentrations and air mass dilution rates from successive observations of nonmethane hydrocarbons in single air masses. *Journal of Geophysical Research: Atmospheres (1984–2012)*, 112.
- BANNAN, T. J., BACAK, A., MULLER, J., BOOTH, A. M., JONES, B., LE BRETON, M., LEATHER, K. E., GHALAIENY, M., XIAO, P. & SHALLCROSS, D. E. 2014. Importance of direct anthropogenic emissions of formic acid measured by a chemical ionisation mass spectrometer (CIMS) during the Winter ClearLo Campaign in London, January 2012. *Atmospheric Environment*, 83, 301-310.
- BARMET, P., DOMMEN, J., DECARLO, P., TRITSCHER, T., PRAPLAN, A., PLATT, S., PRÉVÔT, A., DONAHUE, N. & BALTENSPERGER, U. 2012. OH clock determination by proton transfer reaction mass spectrometry at an environmental chamber. *Atmospheric Measurement Techniques*, 5, 647-656.
- BESSA, V., DARWICHE, K., TESCHLER, H., SOMMERWERCK, U., RABIS, T., BAUMBACH, J. I. & FREITAG, L. 2011. Detection of volatile organic compounds (VOCs) in exhaled breath of patients with chronic obstructive pulmonary disease (COPD) by ion mobility spectrometry. *International Journal for Ion Mobility Spectrometry*, 14, 7-13.
- BLAKE, R. S., MONKS, P. S. & ELLIS, A. M. 2009. Proton-Transfer Reaction Mass Spectrometry. *Chemical Reviews*, 109, 861-896.
- BOHNENSTENGEL, S., BELCHER, S., AIKEN, A., ALLAN, J., ALLEN, G., BACAK, A., BANNAN, T., BARLOW, J., BEDDOWS, D. & BLOSS, W. 2014. Meteorology, air quality, and health in London: The ClearLo project. *Bulletin of the American Meteorological Society*.
- CAPOUET, M., MÜLLER, J. F., CEULEMANS, K., COMPERNOLLE, S., VERECKEN, L. & PEETERS, J. 2008. Modeling aerosol formation in alpha-pinene photo-oxidation experiments. *Journal of Geophysical Research: Atmospheres (1984–2012)*, 113.
- CAPOUET, M., PEETERS, J., NOZIERE, B. & MÜLLER, J.-F. 2004. Alpha-pinene oxidation by OH: simulations of laboratory experiments. *Atmospheric Chemistry and Physics*, 4, 2285-2311.
- COCHEO, V., SACCO, P., BOARETTO, C., DE SAEGER, E., BALLESTA, P. P., SKOV, H., GOELEN, E., GONZALEZ, N. & CARACENA, A. B. 2000. Urban benzene and population exposure. *Nature*, 404, 141-142.
- DOLGOROUKY, C., GROS, V., SARDA-ESTEVE, R., SINHA, V., WILLIAMS, J., MARCHAND, N., SAUVAGE, S., POULAIN, L., SCIARE, J. & BONSANG, B. 2012. Total OH reactivity measurements in Paris during the 2010 MEGAPOLI winter campaign. *Atmospheric Chemistry and Physics*, 12, 9593-9612.
- EHHALT, D. & SCHMIDT, U. 1978. Sources and sinks of atmospheric methane. *Pure and Applied Geophysics*, 116, 452-464.

Chapter five: Case study - Measuring urban air samples in London, UK, with enhanced sensitivity

- ELLIS, A. M. & MAYHEW, C. A. 2014. *Proton Transfer Reaction Mass Spectrometry: Principles and Applications*, Wiley.
- GOLDSTEIN, A. H. & GALBALLY, I. E. 2007. Known and unexplored organic constituents in the earth's atmosphere. *Environmental Science & Technology*, 41, 1514-1521.
- GREEN, T. J., REEVES, C. E., FLEMING, Z. L., BROUGH, N., RICKARD, A. R., BANDY, B. J., MONKS, P. S. & PENKETT, S. A. 2006. An improved dual channel PERCA instrument for atmospheric measurements of peroxy radicals. *Journal of Environmental Monitoring*, 8, 530-536.
- GUENTHER, A. 2002. The contribution of reactive carbon emissions from vegetation to the carbon balance of terrestrial ecosystems. *Chemosphere*, 49, 837-844.
- HAMILTON, J., WEBB, P., LEWIS, A., HOPKINS, J., SMITH, S. & DAVY, P. 2004. Partially oxidised organic components in urban aerosol using GCXGC-TOF/MS. *Atmospheric Chemistry and Physics*, 4, 1279-1290.
- HAMILTON, J. F., RAMI ALFARRA, M., WYCHE, K. P., WARD, M. W., LEWIS, A. C., MCFIGGANS, G. B., GOOD, N., MONKS, P. S., CARR, T. & WHITE, I. R. 2011. Investigating the use of secondary organic aerosol as seed particles in simulation chamber experiments. *Atmospheric Chemistry and Physics*, 11, 5917-5929.
- HARRISON, R. M., DELGADO-SABORIT, J. M., BAKER, S. J., AQUILINA, N., MEDDINGS, C., HARRAD, S., MATTHEWS, I., VARDOLAKIS, S. & ANDERSON, H. 2009. Measurement and modeling of exposure to selected air toxics for health effects studies and verification by biomarkers. *Research report (Health Effects Institute)*, 3-96; discussion 97-100.
- HEALY, R., WENGER, J., METZGER, A., DUPLISSY, J., KALBERER, M. & DOMMEN, J. 2008. Gas/particle partitioning of carbonyls in the photooxidation of isoprene and 1, 3, 5-trimethylbenzene. *Atmospheric Chemistry and Physics*, 8, 3215-3230.
- HENZE, D. K. & SEINFELD, J. H. 2006. Global secondary organic aerosol from isoprene oxidation. *Geophysical Research Letters*, 33.
- HOPKINS, J. R., JONES, C. E. & LEWIS, A. C. 2011. A dual channel gas chromatograph for atmospheric analysis of volatile organic compounds including oxygenated and monoterpene compounds. *Journal of Environmental Monitoring*, 13, 2268-2276.
- JANSSEN, R., VILÀ-GUERAU DE ARELLANO, J., GANZEVELD, L., KABAT, P., JIMENEZ, J., FARMER, D., VAN HEERWAARDEN, C. & MAMMARELLA, I. 2012. Combined effects of surface conditions, boundary layer dynamics and chemistry on diurnal SOA evolution. *Atmospheric Chemistry and Physics*, 12, 6827-6843.
- KROLL, J. H. & SEINFELD, J. H. 2008. Chemistry of secondary organic aerosol: Formation and evolution of low-volatility organics in the atmosphere. *Atmospheric Environment*, 42, 3593-3624.
- LU, K., ROHRER, F., HOLLAND, F., FUCHS, H., BOHN, B., BRAUERS, T., CHANG, C., HÄSELER, R., HU, M. & KITA, K. 2012. Observation and modelling of OH and HO₂ concentrations in the Pearl River Delta 2006: a missing OH source in a VOC rich atmosphere. *Atmospheric Chemistry and Physics*, 12, 1541-1569.
- MCCRACKEN, D. 2013. Real-time measurement of VOCs during SOA formation using PTR-TOF-MS. *MChem report*. University of Leicester.

Chapter five: Case study - Measuring urban air samples in London, UK, with enhanced sensitivity

- NAKAJIMA, T., YOON, S. C., RAMANATHAN, V., SHI, G. Y., TAKEMURA, T., HIGURASHI, A., TAKAMURA, T., AOKI, K., SOHN, B. J. & KIM, S. W. 2007. Overview of the Atmospheric Brown Cloud East Asian Regional Experiment 2005 and a study of the aerosol direct radiative forcing in east Asia. *Journal of Geophysical Research: Atmospheres (1984–2012)*, 112.
- ÖZEL, M. Z., WARD, M. W., HAMILTON, J. F., LEWIS, A. C., RAVENTOS-DURAN, T. & HARRISON, R. M. 2010. Analysis of organic nitrogen compounds in urban aerosol samples using GCxGC-TOF/MS. *Aerosol Science and Technology*, 44, 109-116.
- PARRISH, D. D., KUSTER, W. C., SHAO, M., YOKOUCHI, Y., KONDO, Y., GOLDAN, P. D., DE GOUW, J. A., KOIKE, M. & SHIRAI, T. 2009. Comparison of air pollutant emissions among mega-cities. *Atmospheric Environment*, 43, 6435-6441.
- REN, X., HARDER, H., MARTINEZ, M., LESHER, R. L., OLIGER, A., SIMPAS, J. B., BRUNE, W. H., SCHWAB, J. J., DEMERJIAN, K. L. & HE, Y. 2003. OH and HO₂ Chemistry in the urban atmosphere of New York City. *Atmospheric Environment*, 37, 3639-3651.
- ROGERS, T., GRIMSRUD, E., HERNDON, S., JAYNE, J., KOLB, C. E., ALLWINE, E., WESTBERG, H., LAMB, B., ZAVALA, M. & MOLINA, L. 2006. On-road measurements of volatile organic compounds in the Mexico City metropolitan area using proton transfer reaction mass spectrometry. *International Journal of Mass Spectrometry*, 252, 26-37.
- SALAM, A., BAUER, H., KASSIN, K., MOHAMMAD ULLAH, S. & PUXBAUM, H. 2003. Aerosol chemical characteristics of a mega-city in Southeast Asia (Dhaka–Bangladesh). *Atmospheric Environment*, 37, 2517-2528.
- STONE, E. A., LOUGH, G. C., SCHAUER, J. J., PRAVEEN, P. S., CORRIGAN, C. E. & RAMANATHAN, V. 2007. Understanding the origin of black carbon in the atmospheric brown cloud over the Indian Ocean. *Journal of Geophysical Research: Atmospheres (1984–2012)*, 112.
- VON SCHNEIDEMESSER, E. & MONKS, P. Are megacity's oxidizing environments changing? EGU General Assembly Conference Abstracts, 2010. 4570.
- VON SCHNEIDEMESSER, E., MONKS, P. S. & PLASS-DUELMER, C. 2010. Global comparison of VOC and CO observations in urban areas. *Atmospheric Environment*, 44, 5053-5064.
- WARNEKE, C., DE GOUW, J. A., KUSTER, W. C., GOLDAN, P. D. & FALL, R. 2003. Validation of atmospheric VOC measurements by proton-transfer-reaction mass spectrometry using a gas-chromatographic pre-separation method. *Environmental science & technology*, 37, 2494-2501.
- WATSON, R., MEIRA FILHO, L., SANHUEZA, E. & JANETOS, A. 1992. Greenhouse gases: sources and sinks. *Climate change*, 92, 25-46.
- WHITE, I. R., GOODALL, I., BARBER, S., WYCHE, K. P. & MONKS, P. S. Gas Phase Measurements of VOCs during the ACIDPRUF Chamber Studies. ACID-PRUF Annual Science Meeting, Nov 22nd 2012. 2012 Manchester, UK.
- WILSON, A. D. 2012. Review of electronic-nose technologies and algorithms to detect hazardous chemicals in the environment. *Procedia Technology*, 1, 453-463.
- ZHAO, J. & ZHANG, R. 2004. Proton transfer reaction rate constants between hydronium ion (H₃O⁺) and volatile organic compounds. *Atmospheric Environment*, 38, 2177-2185.

6 Chapter six: Conclusion

The efficient detection of VOCs is crucial in many areas of study; ranging from atmospheric chemistry and medical diagnosis, to the food sciences and homeland security. A variety of techniques exist that can study VOCs, such as GC-MS and SIFT-MS. However PTR-MS offers a good compromise between sensitivity, size, cost, mass resolution and time resolution and is also a soft ionising technique. This thesis aimed to investigate what improvements can be made to PTR-MS through the addition of an ion funnel and also by changing buffer gas composition.

Chapter one put into context the importance of VOCs, as well as the challenges such analysis involves. Current analysis methods were discussed including the instruments that lead to the creation of PTR-MS. A few of the many applications where PTR-MS has proved useful were explored, in order to recognise the wide reaching implications of such an instrument and any future improvements that could be yielded.

Chapter two detailed some of the fundamental aspects behind PTR-ToF-MS and described the instruments that were used in the work in this thesis. A comparison of ionisation techniques was discussed as well as the thermodynamics and kinetics behind proton transfer reactions. The validation and quantification of the data were also described.

6.1 Enhanced sensitivity

Chapter three explored the potential for radio frequency ion funnel technology installed within the drift tube to enhance the sensitivity of a PTR-MS instrument. A standard drift tube was modified in order to allow it to operate as both a conventional drift tube and as an ion funnel. This is the first time a combined drift tube/ion funnel has been coupled to a mass spectrometer and as a result, a much higher sensitivity was achieved for the selected test VOC species. One of the major factors limiting the sensitivity of conventional PTR-MS instruments

comes from the ion transmission through the micro orifices used in the differential pumping stages of the instrument resulting in only a small proportion of ions being transmitted from the drift tube into the mass analyser. Therefore by increasing the ion transmission through the use of an ion funnel, a higher fraction of the ions reach the mass analyser and can be detected. This drift tube/ion funnel set-up could be easily coupled to any type of mass analyser that is routinely used with PTR-MS and could therefore be of great benefit in many areas of research.

The RF-funnel was successful in its aim. The sensitivity enhancement when changing from the standard drift tube (DC-mode) to the ion funnel (RF-mode) resulted in an increase of over two orders of magnitude for many of the compounds analysed. Acetaldehyde, formic acid, acetone, methacrolein and cyclohexanone showed an increase in sensitivity of over two orders of magnitude. Trans-2-butene, pro-pionaldehyde, benzene, limonene, β -pinene, and bromobenzene all showed an increase in sensitivity of over one order of magnitude. Methanol, methyl acetylene and β -caryophyllene all showed an increase in sensitivity albeit below a factor of x10. Crucially no compounds showed a decrease in sensitivity when using the RF ion funnel, suggesting this new hardware would yield benefits for PTR-MS systems across a very wide range of analyte compounds.

6.2 Controlling collision energy

Having the ability to affect the fragmentation of certain molecules and potentially reduce the fragmentation of these molecules allows PTR-MS spectra to be analysed more easily. Furthermore, several applications now have buffer gases that are not pure nitrogen (or air) and/or contain several percent mixing ratios of other components such as CO₂.

Chapter four investigates changing the buffer gas composition and how this affects the collision energy conditions within the drift tube, in order to identify any potential benefits in doing so. Work presented in this chapter demonstrated how the conventional 'Le-ToF' PTR-MS instrument could be successfully operated under argon buffer gas conditions as set out by Inomata and co-

workers (Inomata et al., 2008), without any physical modification. Limonene was successfully analysed at 40 Td and had improved sensitivity and reduced fragmentation when compared to 'standard' conditions of 100 Td for when nitrogen buffer gas was used.

When considering the distribution of hydronium ions and its hydrated clusters across a range of E/N s, both buffer gases produced similar patterns. The distribution in argon buffer gas was however, reduced by approximately 40 Td for equivalent cluster ratios. Using these results it was possible to find two different E/N values (one for nitrogen buffer gas and one for argon buffer gas) that correspond to the same ratio of hydronium to hydrated hydronium $[H_3O^+]:[H_3O^+ \cdot H_2O]$.

Many recent applications of PTR-MS involve sampling complex sample matrices in the field, as opposed to single component lab based experiments. These complex matrices often contain not only a large number of trace level VOCs but also large quantities of other gases, which have the potential to alter the buffer gas make-up. Applications of PTR-MS are moving away from lab-based, single component experiments and into the field, where complex samples contain not only the target VOCs but also high concentrations of other species which potentially alter buffer gas composition significantly and this has been investigated by changing the buffer gas in the PTR-MS system. In order to investigate the effects of having a portion of the buffer gas altered, a detailed study into the use of nitrogen/argon buffer gas mixtures show that the sensitivity of various compounds is highly compound specific and varies by not only E/N but also by the buffer gas make-up.

A comparison between three regimes was carried out in order to compare individual spectra under different experimental conditions: equivalent E/N ratios, equivalent kinetic energies and equivalent hydronium ratios. Fragmentation reduction was successfully achieved for both limonene and hexane when equivalent hydronium ratios and equivalent collision energies were used for an argon buffer gas compared to a nitrogen buffer gas.

When a complex mixture is analysed, i.e. engine exhaust emissions, then a reduction is seen in the number of peaks present at various heights by changing the buffer gas from nitrogen to argon. Overall there is a slight reduction in the number of peaks observed and with further improvement this could simplify analysis of complex VOC mixtures.

6.3 Urban air measurements

Since its inception, PTR-MS has been utilised in the field of atmospheric chemistry due to its ability to measure atmospherically relevant VOCs. With the enhanced sensitivity that RF-PTR-ToF-MS affords, species previously only detectable in chamber studies can potentially be detected in experiments sampling urban air.

The ClearfLo campaign proved the perfect platform to assess the performance of the RF-PTR-ToF-MS and compare this to the operation of a standard PTR-ToF-MS. The ClearfLo winter IOP demonstrated that the standard PTR-ToF-MS could measure VOCs over a weekly time frame at high temporal resolution (1 min). These results showed good agreement with 2D-GC-MS measurements of acetone, butene, benzene, toluene, and xylene. However because 2D-GC-MS only acquires one data point per hour, it can miss many features that are obtained when acquiring 1 min data via PTR-ToF-MS. When assessing a person's exposure to pollution it is vital for high time resolution data to be obtained. This time resolution data, also allows for a more accurate source apportionment of VOCs and oVOCs.

A larger number of ion peaks were detected with the RF ion funnel instrument in the summer IOP compared to the winter IOP as a result of the increased sensitivity offered by the RF-PTR-ToF-MS. Many of these ions signals were also observed during the ACIDPRUF chamber study of alpha-pinene oxidation, meaning that these compounds could be oVOC products from the oxidation of bVOCs. Although these compounds have previously been observed in chamber studies where concentrations are higher, they pose an observational challenge at the lower concentrations present in ambient air.

Unfortunately, long time series of a week or more (like those obtained using the PTR-ToF-MS during the winter IOP) were unobtainable with the RF-PTR-ToF-MS due to instrument instability. Better temperature control is required when operating the RF-PTR-ToF-MS and therefore speciation of those compounds was not possible. The system could be modified with the flight tube and other components being temperature controlled in order to minimise this problem. Adding an internal standard, such as bromobenzene, could also be used to help track sensitivity changes in real time throughout the entire experiment.

6.4 Ongoing challenges

Whilst the RF-PTR-ToF-MS had substantial improvements in sensitivity, background chemical signals currently limit the achievable limits of detection. Components, such as o-rings, could be changed as these background chemical signals are not visible in the LE-ToF which uses o-rings manufactured from a different material, therefore this problem appears relatively simple to solve.

Overall the RF-PTR-ToF-MS performed very well in the laboratory; however the issue was a lack of stability during field deployment. Temperature controlling the various components of the instrument as well as utilising an internal calibrant would lead to a consistent sensitivity and a stable instrument suitable for future deployment.

The many aspects that can be altered within the system, and the fine tuning and balance required for successful analysis, creates a situation where investigating the change of buffer gas is far from trivial. However, with continued study there is no reason to believe that this could not be of benefit in numerous applications.

6.5 Future work

The RF-PTR-ToF-MS will be able to perform successfully in the field and measure more VOCs than a standard instrument, once certain hurdles have been overcome. Therefore, it is sensible that the RF-PTR-ToF-MS is deployed to measure atmospheric samples again in further field work in the near future. Alternatively, because of the high sensitivity available, it is now possible to carry

out chamber studies at lower concentrations, making them more atmospherically relevant. RF-PTR-ToF-MS could also be deployed for other monitoring situations, such as in a hospital to monitor VOC profiles on patients' breath for diagnostic purposes; indeed this is currently where the RF ion funnel instrument used in this thesis is being tested.

A comprehensive investigation into a wide range of VOCs (in order to catalogue the new fragmentation patterns when using different buffer gas compositions) could be carried out to ascertain which applications are most appropriate for different buffer gas compositions. There is also the potential to combine this change in collision energy, brought about by a different buffer gas, with an ion funnel equipped instrument. This could result in buffer gases that alter the fragmentation and also reduce sensitivity, still being a viable option, as the ion funnel could enhance the overall sensitivity of the instrument.

6.6 Final remarks

PTR-MS has already been proven to be a useful technique for measuring VOCs and is being utilised in many areas. It has proved successful in atmospheric chemistry, breath analysis and has the potential to play a larger role in homeland security, forensic science and food sciences. PTR-MS continues to still improve, with lower LoDs being achieved regularly. And with the benefits that altering the collision energy in the drift tube could yield, there are even more opportunities for PTR-MS to be developed further and tuned to optimise the detection of specific target gases. With the large number of current applications, and the many more that will surely arise over the coming years, PTR-MS will no doubt continue to have wide ranging implications in any area VOCs are prevalent.

6.7 References

INOMATA, S., TANIMOTO, H. & AOKI, N. 2008. Proton transfer reaction time-of-flight mass spectrometry at low drift-tube field-strengths using an H₂O–rare gas discharge-based ion source. *J. Mass Spectrom. Soc. Jpn*, 56, 181-187.